POLITECNICO DI TORINO
Repository ISTITUZIONALE

Frontal Polymerizations: From Chemical Perspectives to Macroscopic Properties and Applications

Original
Frontal Polymerizations: From Chemical Perspectives to Macroscopic Properties and Applications / Suslick, B.A., Hemmer, J., Groce, B.R., Stawiasz, K.J., Geubelle, P.H., Malucelli, G., Mariani, A., Moore, J.S., Pojman, J.A., Sottos, N.R.. - In: CHEMICAL REVIEWS. - ISSN 0009-2665. - ELETTRONICO. - 123:6(2023), pp. 3237-3298. [10.1021/acs.chemrev.2c00686]

Availability:
This version is available at: 11583/2976342 since: 2023-03-22T13:49:23Z

Publisher:
ACS

Published
DOI:10.1021/acs.chemrev.2c00686

Terms of use:

This article is made available under terms and conditions as specified in the corresponding bibliographic description in the repository

Publisher copyright

(Article begins on next page)

07 October 2026

CHEMICAL REVIEWS

pubs.acs.org/CR

Review

Frontal Polymerizations: From Chemical Perspectives to Macroscopic Properties and Applications

Benjamin A. Suslick,* Julie Hemmer, Brecklyn R. Groce, Katherine J. Stawiasz, Philippe H. Geubelle, Giulio Malucelli, Alberto Mariani, Jeffrey S. Moore,* John A. Pojman, and Nancy R. Sottos

Cite This: *Chem. Rev.* 2023, 123, 3237−3298

Read Online

ACCESS | Metrics & More | Article Recommendations

ABSTRACT: The synthesis and processing of most thermoplastics and thermoset polymeric materials rely on energy-inefficient and environmentally burdensome manufacturing methods. Frontal polymerization is an attractive, scalable alternative due to its exploitation of polymerization heat that is generally wasted and unutilized. The only external energy needed for frontal polymerization is an initial thermal (or photo) stimulus that locally ignites the reaction. The subsequent reaction exothermicity provides local heating; the transport of this thermal energy to neighboring monomers in either a liquid or gel-like state results in a self-perpetuating reaction zone that provides fully cured thermosets and thermoplastics. Propagation of this polymerization front continues through the unreacted monomer media until either all reactants are consumed or sufficient heat loss stalls further reaction. Several different polymerization mechanisms support frontal processes, including free-radical, cat- or anionic, amine-cure epoxides, and ring-opening metathesis polymerization. The choice of monomer, initiator/catalyst, and additives dictates how fast the polymer front traverses the reactant medium, as well as the maximum temperature achievable. Numerous applications of frontally generated materials exist, ranging from porous substrate reinforcement to fabrication of patterned composites. In this review, we examine in detail the physical and chemical phenomena that govern frontal polymerization, as well as outline the existing applications.

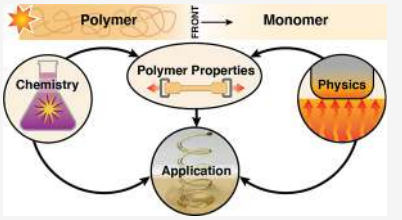

CONTENTS

1. Introduction 3238
 1.1. Conventional High-Energy Curing of Thermosets and Bulk Polymerization Reactions 3238
 1.2. What is Frontal Polymerization? 3238
2. Characteristic Features of Frontal Polymerization 3241
 2.1. Detection and Visualization of Polymerization Fronts 3241
 2.2. Macroscopic Metrics Associated with Propagating Fronts 3242
  2.2.1. Front Velocity and Acceleration 3242
  2.2.2. Ignition and Pre-Steady State Duration 3243
  2.2.3. Temperature Field 3243
  2.2.4. System Lifetimes 3244
  2.2.5. Monomer Conversion and Degree of Conversion 3244
 2.3. Structural and Mechanical Properties of Frontally Derived Polymers 3245
3. Governing Physics: Heat Transport and Instabilities 3245
 3.1. Heat Equation in Frontal Polymerization 3246
  3.1.1. Power Density Generated by the Chemical Polymerization Reaction 3246
  3.1.2. Power Density Transported by Conductive Thermal Diffusion 3247
  3.1.3. Power Density Lost to the Surroundings 3247
 3.2. Instabilities in Frontal Polymerization 3247
 3.3. Geometric Influences on Front Propagation 3249
4. Chemistries of Existing Frontal Polymerization Systems 3250
 4.1. Frontal Ring-Opening Metathesis Polymerization 3250
  4.1.1. Mechanism and Background 3250
  4.1.2. Unusual Catalyst Design Principles: Tempering FROMP Reactivity via Inhibition 3251
  4.1.3. Copolymerizations 3252
  4.1.4. Mechanical Properties of FROMP Polymers 3254
  4.1.5. Non-Thermal Initiation Methods 3254
  4.1.6. Frontal Ring-Opening Metathesis Oligomerization 3255
 4.2. Frontal Cationic Polymerizations 3255
  4.2.1. Epoxy and Oxetane Ring-Opening Polymerization 3255

Received: October 5, 2022
Published: February 24, 2023

Downloaded via 79.44.216.157 on March 22, 2023 at 13:42:27 (UTC).
See https://pubs.acs.org/sharingguidelines for options on how to legitimately share published articles.

ACS Publications

© 2023 The Authors. Published by American Chemical Society

https://doi.org/10.1021/acs.chemrev.2c00686
Chem. Rev. 2023, 123, 3237−3298

4.2.2. Tin-Catalyzed Polyurethane Synthesis 3258
4.3. Frontal Radical Polymerizations 3259
4.3.1. Mechanistic Considerations 3259
4.3.2. Ignition Techniques 3259
4.3.3. Radical Initiators 3260
4.3.4. Monomer Effects on Propagation 3262
4.3.5. Solvent Considerations 3264
4.3.6. Fillers and Additives 3265
4.4. Stoichiometric Frontal Curing 3266
5. Applications of Frontal Polymerization 3266
5.1. Hydrogels 3266
5.1.1. Synthesis, Porosity, and Swelling 3267
5.1.2. Ion Removal Reagents 3269
5.1.3. Drug Encapsulation and Delivery 3270
5.1.4. Synthesis of Interpenetrating and Supramolecular Polymer Networks 3271
5.1.5. Chemical Sensors 3272
5.1.6. Self-Healing Materials 3272
5.2. Functionally Gradient Materials 3274
5.3. Instability Driven Spontaneous Patterning 3275
5.4. Composite Materials and Additive Manufacturing 3276
5.4.1. Substrate Consolidation and Reinforcement 3276
5.4.2. Frontal Geopolymerization 3277
5.4.3. Frontally-Derived Adhesives 3278
5.4.4. Frontally Polymerized Artwork 3279
5.4.5. Photoluminescent and Thermochromic Composites 3279
5.4.6. Generation of Microvascular Networks and Microfluidic Devices 3281
5.4.7. Large-Scale Fabrication, 3D-Printing, and Additive Manufacturing 3281
6. Summary and Outlook 3284
6.1. Summary: Where are We Now? 3284
6.2. Outlook: Where Do We Go from Here? 3285
Author Information 3285
Corresponding Authors 3285
Authors 3285
Author Contributions 3286
Notes 3286
Biographies 3286
Acknowledgments 3287
Abbreviations, Terms, and Symbols 3287
References 3288

1. INTRODUCTION

1.1. Conventional High-Energy Curing of Thermosets and Bulk Polymerization Reactions

Many industrial-scale applications require structurally lightweight, high-strength materials. The aerospace,[1−3] automotive,[4] infrastructure,[5] and energy[6] sectors employ components made of composite materials that are comprised of highly cross-linked thermosets in conjunction with a reinforcing medium (e.g., aluminum, glass, or carbon fillers). In the case of modern commercial aircraft, such as the Boeing 787 or Airbus A350XWB, composites represent nearly 50% of the total weight, and are expected to increase in demand in the coming decades.[2] Traditional, energy inefficient thermoset curing technologies involve elevated temperatures (≈200 °C) over an extended time frame (≈5−20 h) in a closed, high pressure autoclave or oven.[7] Moreover, the dimensions of the reactor depend on the size of the desired object; large objects, therefore, necessitate sufficiently sized forming or containment apparatuses (i.e., an autoclave), which incurs an initial capital investment in addition to the associated energy and materials costs.[1,3,7]

A related, but often undervalued issue involves the environmental impacts associated with the operation of batch curing devices, which encompass the entire life-cycle of the final product.[8] The fabrication of the fuselage of a Boeing 787, for example, requires curing of several massive (≈2 tons) sections comprised of carbon-fiber-reinforced thermoset polymer composite materials.[3] Lifecycle assessment of one such tubular section estimated that manufacturing requires an energy consumption of 1.6×10^4 kWh (≈58 GJ).[3]

Separate from curing processes that irreversibly form extended cross-linked networks, bulk polymerizations (BP) of non-cross-linkable monomers afford linear or branched thermoplastics.[9,10] In the adopted processing conditions, thermoplastics do not undergo irreversible chemical reactions upon heating, whereas thermosets form covalent linkages between polymer chains (i.e., curing). While examples of low-temperature curing processes exist (e.g., room temperature vulcanization of bicomponent silicones or RTV2), most structural thermoset composites are produced at temperatures exceeding 100 °C.[7] BP formulations (i.e., solvent-free) contain monomers with the possible addition of initiators, catalysts, or additives, as necessary. These components are thoroughly mixed and then transferred into heated (and often pressurized) reactor vessels or cast-molds.[9] Polymerizations initiate uniformly through the entire reaction media, without a well-defined monomer-to-polymer interface. The exothermicity associated with these neat polymerization techniques may present a heat dissipation safety challenge; efficient heat removal is required to avoid potentially dangerous run-away reactions.[9] The generated heat is typically wasted, rather than being harvested for productive applications.

Given the rapid changes to global climate patterns attributed to combustion derived green-house gas emissions,[11] new curing and polymerization processes must exhibit improved efficiencies and lower environmental impacts.[12] In this context, frontal polymerization (FP) has emerged as a low-energy alternative for synthesizing thermoset polymers and moldable thermoplastics. Henceforth, we refer to the formation of both cross-linked and non-cross-linked networks as frontal polymerizations.

1.2. What is Frontal Polymerization?

Frontal polymerization is a self-perpetuating reaction, wherein an initial stimulus (e.g., thermal or photo) induces a localized reaction zone, the so-called "polymerization front". The heat released from the exothermic polymerization in this zone provides sufficient temperature increase to initiate additional polymerization events at the boundary between polymer and unreacted monomer phases, which often results in planar propagation. This is perhaps best described in analogy to the falling of dominoes arranged in a line (Figure 1). Initially, the upright dominoes exist in a local energy minimum. Unperturbed, the dominoes remain motionless. An external force, say for example from a finger, provides sufficient energy to knock a single domino over (i.e., surpass a kinetic barrier). In this fashion, the trigger transforms potential energy into kinetic energy. As the domino falls, it transfers some of this

https://doi.org/10.1021/acs.chemrev.2c00686
Chem. Rev. 2023, 123, 3237−3298

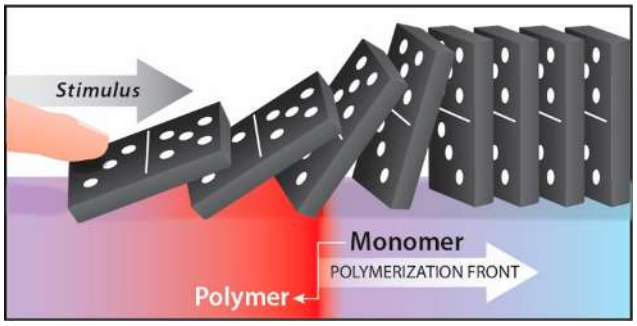

Figure 1. Generalized representation of FP compared to falling dominoes. Top: An initial force provides sufficient energy to induce a domino effect. Bottom: An initial energy stimulus (e.g., heat) initiates a self-sustaining, propagating polymerization front.

kinetic energy onto an adjacent tile, which then has sufficient energy to overcome its own barrier. In this way, the dominoes fall one after another in a self-sustaining and predictable way. This analogy elegantly describes an ideal propagation event.

Nonplanar fronts also exist, and section 3 details the underlying causes associated with thermal and convective instabilities. Except for the ignition by an exogenous source, no additional external energy input is needed as the heat generated by the chemical reaction (i.e., monomer transforming into polymer) sustains the process. Self-perpetuation occurs by way of heat transport (see section 3) through the polymerizable medium until complete monomer conversion occurs. The polymerizable medium is typically in a liquid or gel phase, but in the case of composites, the inclusion of a chemically inert reinforcement phase (i.e., filler) influences to the heat transport.

A bibliometric analysis of the history of FP is possible using the method known as reference publication year spectroscopy (RPYS). First introduced by Marx et al.,[13] this technique quantifies the frequency with which references are cited (i.e., cited references, CR) in the publications of a specific research field. The findings from RPYS are reported as a plot of total CR for papers published in a given year vs the publication year (Figure 2, gray bars). From this data, the difference from the 5-year median of the CRs (Figure 2, red curve) against publication year is calculated. Historically important works manifest as pronounced peaks in the difference curves (i.e., highly cited). RPYS is implemented using the tool CitedReferencesExplorer (CRExplorer), which analyzes the CRs in a publication set retrieved from common bibliometric databases, such as Web of Science (WoS, Clarivate Analytics). For a WoS search on "Frontal Polymerization" conducted on September 1, 2022, we found 769 FP publications with 26 319 nondistinct CRs. The RPYS analysis revealed four distinct time periods of seminal papers that contributed to the FP literature: (1) before the discovery of FP, a handful of elementary publications appear dealing with combustion science and polymerization; (2) starting from 1972, papers on the discovery of FP appear, exclusively from scientists of the former Soviet Union (USSR); (3) ca. 1990, publications investigated and established the fundamental chemistries of FP; and (4) after ca. 2005, publications emerge related to engineering science (i.e., applications) of FP. Key early references identified by RPYS are provided in Figure 2.

The first usage of the term "frontal" in the context of polymerization originated from the former USSR in the early 1970s.[14−27] These early works described the self-perpetuating radical polymerization of methyl methacrylate under intense pressures in sealed reaction chambers (on the order of 10^2 to 10^3 atm). The pressure involved in such systems, however, precludes their practical implementation in commercial or industrial settings. Between the 1970s and early 1990s, a significant research effort existed in USSR to develop large-scale frontal reactors; given political pressure and censorship within Soviet science, dissemination of science outside of the country was limited until after the fall of the USSR in 1991.[28] The results on FP from the USSR era are nicely summarized in early reviews by Pojman et al.[29,30] and Davtyan et al.[31] and will not be discussed further here.

FP provides several advantages compared to other polymerization modes. Existing industrial methods, such as those employed to fabricate thermosets, often require prolonged heating at elevated temperatures inside large autoclaves. In contrast, FP reactions exhibit superior energy efficiencies through the elimination of the continuous external heating requirement.[7] Additionally, frontal temperatures typically exceed those of batch reactors, which manifests as faster observed polymerization rates and shorter fabrication times. The mechanical properties of frontally prepared polymers are often comparable to, if not better than, those derived from other methods as a result of higher monomer conversions and degree of cross-linking (sometimes indicated as the degree of conversion, α).[32−34] Theoretical studies have also investigated differences between bulk polymerizations and FP in the context of fabricating fiber-reinforced composites.[35]

Despite these advantages, several limiting factors exist. FP necessitates highly reactive monomers to self-propagate. As an unintended consequence, some monomer systems undergo spontaneous polymerization (SP) at or near ambient temperatures.[36] In the context of this review, we differentiate FP and SP as separate modes of polymerization. While FP and SP are both types of BP (i.e., neat resins), the associated reaction/thermal profiles distinguish them from commonplace industrial methods. Typical industrial BP occur at a fixed temperature, where polymerization occurs uniformly throughout the reaction media. In contrast, FP and SP proceed nonuniformly. In the former case, a well-defined and predictable thermal gradient exists. In contrast, SP occurs at ambient conditions in the absence of an initiating trigger. Typically, SP is uncontrolled without a well-behaved thermal profile and typically provides materials of variable properties.

In addition, some of these systems induce autoacceleration phenomena (also known as the gel or Trommsdorff−Norrish effect).[37−40] Contrary to most reaction types where observed rates decrease with substrate consumption, autoaccelerating polymerizations exhibit rate enhancements as the monomer concentration decreases. Increased viscosity due to increasing polymer chain length over the course of polymerization results in reduced termination rates that net an overall increase in the observed rate of monomer consumption.[37] Hence, low polymerization onset temperatures require substantially colder working conditions to avoid SP and favor FP.

On the other hand, mitigation of heat-loss from the front to the surroundings is a separate but equally important challenge. Front quenching may occur via heat-loss to the surroundings, as this lowers the temperature at the front below a critical point required to self-sustain FP. Quenching also results when an insufficient monomer, initiator, or catalyst volume fraction exists in the polymerizable medium, the polymerization rate is

https://doi.org/10.1021/acs.chemrev.2c00686
Chem. Rev. 2023, 123, 3237−3298

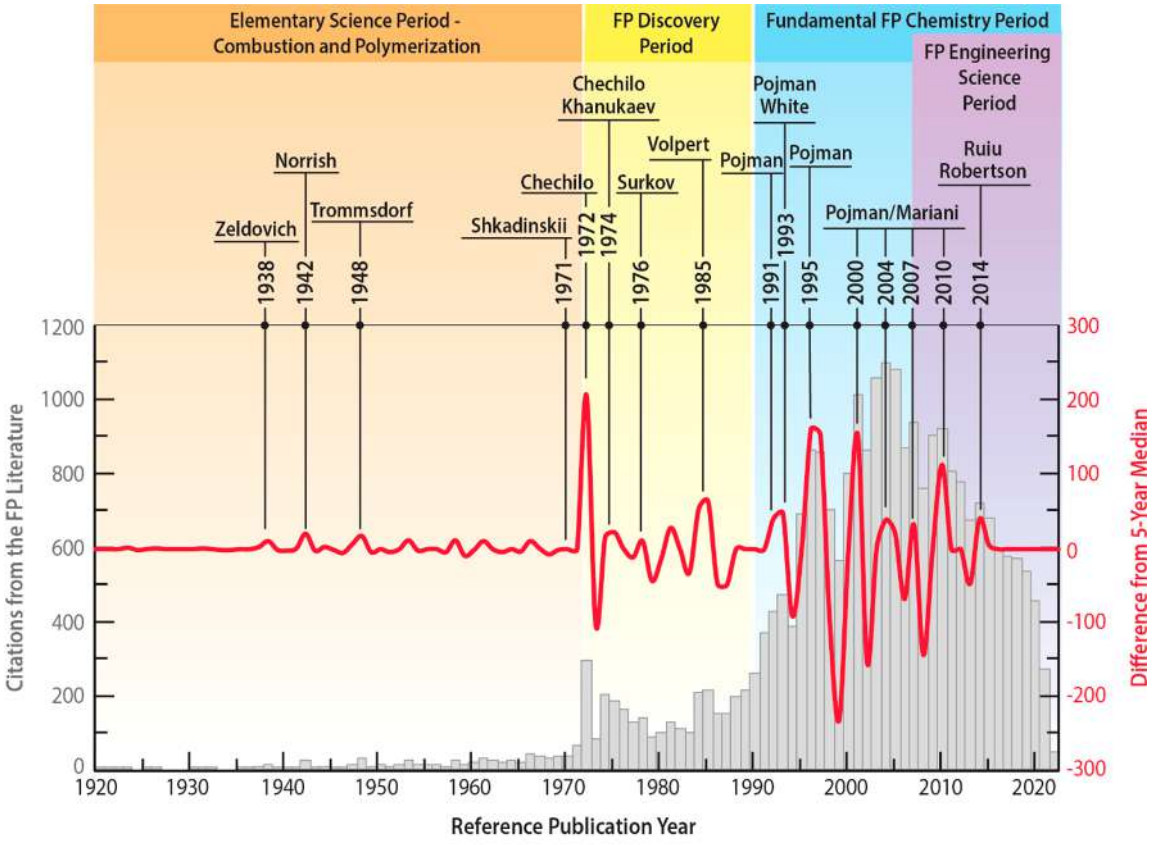

Year	Key Early References (pre 1995)	Total Citations	Cited by FP Literature
1938	Zeldovich and Kamenetzki, A theory of thermal propagation of flame. *Acta Physicochimica URSS* **1938**, 9, 341.	47	6
1942	Norrish *et al.*, Catalyzed polymerization of methyl methacrylate in the liquid phase. *et al. Nature* **1942**, 150, 336.	329	24
1948	Trommsdorff *et al.*, Polymerization of methyl methacrylates. *Makromolekulare Chemie* **1948**, 1, 169.	487	24
1971	Shkadinskii *et al.*, Propagation of a pulsating exothermic reaction front in the condensed phase. *Combust. Explos. Shock Waves* **1971**, 7, 15.	170	17
1972	Chechilo *et al.*, Phenomenon of Polymerization Reaction Spreading. *Dolk. Akad. Nauk SSSR* **1972**, 204, 1180.	252	217
1974	Chechilo *et al.*, Structure of Polymerization Wave Front and on Mechanism of Polymerization Reaction Spreading. *Dolk. Akad. Nauk SSSR* **1974**, 214, 1131.	27	47*
1974	Khanukaev *et al.*, Theory of polymerization-front propagation. *Combust. Explos. Shock Waves* **1974**, 10, 17.	6	5
1974	Khanukaev *et al.*, Theory of the propagation of a polymerization front. *Combust. Explos. Shock Waves* **1974**, 10, 562.	16	16
1976	Surkov *et al.*, Calculation of Steady-State Velocity of Reaction Front During Epoxide Oligomer Curing by Diamines. *Dolk. Akad. Nauk SSSR* **1976**, 228, 141.	11	25*
1985	Volpert *et al.*, Propagation of the caprolactam polymerization wave. *Combust. Explos. Shock Waves* **1985**, 21, 443.	9	9
1991	Pojman, Traveling fronts of methacrylic acid polymerization. *J. Am. Chem. Soc.* **1991**, 113, 6284.	205	174
1993	Pojman *et al.*, Traveling fronts of addition polymerization with a solid monomer. *J. Am. Chem. Soc.* **1993**, 115, 11044.	83	70
1993	White *et al.*, Simultaneous lay-up and in situ cure process for thick composites. *J. Reinf. Plast. and Compos.* **1993**, 12, 520.	41	32
1994	Nagy *et al.*, Thermochromic composite prepared via a propagating polymerization front. *J. Am. Chem. Soc.* **1995**, 117, 3611.	103	90

Figure 2. Reference publication year spectroscopy of the term "Frontal Polymerization" in a Web of Science search conducted on September 1, 2022. Plot: Gray bars represent the total citations by the FP literature for papers published in a given year as a function of the publication year. The red curve is the difference from the 5-year median value. Key references correspond to well-defined peaks in the red trace. Four time periods of publication exist and correspond to distinct phases of the development of FP. Table: Key early references (pre-1995) are provided, with the associated authors, titles, total citation count, and citations from the FP literature. *The FP citations exceed the total citation count likely as the result from an error in the WoS database.

https://doi.org/10.1021/acs.chemrev.2c00686
Chem. Rev. 2023, 123, 3237−3298

too slow, or the heat of polymerization is too small. Indeed, front quenching is problematic as the resultant polymers exhibit nonuniform properties. From a chemical perspective, many polymerization motifs are plagued by undesired termination reactions or slow background gelation. In radical chain polymerizations, for example, coupling events reduce the concentration of reactive species able to add monomer within the reaction media, thereby dampening the observed polymerization rate.[37] Similarly, gel-state resins that result from partial prepolymerization exhibit reduced monomer concentration compared to the initial, liquid-state reaction conditions. The lowered potential energy in such resins may slow (or even prevent) propagation under FP conditions.[41] Nevertheless, recent work from Robertson et al.[32] achieved successful gel-state FP and adapted this technique to applications that require processing of viscoelastic materials (e.g., 3D-printing). Reactor boundary conditions dictate the magnitude of heat-loss in FP regime.[42] Thermally insulated reaction vessels, for example, dissipate heat more slowly than those comprised of conductive materials. Thermal insulation facilitates efficient heat transfer through the reaction media. The effective volume to exposed surface area (i.e., at the reactor boundary) ratio, as well as the reactor shape, play a critical role in heat-loss.[43,44]

Autoacceleration and front quenching may be viewed as two extreme cases of a shared phenomenon: the balance between chemical reaction and heat transfer rates. From this point of view, autoacceleration occurs when the kinetic and thermodynamic aspects of the chemical reaction prevail. In contrast, the front quenching exists in a heat-transfer governed regime, where insufficient heat generation per unit time cannot compensate for heat-loss.

To mitigate these challenges, an ideal FP system must remain inert for extended lengths of time (i.e., display a long pot-life) prior to the introduction of the exogenous triggering stimulus. These systems display resilience to undesired, background polymerization (either gelation or SP) under ambient conditions prior to front ignition. Additionally, resins must not exhibit premature front quenching after ignition. The latter consideration is described by the "propagating lifetime" of the system. In a hypothetical scenario where an infinite quantity of monomer exists, we define this value as the maximum length of time after ignition that a front propagates before either front quenching or autoacceleration occurs, given a nonsteady state condition. The propagating lifetime depends primarily on the reactor vessel specifications (e.g., boundary conditions, surface-area-to-volume ratio) and its resistance to heat-loss rather than the fundamental chemical properties. Short propagating lifetimes pose challenges toward the implementation of FP to 3D-printing.

Our goal in this review is to provide a complete picture of FP that bridges the gap among the governing chemical, physical, and mechanical phenomena. Given the interdisciplinary nature of the field, this review aims to provide a common ground to facilitate fruitful discussions. To our knowledge, this is the first review that comprehensively covers each of these details for a general audience. The four existing FP reviews cater to a highly specialized community and focus on specific subtopics (e.g., composite manufacturing).[29,30,45,46] As mentioned previously, the first review by Pojman and co-workers[29] in 1996 summarized the early Russian FP works that were otherwise inaccessible to non-Russian audiences. In 2012, Pojman[30] contributed a FP review chapter to the book *Polymer Science: A Comprehensive Reference*. More recently in 2022, Pojman[45] described FP exclusively in the context of composite manufacturing as a chapter of the *Encyclopedia of Materials: Plastics and Polymers*. Sadly, books have fallen out of style as easily accessible, widespread repositories of knowledge. While a recent review in *Prog. Polym. Sci.* by Li and co-workers[46] surveys the FP literature, it fails to critically analyze the field from an *ab initio* (i.e., first-principles) viewpoint; it best serves experts in the field as a reference list. To attract and engage the uninitiated, a general review must offer an entry point to *all* disciplines.

To this end, this review is organized into six sections, as outlined above. After this general introduction section, section 2 focuses on the common measurable metrics used to assess the efficacy of FP reactions, as well as a brief general discussion of key mechanical properties. Section 3 approaches the physics of FP by deriving the phenomena associated with heat transport, which govern the success of a frontal system. Section 4 outlines the chemical space (i.e., polymerization mechanism) and the relationship between FP compositions (i.e., monomer, initiator/catalyst, additives) and polymer properties. Section 5 provides an exhaustive survey of applications that exploit FP. The past five years have seen an explosive growth of application-driven FP developments. Indeed, a majority of new frontal systems describe the adaptation of FP to specific technologies (e.g., manufacturing, chemical sensing, composite production). As a result, we believe that a comprehensive review of the application space provides new insights for experts and new-comers alike. Lastly, section 6 provides our vision for future FP endeavors and concepts for the field to consider moving forward.

2. CHARACTERISTIC FEATURES OF FRONTAL POLYMERIZATION

2.1. Detection and Visualization of Polymerization Fronts

Optical imaging (i.e., the human eye or a digital camera) provides the most direct measurement of the front position (Figure 3); indeed, even an undergraduate student equipped with a ruler is sufficient to record front velocity, as described in an educational laboratory procedure by Pojman and co-workers.[47] A digital camera or camcorder in conjunction with modern analytical software packages enables enhanced spatial and temporal resolution, as well as better detection of complex front dynamics caused by thermal instabilities (see section 3.2). Optical imaging, however, relies on a substantial refractive

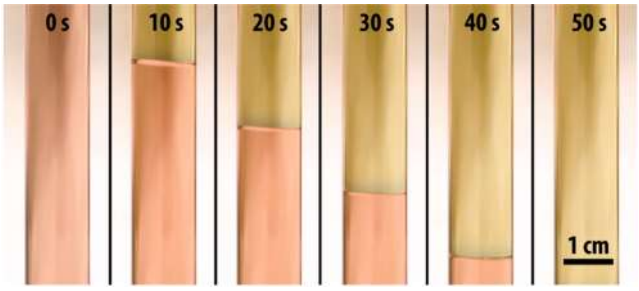

Figure 3. Time evolution of a reaction front in a neat resin of dicyclopentadiene. An initial thermal trigger initiates frontal ring-opening metathesis polymerization to convert liquid monomer (orange) into a solid thermoset polymer (yellow). Figure reprinted with permission from *ACS Macro Lett.* **2017**, *6*, 609−612.[52] Copyright 2017, American Chemical Society.

https://doi.org/10.1021/acs.chemrev.2c00686
Chem. Rev. 2023, 123, 3237−3298

index (or color) difference across the interface of the hot polymer and cool monomer phases.[48,49] In cases with negligible differences, the position of the reaction interface is ambiguous and difficult to track. Several alternative approaches circumvent these limitations, such as thermographic imaging or addition of reactive dyes (*vide infra*).[29,48,50]

Masere and Pojman[48] designed a polymerization formulation to include a reactive, colored indicator, such as bromophenol blue; under the reaction conditions associated with radical polymerizations (see section 4.3), this colored indicator undergoes a marked color change, thereby allowing for rapid visual detection of the reaction front. The authors attributed the change in photophysical properties to the radical scavenging behavior of bromophenol blue. In theory, any additive (e.g., thermochromic or fluorescent compounds) that does not interfere with the polymerization and undergoes a marked change in light absorption (or emission) within the reaction zone may aid in front position determination. Indeed, recent work from Lloyd et al.[51] demonstrated that the inclusion of a thermochromic additive (i.e., *N*,*N*′-di-*sec*-butyl-*p*-phenylenediamine) into FP resins records the thermal history during front propagation. Specifically, regions that achieve front temperatures exceeding ≈200 °C underwent a color change from purple to colorless, which is presumed to result from mesolytic cleavage of reasonably stable radical cation adducts of the diamine additive. More importantly, inclusion of this additive did not alter the metrics associated with front propagation.

Adaptation of infrared thermographic imaging to FP enables the observation of the heat-transfer dynamics. A recent publication by Bansal et al.[53] studied curing of thin acrylate films on wood surfaces by FP and employed thermographic visualization to extract the front position as a function of time, as well as the time-dependent temperature behavior (Figure 4).

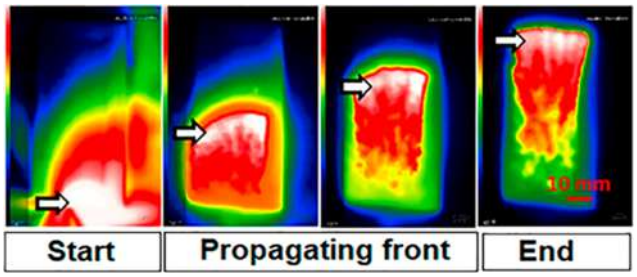

Figure 4. Infrared thermographs of FP of a mixed wood-polymer composite material provide insight into frontal dynamics. The edge of the front is indicated by the arrows. Reprinted and adapted with permission from *ACS Macro Lett.* **2020**, *9*, 169−173.[53] Copyright 2020, American Chemical Society.

Real-time video of the propagating heat wave is available in the Supporting Information provided by Bansal et al.[53] While this experimental procedure has become commonplace, it only provides temperature information at the sample surface, since detection involves IR radiation emitted via a blackbody cooling mechanism (see section 3).[54] Accurate measurements with this technique require IR transparent reaction vessels to avoid adventitious absorption by the container itself; this is particularly problematic for FP reactions housed in glass test-tubes. Changing the apparatus material or switching to an open-mold setup, however, greatly impacts thermal instabilities and front propagation. In contrast to thermographic imaging, an embedded thermocouple at a predetermined location in the reaction vessel provides accurate temperature measurements within the reaction zone. In this context, the judicious application of both techniques best describes the system.

For nontransparent materials comprised of opaque filler components (e.g., structurally reinforced composites, porous materials, stone, etc.) with polymers generated frontally, traditional visualization techniques are not applicable. In these select cases, high energy spectroscopic analyses are able to identify structural features *ex post facto*. In the consolidation of porous stones, for example, X-ray tomography was successfully utilized to determine the efficacy of structural reinforcement provided by polymers generated frontally *in situ*.[50,55] X-ray based techniques, however, are difficult to implement, especially in a time-resolved fashion, and therefore remain impractical for many frontal applications.

2.2. Macroscopic Metrics Associated with Propagating Fronts

Direct comparisons of otherwise disparate FP systems require a uniform set of well-defined parameters to describe the often-complex nature of the propagating heat wave. Variable experimental design specifications (e.g., chemical mechanism operative in the polymerization, reactor dimensions and material, additives, etc.) obfuscate meaningful comparisons between systems in this field. A discussion of the variables and the techniques involved in their measurement, therefore, is warranted to aid in subsequent analyses of the various frontal systems. While a set of standardized practices and terminologies exist, we propose several additional facets (*vide infra*) that are relevant when evaluating the efficiency of new FP experiments. The parameters related to front velocity and temperature typically are experimentally determined by the methods outlined in section 2.1.

2.2.1. Front Velocity and Acceleration. One of the most obvious characteristic features of FP is the velocity at which the reaction zone propagates through the monomer solution. In the simplest case of a 1D linear front, the steady-state velocity is defined as $v_f = dx/dt$, where x is position and t is time; typical values range from 0.5−10 cm min^{-1} as observed in Figure 5, though significantly higher and lower values also exist

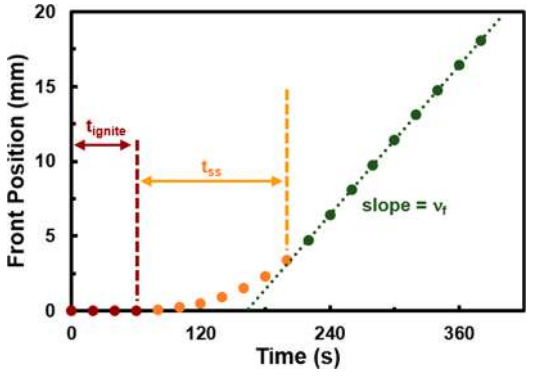

Figure 5. Generic plot of a front position profile. At $t = 0$, an external stimulus is applied to ignite the system. After a length of time (t_{ignite}), a visible front starts to propagate. The presteady state time (t_{ss}) reflects the length of time required to achieve a constant frontal velocity (v_f) after ignition. The frontal velocity is determined from the slope of the linear fit of the green section. The parameters in this general schematic are as follows: t_{ignite} = 60 s, t_{ss} = 140 s, and v_f = 5 mm min^{-1}.

https://doi.org/10.1021/acs.chemrev.2c00686
Chem. Rev. 2023, 123, 3237−3298

in several cases. In the 1960s, analytical expressions for front velocities were proposed for zeroth- and first-order, as well as autocatalytic chemical reactions.[56] The primary parameters that describe the correlation with the experimental observations include the thermal conductivity of the reaction media, polymerization enthalpy and activation energy.[56] Similarly, heat dissipation and the possible occurrence of concomitant physical or chemical transformations must also be considered. The transient acceleration of the front ($a_f = dx^2/d^2t$ in the 1D linear case) that occurs immediately after the ignition step has not been widely studied, but may relate to autoacceleration ($a_f \gg 0$) or front quenching ($a_f < 0$) phenomena. Systems that exhibit thermal instabilities, as presented in section 3.2, may undergo an alternation of positive and negative acceleration modes.[57]

2.2.2. Ignition and Pre-Steady State Duration. Perhaps unsurprisingly, instantaneous ignition of thermal fronts does not occur; a transient period exists prior to front propagation, during which a critical quantity of heat is transferred from the external stimulus to the ignition zone. Two different time parameters describe these transient dynamics, as depicted in Figure 5. The ignition time, t_{ignite}, reflects the length of time that the external stimulus is applied prior to visible front formation. This has also been referred to as the front start time,[58−64] but we favor the usage of t_{ignite} as it is less ambiguous. The energy required to trigger front formation divided by t_{ignite} provides a power value (measured in Watts), and is quantifiable for photoignited fronts.[59] The input power triggers the chemical reaction by providing sufficient energy to overcome the kinetic barriers (i.e., activation energy) associated with initiation and subsequent propagation steps. Separately, the rising temperature preheats fresh monomer ahead of the polymerization front via the physical process of heat transfer.[65]

A second, but related, feature of the initial frontal period is the presteady state time, t_{ss}, which indicates the transient regime after front generation for v_f to reach a constant value.[58] Large t_{ignite} values are problematic since they exacerbate competitive heat-loss; if heat transfer to the surroundings dominates (due to high thermal conductivity or the convective effect), a long t_{ignite} will not provide enough energy to trigger front formation. Similarly, longer t_{ss} afford nonuniform front conditions, which complicate the frontal process and may even lead to heterogeneous materials. An example of this occurs in systems that undergo cross-linking. Long t_{ss} values enable differences in the degree of cross-linking as a function of distance throughout the polymer. Despite the importance of t_{ignite} and t_{ss}, most literature reports provide only v_f, which limits meaningful analyses of the ignition dynamics and the reinforcing feedback between initiation and propagation.

2.2.3. Temperature Field. The velocity and temperature of the front are often highly correlated; for example,[56] fast moving fronts typically display higher frontal temperatures than slow moving fronts. Computationally, the temperature evolution is evaluated as a function of position and time. In a typical experiment, a thermocouple junction at a fixed position (Figure 6A and B) records the time-evolution of the temperature, whereas an IR thermograph displays the spatial temperature field at a fixed time (Figure 6C). Both techniques highlight three discrete regimes: (i) monomer preheating, (ii) the reaction front, and (iii) polymer cooling. The first results from heat transfer, either from the ignition source or from the polymerization enthalpy, and is defined by a smooth (and

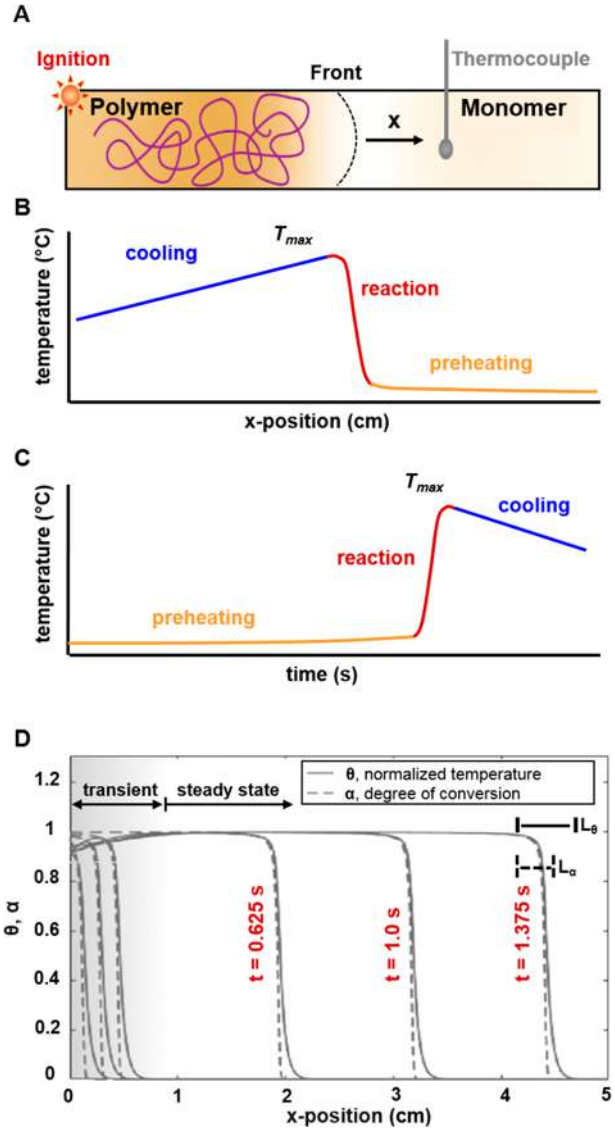

Figure 6. Temperature field evolution as a function of time and space. A: General schematic of FP at a fixed time period after ignition. B: Typical spatial evolution of the front temperature at a fixed time period after ignition, where "*x*-position" refers to distance from the ignition site. Three discrete regimes exist, the first of which involves preheating of the monomer via heat transfer (orange region). The red region exhibits a rapid temperature change due to the exothermic polymerization reaction in the front. Finally, cooling of the hot polymer occurs in the blue section. C: Typical temporal evolution of the front temperature at a fixed distance, as measured by an embedded thermocouple junction. D: Simulated frontal conversion (α) and normalized temperature (θ) profiles at different times, which indicate an initial transient propagation motif prior to achieving a steady-state. The normalized temperature θ is unitless and defined as $(T - T_0)/(T^0_{max} - T_0)$, where T_0 is the initial reaction temperature and T^0_{max} refers to the maximum front temperature at an initial $\alpha_0 = 0$. The reaction front exhibits two characteristic length scales, L_θ and L_α. L_θ refers to the spatial length (in cm) between positions in the front that exhibit a maximum and minimum θ value. L_α refers to analogous spatial length (in cm) in relation to degree of conversion, α. Note that both L_θ and L_α vary with initial α_0 and θ_0 values. This model does not consider cooling. Reprinted and adapted with permission from *J. Appl. Polym. Sci.* **2019**, *136*, 47418.[69] Copyright 2018, Wiley Periodicals, Inc.

https://doi.org/10.1021/acs.chemrev.2c00686
Chem. Rev. 2023, 123, 3237−3298

ideally flat) temperature gradient in both space and time. In the front region, monomer rapidly transforms into polymer with a concurrent heat-release and is characterized by a sharp thermal gradient. The final regime occurs after the front has polymerized the reaction media. The polymer spontaneously cools as the excess heat is lost to the surroundings.

For systems that exhibit well-behaved, smooth front propagations, a sensor that captures the time evolution of the temperature sufficiently characterizes the process. In particular, the maximum temperature of the front (T_{max}) is the most reported metric as it provides an easily comparable value. This simplistic observable, however, only provides information averaged over a small section and usually depends on the position of the sensor. Indeed, as the system is not adiabatic, temperature gradients likely exist between the reactor center and its boundaries. Moreover, fronts often deviate from the ideal smooth propagation motif, as highlighted in several studies that report the complexity of the temperature field evolution during FP (e.g., hot spots, spin-modes, fingering).[57,66−68] For instance, Figure 2 illustrates nonidealized behavior that results from the coupling between diffusive-convective transport modes and gravity. These complex instabilities are described in further detail in section 3.2.

Computational models, such as that described in Figure 6D, employ a normalized temperature θ.[41] This unitless value is defined as $\theta = (T - T_0)/(T^0_{max} - T_0)$, where T_0 is the initial reaction temperature and T^0_{max} refers to the maximum front temperature achieved in during FP (i.e., an initial degree of conversion, $\alpha_0 = 0$; see section 2.2.5). The characteristic length (L_θ) of the reaction front is easily visualized in Figure 6D; the length of the front is defined as the spatial distance between the maximum ($\theta = 1$) and minimum temperature ($\theta = 0$).

2.2.4. System Lifetimes. The so-called "pot-life" is a loosely defined term that typically reflects the length of time that a FP monomer system remains viable for frontal polymerization prior to the onset of SP. The literature definitions, however, vary as pot-life does not inherently specify the temperature at which it is measured. In this context, we propose two narrowly defined parameters that describe the viability of a frontal formulation. The *storage lifetime* reflects the length of time that a reaction mixture is stable at a specified temperature before background polymerization precludes its use for FP. Practical applications require long storage lifetimes; a batch of monomer must not undergo SP until it is intentionally ignited. This feature is particularly important in composite material fabrication. The production of carbon fiber-reinforced polymers, for example, requires the infusion of the reactive mixture into the porous substrate prior to polymerization.[32] Similarly, applications involving the consolidation of stone (e.g., historical artifacts) or adhesives also require long storage lifetimes. Significant research efforts have centered on increasing the storage lifetimes from minutes[70−73] to hours,[74−77] and in some cases days.[52,78] Section 4 provides a detailed analysis of the various factors that dictate the storage lifetimes.

A related, but often ignored, parameter is the *propagating lifetime*, which we define as the length of time that a hot front propagates before stalling out or undergoing SP. In contrast to the storage lifetime, the active lifetime denotes the resiliency of the system to heat-loss and uncontrolled autoacceleration. For manufacturing purposes, a self-sustaining front must possess a sufficiently long propagating lifetime to support industrial-scale applications. The primary difference between storage and propagating lifetimes is the relation to the ignition event. Storage lifetime reports on the resilience of frontal formulations to any process that occurs prior to front generation. It is most relevant to applications that require extensive preprocessing of the reaction system. In contrast, the propagating lifetime reflects the stability of the polymerization front to exogenous forces (e.g., heat-loss), with direct ramifications toward the processing window of the final product.

2.2.5. Monomer Conversion and Degree of Conversion. If no side reactions occur, monomer conversion or the degree of conversion (α) denotes the mole fraction of monomer transformed to polymer during polymerization at a given time. For a specific polymer architecture (e.g., linear, branched, network), the mechanical properties are highly correlated to α. When $\alpha = 0$, no polymer chains exist. At the other extrema ($\alpha = 1$), complete monomer consumption occurs. The state bounded by these extremes ($0 < \alpha < 1$) contains a mixture of species characterized by various degrees of polymerization. Indeed, the initial degree of conversion (α_0) tunes the rheology of the polymerization medium for a specific application. For example, 3D-printing requires a gel-like monomer formulation ($\alpha_0 \approx 0.3$) with specific viscoelastic and shear-thinning properties.[32] The polymerization front exhibits a second characteristic length (L_α) dependent on the gradient in degree of conversion.[41] Similar to L_θ described in section 2.2.3 and Figure 6D, L_α refers to the spatial length of the front between positions at a maximum and minimum α values.

Several techniques measure the overall monomer conversion. In a typical differential scanning calorimetry (DSC) experiment, changes in heat flow or heat capacity are measured as a function of time or temperature compared to a reference standard.[37] For a given sample, two identical heating ramps are applied, the first of which measures the heat required to complete polymerization. The second scan provides a reference for the fully polymerized sample. The conversion, therefore, is measured by the difference in exotherm area between the two scans.[52,73,79−90] DSC is the favored technique, since several temperature rates are necessary to construct a reliable kinetic model that accounts for changes in α and frontal temperature: $d\alpha/dt = f(\alpha, T)$.

Thermogravimetric analysis (TGA) elucidates mass loss of a sample as a function of time or temperature. This technique has been employed as an indirect method to calculate conversion. Changes in mass correlate to volatilization of monomers or thermal decomposition products, and depends on the selected atmosphere (i.e., inert or oxidizing). Additionally, TGA provides useful information on small molecule release. Under appropriate conditions, the amount of residual monomer contained within the polymer network is quantifiable by the associated mass loss.[84,91−93] This technique is better suited toward quantifying the products derived from thermal degradation of the material. Furthermore, TGA coupled with Fourier-transformed infrared spectroscopy (TG-FTIR analysis) or mass-spectrometry (TG-MS analysis) provides detailed chemical information on gaseous species evolved during pyrolysis.

A third, albeit crude, technique to measure conversion involves the physical extraction of monomer contained in a thermoset polymer. This relies on a marked difference in solubilities between the two species; soluble monomers

https://doi.org/10.1021/acs.chemrev.2c00686
Chem. Rev. 2023, 123, 3237−3298

embedded in insoluble polymers are extracted with repeated solvent treatment (e.g., Soxhlet extraction). The mass difference between the untreated polymer and the washed polymer (after removing volatile components under reduced pressure) provides very rough indirect information about the monomer(s) conversion, much like other forms of gravimetry.[33,61,86] Moreover, this technique is limited to thermoset networks. For thermoplastics, both residual monomer and low MW polymeric species may solubilize, thus artificially skewing the apparent conversion. Instead, *in situ* spectroscopic methods (e.g., NMR spectroscopy or size-exclusion chromatography) enable time-resolved quantification of monomer conversion for soluble polymers.

2.3. Structural and Mechanical Properties of Frontally Derived Polymers

The physical and mechanical properties of frontally derived polymeric materials must be similar to (if not superior than) those derived from traditional methods for broad applicability of FP. Before discussing the various effects that determine the features of the frontally derived polymers, a brief discussion of the various mechanical metrics as compared to bulk polymerization derived materials is warranted.[37,94]

The most important mechanical and thermochemical features include elasticity (i.e., Young's (E) and Shear (G) Moduli), viscoelasticity (i.e., Storage (E') and Loss (E'') Moduli), tensile strength, hardness, transition temperatures (*e.g.*, T_g), average molecular weight (M_n), dispersity ($Đ$), and swellability (as measured by the swelling ratio, SR%). Most polymers, such as polyacrylates, display E values in the range of 0.1 to 10 GPa.[94] The variance in this range, however, reflects differences in composition as well as microstructural features (e.g., crystallinity, porosity) derived from the polymerization process itself (i.e., stirred BP, SP, FP). Additionally, mechanical properties (*e.g.*, E) are temperature dependent, as described in an idealized scan from dynamic mechanical analysis (DMA; Figure 7).

The existence of multiple transition temperatures reflects different responses of a material under heating. In an idealized amorphous thermoplastic (i.e., low to medium M_n), several low-temperature transitions related to local bending/stretching and side chain motions occur. The most commonly compared variable, the glass-transition temperature (T_g), indicates the onset of long-range main chain movement. As the temperature exceeds the T_g, long-range segmental motion within the polymer chains occurs alongside a loss in elastic response (*i.e.*, E') to afford a rubbery material. For thermoplastics below a critical chain-entanglement, M_n, a melting temperature exists whereby interchain slippage results in free fluid-flow. In contrast, cross-linked amorphous thermosets (or exceedingly high M_n polymers) cannot undergo global chain-slippage and do not possess T_m values. Typically, such thermosets degrade prior to achieving free-flow.

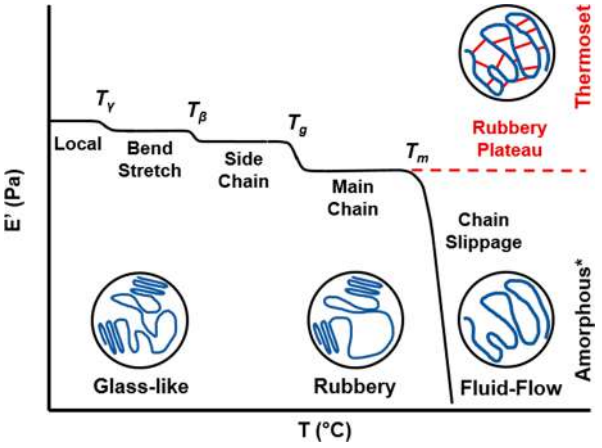

Figure 7. Idealized DMA schematic of the microstructure and mechanical properties of an amorphous polymer (black, solid line) and a cross-linked thermoset (red, dashed line). The type of internal motion experienced in a material relates with its temperature, as reflected in the transition-temperatures. *Assuming a low to medium M_n.

A possible difference between polymers derived from FP and SP may manifest as a result of differences in the T_g. In general, FP affords polymers with slightly higher T_g values than their classical counterparts (mostly by about 5−10 °C), as is observed in several examples.[76,82,89,95] While there might be various causes for such differences, it is likely that FP provides higher conversion and degree of cross-linking than analogous SP conditions. In turn, this reduces the quantity of residual monomers within the network that can act as plasticizers.

For many potential FP applications, such as aircraft component fabrication, additional weight or volume constraints require high-performing load bearing materials. A two-dimensional material selection chart (also known as an Ashby chart) correlates a desired mechanical parameter (*e.g.*, E) as a function of a constraint (e.g., density ρ).[96,97] In this regard, composites are beneficial as they display desirable mechanical properties from each component without the weight associated from metallic or ceramic analogues. With frontal curing, more energy efficient manufacturing procedures are possible compared to batch derived (e.g., autoclave cured) congeners.

3. GOVERNING PHYSICS: HEAT TRANSPORT AND INSTABILITIES

Heat transport and the associated mechanisms are critical to successful FP. Given the complex physics that govern heat transport, a short discussion of the definitions and terminology associated with the various modes of heat transport is warranted. Additionally, it is worth distinguishing the related concepts of heat and temperature; the former describes the flow (or change) of internal energy (measured in J) within a system. Temperature, on the other hand, provides a measurement of the average kinetic energy associated with the vibration of molecules comprised in the system (measured either in °C or K in SI units). Due to entropic considerations, heat redistributes itself to average out the thermal energies of two objects (often called bodies). Heat flows away from a hot body (source) into another cold body (sink) until thermal equilibrium is achieved.

Four mechanisms exist in heat transport: conduction, convection, advection, and radiation. Conduction occurs as the result of direct contact between two bodies; the movement and vibration of atoms and molecules transfers kinetic energy in a manner similar to that observed in billiard balls (i.e., collisions). Conduction is the largest mode of heat transport in solids, but also occurs in liquid and gas phases.

Heat transport via bulk fluid flow is classified as convection, which couples mass and energy diffusion within a fluid. Typically, an external force (e.g., gravity) drives a density-driven fluid motion; more dense materials sink whereas less dense ones float. Additionally, hotter objects are typically less

https://doi.org/10.1021/acs.chemrev.2c00686
Chem. Rev. 2023, 123, 3237−3298

dense than cold ones. The mass diffusion of hot and cold bodies in a system provides direct contact for the associated molecules to transfer kinetic energy in a manner similar to that described in conduction. Indeed, convection may be viewed as a subset of conduction where fluid motion also occurs. Advection is similar to, but not the same as, convection. In advection, heat and mass are transported in a nondiffusive process; a flow of fluid moves a *different* material through space (i.e., nonhomogenous systems, emulsions, etc.). In the process of mass transport, thermal exchange between the material and the flowing fluid occurs. The movement of silt in a river provides a good example of an advective process.

The final mechanism for heat transport involves photon-based energy changes. In such radiative processes, high energy molecules undergo photorelaxation; the internal energy of the molecule is reduced upon the expulsion of a photon with energy of $h\nu$, where h is Planck's constant and ν is the photon's frequency (in cm^{-1}). Radiative cooling is unique from conduction, convection, and advection as cooling can occur in a vacuum; direct molecular contact between the source and sink is not required for photon expulsion. Radiative cooling primarily occurs in extremely hot systems, such as stars or other black bodies, with temperatures greater than 1000 K. Radiative cooling does occur to some degree at lower temperatures. Glowing hot metals or the human body, for example, undergo radiative processes, and are observable with an IR thermographic camera (see section 2.1).

Given the definitional insights above, the total heat flow within a system is described by the heat equation, as derived below.

3.1. Heat Equation in Frontal Polymerization

Successful FP requires a delicate balance of reaction rates, exothermicity, and efficient heat transport into unpolymerized media while minimizing losses to the surroundings (Figure 8). To provide an analytical insight, these physical phenomena are modeled by a series of coupled differential equations, and detailed derivations exist in several key references.[41,57,66−69,98−101] For the purposes of this review, we will briefly describe the heat equation and its implications for FP.

Let the variable Q be defined as the total heat energy per volume in a material ($J\ m^{-3}$). The evolution of this energy with time ($\partial Q/\partial t$ in $W\ m^{-3}$) is proportional to the temperature time-derivative[35,41,57]

$$\frac{\partial Q}{\partial t} = \rho C_p \frac{\partial T}{\partial t} \tag{1}$$

where C_p is the specific heat capacity of the material ($J\ kg^{-1}\ K^{-1}$) and ρ is the corresponding density ($kg\ m^{-3}$). The power density associated with heat transport is defined by $\partial Q/\partial t$ and depends on both on time (t) and position (x in the 1-D case). Conservation of energy stipulates that the power density must equal any spatial change in the heat flux (Φ) that is going into or out of a control volume (see the circle located at a given x-position in Figure 8). This is also stated mathematically in eq 2:

$$\frac{\partial Q}{\partial t} = \sum \frac{\partial \Phi}{\partial x} \tag{2}$$

In the context of a typical FP, three main terms exist in this sum: (1) heat generated by polymerization, (2) heat transported via thermal diffusion through the monomer and polymer phases, and (3) heat lost to the surroundings

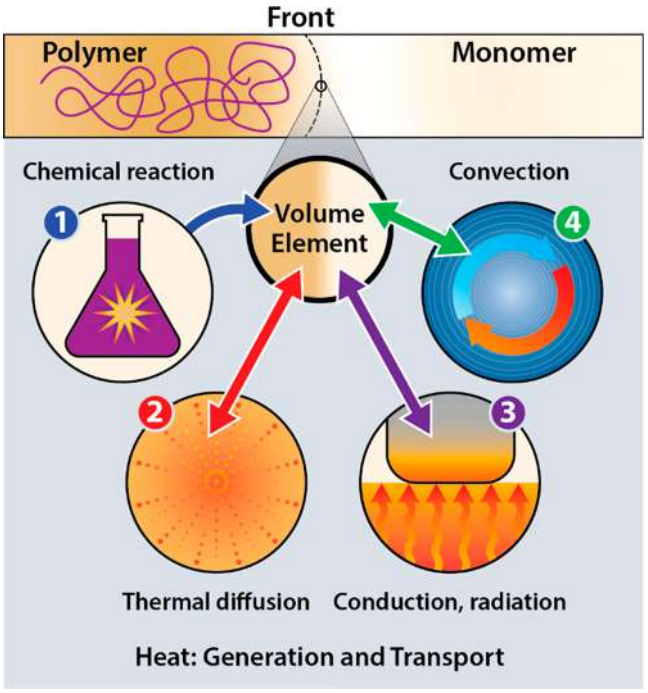

Figure 8. Illustration of heat conservation for a control volume across the front in a FP reaction. The power density, $\frac{\partial Q}{\partial t}$, evolves with time due to 4 main physical mechanisms: chemical reaction (**1**), thermal diffusion (**2**), conductive/radiative heat-loss to the surroundings (**3**), and fluid-motion (convection and advection, **4**).

primarily via convection. To a lesser degree, advection (fluid-flow) and radiative cooling contribute to heat transport. Heat transported in a nonhomogeneous fashion results in the generation of a variety of thermal instabilities and is detailed further in section 3.2.

3.1.1. Power Density Generated by the Chemical Polymerization Reaction. Since polymerization events provide heat, the enthalpy and rate of polymerization must be considered. The heats of polymerization for most common monomers are known (ΔH_p or H_r, $J\ g^{-1}$) and are discussed in detail in section 4. As a side note, these two terms are used interchangeably; chemists favor the former, whereas the latter is commonplace among physicists and engineers. The rate of polymerization exhibits a modified Eyring- or Arrhenius-like behavior.[41,57] One key difference, however, exists since α may exert autoacceleration behavior over time via the gel effect (for free-radical polymerization).[40] Multiple reaction models exist to capture such effects, as described by Kessler and White.[102] The rate component, therefore, is described by the change in degree of polymerization with time as is illustrated in eq 3 with an nth-order reaction model[41]

$$\frac{\partial \alpha}{\partial t} = A e^{\left(-\frac{E_a}{RT}\right)}(1-\alpha)^n(1 + k_{acat}\alpha) \tag{3}$$

where A is the Arrhenius pre-exponential factor (s^{-1}), E_a is the activation energy for the reaction ($J\ mol^{-1}$), R is the universal gas constant ($J\ mol^{-1}\ K^{-1}$), k_{acat} is a unitless autoacceleration coefficient, and n is a constant associated with the reaction motif. Fits of DSC experimental curves to an appropriate model provide approximate values to these parameters. Taking the material's density and enthalpy of polymerization, the power density of the polymerization is described in eq 4.[41,57]

https://doi.org/10.1021/acs.chemrev.2c00686
Chem. Rev. 2023, 123, 3237−3298

$$\frac{\partial \Phi_{poly}}{\partial x} = \rho H_r \frac{\partial \alpha}{\partial t} \quad (4)$$

3.1.2. Power Density Transported by Conductive Thermal Diffusion. The vector form of the change in heat flux through a surface of a given material ($\overrightarrow{\Phi_q}$, W m^{-2}) is dictated by Fourier's law in eq 5,

$$\overrightarrow{\Phi_q} = -\kappa \nabla T \quad (5)$$

where κ is the thermal conductivity of the material (W m^{-1} K^{-1}), and ∇T is the spatial gradient of the temperature field (K m^{-1}). As a side note, several intriguing possibilities exist to modulate the effective κ of a homogenized material, such as the inclusion of conductive wires within the reaction apparatus.[69]

When considering unidirectional diffusion through uniform and homogeneous materials, the following scalar approximation exists:

$$\Phi_q = -\kappa \frac{\partial T}{\partial x} \quad (6)$$

Assuming a uniform thermal conductivity, the spatial variation of the heat-flow (W m^{-3}), therefore, is described by eq 7:

$$\frac{\partial \Phi_q}{\partial x} = -\kappa \frac{\partial^2 T}{\partial x^2} \quad (7)$$

3.1.3. Power Density Lost to the Surroundings. Most numerical studies consider adiabatic conditions, and ignore heat loss. As mentioned previously, heat loss strongly affects front propagation, including in the form of premature front quenching due to cooling and thermal instabilities. Heat loss may occur via four different mechanisms: radiative, conductive, convective, and advective. In radiative cooling in the absence of vacuum, a gray-body emits photons to reduce its internal energy, which are absorbed by the surroundings. The associated change in flux is given in eq 8

$$\frac{\partial \Phi_{loss,radiative}}{\partial x} = \mu(T^4 - T_s^4) \quad (8)$$

where μ (W m^{-3} K^{-4}) is a material constant, T is the surface temperature (K) of the radiating body, and T_s is the temperature of the surroundings (K). Alternatively, radiative and conductive heat loss can be modeled as boundary conditions rather than explicitly solved in the partial differential equations.

Conductive, convective, and advective cooling require contact with another medium. Recent FP modeling efforts have studied the effects of added filler (glass, steel, carbon fiber)[69,103,104] or reaction apparatus material on conductive heat loss,[105] as well as convective heat transport to the surrounding air.[106] Fourier's law accounts for conductive transport by creating numerical subdomains that correspond to the surroundings. Convective cooling can be modeled by Newton's law of cooling as given in eq 9

$$\frac{\partial \Phi_{loss,conv}}{\partial x} = h\frac{P}{S}(T - T_s) \quad (9)$$

where h is the heat transfer coefficient (W m^{-2} K^{-1}), and P (m) and S (m^2) are the perimeter and surface area of the domain cross-section, respectively.[106−108]

Combining eqs 7−9, a final 1-D expression of heat conservation describes the evolution of temperature with time inside a control volume:

$$\rho C_p \frac{\partial T}{\partial t} = \frac{\partial Q}{\partial t} = \frac{\partial \Phi_{poly}}{\partial x} - \frac{\partial \Phi_q}{\partial x} - \frac{\partial \Phi_{loss}}{\partial x} \quad (10)$$

$$\rho C_p \frac{\partial T}{\partial t} = \rho H_r \frac{\partial \alpha}{\partial t} + \kappa \frac{\partial^2 T}{\partial x^2} - \mu(T^4 - T_s^4) - h\frac{P}{S}(T - T_s) \quad (11)$$

As discussed in section 2.2.3, ideal FP systems only exhibit large temperature changes in close proximity to the reaction zone (i.e., small L_θ and L_α on the scale of 0.1 to 1 mm). The final governing eq 11 illustrates several key physical properties that modulate effective front propagation. Fast, highly enthalpic polymerization processes, as well as efficient heat transport within the monomer solution, are required for front propagation. The choice of monomer, catalyst, or initiator impacts the reaction rate and enthalpy. The thermal conductivity and heat capacity of the reaction media dictate the efficacy of heat transfer through the unpolymerized medium. Heat loss is mitigated primarily by minimizing the exposed surface area of the experimental apparatus (e.g., maximizing the volume-to-surface area ratio), though monomers with high heat capacities will functionally reduce the heat loss as well. Several recent studies exploited the balance between heat generation and transport to produce varied morphologies within a single FP event, in a fashion akin to pattern printing.[51,109]

3.2. Instabilities in Frontal Polymerization

Ideal FP exhibits uniform, steady propagation, particularly for structural applications that require homogeneous physical or mechanical properties throughout the material. In contrast, convective or thermal instabilities may contribute to undesirable, premature front termination; specifically, the sharp thermal and cure gradients proximal to the front, as well as external perturbations (gravity, boundary conditions, fluid-flow), may induce front quenching phenomena. Not all systems that exhibit convective or thermal instabilities, however, terminate precipitately. Complete polymerization can still occur with nonplanar fronts. Early work from the USSR described theoretical models and some supporting experimental evidence related to front propagation in polymerization and other combustion-like reactions;[16,18,20,22−24,26,27,110−112] moreover, these reports examined instabilities arising from nonequilibrium propagation modes (e.g., thermal spin-modes).[22,19,21,25]

Buoyancy-based convective instabilities in liquid-to-liquid systems are particularly problematic for FP.[30,66,98,101,113−116] Rayleigh−Taylor fingering (Figure 9A) occurs in vertical-descending fronts where the more dense polymer phase exists atop the less dense monomer. Double-diffusive convection results from differences in diffusion rate of two separate phenomena (i.e., heat and mass) across an otherwise stable system. In FP, heat transfer occurs at a faster rate than mass transport, and leads to the generation of thermal "fingers".[113] These densely packed fingers exhibit smaller diameters than those derived by Rayleigh−Taylor instabilities (Figure 9B). While double-diffusive convection is exceedingly rare in FP, such effects may influence front propagation with an applied acceleration (e.g., from gravitation or centrifugal force).[117] As

https://doi.org/10.1021/acs.chemrev.2c00686
Chem. Rev. 2023, 123, 3237−3298

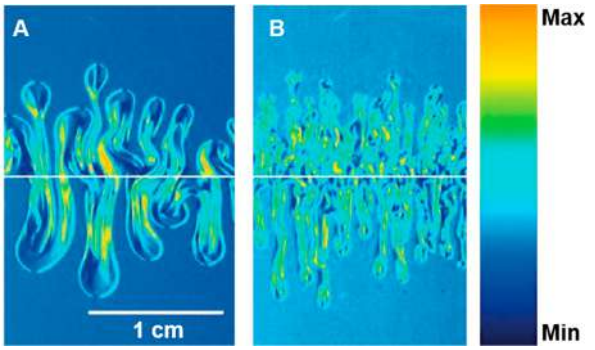

Figure 9. Changes in refractive index arising from Rayleigh−Taylor (A) and double diffusive convection (B). The centered horizontal line represents the initial contact position between the two fluids. Reprinted and adapted with permission from *Phys. Fluids* **2013**, *25*, 014103.[113] Copyright 2013, AIP Publishing.

depicted in Figure 4, thermographic imaging highlights heterogeneous temperature phenomena in FP that arise from these instabilities.[29,53]

Propagating polymerization fronts share features akin to those observed in flame propagation. Indeed, similar mathematical equations are used to describe these systems.[101,110] A dimensionless parameter, known as the Zeldovich number (β), describes the bifurcation behavior of flame propagation in gas-phase combustion reactions, and is given in eq 12,

$$\beta = \frac{E_a}{RT_b^2}(T_b - T_u) \tag{12}$$

where E_a is the reaction activation energy (J mol^{-1}), R is the ideal gas constant (J mol^{-1} K^{-1}), and T_b and T_u are the temperatures (K) of the burnt gas and unreacted material, respectively. Typical combustion reactions exhibit β in the range of 8 to 20,[118] though this value depends on the identity of the reactants.

The onset conditions for nonuniform thermal front propagation is determined by the relation of the calculated β to a critical value (β_c), as determined by linear stability analysis (LSA).[67,118] This analysis provides insights into thermal instabilities that result from thermal transport. In the FP of methacrylic acid, for example, uniform reaction fronts exist when $\beta < \beta_c = 8.4$.[119] In contrast, periodic and pulsating hot spots arise when $\beta > \beta_c$, which manifest as helical or corkscrew-like propagation events. Unfortunately, the specific value of β_c is not constant for all substrates, and a rather laborious LSA is required for each monomer to calculate the associated β_c. Solovyoy et al.[57] demonstrated with simulations that the reactor dimensions affect the propagation mode. The specific nature of these thermal spin-modes (i.e., number of propagation heads) depend on the size and composition of the reactor,[43] in addition to the monomer type and concentration (Figure 10).[16,22,19,21,25,119,120]

The flow of liquid monomer ahead of the propagation front creates or enhances existing instabilities; some frontal systems undergo thermal expansion during polymerization that exert a force on the monomer phase, resulting in a thermo-chemical front coupled with mass-flow.[121,122] In such examples, the sharp temperature gradient, along with a potential surface-tension mismatch between the polymer and monomer phases, induces Marangoni flow.[123,124] This advective transport is

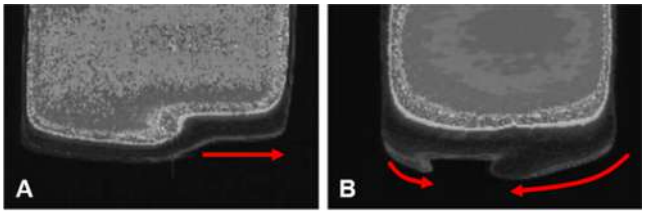

Figure 10. Experimental observations of a single- (A) and double-headed (B) spin modes in **HDDA** (1,6-hexanediol diacrylate; A) and **TMPTA** (trimethylolpropane triacrylate; B) FP. The existence of these spin modes depends on the passive diluent concentration of diethyl phthalate in the monomer solution. Reprinted and adapted with permission from *Chaos* **1999**, *9*, 315−322.[119] Copyright 1999, AIP Publishing.

modeled by $\rho C_p \vec{u}.\nabla T$, where $\vec{u}$ is the fluid velocity (m s^{-1}); a recent report highlighted that spatial patterning in reaction-diffusion processes is highly impacted by the introduction of an intentional fluid-flow.[125]

Most recently, Tiani et al.[108] and Gao et al.[126] numerically studied the effect of reaction thickness on FP. In the absence of thermal cooling at the boundary (i.e., inside an insulator), a uniform planar front exists. In contrast, open-mold systems with nonuniform heat loss from one (or more) boundaries exhibit convection driven instabilities that dramatically vary with the layer thickness. Unsurprisingly, fronts generated from thin layers are most sensitive to heat loss (Figure 11). As the

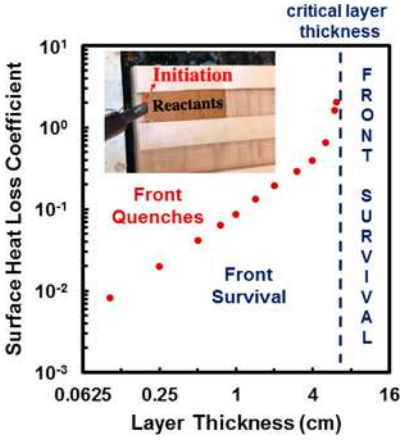

Figure 11. Plot of the surface heat loss coefficient (unitless) as a function of layer thickness for FP systems. A critical layer thickness exists whereby the energy imparted from the reaction outcompetes heat-loss regardless of the efficiency of heat transfer to the surroundings. Figure reprinted and adapted with permission from *J. Phys. Chem. B.* **2022**, *126*, 3607−3618.[108] Copyright 2022, American Chemical Society.

layer thickness increases, fronts become more resilient to heat transfer to the surroundings. Below a critical layer thickness, the efficiency of heat-loss dictates whether a front quenches or propagates. For thicker layers, the reaction outcompetes thermal cooling. Similar to the layer thickness study by Tiani et al.,[108] instabilities in thin-film geometries with thermally insulating substrates were recently reported by Gao et al.[126]

The existence of convective and thermal instabilities has significant repercussions for FP chemistries and FP-derived materials.[114] In certain structural applications that require homogeneous features, for example, these nonuniform

https://doi.org/10.1021/acs.chemrev.2c00686
Chem. Rev. 2023, 123, 3237−3298

propagation motifs induce hot-spots that may negatively affect the properties of the final polymer. As discussed in section 3.1, high surface area contact increases the heat dissipation rates. Fingering disrupts the frontal interface to increase the total thermal contact area in the hot front, thereby increasing the heat flow away from the reaction zone. This heat is transferred to fresh, but cold monomer at varying depths. This broadens the reaction front and depresses the corresponding frontal velocity. Additionally, discontinuities may exist at the finger interfaces, which behave as fault lines within the polymer. Hence, such polymers exhibit substantially reduced strengths compared to those derived from stable fronts. In extreme cases, fingering prohibits propagation and leaves sizable holes in the product.[114]

Several methods were investigated to dampen or suppress the effects of convective instabilities in FP. Nagy and Pojman[114] described an experimental apparatus that spun the reaction vessel at rates between 1300 and 3200 rpm. The spinning motion inhibited fingering but also generated conical front shapes due to the applied centrifugal force. It is unclear what effects, if any, a conical reaction surface has on the polymer's mechanical properties. Other systems have successfully employed fillers to increase the density and viscosity of the monomer solution, thereby suppressing buoyancy-induced instabilities.[127] Pojman et al.[128] dispersed monomer in a salt water solution to inhibit convective fingering.

Monomer design may reduce density driven instabilities; linear monomers display reduced densities compared to their polymeric products, which manifests as a shrinkage in volume.[129−131] The change in density during FP of linear monomers, as well as the associated volume shrinkage, introduce advective fluid flow and Rayleigh−Taylor instabilities. Indeed, early work from Mariani and co-workers[132] described such observations as the "rain-storm" effect. Additionally, the shrinkage stress depresses the mechanical strengths of the resultant polymers. Ring-opening polymerization reactions, on the other hand, are resistant to such density changes; cyclic monomers display densities that better match those of the final polymer. An extensive body of research focused on minimizing shrinkage exists, such as the development of so-called "expanding monomers" (Figure 12).[129−131] The design of new frontal monomers or additives, therefore, may benefit from such insights. Indeed, FP with expanding fillers were reported by Scognamillo et al. in 2014;[133] frontal formulations included microspheres (Expancel #80 from Expancel, Inc.) that expand upon heating, and the resultant frontally derived polymers underwent significant volume increases compared to the initial resin volume (≈50−250%).

In parallel, recent work from the Lloyd et al.[51] exploited thermal instabilities associated with FP to produce patterned materials with unique morphologies and heterogeneous mechanical properties in a single manufacturing step. While discussion of this work in finer detail is found in section 5, there are interesting parallels to combustion-type syntheses. A review by Varma and Lebrat[17] describes the generation of inorganic materials by combustion reactions. As with FP, such reactions involve a self-sustaining and propagating reaction front. Combustion reactions also exhibit thermal instabilities (namely, spin-modes) under certain conditions. Two reaction models describe stable (i.e., equilibrium mechanism) and unstable (i.e., nonequilibrium mechanism) combustion propagation (Figure 13). In the former case, a rise in the heat

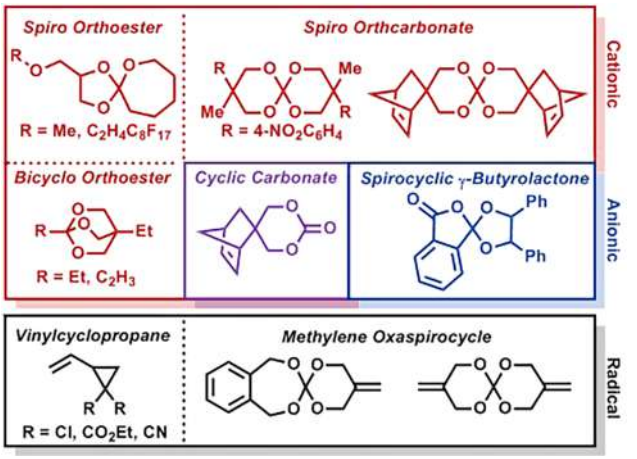

Figure 12. Example structure architectures for expanding monomers. The polymers derived from these cyclic monomers fill a larger volume (and lower density) than the initial resin conditions. As a general design principle, a fast polymerization step occurs prior to a slow secondary ring-opening isomerization step. These monomers are compatible with cationic-, anionic-, and/or radical-type polymerizations.[131]

generation rate occurs concurrently with a sharp temperature spike. The increase in the degree of conversion, α, lags behind, with an onset that approximately corresponds to the maximum heat generation rate. The equilibrium mechanism exhibits four discrete reaction regimes: unreacted reagents ahead of the front, preheating as the front approaches, synthesis, and final product formation. The nonequilibrium case, in contrast, displays a complex relationship between the heat generation rate, reaction temperature gradient, and α. A slow (and constant) increase to the reaction temperature occurs and is closely followed by substrate consumption, as reflected in changes in α. Moreover, α does not directly reflect the product generation rate; instead, intermediates formed during high-temperature reactions undergo subsequent chemical steps (i.e., "structuring") to generate the final product. Thermal spin modes likely occur through nonequilibrium front propagation.

These models also suggest that the initiation conditions dictate the fate of propagation and the existence of potential intermediate phases. The energy added to the system during initiation, for example, may bias propagation toward a specific mechanism. High energy (or large thermal flux) initiation typically favors an equilibrium mechanism. In contrast, low temperature initiation (or low thermal flux) may induce a nonequilibrium-type propagation mode. This latter mode likely leads to the formation of gel-state intermediate structures. One may think of the subsequent cross-linking events as material "structuring". Better understanding of the underlying physics of thermal instabilities enables prediction and clever exploitation to generate patterned materials.[51]

3.3. Geometric Influences on Front Propagation

The front direction and the orientation of the reaction apparatus impact propagation. For vertically aligned systems, ignition occurs either in a descending or ascending mode. Descending fronts traverse coincident with gravitational forces; as a consequence, convective instabilities rapidly occur if the resultant polymer exists in a liquid state. In this case, the dense polymer sinks due to Rayleigh−Taylor effects.[134] Solid polymer products, however, are physically "locked" into place and buoyant instabilities do not present a major issue. In

https://doi.org/10.1021/acs.chemrev.2c00686
Chem. Rev. 2023, 123, 3237−3298

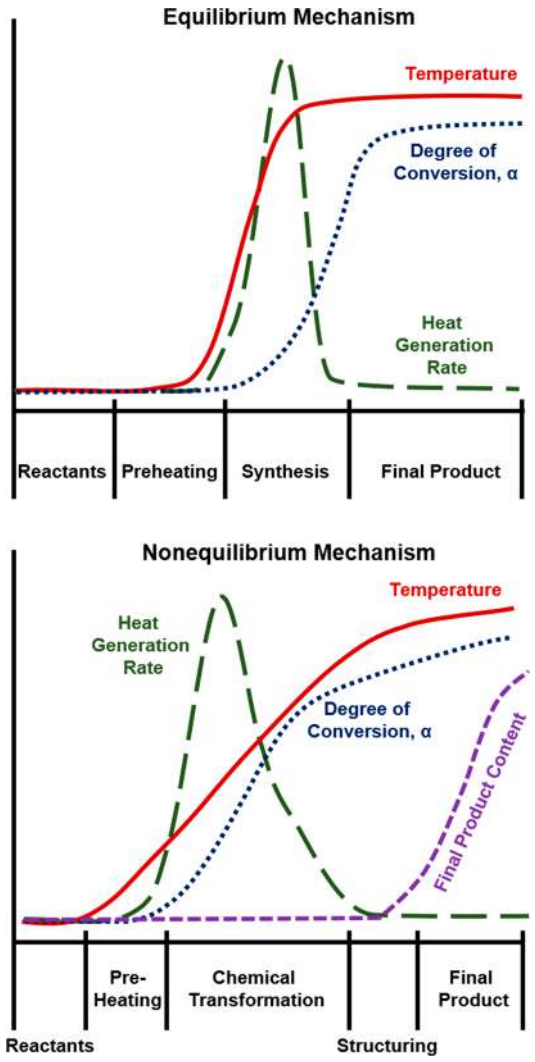

Figure 13. Generalized reaction mechanisms for adiabatic structures generated from combustion waves. Top: Equilibrium mechanism, whereby product formation occurs concurrently with substrate consumption. Bottom: Nonequilibrium mechanism, where the final product forms *after* the combustion event. Species generated during combustion decompose to generate the final products. Figure adapted with permission from *Chem. Eng. Sci.* **1992**, *47*, 2179−2194.[17] Copyright 1992, Elsevier Ltd.

contrast, ascending fronts exhibit extreme sensitivity to buoyancy-driven convection. As the reaction proceeds, hot monomer rises and is replaced from above by colder monomer.[116]

Nonvertically aligned systems exhibit angle-dependent velocities, as shown in a study by Bazile et al.[134] Specifically, trigonometric constraints influenced convection as well as the propagation. In the ideal case (Figure 14A), the front is coplanar with the ground because of buoyancy-driven convection and traverses along the displacement angle, θ. In reality, however, convection cannot fully flatten the front and the front is displaced by an angle of ζ (Figure 14B). Hence the total displacement angle is defined by φ, which is defined as $\theta - \zeta$. In either case, however, the observed axial velocity (ν_φ) increases with tilt angle by the trigonometric relationship, $\nu_\varphi/\nu_0 = \cos(\varphi)^{-1}$ (Figure 14C).[134]

Not all frontal systems travel as a 2D cross-section, where perpetuation occurs in a fashion akin to the theoretical plate

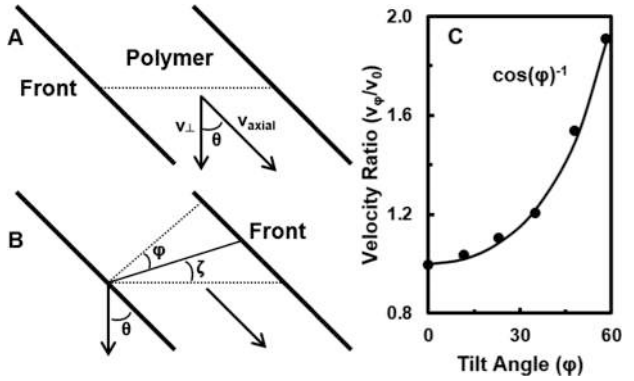

Figure 14. Geometric influences on front propagation where the reaction vessel is offset by an angle, θ. A: Idealized front geometry arises in the absence of thermal instabilities. Front propagation occurs with a velocity ν_{axial}. B: Actual front geometry. Convection induces a deviation in the front geometry such that the front is no longer coplanar with the ground (offset by ζ) and deviates via the corrected angle φ. C: Velocity ratio (ν_φ/ν_0) as a function of angle φ. Figure adapted with permission from *J. Polym. Sci., Part A: Polym. Chem.* **2002**, *40*, 3504−3508.[134] Copyright 2002, Wiley Periodicals, Inc.

model invoked in chromatography. Binici and co-workers[135] described a spherically propagating frontal system (Figure 15).

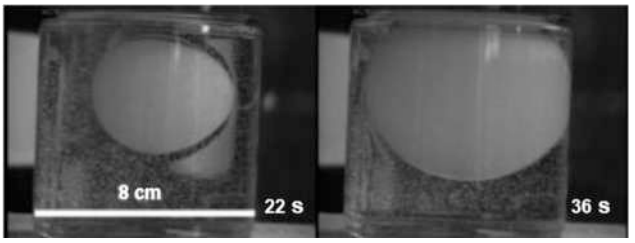

Figure 15. Spherical front propagation occurs via photoinitiated radical polymerization from a reaction mixture containing 1,6-hexanediol diacrylate (**HDDA**, 35%), DMSO (53%), diethyl phthalate (12%), and fumed silica (6.7%). The thermal radical source was ammonium persulfate (APS). The photoinitiator, Irgacure 184, was injected into the center of the reaction mixture and ignited by UV-light. Figure reprinted and adapted with permission from *J. Polym. Sci., Part A: Polym. Chem.* **2006**, *44*, 1387−1395.[135] Copyright 2006, Wiley Periodicals, Inc.

To ensure spherical propagation, fumed silica as an added thickening agent eliminated convection and allowed for direct injection of a photoinitiator without significant mixing. Ignition occurred at the center of the reaction vessel after triggering by a UV-light source (3 mW, 365 nm). Such viscosity dependencies on propagation motif were also observed by Bidali et al.;[132] high viscosity reaction media favor spherical propagation. The chemical details of similar photoinitiated frontal radical polymerizations are described in further detail in section 4.3. The ability to control propagation geometry and final polymer shape may find applications in 3D printing or composite patterning.

4. CHEMISTRIES OF EXISTING FRONTAL POLYMERIZATION SYSTEMS

4.1. Frontal Ring-Opening Metathesis Polymerization

4.1.1. Mechanism and Background. Ring Opening Metathesis Polymerization (ROMP) has emerged as a versatile

https://doi.org/10.1021/acs.chemrev.2c00686
Chem. Rev. 2023, 123, 3237−3298

reaction motif over the last two decades,[136−138] particularly in the synthesis of robust materials. Olefin metathesis exploits reversible C−C bond scissions to exchange alkene fragments from two different substrates under thermodynamically controlled conditions; as a consequence, metathesis-like transformations often provide a mixture of products (*e.g.*, *E*- and *Z*-isomers, oligomers, polymers). The relative stabilities of each species dictate the observed product distribution (i.e., selectivity) after a sufficiently long reaction period. Transition-metal ROMP catalysts comprised of Ru,[136,139,140] Mo,[141] or W[137,141] exist, and the choice of metal center influences the reactivity and air-sensitivity of the catalyst.

Most practical applications employ Ru-alkylidene complexes owing to their enhanced stability in air. Indeed, commercial chemical vendors sell several generations of these so-called "Grubbs" catalysts (Chart 1).[140] These catalysts display a

Chart 1. Typical Commercially Available Grubbs-Type Ru Metathesis Catalysts

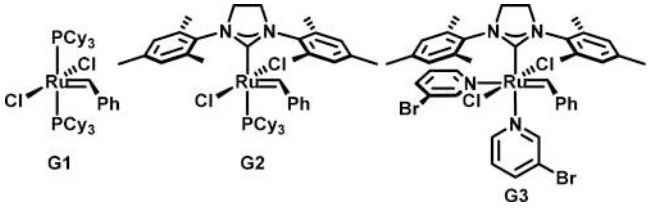

Schrock-type metal carbene (M = CHR) as a common structural motif. The first-generation of Grubbs catalysts (**G1**) possess phosphine auxiliary ligands, whereas generations two and three (**G2** and **G3**, respectively) contain *N*-heterocyclic carbenes (NHCs). In general, the reactivity of NHC-bearing catalysts surpasses that of phosphine-bound complexes. For nonfrontal systems, a volume of catalyst development research has investigated a wide variety of parameters in search of highly reactive and selective catalysts; for instance, NHC chelation affords highly *Z*-selective catalysts,[142−144] while addition of other X- or L-type ligands enables rapid initiation.[145,146] One such example, **G3**, bears highly labile pyridine auxiliary ligands and this feature has been effectively exploited in ROMP to generate polymers with exceedingly uniform dispersities.[139,140]

The generally accepted mechanism of ROMP with **G2** (Scheme 1), as elucidated at temperature far below those achieved in FROMP, involves an initial dissociative ligand exchange of a labile ligand (e.g., PCy_3) for olefin (e.g., dicyclopentadiene, **DCPD**) to generate the bottom-bound intermediate **A**.[138] A metal mediated [2 + 2] cycloaddition occurs to form a metallacyclobutane species (**B**). Retro [2 + 2] cycloaddition may reform **B** or proceed productively to generate a new olefin containing Ru alkylidene species (**C**). Subsequent Ru assisted ring opening interactions occur with fresh substrate to propagate the polymer chain in a living fashion (i.e., without self-termination) to generate **D**. A second, ring opening reaction may occur with side-chain olefin functionalities in **D** to result in a highly cross-linked polymer as depicted in **E**; cross-linking, however, occurs to a lesser extent than the initial propagation steps. These mechanistic insights, however, assume reaction temperatures < 100 °C. On the other hand, typical FROMP reactions proceed at temperatures exceeding 200 °C, albeit for very short time periods. These elevated temperatures may result in competitive catalyst decomposition reactions (i.e., nonliving

Scheme 1. Initiation, Propagation, and Crosslinking Mechanisms for the ROMP of Dicyclopentadiene Catalyzed by G2

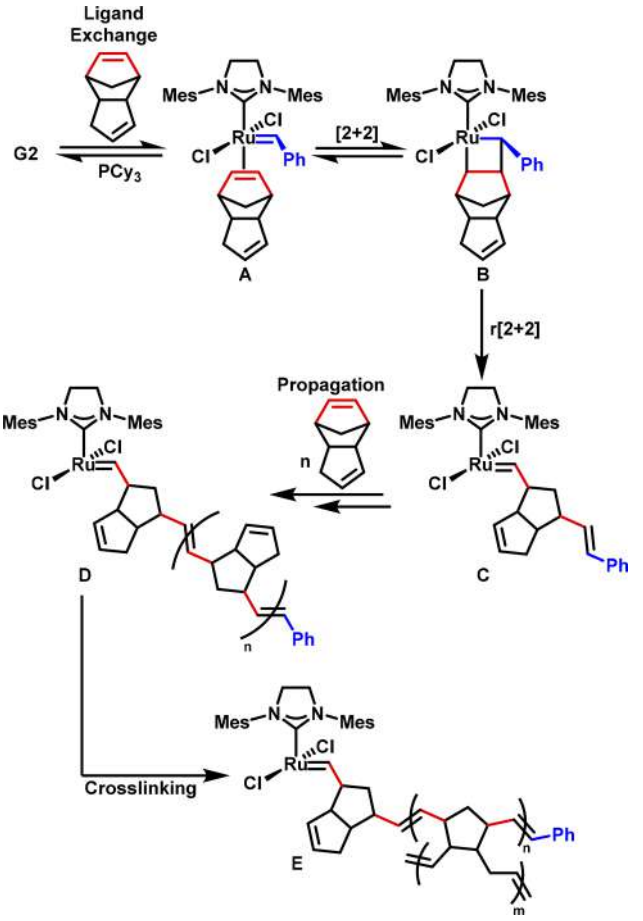

polymerization), though the details of such processes are not yet understood. Recent work from Alzate-Sanchez et al.[393] suggests that the metathetic activity of **G2** after FROMP is retained; the catalyst survives FROMP and can induce chain-extension when fresh monomer is introduced.

Reactant volatility also poses a significant challenge to FP; low-boiling monomers undergo an evaporative phase-change, which introduces void-spaces as the monomer gas escapes the resin. Monomer stability is an additional draw-back that stems from the temperatures achieved during FROMP; for example, **DCPD** undergoes retro-Diels−Alder chemistry at temperatures above ≈150 °C to provide cyclopentadiene in a process known as "cracking." The exceedingly low boiling point of cyclopentadiene (≈ 40 °C) exacerbates the inherent volatility of the monomer resin (for reference, *endo*-**DCPD** has a boiling point of 170 °C). Ideal FROMP monomers, therefore, must exhibit high decomposition onset temperatures and boiling points.

4.1.2. Unusual Catalyst Design Principles: Tempering FROMP Reactivity via Inhibition. Systems employing FROMP have heavily employed **DCPD** or norbornene derivatives as the monomer of choice (refs 32, 35, 41, 51, 52, 69, 72, 73, 76, 105, 126, 147−170). As stated previously, the heat released by polymerization (ΔH_p) dictates the feasibility toward frontal application; as a catalytic process, the total quantity of heat released in ROMP depends only on the monomer itself, assuming that the reaction reaches

https://doi.org/10.1021/acs.chemrev.2c00686
Chem. Rev. 2023, 123, 3237−3298

completion. In other words, ΔH_p describes the thermodynamics of the polymerization event. Indeed, ROMP is predicated on an enthalpic driving force afforded by the ring opening of highly strained cyclic alkenes. Unsurprisingly, substantial heat generation occurs in neat ROMP resins; for example, the heat released in the polymerization of *endo*-**DCPD** with **G2** is 353 J g^{-1}.[147]

While the thermodynamic favorability is essential for successful adaptation to FROMP, the rate of heat generation presents major challenges. The rate of catalysis (k_{obs}) directly influences *how fast* thermal energy is added to the system. Stable FROMP systems require that the catalytic rate at least matches the rate of heat-loss; systems with lower catalytic activities suffer from undesired stalling of the front, whereas highly active catalysts typically induce SP via autoacceleration, and therefore possess short active lifetimes. Highly reactive FROMP catalysts pose an additional limitation in their short storage lifetimes, which are a direct result of the room temperature kinetics. Rule and Moore[171] estimated the activation enthalpies ($\Delta H^{\ddagger}$) and entropies ($\Delta S^{\ddagger}$) for *exo*- and *endo*-**DCPD** ROMP catalyzed by **G1** (4 mM in toluene-d_8). The activation parameters for the ROMP of *exo*-DCPD were calculated to be $\Delta H^{\ddagger}$ = 82 kJ mol^{-1} and $\Delta S^{\ddagger}$ = 28 J mol^{-1} K^{-1}, whereas the *endo*-isomer exhibited a $\Delta H^{\ddagger}$ = 66 kJ mol^{-1} and $\Delta S^{\ddagger}$ = −52 J mol^{-1} K^{-1}.[171] From these activation parameters, the observed solution-state first-order rate constants at 20 °C for the *exo*- and *endo*-substrates were determined to be 3.7 × 10^{-1} and 1.9 × 10^{-3} s^{-1}, respectively.[171] The specific powers ($P \equiv \Delta H_p \times k_{obs}$) of *exo*- and *endo*-**DCPD** solutions at 20 °C are approximately 8000 and 460 W kg^{-1}, respectively. These parameters correspond to rapid reactivity under mild temperatures. Formulations comprised only of substrate and **G1**, therefore, display disappointingly short storage lifetimes, as reflected in the short half-lives (e.g., 34 s for *endo*-**DCPD**). Additionally, these parameters suggest that *exo*-**DCPD** is a more reactive substrate and, therefore, is less likely to provide easily controllable fronts in FROMP.[73]

Despite these challenges, several examples of FROMP systems exist with the aid of catalytic inhibitors to temper background reactivity at ambient temperatures. The approach runs counter to most catalyst design principles that favor faster, more reactive catalysts. Such inhibitors slow the rate of heat generation via a competitive binding mechanism (Scheme 2). Catalysis requires the existence of an open coordination site at the Ru center for olefin to bind prior to metallocycle formation, as described by K_{eq}. The presence of added ligand gives rise to off-cycle equilibria to generate inactive Ru-L adducts (K'_{eq} and K''_{eq}), which functionally reduces the concentration of active intermediates. The concentration of such off-cycle species depends on the relative binding strength of L (and PCy_3) compared to incoming olefin. Hence, a reduction in observed catalytic rate occurs, and by extension the rate of heat generation decreases, despite a constant k_{cat}. This mode of action necessitates that facile ligand dissociation occurs near the front temperature (i.e., T_{max}) but not at storage temperatures. Unfortunately, these systems are limited by the reversibility of inhibitory ligand coordination, as the ligand exchange equilibria (K_{eq}, K'_{eq}, and K''_{eq}) are temperature dependent. At ambient conditions, there exists a nonzero population of highly active species, which results a background reaction that brings about gelation in the case of **DCPD**.

Scheme 2. Competitive Inhibition in FROMP with Added Ligands

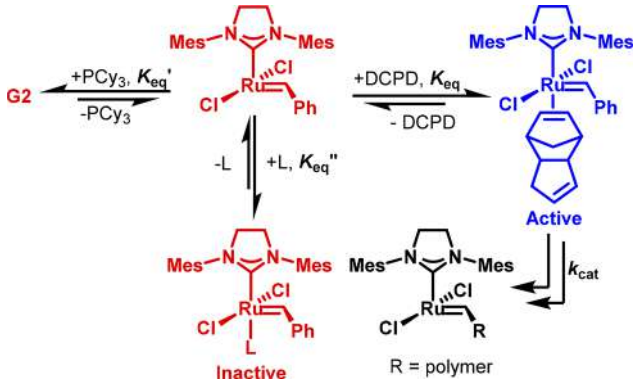

Several types of inhibiting ligands successfully control FROMP: triaryl phosphines,[72] trialkyl phosphites,[52] electron-rich pyridines,[73,148] and hindered olefins.[76] The first example, published by Pojman and co-workers,[72] achieved storage lifetimes of ≈20 min at 35 °C by the addition of PPh_3 to the reaction formulation (2.7 equiv relative to **G1**, with catalyst loading of ≈100 ppm). Inside a 15 mm inner diameter test tube, frontal behavior (ν_f = 0.6 cm min^{-1}; T_{max} = 162 °C) was achieved after ignition with a thermoelectric heater. Negligible prefrontal exotherms were detected, which indicated that background reactivity did not occur on the frontal time scale. The concentration of PPh_3 was varied and the results indicated that only a small inverse relationship existed between PPh_3 concentration on ν_f. In contrast to inhibitory ligand, decreases in **G1** loading resulted in concurrent reductions in both ν_f and T_{max}; stable fronts were not observed with catalyst loadings under 71 ppm or above 500 ppm. Interestingly, a linear correlation of T_{max} to catalyst loading existed.

Subsequent reports investigated other inhibitors for FROMP, and the frontal parameters for these studies are summarized in Table 1.[52,73,76,147,148] While the specific conditions employed across these reports vary (e.g., reactor diameter, cosolvent), several identifiable trends exist. FROMP catalyzed by **G2** provides hotter, faster fronts than those derived from **G1** systems, perhaps unsurprisingly given that **G2** is a better catalyst for bulk ROMP. For example, **G2** systems exhibit faster ν_f (by an order of magnitude in some cases) at lower loadings than the analogous resin mixtures with **G1** as the catalyst.

For all inhibitors tested, the storage lifetime has an inverse relationship to ν_f. These two parameters are tunable through the ancillary ligand loading; at higher concentrations, the background ROMP activity has been dampened to afford a more robust, storable formulation at the expense of slowing ν_f and reducing T_{max}. One must, therefore, balance the merits of frontal propagation against storage lifetime. Trialkyl phosphites provide the best storability, with lifetimes up to 30 h in some cases. By this metric, $P(O^nBu)_3$ performs the best, whereas dimethylamino pyridine (**DMAP**), limonene, and PPh_3 exhibit the highest propensity to undergo spontaneous polymerization. It seems that the π-acidity and sterics of the inhibitory ligand define the resistance of the system to undesired gelation.

4.1.3. Copolymerizations. Several examples of copolymerization under phosphite dampened FROMP exist (Scheme 3).[147,149,150,153,170] Functionalized mononorbornene and linked dinorbornene monomers underwent random copoly-

https://doi.org/10.1021/acs.chemrev.2c00686
Chem. Rev. 2023, 123, 3237−3298

Table 1. Typical Frontal Parameters for the FROMP of DCPD with Added Inhibitor Catalyzed by Grubbs-Type Complexes

inhibitor[a]	inhibitor loading range (ppm)[b]	catalyst loading (ppm)[c]	ν_f range (cm min^{-1})[b]	T_{max} range (°C)[b]	storage life (h)[b,d]
PPh_3[72]	330	122 (**G1**)	0.6	162	0.3 {35}
$P(OMe)_3$[52e]	100−800	100 (**G2**)	7−1	215−175	1−4 {23}
$P(OEt)_3$[52e]	100−800	100 (**G2**)	7−1	215−175	3−15 {23}
$P(O^nBu)_3$[52e]	100−800	100 (**G2**)	7−1	215−175	5−30 {23}
DMAP[148e]	170	170 (**G1**)	0.9	197	0.16 {30}
	60−500	60 (**G2**)	7.5−2.2	197−198	0.3−0.5 {30}
(*R*)-limonene[76]	10000−200000	80 (**G2**)	29−9	187−162	0.4−10 {22}

[a]References are given in brackets. Glass test tubes were employed as the reactor vessel with inner diameters of 1.3−1.5 cm. FROMP was initiated by exposure to a soldering iron. [b]Values given correspond to the lower and upper limit of inhibitor loading provided. [c]Catalyst is given in parentheses. [d]Storage temperature in °C given in curly brackets. [e]Catalyst was added to the monomer as a solution in 0.4 mL toluene.

Scheme 3. Copolymerization of Mono- or Di-Norbornene Derivatives with DCPD

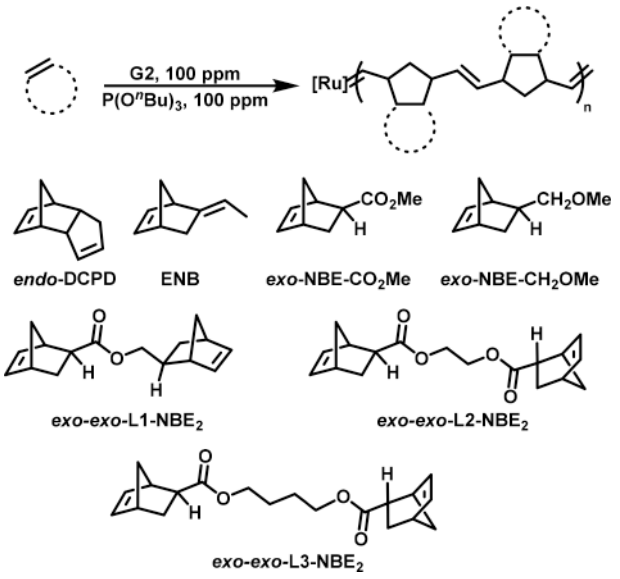

[a]Data reported in *ACS Macro Lett.* **2019**, 8, 846−851.[147]

merization with **DCPD**. The heat associated with the homopolymerization of these monomers is given in Table 2; mononorbornenes produce more heat per gram since the reactive olefin functionality represents a larger percentage of the molecular weight.

In the copolymerization of *endo*-**DCPD** and mononorbornene monomers, the observed ν_f and ΔH_p obey a linear relationship that is dependent on the wt % of substrates.[147] This so-called "mixing rule" predicts that the mixtures of substrates will exhibit properties that are proportional to the weighted average of the pure components. In contrast to the mononorbornene monomers, mixtures of **DCPD** and linked

Table 2. ΔH_p and ν_f for the Homopolymerization of Norbornene-Derived Monomers[a,b]

monomer	ΔH_p (J g^{-1})	ν_f (cm min^{-1})
endo-**DCPD**	353 ± 5	6.0
ENB	420 ± 7	8.2
exo-**NBE-CO$_2$Me**	320 ± 10	6.7
exo-**NBE-CH$_2$OME**	325 ± 5	3.9
exoexo-**L1-NBE$_2$**	273 ± 7	5.8
exoexo-**L2-NBE$_2$**	260 ± 5	3.7
exoexo-**L3-NBE$_2$**	250 ± 5	2.8

[a]Determined by integration of the DSC exotherm associated with the polymerization event. [b]Data found in *ACS Macro Lett.* **2019**, *8*, 846−851.[147]

dinorbornenes afford copolymers that deviate from the empirical mixing rule. In the copolymerization, these mixtures provide ν_f that are larger than either of the pure substrates alone, despite the linear proportionality of ΔH_p to the composition. This nonmonotonic relationship is attributed to an increased local olefin concentration afforded by the tethered substrates, as the average distance a dinorbornene substrate must travel to approach the catalytically active Ru-site is diminished. Stated differently, the reaction rate is less dependent on substrate diffusion in such mixtures than pure **DCPD**. As the dinorbornene composition passes a critical wt %, however, a higher degree of cross-linking limits chain mobility and reaction rate. A second example from Dean et al.[149] investigated FROMP in systems with **DCPD** diluted with cyclooctadiene (**COD**) and is discussed further in section 5.2.

While most studies of FROMP focus on the fabrication of thermoset materials, several examples exist that afford linear polymers in the absence of **DCPD**. As examples, successful FROMP occurs with **COD** or partially hydrogenated **DCPD** bearing a pendent cyclopentane instead of a cyclopentene (i.e., 2,3,3*a*,4,7,7*a*-hexahydro-1*H*-4,7-methanoindene).[393] The resultant soluble polymers enable traditional characterization methods to deduce aspects of the polymer's microstructure and molecular weight. Perhaps unsurprisingly these linear polymers exhibit M_n in the range of 10^5 to 10^6 Da; while one may be tempted to invoke a mechanistic argument, we suspect that such observations simply result as a function of the formulation composition. Typical solution-state ROMP experiments often target low to medium molecular weights (i.e., M_n < 10^5 Da). In contrast, a standard FROMP resin contains a monomer-to-initiator ratio on the order of 10^4 to 10^5. Correspondingly, at full monomer consumption these polymers exhibit large M_n values. For formulations that contain **DCPD**, however, cross-linking events convolute attempts to study the molecular weights. Indeed, M_n is not defined for a cross-linked material and the molecular weight between cross-links (M_x) is used as a descriptor instead; typical p(**DCPD**) materials possess M_x on the order of 10^3 to 10^4 Da.

Davydovich et al.[170] described frontal copolymerizations of **DCPD** and 2,3-dihydrofuran (**DHF**). Perhaps unsurprisingly, **DHF** dampens ν_f as it forms a less reactive Fischer carbene of the type [Ru = CH_2OR] after ring-opening. The inclusion of **DHF** also imparts new functionality into the backbone of the p(**DCPD**-*co*-**DHF**) thermosets. Treatment with acid induces C−O scission that deconstructs the cross-linked thermoset into smaller, soluble oligomeric species. A related upcycling strategy by Lloyd and co-workers[172] utilized 6- and 7-membered cyclic olefin comonomers bearing silyl-ether

https://doi.org/10.1021/acs.chemrev.2c00686
Chem. Rev. 2023, 123, 3237−3298

linkages in the backbone of the heterocycle. The resulting **DCPD** thermosetting copolymer exhibits robust mechanical properties until treated with fluoride, which induces Si−O fragmentation along the polymer backbone to provide soluble oligomeric products. A subsequent study demonstrated that deconstruction and remanufacturing of such materials also occurs via carboxylic acid catalyzed dynamic exchange of bifunctional silyl ether groups.[173] These works highlight new directions for thermoset end-of-life management. One may rightly wonder, however, whether such transformations truly address the problem of polymer waste; on their own, these advances convert solid polymer waste into smaller, perhaps less inert oligomeric waste. To this end, ongoing efforts must focus on closing the loop by developing methods to efficiently repolymerize these deconstruction products.

4.1.4. Mechanical Properties of FROMP Polymers. A small subset of FROMP reports investigated the effects of inhibitor choice on physical properties of FROMP polymers.[32,76] Alzari et al.[76] elucidated the role of (*R*)-limonene on the elastic moduli, T_g, and SR% values associated with p(**DCPD**). Polymers generated from formulations containing higher concentration of limonene display less stiff behavior, as reflected in the reduction in E from 3.2 to 0.3 GPa with an increase in limonene content from 5 to 20 mol %, respectively. Under dynamic stress, polymers with increased limonene content display reduced E', with a concurrent increase to E''. These effects are borne out in the transition temperature of the polymer. For reference, cross-linked p(*endo*-**DCPD**) prepared by classical batch ROMP methods exhibits a T_g in the range of 140 to 165 °C.[174] In comparison, a frontally prepared sample of p(**DCPD**) displayed a T_g of 172 °C. With added competitive olefin, a marked drop in T_g occurs. At 5 mol % limonene, the polymer displays a T_g of 128 °C, which is further decreased to 43 °C at 20 mol % limonene. Chain transfer induced by limonene interrupts cross-linking events, thereby depressing the T_g. A related change in the SR% of the polymers after submersion in tetrahydrofuran exists; enhanced swellability (up to 300%) results from increased limonene content, and by extension increased porosity.

Polymers derived from trialkyl phosphite formulations, however, display mechanical properties nearly identical with conventionally cured p(**DCPD**).[32] Indeed, catalytic mixtures of **DCPD** with 100 ppm of **G2** and $P(O^nBu)_3$ afford highly cross-linked polymers, as is reflected in the large E values (≈2 GPa), tensile strengths (≈50 MPa), and fracture toughnesses (K_{IC} ≈ 2.7 MPa $m^{1/2}$); these parameters are identical within error to bulk cured analogues.

The inclusion of solvent in FROMP formulations dramatically affects the mechanical properties of the resultant polymers. Until very recently, FROMP systems required a solvent to dissolve the catalyst, since **G1** and **G2** are not particularly soluble in neat monomer. Solvents with high boiling points, such as phenyl cyclohexane (238 °C), circumvent adventitious bubble formation associated with solvent vaporization. Solvent, however, acts as a plasticizer in the final polymer to reduce the T_g. A recent report from Ivanoff et al.[150] demonstrated that solvent-free formulations are viable for FROMP. Extended sonication of **G2** (≈100 ppm) and $P(O^nBu)_3$ (equimolar relative to Ru) in a 95:5 mixture of **DCPD**/**ENB** afforded a homogeneous, clear formulation capable of FROMP. The solvent-less formulation exhibits a ΔH_p of 380 J g^{-1}, which is larger than that observed in an analogous formulation with 3 wt % phenylcyclohexane (360 J g^{-1}). Unsurprisingly, faster front velocities existed under solvent-free conditions. The exclusion of solvent provided a polymer with a T_g of 161 ± 7 °C, which is noticeably larger than observed with solvent containing polymers (138 ± 1 °C).

Recent work from Suslick et al.[153] adapted 9 commercially available ruthenium alkylidene complexes for FROMP; subtle variations in the catalyst architecture (e.g., NHC identity) and resin formulation (e.g., inhibitor loading) greatly influenced the FP process and the mechanical properties of the final polymer products. The largest differences occurred in frontal polymers generated by catalyst bearing a chelating NHC ligand; unlike typical FROMP polymers, the resulting materials exhibited elastomeric properties (i.e., large failure strain, low T_g, small E). Additionally, some catalyst formulations afforded polymers with multiple transition temperatures, as determined by DMA. At present, the operative mechanism for such property differences is not known; changes in catalyst selectivity (e.g., reactivity ratios) may dictate these atypical features. In a subsequent report, Suslick et al.[165] investigated the use of a bis(NHC) complex as a latent catalyst for FROMP. In the absence of an activation reagent (i.e., coinage metal halide), this complex cannot undergo a ligand dissociation step necessary for substrate binding and ring-opening to occur. The pot life of this latent species is nearly 2 months; after this time, background gelation occurs and forms a stiff gel incapable of FROMP. In the presence of CuX type species, however, facile NHC transmetalation occurs from Ru to Cu. The resultant active species then rapidly catalyzes FROMP after a thermal trigger. Most importantly, this work employed statistical methods to probe the correlations present (e.g., the relationship between T_{max} and T_g).

4.1.5. Non-Thermal Initiation Methods. Stawiasz et al.[151] recently reported the first example of light-triggered FROMP employing **G2**/$P(O^nBu)_3$ as the catalyst precursor. A range of UV-A light sources, including low-power LEDs (375 nm, 318 mW cm^{-2}), ignited FROMP efficiently within 6 min; increases in the power output of the light source to 4.75 W cm^{-2} (at 365 nm) dramatically decreased t_{ignite} to under 1 min. Control experiments determined that background temperature increases caused by the photosource did not occur, which ruled out adventitious thermal ignition. Successful ignition required that the incident light match the major absorption band of **G2** (λ_{max} = 342 nm), which suggests that photoassisted phosphite dissociation occurs to unmask the active 14 electron species. Indeed, photoignition presents interesting possibilities for controlled multifront FROMP, as well as high-resolution patterning applications. In a subsequent report, Stawiasz et al.[164] investigated photoactivated dual-component FROMP system with the bis(NHC) complex described previously by Suslick et al.[165] This work cleverly employed a photoredox mediator (e.g., pyrylium or acridinium salts) to transform Cu^{II} species into Cu^{I} *in situ* after irradiation with blue light (λ_{max} = 455 nm). Catalyst activation then occurs via NHC transmetalation. A series of control experiments ruled out adventitious thermal activation; during the course of photoactivation, the resin temperature remains constant and below the thermal onset temperature measured by DSC.

Photothermal ignition is possible with the addition of a strongly light-absorbing filler, as observed in a recent example from Dean et al.[152] The inclusion of carbon black nanoparticles into a **DCPD** resin enabled efficient photothermal heating; irradiation of suspended carbon black with a Hg vapor light source (Novacure N2001, Artisan Technology Group) raised

https://doi.org/10.1021/acs.chemrev.2c00686
Chem. Rev. 2023, 123, 3237−3298

the resin temperature enough to ignite a polymer front. In control experiments with a resin composition containing 1 wt % carbon black and no catalyst, 2 min of irradiation at a power of 2 W cm^{-2} elevated the resin to nearly 70 °C. Additionally, the total energy input required to photothermally ignite a front scaled with the quantity of carbon black. Without the absorbing material, nearly 1.2 kJ of energy was required to initiate FROMP. In contrast, formulations with 1 wt % carbon black ignited with an input of nearly 40 J. The final polymers displayed similar T_g values (≈140 °C) to that of neat p(**DCPD**) derived from thermally ignited FROMP. The largest difference between the photothermal and thermal resins is the color—unsurprisingly, added carbon imparts a black color to the polymer.

4.1.6. Frontal Ring-Opening Metathesis Oligomerization. The insolubility of thermoset materials complicates efforts to understand chemical-level details, particularly those involving the nature of cross-linking. For p(**DCPD**) as an example, it is estimated that ≈15% of the pendent cyclopentene fragments undergo ring-opening.[175] Suslick, Alzate-Sanchez, and Moore[169] recently developed methodology to frontally synthesize and characterize soluble oligomers of **DCPD**. Specifically, the incorporation of a terminal olefin chain-transfer agent (CTA) into FROMP resins prevents cross-linking and network formation. Chain-transfer occurs by cross-metathesis between the CTA and the growing oligomer chain. Front generation and propagation occur at a variety of **DCPD** to CTA molar ratios; successful FROMO occurs in resins with ratios in the range of ≈5 to 35. Resins comprised primarily of CTA undergo homocross-metathesis and do not generate oligomer (or polymer). At the other extreme, resins with minimal CTA generated cross-linked materials. Such cases are best described as FROMP.

The solubility of o(**DCPD**) in organic solvents enabled solution-state characterization types; NMR spectroscopy and size exclusion chromatography provided details about the molecular weight distribution. The authors employed Kendrick mass-analysis to extract details related to chain-end speciation and cyclopentene ring-opening, otherwise unobtainable through conventional characterization tools. While a detailed discussion of this technique is beyond the scope of this work, a tutorial by Fouquet[176] and an editorial by Suslick et al.[177] nicely describe Kendrick mass analysis in the context of polymer chemistry. In the context of FROMO, Kendrick mass-analysis revealed the existence of at least six different classes o(**DCPD**), that varied by chain-end type and number. Species with four or six chain-ends resulted from ring-opening events on the pendent cyclopentene functionality. The results from this work provided convincing evidence that cross-linking in FROMP occurs via cyclopentene ring-opening and not by a direct-addition mechanism.[169]

The resultant telechelic oligomers possess two benefits over the parent monomer. First, o(**DCPD**) is odorless, unlike the foul acrid smell of **DCPD**. Indeed, the pungent aroma of **DCPD** limits its usage for many commercial applications. Second, the reactive chain-ends in o(**DCPD**) enable postoligomerization functionalization, which widens the accessible chemical space for **DCPD**-derived materials. Specifically, alteration of the chain-end identity may impart desirable properties into **DCPD**-based materials (e.g., adhesion promoters). The synthesis of these oligomeric building-blocks is scalable; in some cases, >100 g of oligomer are produced in under a few minutes after thermal initiation.[169]

4.2. Frontal Cationic Polymerizations

4.2.1. Epoxy and Oxetane Ring-Opening Polymerization. Epoxy ring opening polymerization reactions are ubiquitous in the synthesis of both practical and advanced polymers employed in coatings, adhesives, and castings.[178] Indeed, a massive global demand for thermoset epoxy resins exists, particularly for applications which require lightweight and robust materials (e.g., Boeing 787 Dreamliner parts);[2] the global production of epoxy resins exceeded 3 million metric tons in 2000, with an estimated value of ≈20 billion USD.[2] While most industrially prepared composites are amine cured epoxies, other methods used in academic research often involve a strong acid-initiated mechanism, as depicted in Scheme 4. Initial monomer activation occurs by protonation of

Scheme 4. General Mechanism for Acid-Catalyzed Cationic Epoxy Ring-Opening Polymerizations

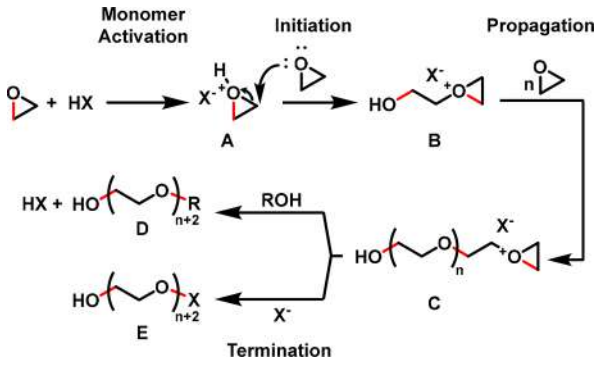

the oxirane (or other larger cyclic ethers) with a proton source (HX) to generate an electrophilic oxonium adduct (**A**). Subsequent nucleophilic attack by additional monomer (**B**) initiates and propagates the growing polymer (**C**). Termination typically occurs by interaction with an added alcohol (or water) to produce the final poly(epoxide) and acid regeneration (**D**). If the counterion (X) is sufficiently nucleophilic, then attack on the growing polymer occurs to afford an X-capped epoxy polymer, akin to **E**. As a consequence, polymers derived from this termination route display low molecular weights with monofunctional monomers. Typical proton sources, therefore, contain counterions that exhibit poor nucleophilicity (e.g., $CF_3CO_2^-$, FSO_3^-, $CF_3SO_3^-$) as to achieve better control over termination.[37]

Frontal epoxy ring-opening polymerizations display reduced heat generation rates compared to FROMP, which results in slower propagation rates. The second order rate constant for epoxide ring-opening spans a wide range of values from 10^{-2} to 10^{-10} M^{-1} s^1. As an example, the rate constant for cyclohexene oxide polymerization by an aluminum amine-phenolate catalyst is 9.5×10^{-4} M^{-1} s^{-1} as measured at room temperature, which corresponds to a k_{obs} of 1.9×10^{-5} s^{-1} at a catalyst loading of 0.2 mol % (20 mM).[179] Alongside the heat of polymerization for cyclohexene oxide (0.99 kJ g^{-1}),[180] the specific power in this example is 18 W kg^{-1} at 22 °C. With this crude benchmark, it is of no surprise that epoxy-based frontal systems display longer storage lifetimes than FROMP without added inhibitors, since the rate of heat generation is at least 2 orders of magnitude less than that described in section 4.1.2.

The primary initiators employed in cationic FP are photoacid generators (PAGs),[34,62,64,80,83,181−190] amine-boron trifluoride adducts,[74,83,133] or cross-linking polyamines.[82,191,192]

https://doi.org/10.1021/acs.chemrev.2c00686
Chem. Rev. 2023, 123, 3237−3298

While the mode of propagation with these curing agents matches that of the general mechanism in Scheme 4, several differences in monomer activation and initiation exist. Radical induced cationic FP employs PAGs as the curing agent, typically in conjunction with added thermal radical sources (e.g., organic peroxides). Hypervalent iodine reagents undergo light assisted acidification and until 2020 were the only PAG motif employed for cationic FP. Initial photoexcitation of diaryliodonium salts with UV light forms a highly reactive excited state (Scheme 5A).[193] This excited state relaxes either

Scheme 5. Various Initiation Techniques Employed in Cationic FP, Which Involve UV-Triggered Cation Formation (A), Amine-Boron Trifluoride Adducts (B), or Polyamine Comonomers (C)

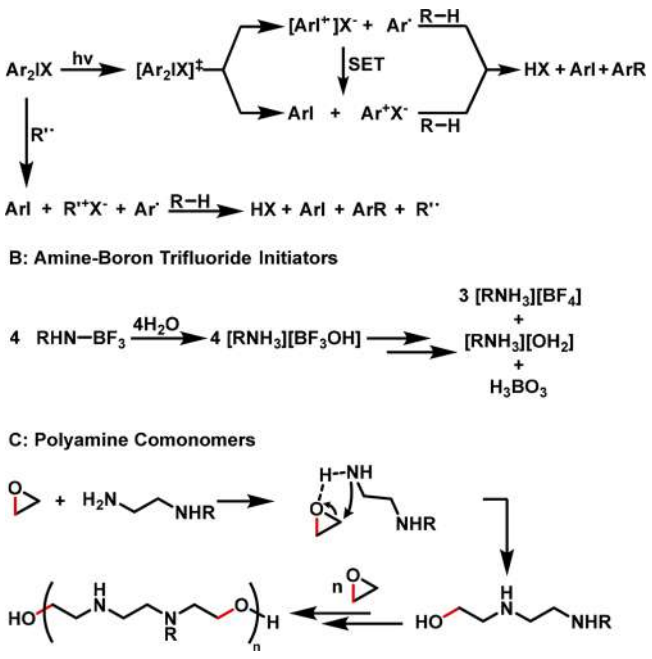

by homolytic or heterolytic Ar−I scission; radicals generated in the former pathway abstract hydrogen atoms from C−H bonds (e.g., Ar−H), which generates an acid, HX. Alternatively, single electron transfer from the aryl radical to the monoaryl iodonium species to generate ArI along with aryl cations, which act as potent electrophiles that interact with C−H bonds to generate HX.[193] Alongside iodonium reagents, several successful examples of sulfonium,[190,194] bismuthonium,[185] and pyrylium[185] based PAG architectures as photoinitiators have been reported.

Light penetration through a large volume of monomer, however, limits the use of PAGs for frontal processes.[34,62,181,182] Indeed, a percentage of incoming photons are diffracted or absorbed by initiators (and monomers) in the formulation, and thus give rise to a photon gradient through the material. PAG molecules on the surface receive more photons than those deeper within the material, which results in nonuniform rates of polymer initiation and propagation. Hence, the surface undergoes a higher degree of conversion than the deeper polymer layers. UV-triggered cationic oxetane polymerizations, as reported by Crivello,[181] illustrated that uniform polymerization occurs only in thin films of 2 mm or less. In a related system, Mariani and co-workers[80] determined that higher monomer conversions exist in the presence of an added thermally degradable radical source. The heat produced from photoinduced polymerization causes homolytic thermolysis of the radical source. Subsequent interaction of the resultant radical species with unreacted PAG molecules perpetuates the polymerization. As a net effect, the initiation process may efficiently occur at depths otherwise inaccessible to the light trigger, thereby enabling quantitative monomer consumption. Specifically, successful FP with diaryliodonium PAGs exploits the thermolysis of added benzoyl peroxide (**BPO**)[80] or 1,1,2,2-tetraphenylethylenediol (**TPED**).[34,62,64,182,184,186−188,195]

Amine-boron trifluoride initiated FP occurs by background reaction with residual moisture. These adducts react readily with water (Scheme 5B) to form a transient, solvent separated species, $[RNH_3][BF_3OH]$. The cationic amine initiates polymerization, whereas the anionic species rapidly decomposes into boric acid through a series of complex disproportionation reactions.[196] Reported frontal polymerization reactions typically occur under ambient atmospheres without rigorous water exclusion, so it is reasonable to assume that cationic amine exists to an appreciable extent in solution. Unfortunately, the amine-boron trifluoride adducts added in these FP reactions consist of proprietary, commercial brands, thereby obfuscating meaningful comparisons. For reference, Scognamillo et al.[74,133] used initiators produced by Leepoxy (namely, Leecure B-110 or B-950).

Finally, polyamines (e.g., diethylenetriamine [**DETA**], tris(2-aminoethyl)amine [**TREN**]) have found use in the design of highly cross-linked epoxy copolymers;[197] **DETA** cures glycidyl ether at ambient temperatures through a mechanism akin to that of Scheme 5C.[197] Monomer activation occurs by complexation with the amine. In the high concentrations employed in this type of polymerization (≈ equimolar to monomer), a subsequent copolymerization event forms an amine-oxirane adduct, which acts as a reactive ring-opening nucleophile. Hence, such polyamine initiated frontal systems form epoxy-amine copolymers.[197]

Reported frontal cationic ring-opening polymerizations exclusively involve the cyclic ethers depicted in Chart 2 (refs

Chart 2. Common Cyclic Ether Monomers Employed for Cationic Ring-Opening FP

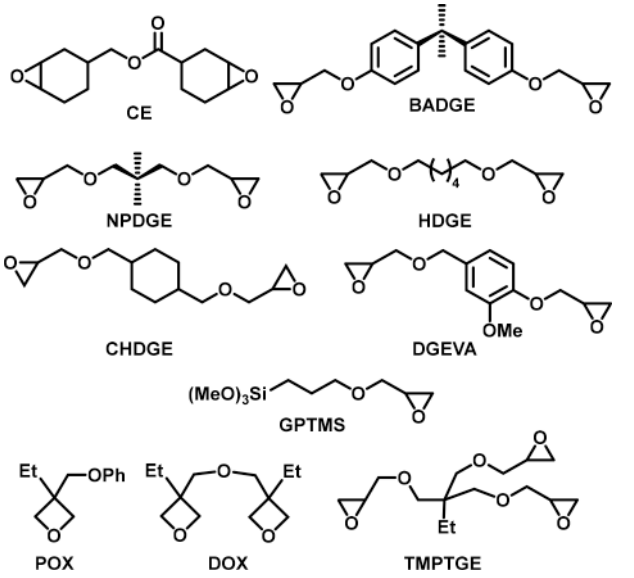

https://doi.org/10.1021/acs.chemrev.2c00686
Chem. Rev. 2023, 123, 3237−3298

34, 62, 64, 74, 80, 82, 83, 133, 181, 191, 192, 195). Indeed, one may notice that a majority of the successful monomers employed possess *two* reactive sites; in general, monofunctional epoxies undergo front-quenching in the absence of a cross-linkable comonomer. While the exact cause is not known, it is possible that the addition of cross-linkers increases the local monomer concentration and boosts the observed heat generation rate, thereby avoiding heat-loss driven quenching. Alternatively, it is possible that differences in the energy density of mono- vs bifunctional epoxies account for this observation. As the products with this form of FP are thermosets, metrics related to microstructure and molecular weight are difficult to parse. To the best of our knowledge, the cross-link density (M_x) has not been determined for epoxy FP.

While most examples include an inert inorganic filler, initial reports by Mariani et al.[80] and Crivello[181] demonstrated that unfilled monomer formulations support stable fronts. For example, UV-triggered polymerization of 3,4-epoxycyclohexylmethyl-3′,4′-epoxycyclohexanecarboxylate (**CE**) occurs in the presence of [4-(2-hydroxytetradecyl)oxy]-phenyliodonium-SbF_6 (**HOPH-SbF_6**) or [(4-(octyloxy)-phenyl]phenyliodonium-SbF_6 (**IOC-8 SbF_6**) as soluble PAG salts with **BPO** as a thermal co-initiator.[80] The concentrations of the PAG and thermal radical source influenced the observed frontal velocities and temperatures. Sustainable fronts only existed in formulations containing between 1 and 3 mol % iodonium; at low concentrations, the polymerization front exhibited a ν_f of 3.2 cm min^{-1} with a T_{max} of 250 °C. While increases in PAG loading afforded faster fronts (up to ≈5 cm min^{-1}), the maximum temperatures decreased to 232 °C. In contrast, front velocity and temperature increased linearly with thermal radical loading. These results illustrate a typical trend in related systems: more initiator affords faster, hotter fronts in a set range. At a critical quantity of initiator, SP occurs.

Unsurprisingly, the monomer identity impacts the frontal parameters, as evidenced in the examples reported by Liska and co-workers[62] in Table 3. Neat mixtures of bis(epoxy) monomers with **IOC-8 SbF_6** and **TPED** afforded stable fronts after UV irradiation (320−500 nm at 500 mW cm^{-2}) for a set length of time (t_{ignite}). While minor variations in the ignition time exist, these formulations rapidly ignited within 23 ± 12 s on average. No clear correlation between the ignition time and the frontal velocity seems to exist; 1,6-hexanediol diglycidylether (**HDGE**) as a monomer provides a faster front than CE despite requiring twice as long to ignite. Similarly, T_{max} does not exhibit a clear dependency on ν_f; out of the substrates tested, **HDGE** and cyclohexanedimethanol diglycidylether (**CHDGE**) provide the fastest fronts despite a ΔT_{max} of 41 °C. It is not immediately clear which factors dictate the variation in frontal parameters. The authors also noted that bubble formation occurs in the polymerizations with all monomers except bisphenol A diglycidyl ether (**BADGE**).[62] Bubble formation results from small-molecule evaporation/boiling phenomena. In this context, monomer or initiator decomposition occurs with **CE**, **NPDGE**, **HDGE**, and **CHDGE** to generate low-vapor pressure byproducts. Most cationic ring-opening systems employ **BADGE** as it supports robust and stable fronts. More recently, Groce et al.[183] reported on radical-induced cationic frontal vinyl ether polymerization using an initial thermal stimulus.

Table 3. Frontal Properties of Bis(Epoxy) Monomers under UV-Ignited Conditions[a,b]

monomer	MW (g mol^{-1})	T_{max} (°C)	ν_f (cm min^{-1})	t_{ignite} (s)
CE	252	176	26.2	31
BADGE	340	173	2.7	38
NPDGE	216	169	19.9	10
HDGE	230	181	28.6	12
CHDGE	256	140	37.9	23

[a]Conditions: Monomer (15 g), **TPED** (1 mol %), and **IOC-8 SbF_6** (1 mol %) were irradiated for a length of time (t_{ignite}). [b]Data found in ref 62.

The polymerization of the oxetane substrates 3-ethyl-3-(phenoxymethyl)oxetane (**POX**) and 3,3′-(oxybis-(methylene))bis(3-ethyloxetane) (**DOX**) under UV-activated and thermally ignited cationic polymerization conditions generated slower, colder fronts than the epoxy analogues.[180] At 1 mol % **HOPH-SbF_6**, **DOX** underwent FP characterized by a T_{max} of ≈160 °C and ν_f of 14 cm min^{-1}. The reduction in ring strain in oxetanes lowers the exothermicity of ring-opening. The heats of polymerization of ethylene oxide and oxetane, for example, are 2.9 and 1.4 kJ g^{-1}, respectively. Despite the lower exothermicity, rapid temperature time-evolutions existed within the reaction zone (135 °C s^{-1} with **POX**), which manifested as a narrow, well-defined front. Crivello[181] observed that background temperature increases occur with **DOX** (20 °C over 4 min), which implicates a reasonable degree of SP as well as a poor storage lifetime. In contrast, formulations consisting of **BADGE**, **TPED**, and **IOC-8 SbF_6** are stored at 50 °C for at least 2 h without discernible SP or gelation.[62] One might expect, therefore, that the storage lifetime of the system is determined by kinetics differences in the ignition process rather than by thermodynamic differences inherent to the substrates.

Polymerizations in the presence of added inert diluents provide physical properties otherwise difficult to access with unfilled epoxy polymers.[191] Inorganic fillers impart enhanced heat resistance to the polymer matrices in which they are embedded. Section 5 is dedicated to a thorough discussion of such implications to composite materials synthesis. While a diverse of applications exist for composite materials, the

Table 4. Filler Dependent Frontal Properties of Hybrid Inorganic−Poly(Epoxy) Materials

monomer	filler	filler loading range	conditions[a]	T_{max} range (°C)	ν_f range (cm min^{-1})
BADGE[192]	Montmorillonite	0−8 phr	A	236−203	0.9−0.8
BADGE[34]	Calcinated Mica	5−15 phr	B	−	4.0−3.7
TMPTGE[74]	Fumed Silica	0−15 phr	C	275−240	3.2−1.2
TMPTGE[74]	Kaolin	0−80 phr	C	275−185	3.2−0.9

[a]Reaction conditions for A: **BADGE** (11 mmol), **DETA** (7.2 mmol), soldering iron initiated; B: **IOC-8 SbF_6** (8 mol %), **TPED** (8 mol %), UV-ignited. T_{max} was not recorded; C: **Leecure B-110** (15 phr), **TMPTGE** (10 g), soldering iron ignited.

https://doi.org/10.1021/acs.chemrev.2c00686
Chem. Rev. 2023, 123, 3237−3298

chemical effects of diluents on the frontal process itself remain challenging. In general, diluting reactive monomers with nonparticipating reagents changes the heat transfer in two ways. A reduction in the heat generation rate occurs as a smaller wt % of the mixture undergoes polymerization (i.e., reduced energy density). Second, the added filler acts as a heat-sink. These factors manifest in an inverse relationship between filler content and ν_f.

Most frontal epoxy formulations contain additives, typically comprised of silicates or main group metal oxides.[62,74,82,133,191,192] Fully inorganic additives (e.g., fumed silica,[74] kaolin,[74,133] mica,[34] montmorillonite[192]) follow the general trend described above. The specific choice in filler, however, determines the degree of dampening for T_{max} and ν_f. While the specific reaction conditions vary greatly among the examples provided in Table 4, discernible effects of filler on frontal properties exist. Regardless of the filler identity, an upper diluent concentration limit exists in formulations able to support stable fronts. In general, kaolin accesses the largest working dopant range; FP occurred in mixtures of trimethylolpropane triglycidyl ether (**TMPTGE**) containing up to 80 phr kaolin by mass, with only a 3-fold decrease in ν_f. In contrast, monomer blends with added montmorillonite, fumed silica, or mica only proceed frontally with concentrations under 15 phr by mass. A combination of filler properties (i.e., thermal conductivity, specific heat capacity, shape, size, and aspect ratio) likely govern the effects of filler on the front parameters; similarly, the interface of the curing resin and the filler surface perturbs front propagation.

Scognamillo and co-workers[133] employed the use of fillers to change the viscosity of frontal resins. Specifically, the chosen materials displayed thermal expansion or defoaming behavior. The addition of microspheres impregnated with gaseous hydrocarbons reduced T_{max} and ν_f of fronts derived from **TMPTGE** initiated by Leecure B-110. As a result of low thermal conductivity, trapped gases within the resin provide an insulating pocket that may modify the diffusion of the overall material and potentially disrupt heat and front propagation. The resultant semiporous polymers display inferior mechanical properties when compared to additive-free analogues. In contrast to thermal expansion agents, defoaming agents increase the observed frontal parameters. The authors proposed that the defoaming agents, which are a proprietary mixture of xylene and functionalized acetates (BYK 070N), improved thermal diffusion through the sample by filling void spaces generated during polymerization (i.e., better thermal conductivity compared to air).[133]

4.2.2. Tin-Catalyzed Polyurethane Synthesis. Frontal processes exist that produce polyurethanes, albeit far fewer in number than that of epoxide ring-opening reactions.[71,75,132,198−200] The prototypical example by Fiori and co-workers[71] investigated the copolymerization of ethylene glycol with 1,6-hexyldiisocyanate (and added catechol), as depicted in Scheme 6. Polyurethane manufacture occurs in a bimolecular fashion. The added Sn^{IV} reagent (typically dibutyl tin dilaurate, **DBTDL**) acts as a Lewis acid catalyst; initial coordination of the isocyanate activates the substrate toward nucleophilic attack by the added diol. Subsequent proton transfer affords a carbamate species, terminated on either end by alcohol and isocyanate functionalities. Further polymerization events occur through a step-growth mechanism to afford the final polyurethane species; step-growth polymers with desirable mechanical properties require higher conversion than those generated in chain propagation mechanisms, since the average molecular weight is exponentially proportional to conversion.[37]

In the initial report by Fiori[71] and a subsequent follow-up,[200] the monomer resin required the use of DMSO as a solvent to ensure uniform resin viscosity and rheological behavior during FP. Increased dilution with DSMO, however, depressed T_{max} and ν_f, which was attributed to termination steps that resulted from interaction with residual moisture in the solvent. A nearly linear relationship between T_{max} and Sn loading exists. For example, T_{max} rose from 177 to 210 °C upon a 4-fold increase in catalyst concentration (0.5 to 2.0 mol %, respectively). The frontal velocity displayed a similar linear increase from 0.4 to 0.9 cm min^{-1}. Increases in catechol content dampened the frontal temperature and velocity through an inhibitory mechanism where competitive coordination to the Sn center depresses the active catalyst concentration and observed catalytic rate. In the absence of catechol, however, instantaneous background polymerization occurs within seconds; formulations with at least 0.5 wt % catechol displayed enhanced storage lifetimes of 25 min.[71]

Compared to analogous batch conditions, polyurethanes generated frontally exhibited significantly higher inherent viscosities (0.76 vs 0.23 dL g^{-1}) and, therefore, larger molecular weights. Interestingly, the DSC traces of the resultant frontal polyurethanes displayed two different transition modes. The lower, sigmoidal-like transition occurred at 37 °C and corresponds to the T_g. The second feature, however, existed as a large endotherm at 167 °C, indicative of a T_m. This semicrystalline material (degree of crystallinity = 31−48%), therefore, is a rare example of a nonamorphous frontal polymer.[71,200] Two follow-up reports by Mariani and co-workers[199,200] expanded the substrate scope to include longer-chain diols and aromatic isocyanate monomers in the synthesis of semicrystalline frontally derived polymers.

Chen and co-workers[198] examined the FP of 2,4-toluene diisocyanate with a macromolecular diol, poly(propylene oxide)glycol, catalyzed by tin bis(2-ethylhexanoate). This less active Sn source afforded longer storage lifetimes of 6 h without an inhibition reagent. Unsurprisingly, the addition of a less active catalyst, in conjunction with a low energy-density polymeric diol, afforded slow moving fronts (ν_f = 0.1−0.3 cm min^{-1}) characterized by fairly low T_{max} values (≈90 °C). In contrast to the unique morphologies observed by Fiori et al.,[71] these polyurethanes displayed only amorphous characteristics (T_g = −43.5 °C).[198] Despite the successes of Sn-catalyzed polyurethane synthesis as a frontal method, other urethane containing systems merely employ the carbamates as linkers to large, macromolecular diacrylate monomers;[75,201] these frontal formulations do not react *via* Sn-catalysis but instead occur by free-radical polymerization (*vide infra*).

Scheme 6. Typical Conditions for the FP Diols and Diisocyanates

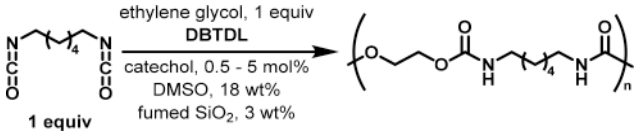

https://doi.org/10.1021/acs.chemrev.2c00686
Chem. Rev. 2023, 123, 3237−3298

4.3. Frontal Radical Polymerizations

4.3.1. Mechanistic Considerations. Free-radical polymerizations are the most common type of frontal systems, with over 80 published reports as of 2022 (refs 29, 33, 34, 44, 47−50, 53, 60−63, 70, 77−79, 81, 84−93, 95, 114, 127, 134, 199, 201−259). Three distinct mechanistic regimes exist for chain growth radical polymerizations (see the simplified Scheme 7). Activation of an initiator occurs *via* decomposition

Scheme 7. Simplified General Mechanism for Chain-Growth Free Radical Polymerization[a]

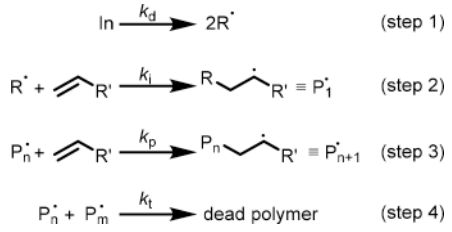

[a]Chain transfer and termination due to primary radicals are not depicted.

to give rise to primary radicals (at a rate of k_d, step 1). Interaction of the resultant radical with a monomer initiates the polymerization to generate a growing polymer chain at a rate of k_i (step 2). Subsequent reaction with monomer increases the chain length by one unit (step 3); propagation continues at an average rate of k_p until a termination event occurs. Chain termination proceeds through radical coupling or disproportionation reactions, with an averaged observed rate k_t (step 4). In the former, radical annihilation leads to a single, dead polymer typically incapable of re-entering the polymerization event. The radical disproportionation pathway, however, occurs by β-hydrogen transfer between the two species, where one of the resultant products contains a degree of unsaturation.

Each of the fundamental steps in this chemical polymerization mechanism relates to various frontal process parameters. The choice of initiator affects the k_d and k_i values; faster initiator decomposition depresses the length of time required for front generation (i.e., shortened t_{ignite} and t_{ss}). In contrast, long-lived and persistent initiators (i.e., characterized by small k_d) provide frontal formulations with the longest storage lifetimes. While k_i and k_d refer to different chemical steps and are often of different orders of magnitude, most computational engineering studies either average the two values or reduce the complexity of the chemical mechanism to a single-step reaction. Typically, an implied kinetic model is fit to DSC data.[68,225] The propagation rate (k_p) is dictated by the choice of monomer and is independent of the initiator. Indeed, nearly all heat generated during radical polymerization occurs in the propagation step. Thus, k_p provides a reasonable approximation for the rate at which heat is generated and governs T_{max} and ν_f. Front quenching results when k_t is competitive with k_p. To increase the heat released per unit time, it is necessary to increase the radical concentration present in the system. As a side effect, the larger number of radical species results in a higher probability of chain termination. In turn, this affects the molecular weight of the obtained polymers. However, this is generally not a problem in FP as the majority of systems undergo cross-linking.

Efficient frontal radical polymerizations require fast initiation and moderate propagation rates. Indeed, the choice of monomer and initiator dictates the viability toward FP. Systems comprised of initiators with slow homolytic cleavage rates more readily undergo competitive heat-loss. In contrast, highly reactive initiators exhibit poor ambient temperature stability, which precludes extended storage lifetimes. The thermodynamics and kinetics associated with this polymerization motif requires that substrates and initiators display Goldilocks-like behavior to be "just right" for sustainable FP.

In 1991, Pojman[222] described one of the first frontal systems performed under ambient pressures. Previous reports from the former USSR employed metal reactors for high pressure FP. In contrast, Pojman[222] directly observed the front formation of methacrylic acid (**MAA**) with benzoyl peroxide (**BPO**) after thermal ignition in a glass test tube. These fronts required a t_{ss} of 2 min to reach a steady-state velocity (ν_f = 1 cm min^{-1}). The observed thermal-spatial gradient of approximately 180 °C cm^{-1}, as well as a large T_{max} of 195 °C, indicated the existence of a narrow, hot reaction zone. The temperatures achieved with this formulation, however, surpassed the boiling point of **MAA** (163 °C), and induced undesirable monomer vaporization, as well as double-diffusive convection. The resultant polymers, as a result, exhibited a nonuniform molecular weight distribution ($Đ \approx 4$).

4.3.2. Ignition Techniques. Four main ignition categories exist for frontal free-radical polymerizations: thermal (refs 29, 33, 44, 48, 53, 70, 78, 79, 81, 91−93, 95, 127, 134, 167, 203−207, 210, 211, 215−217, 219−224, 226, 235, 238, 241−243, 246−248, 253, 255, 256, 258, 260, 261), photo (refs 58−60, 135, 167, 255, 257, 259, 262−269), plasma (refs 270−273), and magnetocaloric (refs 206, 239). Thermal triggering typically involves the use of a soldering iron or oil bath to heat a localized region. More controlled thermal initiated systems may involve the use of an embedded resistive wire at a fixed volatage and amperage. Thermal ignition typically requires ≈10 to 120 s, depending on the resin composition and boundary conditions. Photoinitiators follow the same mechanism as that described above for epoxide ring-opening polymerizations (section 4.2.1), where a mixture of UV-active and thermal radical sources provide more uniform radical concentrations.[58−60,135] Recent work from Gary et al.[255] demonstrated that the inclusion of iodonium PAG salts enable both photo and thermal initiation modes with acrylate monomers.

A subset of systems have employed directed CO_2-lasers with IR-wavelength photons (λ_{max} = 10.6 μm) to induce highly focused heating in the rection zone.[207,262−264,266,267] In contrast to nondirected thermal initiation, CO_2-lasers provide incredibly short ignition times ($t_{ignite} \approx 1-10$ s) as a result of higher energy density.[263] Plasma ignited systems follow a similar premise to CO_2-lasers in that intense local heat transfer occurs. Chen and co-workers[271] reported the first usage for FP applications; a high energy, air plasma (∼1−10 eV, where 1 eV corresponds to a T = 11000 K) rapidly induced ignition in seconds. The same group[206,239] also reported the use of magnetocaloric-type ignition. In these systems, the reaction formulation included super paramagnetic Fe_3O_4 nanoparticles (SPIONs).[274] Under an applied and oscillating magnetic field, spontaneous spin alignment occurs within the SPION, which corresponds to an overall reduction in the entropy of the system with a concurrent heat release (i.e., dielectric

https://doi.org/10.1021/acs.chemrev.2c00686
Chem. Rev. 2023, 123, 3237−3298

heating).[274] This heat triggers FP, which ignites after a few seconds of exposure to a 450 kHz magnetic field.[206,239]

Two notable examples deviate from the ignition methods outlined above. Lewis et al.[275] and Evstratova et al.[63] described an isothermal frontal formulation that exploits the gel effect. Unlike other FP reactions, the experimental procedure (Figure 16) does not involve a localized hot spot to induce

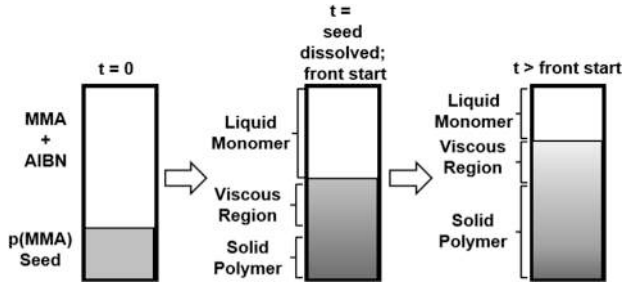

Figure 16. Experimental schematic for the isothermal FP of **MMA** initiated by a p(**MMA**) seed. Figure adapted with permission from *Polym. Sci., Part A: Polym. Chem.* **2005**, *43*, 5774−5786 and *Polym. Sci., Part A: Polym. Chem.* **2006**, *44*, 3601−3608.[63,275] Copyright 2006, Wiley Periodicals, Inc.

polymerization. Instead, a mixture of 20 mM azobis(isobutyronitrile) (**AIBN**; see section 4.3.3, Chart 3) and

Chart 3. Common Initiators for Free-Radical Polymerizations[a]

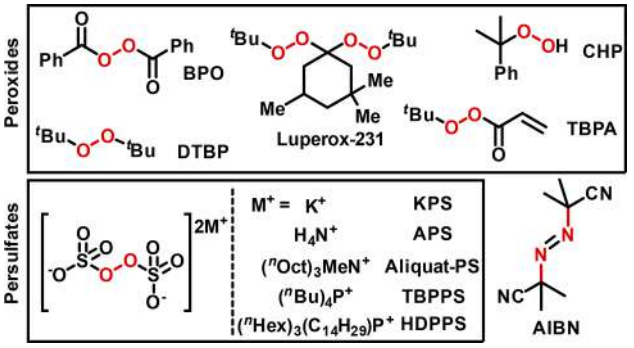

[a]The bonds in red undergo homolytic scission after a triggering event.

methyl methacrylate (**MMA**, see section 4.3.4, Chart 4) was layered atop a p(**MMA**) seed inside a glass cell heated to approximately 65 °C. In this example, **MMA** diffuses into the p(**MMA**) seed, and due to the aforementioned Trommsdorff−Norrish effect, diffusion of the propagating radical is depressed. This results in an increase of radical concentration that rises the polymerization velocity. Additionally, the decrease in diffusivity gives rise to larger molecular weights. Isothermal FP proceeds more slowly ($\nu_f \approx 0.2$ cm h^{-1}) than other thermally ignited fronts, as a result of significantly slower k_p. Additionally, long induction periods upward of 1 h exist prior to front ignition. A typical plot of temperature as a function of time is nearly flat; the temperature of the system remains at a steady-state prior to gel-point of the system. At the gel-point, spontaneous polymerization occurs in the remaining liquid monomer.

Water triggered systems were explored by Pujari et al.[227] in the polymerization of acrylamide (**Am**, See section 4.3.4, Chart 4) with potassium persulfate (**KPS**, see section 4.3.3, Chart 3)

Chart 4. Monomers for Frontal Free-Radical Polymerization

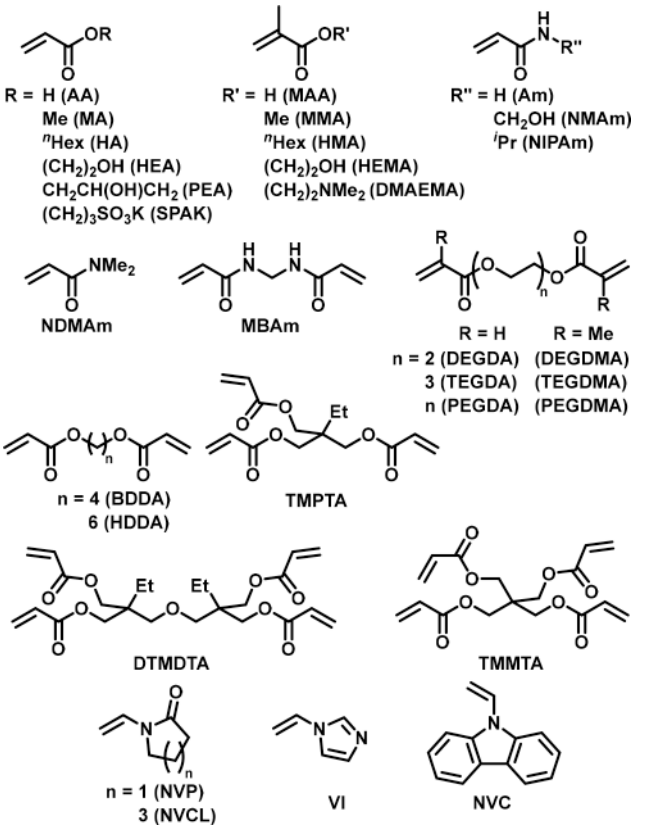

as a radical source. To trigger polymerization, water is added atop the monomer solution (∼10 wt %) at ambient temperature (≈30 °C), which slowly generates aqueous persulfate species that undergo homolytic dissociation.[227] After a long induction period (≈80 min), front formation occurs, as indicated by the concurrent rise in temperature. The final polymer products from this method exhibit a high degree of porosity and broad dispersities ($Đ = 3.0 \pm 0.5$).

4.3.3. Radical Initiators. As the section title implies, frontal free-radical polymerization requires the addition of a radical source, and the most common compounds are given in Chart 3. The majority of free-radical FP systems employ "traditional" peroxide- or azo-derived initiators, such as **BPO** or **AIBN**. Increasingly, **Luprox-231** is the initiator of choice, as it exhibits excellent room temperature stability and is miscible with a wide range of monomers. Upon exposure to one of the exogenous triggers discussed above, peroxides, persulfates, and certain azo compounds undergo homolytic scission. The resultant radical species induce polymerization, and the associated heat prompts additional decomposition of initiators in proximity to the reaction zone. The storage lifetimes of free-radical systems, therefore, are dictated by background radical formation from the thermally reactive additives.

The decomposition rates (k_d) and half-lives ($t_{1/2}$) of selected initiators are provided in Table 5 at various decomposition temperatures (T_D). Formulations with long storage lifetimes correspond to the use of thermally persistent species; in exchange, however, the resultant fronts travel with slower velocities, since a reduction in the effective radical concentration occurs with slower k_d (*vide infra*). Interestingly, Gugg and co-workers[269] demonstrated that methacrylate-based peroxides (*e.g.*, *tert*-butylperacrylate, **TBPA**) frontally copoly-

https://doi.org/10.1021/acs.chemrev.2c00686
Chem. Rev. 2023, 123, 3237−3298

Table 5. Initiator Homolytic Decomposition Rates (k_d) and Half-Lives ($t_{1/2}$) for Selected Radical Initiators at Specified Temperatures T_D[a]

initiator	T_D (°C)	k_d (s^{-1})	$t_{1/2}$
AIBN[a]	40	4.8×10^{-7}	16.6 days
BPO[a]	25	6.4×10^{-5}	3 h
DTBP[a]	80	7.8×10^{-8}	103 days
Luperox-231[a]	85	6.9×10^{-6}	1.2 days
TBPA[b]	100	1.5×10^{-5}	13 h
KPS[c]	50	1.0×10^{-6}	8 days
APS[d]	30	4.5×10^{-5}	4 h
TBPPS[d]	30	9.0×10^{-6}	21 h
HDPPS[d]	30	1.4×10^{-5}	14 h

[a]Measured in benzene solutions as reported by Dixon in *Polymer Handbook*, 4th ed.[276] [b]Measured in a benzene solution as reported in *Macromol. Rapid Commun.* **2011**, *32*, 1096−1100.[269] [c]Measured in 0.1 M $NaOH_{(aq)}$ solutions as reported in *J. Am. Chem. Soc.* **1951**, *73*, 3055−3059.[277] [d]Calculated from the Arrhenius data provided in *Macromolecules* **2008**, *41*, 5191−5196.[215]

merize with **HDDA** to provide reactive branched peroxide intermediates. These species undergo subsequent fragmentation with a 10 h half-life of nearly 20 °C lower than the starting initiator to provide cross-linked thermosets.

The radical source dictates the degree of homogeneity at the front, especially when considering possible side products. Some radical species generate volatile byproducts as a result from either decomposition or interaction with other species present in the environment. In this regard, **AIBN** necessarily provides N_2 *en*-route to polymerization ignition; at high temperatures, **BPO** may decompose to release CO_2. Peroxide initiators, such as **DTBP**, **Luperox-231**, and **TBPA** may thermally decompose to generate volatile organics (e.g., acetone, methane). At frontal temperatures, these products volatilize to form gas pockets within the monomer solution, which disrupt the homogeneity of the product. Hence, the mechanical properties of the resultant polymers suffer due to the vacant spaces generated by these bubbles.[216] Substantial efforts have focused on the development of "gas-free" initiators, such as the persulfate species listed in Chart 3.[69,79,81,215] Unlike other initiators, these species are advantageous as they do not produce volatile byproducts during fragmentation. One potential drawback, however, stems from poor solubility of charged species in acrylate monomers. Specifically, the choice of counterion in these salts determines the solubility; DMSO or H_2O are required for obtaining completely homogeneous solutions with **KPS** or **APS**. Development of long-chain alkyl ammonium- or phosphonium-persulfate salts (**Aliquat-PS** or **TBPPS**, for example) by Mariani and co-workers[79,81,215] accessed solvent-free conditions.

As a general trend, the initiator concentration dramatically impacts the frontal parameters; it should be noted that **Aliquat-PS**, **TBPPS**, and **HDPPS** are characterized by higher molecular weights than other initiators. This results in larger wt % despite being equal in molar fraction. Mariani et al.[215] thoroughly studied the effects of initiator identity and concentration on the FP of triethylene glycol dimethacrylate (**TEGDMA**, see section 4.3.4, Chart 4). Formulations with **BPO** or **AIBN** in under 0.5 wt % exhibited fronts with higher T_{max} than those derived from the inorganic species **APS**, **TBPPS**, or **HDPPS**, as depicted in Figure 17. The concentration window with **AIBN** and **BPO**, however, is

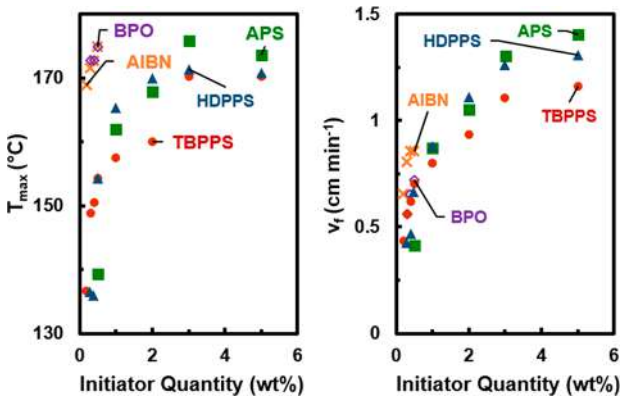

Figure 17. Radical source effects on T_{max} (left) and ν_f (right) as a function of initiator concentration (wt %) and identity in the FP of **TEGDMA**. Figure reprinted and adapted with permission from *Macromolecules* **2008**, *41*, 5191−5196.[215] Copyright 2008, American Chemical Society.

exceedingly narrow; concentrations above 0.5 wt % provide fronts hot enough to potentially degrade the polymer product. In contrast, persulfates can support fronts with large ν_f (≈1.5 cm min^{-1}) at reasonably high loadings (≈5 wt %), but at lower reaction temperatures (<180 °C). Increases in persulfate concentrations yield hotter, faster fronts, and allow for a wide range of T_{max} and ν_f. In respect to practicality, **APS** is commercially available and perhaps more attractive as a cost-effective initiator than other persulfates; on the other hand, the short pot-life may limit its potential utility.

The use of metal assisted redox couples enhances the frontal velocity without sacrificing storage lifetime. Parrinello et al.[70] demonstrated that the dual redox cycle depicted in Scheme 8

Scheme 8. Metal-Mediated Dual Redox Cycle with CHP and an Ascorbic Acid Derivative[70]

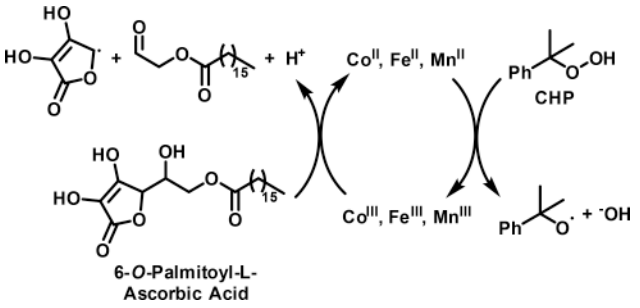

successfully supports fronts with a larger loading of inert filler than with **CHP** alone. For example, a formulation comprised of **CHP**, a triacylate monomer, 6-*O*-palmitoyl-L-ascorbic acid, and Co^{II} source embedded in a polymer network (Intelimer 6050 × 11 from Air Products) provided fronts with up to 100 phr of kaolin filler. In contrast, fronts with **CHP** and monomer alone supported only up to 70 phr kaolin. Additionally, the dual redox cycle provided fronts that were nearly twice as fast (ν_f = 4.0 vs 2.0 cm min^{-1}) and 20% colder (T_{max} = 200 vs 250 °C) than **CHP** alone.

Added nitrogenous co-initiators help to inhibit bubble formation via an organic redox couple. Common redox couples comprised of **BPO**/*N*,*N*-dimethylaniline or **KPS**/*N*,*N*,*N*′,*N*′-tetramethylethylenediamine (**TMEDA**) form carbon-based radicals through the general mechanism depicted in Scheme

https://doi.org/10.1021/acs.chemrev.2c00686
Chem. Rev. 2023, 123, 3237−3298

9.[240] These additives promote O−O bond cleavage rates by forming a charged pair intermediate. Rapid electron and H

Scheme 9. General Redox Mechanism for the Interaction between Radical Sources and Dimethylamines

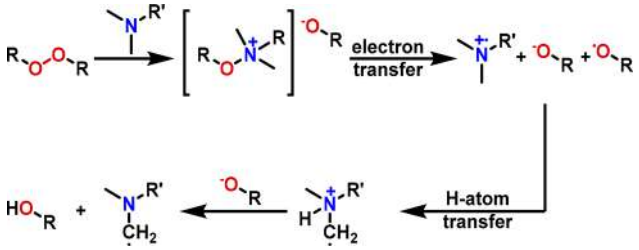

atom transfers occur to provide a carbon-centered radical. A report from Chen and co-workers[240] thoroughly explored the effects such redox couples on FP. Several advantages exist when compared to unadulterated radical sources: faster radical generation rates and less volatile byproducts. These two factors result in a bubble-free front. The room-temperature storage lifetimes are highly dependent on the identity of the ingredients in the formulation; the authors observed that DMSO solutions of **BPO** and hydroxyethyl acrylate (**HEA**, see section 4.3.4, Chart 4) were stable for up to 48 h.[240] In contrast, Pojman and co-workers[70,78,217] observed that neat mixtures of 1,6-hexanediol diacrylate (**HDDA**, see section 4.3.4, Chart 4), **CHP**, and added accelerator spontaneously polymerized within 2 h. In both systems, it was observed that increases in amine concentration (relative to radical initiator) provided colder, slower fronts. Other niche reagents, such as carbon dots,[207] are effective redox partners for FP.

Pojman and co-workers[78,217] described the use of microencapsulated initiators to suppress bubble formation and increase storage lifetimes. Hollow microspheres comprised of polyurea formed a semiporous shell around a **CHP** (≈80 wt %). In conjunction with added cobalt naphthenate as an accelerator, the microencapsulated initiator system exhibited an extended storage lifetime of nearly 5 d compared to nonencapsulated formulations without loss of viability toward FP, as observed with nearly identical front speeds (ν_f = 1.3 cm min^{-1}). Analogous formulations with dissolved and unencapsulated **CHP**, but without accelerator, were reasonably stable for 5 d under ambient conditions. The resultant fronts exhibited a ν_f of 2.7 cm min^{-1}. Excessive bubble formation in this formulation, however, prematurely quenched the front after a few minutes.

While bubble formation during FP presents a major challenge, oxygen assisted inhibition represents an equally important limitation. Radical interception and polymer termination occur with O_2 as it contains a paramagnetic electronic configuration. The ratio of inhibition and propagation rates ($z = k_z/k_p$) defines the efficacy of reaction retardation. As indicated by Odian,[37] the z value of O_2 in the polymerization of **MMA** is roughly 3.3×10^4. This exceedingly large value prevents propagation and reduces the associated heat release, which stifles front perpetuation and reduces the active lifetime. To date, there are a handful of frontal examples that address the effect of O_2 inhibition.[60,135,218,226] These systems include added thiol as a coreagent to enable thermally[218,226] or photolytically[59,278−282] ignited thiol−ene copolymerizations. While the thiol−ene copolymerization pathway generates less heat and occurs at a slower rate than acrylate homopolymerization,[60,218] O_2 inhibition occurs to a lesser extent in systems containing thiols. As a result, the operative polymerization mechanism and the corresponding frontal parameters depend on the relative thiol:acrylate ratio. Indeed, the effects of increasing thiol concentration are complex and therefore difficult to generalize or ascribe to a single cause.

While the vast majority of radical FP reactions employs organo-radical sources, early work from Bidali et al.[248] adapted atom transfer radical polymerization (ATRP) to frontal conditions. ATRP-type reactions involve the use of CuX salts and an organohalide co-initiator (e.g., CBr_4) as a means to generate carbon-centered radical species. The atom transfer step of halide to and from the Cu source serves to control the growing polymer chain; this process provides polymers of exceedingly uniform dispersities. In frontal ATRP, a complex dependency exists between the formulation identity ($[CBr_4]_0$ and $[CuBr]_0$) and the observed T_{max} and ν_f values; specific resin compositions provide values comparable to those observed in "classical" radical FP reactions.[248] Similarly, the T_g values of **TEGDMA** polymers derived from frontal ATRP (≈40 °C) match those of analogous polymers derived from "classical" radical FP or batch conditions.

4.3.4. Monomer Effects on Propagation. Chart 4 provides an exhaustive list of monomers employed in radical FP. In general, formulations employ mixtures primarily composed of monomers bearing one double bond with multifunctional comonomers to achieve the desired degree of cross-linking. The majority of published systems utilize acrylate and acrylamide derived monomers. Other vinyl compounds, such as *N*-vinylpyrrolidone (**NVP**), *N*-vinylcaprolactam (**NVCL**), 1-vinylimidazole (**VI**), and *N*-vinylcarbazole (**NVC**), have found applications in hydrogel syntheses and are discussed further in section 5.1.1.

A plethora of reports have expanded the set of monomers capable of self-propagation, and several of these claim to be the "first published example" for a specified monomer (e.g., **NVP**,[92] *N*-methylolacrylamide [**NMAm**],[93] **Am**,[33] 2-hydroxyethyl acrylate [**HEA**],[205] or diurethane diacrylates[95,260]). The formulation conditions, however, vary with the identity of the monomer and make direct comparisons difficult. Changes in initiator, ignition method, and filler obfuscate monomer specific effects. Despite these challenges, Bynum and co-workers[203] recently examined substitutional effects on acrylate architectures under identical conditions with **Luperox-231** (1 phr) as the radical initiator after thermal ignition. Figure 18 illustrates that a definitive trend between monomer identity and frontal parameters does not exist. Under these conditions, sustainable fronts required the use of di- or triacrylate monomers; hexyl acrylate (**HA**) was unable to support FP because of Rayleigh−Taylor instabilities. In contrast, the fastest fronts were obtained with trimethylolpropane triacrylate (**TMPTA**). The literature has suggested that the molecular weight per acrylate functionality dictates the reactivity, with the justification that filler weight is inert. Despite this assumption, the T_{max} and ν_f do not trend particularly well with the adjusted weight per monomer. A more complete analysis, therefore, requires the consideration of the thermodynamics (ΔH_p) and kinetics (k_p) associated for each monomer. As is the case with epoxy-based FP (see section 4.2.1), details related to microstructure and molecular weight have not been studied.

Table 6 contains the heats of polymerization as well as the rates of bulk polymerization for selected monomers. The

https://doi.org/10.1021/acs.chemrev.2c00686
Chem. Rev. 2023, 123, 3237−3298

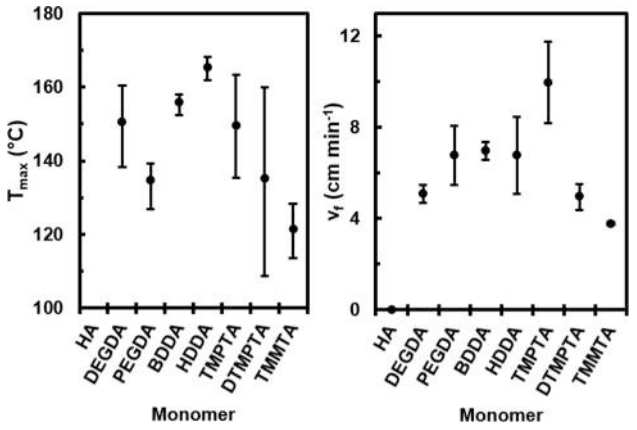

Figure 18. Dependence of monomer identity on T_{max} (left) and ν_f (right) values with **Luperox-231** (1 phr) as the radical source. Monomer **HA** did not provide a propagating front. Figure reprinted and adapted with permission from *J. Polym. Sci., Part A: Polym. Chem.* **2019**, *57*, 982−988.[203] Copyright 2019, Wiley Periodicals, Inc.

specific power-to-weight ratios (P, W g^{-1}) for each monomer are approximated by multiplying ΔH_p by k_p. The propagation rate constants were either used directly or extrapolated from the corresponding Arrhenius parameters. To approximate the initiation process, the effective steady-state radical concentration, $[M^\bullet]_s$ (≈10^{-7} to 10^{-9} M),[37] was employed. The tabulated P values ignore initiator dependent effects (i.e., k_i), as well as termination related phenomena (i.e., k_t), but nevertheless provide a useful comparative metric from which optimal frontal design parameters may be derived.

Acrylate-derived monomers provide better power efficiencies than methacrylate architectures by at least an order of magnitude, as is observed in the difference between **MA** and **MMA** (or **HA** and **HMA**). Indeed, methacrylates polymerize slower than acrylates. Unsurprisingly, inert functionalities within a monomer reduce P. For example, **MA** generates more heat per second per weight than **HA**. The cross-linking acrylates, **HDDA** and **TMPTA**, exhibit reduced P when compared to monoacrylate analogues. On first inspection, this suggests that formulations containing multiacrylate substrates perform less efficiently (i.e., slow ν_f); there are several examples, however, where the opposite trend exists for ν_f: triacylates > diacrylates ≫ monoacrylates.[60,203,218] This may result from an increased local radical concentration that occurs with tethered acrylates. Phrased differently, the average mean path a tethered acrylate must travel during polymerization is shorter than for the monoacrylate counterparts. This affects the k_p and k_t to different extents and results in a net increase to the observed ν_f (i.e., the Trommsdorff−Norrish effect). Acrylamides exhibit P values intermediate to those observed for acrylate and methacrylate derived species.

Macromonomers (e.g., unsaturated polyesters) possess significantly less embodied energy than analogous small molecules, which in turn dramatically influences the FP process. For example, Fiori et al.[261] successfully demonstrated FP of unsaturated polyester resins in the presence of radical initiators (**Aliquat-PS**, **BPO**, and **AIBN**); such resins are

Table 6. Heats of Polymerization, Propagation Kinetic Parameters, and Estimated Specific Powers for Selected Monomers

	monomer	ΔH_p (J g^{-1})[a]	bulk E_a (kJ mol^{-1})[c,d]	A (M^{-1} s^{-1})[d,e]	T (°C)	calc. P (W kg^{-1})[f]
acrylates	**AA**	930 ref (180)	$k_{p,25°C}$ = 4.2 × 10^3 M^{-1} s^{-1} ref (295)		25	39
	MA	907 ref (180)	17.3 ref (296)	1.4 × 10^7	20	100
					150	930
	HA	500 ref (180)	18.5 ref (297)	2.8 × 10^7	20	70
					150	730
methacrylates	**MAA**	738 ref (180)	$k_{p,25°C}$ = 2.2 × 10^3 M^{-1} s^{-1} ref (295)		25	16
	MMA	560 ref (180)	22.4 ref (296)	2.67 × 10^6	20	2
					150	26
	HMA	344 ref (180)	$k_{p,25°C}$ = 1.4 × 10^3 M^{-1} s^{-1} ref (295)		25	5
	HEMA	385 ref (180)	21.9 ref (298)	8.9 × 10^6	20	4
					150	68
acrylamides	**Am**	1120 ref (180)	21 ref (299)	7 × 10^6	20	14
					150	200
	NMAm	738 ref (180)	–	–	–	–
	NIPAm	700[b] ref (180)	$k_{p,aq,pH=7,20°C}$ = 2.7 × 10^4 M^{-1} s^{-1} ref (298)		20	1[g]
crosslinkers	**MBAm**	537 ref (180)	–	–	–	–
	HDDA	650 ref (300)	$k_{p,80°C}$ ≈ 1.5 × 10^4 M^{-1} s^{-1} ref (301)		80	98
	TMPTA	653 ref (300)	$k_{p,80°C}$ ≈ 1.0 × 10^4 M^{-1} s^{-1} ref (302)		40	65

[a]Reported for liquid monomer converted into a crystalline polymer phase. [b]No reported value exists for **NIPAm**. Therefore, this value is approximated by the heat of polymerization for **Am** and the relative ratio of molar masses in the following equation: ΔH_p(**NIPAm**) ∼ ΔH_p(**Am**) × (molar mass **Am**)/(molar mass **NIPAm**). [c]Arrhenius activation energy parameter. [d]Propagation rates, k_p, are estimated at temperature T by the following equation: $k_p = A \times e^{-E_a/RT}$, where R is the fundamental gas constant and assuming that A is temperature independent. For some monomers, only the k_p could be found and is explicitly reported with the corresponding reference, and the relevant conditions are given in the subscript. [e]Pre-exponential Arrhenius factor. [f]The estimated specific power, P, at temperature T was calculated by the following formula: $P \approx k_p \times [M^\bullet]_s \times \Delta H_p \approx A \times e^{-E_a/RT} \times [M^\bullet]_s \times \Delta H_p$, where $[M^\bullet]_s$ is the steady-state radical concentration. Odian[37] noted that $[M^\bullet]_s$ is bounded in the range of 10^{-7} to 10^{-9} M; we assume that 10^{-8} best approximates $[M^\bullet]_s$ and is therefore used for all calculations. [g]Specific heats are provided for the aqueous solution, assuming a concentration of 0.2 M. In this case, the units are W (kg of solution)$^{-1}$.

https://doi.org/10.1021/acs.chemrev.2c00686
Chem. Rev. 2023, 123, 3237−3298

frontally cured by added styrene. These formulations, however, exhibited quite low ν_f in the range of (0.3 to 0.9 cm min^{-1}). In a subsequent report, the same group[260] avoided styrene due to its volatility, and instead substituted **HEA** or diurethane diacrylate (2-[6-(2-acryloyl-oxyethoxycarbonylamino)-hexylcarbamoyloxy]ethyl ester) as comonomers. With these altered resins, ν_f values existed in a larger range (0.3 to 15.5 cm min^{-1}), with T_{max} values of up to 230 °C. Nevertheless, unsaturated polyesters (and styrene) are significantly less reactive than acrylates in free-radical polymerization.

Perry et al.[283] mathematically modeled the effects of monomer composition on ν_f and T_{max} in copolymerization reactions. Perhaps unsurprisingly, the sensitivity of the frontal parameters on the monomer feed depend on the relative reactivity ratios of the two monomers. For reactivity ratios where $r_1 \leq r_2 \leq 1$, a concave relationship exists between ν_f or T_{max} and monomer fraction. That is, copolymerizations proceed with larger T_{max} and ν_f values than the corresponding homopolymerizations. In contrast, the opposite trend exists when $1 \leq r_1 \leq r_2$. Experimentally, copolymerizations of **MAA**, **AA**, or **Am** provided frontal parameters that reasonably matched the theoretically derived values. These results share a similarity with FROMP copolymerizations;[147] mixing rules only apply with monomers of similar reactivities.

Considerable Russian efforts in the mid-1990s to early-2010s focused on the design of metal-containing acrylate monomers.[284−294] Early work from Pomogailo and co-workers[294] investigated FP of first-row transition metal complexes of the type $[M^{II}(\mathbf{Am})_4(H_2O)_2(NO_3)_2]$ (M = Mn, Co, Ni, Zn) as potential platforms to generate inorganic−organic composite materials. Notably, these solid monomers underwent polymerization after melting and in the absence added radical initiators. Instead, the authors suggested that thermal decomposition of nitrate occurs to oxidize the bound **Am** ligands and initiate FP. Interestingly, the choice of metal influenced the ν_f with the following trend: Co^{II} > Ni^{II} > Mn^{II} > Zn^{II}. Unlike linear p(**Am**), however, these coordination polymers likely are cross-linked as they do not dissolve in common organic solvents. Thermomechanical tests of the resultant materials were compared to metal-free p(**Am**). Upon heating, the purely organic polymer enters a viscous-flow state at temperatures near 80 °C. In contrast, the polymers generated from these metal-containing monomers possess an ultimate strain. These data suggest that cross-linking occurs, presumably through coordination at the metal center. Subsequent reports focused on fabrication of composite materials,[285−287,291,293] as well as modeling front propagation through phase transitions.[284,288,290]

4.3.5. Solvent Considerations. The majority of systems employ neat, solvent-free conditions; several monomer-initiator pairs, however, require the use of solvent. As noted above, solvents depress the frontal velocity and temperature in three ways. The heat of polymerization per solution weight decreases as the reactive monomer constitutes a smaller wt% of the total formulation. Second, the observed rate of polymerization decreases in response to dilution. Third, according to its thermal capacity, the solvent acts as a potential heat sink by absorbing heat. The first example of solution-state FP was published by Pojman et al.,[223] in which **Am** and **KPS** were dissolved in DMSO, DMF, or water. After thermal ignition, only DMSO-derived fronts were bubble-free. While propagation does occur in water, vapor formation prohibits ideal polymer morphology. In contrast, DMF solutions exhibit convective instabilities that impede efficient front propagation. These instabilities are somewhat mitigated if *N,N′*-methylenebisacrylamide (**MBAm**; 1 wt %/wt) is added as a comonomer. Solvent dilution accesses tunable ν_f values, which provides a major advantage over neat formulations where monomer concentration is constant. From the data in Figure 19, a near linear correlation exists between monomer

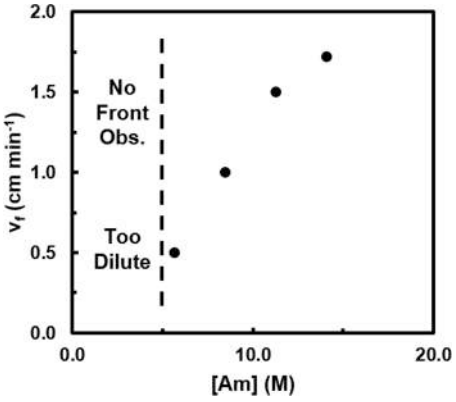

Figure 19. Monomer concentration in DMSO dictates the value ν_f in the FP of **Am** with **KPS** (18 mM) as the radical source. Figure reprinted and adapted with permission from *J. Am. Chem. Soc.* **1996**, *118*, 3783−3784.[223] Copyright 1996, American Chemical Society.

concentration and frontal velocity. Front propagation required an [**Am**] of at least 5 M. Below this value, the high solvent content precluded front ignition and self-propagation.

The vast majority of solvent assisted FP reactions occur in the synthesis of hydrogel materials (see section 5.1 for a detailed disicussion; refs 49, 61, 84−90, 208, 209, 212, 213, 220, 229, 230, 232, 233, 236, 237, 239, 263−267, 270, 271). Frontally derived hydrogels are typically generated from formulations diluted with DMSO, glycerol, or *N*-methyl-2-pyrrolidinone (**NMP**), though several aqueous examples exist.[58,61,208,209,228] Bubble-free aqueous mixtures require T_{max} values below 100 °C, which decreases the initiator's upper concentration limit. For example, the FP of **AA** under aqueous conditions only provided stable fronts with **KPS** loadings in the narrow range of 0.2−0.7 wt %.[58]

In contrast to typical solvents used in solution-state FP, several examples of FP in an ionic medium exist. Reports from Mota-Morales et al.[91,303,304] and Fezende et al.[305] demonstrated that deep eutectic solvent mixtures support polymerization propagation. Unlike traditional ionic liquids with complex charged components capable of facile solvent separation, deep eutectic solvents are comprised of hydrogen bonding donor/acceptor pairs. Typically, one (or both) of these components is a salt (e.g., choline chloride). In the context of FP, **AA**, **MAA**, or **Am** serve as a polymerizable monomer as well as a hydrogen-bond donor. Moreover, deep eutectic solvent mixtures comprised of dual-function monomer (i.e., **AA** or **MAA**) provide fronts nearly three times faster than analogous resins with DMSO-solutions.[305]

Solvent-free polymerizations with high melting point monomers are also possible; solid monomers present a processability challenge in that uniform polymerization fronts require a preceding, narrow molten zone. Undesirable geometric perturbations occur with coincident melting and polymerization events. Additionally, monomer melting is endothermic, which redirects heat away from polymerization

https://doi.org/10.1021/acs.chemrev.2c00686
Chem. Rev. 2023, 123, 3237−3298

and dampens the propagation rate. Despite these obstacles, several solid-monomer systems exist, as highlighted in two examples by Pojman et al.[33,224] Solid reaction mixtures prepared from finely ground **Am** and **AIBN** (or **KPS**) were thermally ignited inside a glass tube; while a distinct molten region was not observed, the front temperatures exceeded the melting point of the monomer (T_{max} = 250 °C). A decrease in the temperature gradient occurred at 160 °C as a result of adventitious imidization, which generates volatile NH_3. A significantly larger thermo-spatial gradient exists in the reaction zone this system (dT/dx = 450 °C cm^{-1}) when compared to liquid or solution state fronts.[224]

4.3.6. Fillers and Additives. Filling materials modulate both the properties of the obtained polymers and the corresponding frontal process parameters. Such composite materials are highly desirable for many applications (see section 5.4). As with cationic epoxy FP (section 4.2.1), a large number of composite materials derived from radical FP exist (refs 33, 53, 84, 88, 127, 210, 213, 235, 242, 245, 246, 250, 251, 270, 306). Two studies by Viner and Viner[127,235] investigated the effects of fillers for frontal cyanate ester polymerizations. The base formulation in these studies consisted of **TMPTA** and **Luperox-231** (10.4 phr). In addition to this, a dicyanate resin (1,1-bis(4-cyanatophenyl)ethane, **Primaset LeCy**) in aniline (3.6 phr) was added to form a binary monomer mixture. An inert filler, either fumed silica (**Cab-O-Sil M-5**) or kaolin (**Polygloss 90**), thickened the formulations and altered the processability of the prepolymer mixtures. An additional test sample included both these inorganic fillers. The resultant preignited materials with silica displayed putty-like consistencies, whereas the inclusion of kaolin provided a more fluid-like mixture.

The filler and compositional effects on the frontal parameters are given in Figure 20. In contrast to the observed trends with filled epoxy systems, Viner observed that kaolin dampened the frontal parameters substantially more than fumed silica. Increases in the acrylate mass percentage amplified these effects, particularly with v_f; fronts derived from silica-filled formulations propagated at nearly double the velocity of the kaolin analogues.[127] Differences in convection

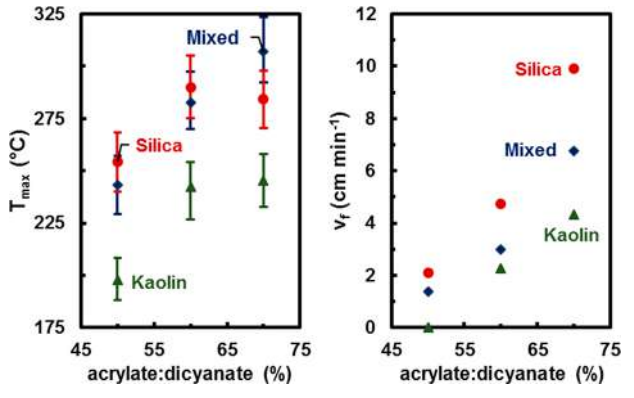

Figure 20. Plots of T_{max} (left) and v_f (right) values as a function of filler and monomer composition. Acrylate portion corresponds to a mixture of **Luperox-231** (10.4 phr) in neat **TMPTA**. Dicyanate portion corresponds to **Primaset LeCy** in aniline (3 phr). The ratio of acrylate:dicyanate corresponds to the mass percent of two different components in the final formulation. Figure reprinted and adapted with permission from *J. Phys. Chem. B.* **2011**, *115*, 6862−6867.[127] Copyright 2011, American Chemical Society.

rationalized this behavior; the higher viscosity of silica containing mixtures prevented buoyancy-driven convection to a greater degree, thereby mitigating convection driven heat-loss processes.

A subsequent report by Viner[235] investigated a 2-dimensional binary system, whereby the heat from one FP ignites a second event. Specifically, a strip composed of acrylate monomers was thermally ignited to propagate a front in one direction. The residual heat from the acrylate strip ignited a dicyanate strip to induce the ignition of a second, orthogonally propagating front. Due to differences in reactivity, the range of accessible v_f for the acrylate front was significantly larger than that for the dicyanate ester front (30−70 vs 0.5−2 cm min^{-1}, respectively).[235]

More recently, Lessard et al.[167] described a tandem FROMP to frontal radical polymerization (FRaP) system as depicted in Figure 21. The propagation behavior, and resultant material

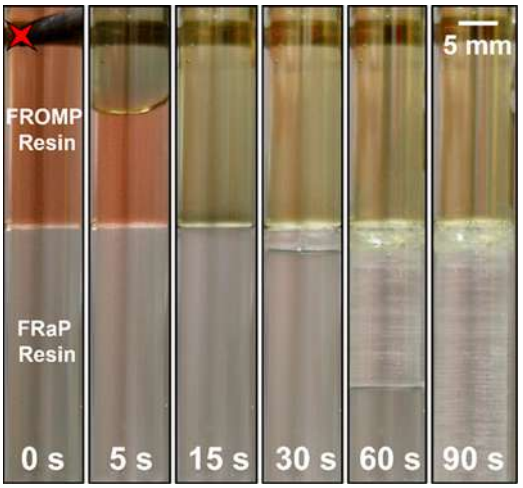

Figure 21. Time evolution of tandem FROMP to frontal radical polymerization (FRaP). This method fabricates layered, biphasic materials after thermal initiation in the topmost FROMP layer. Figure reprinted with permission from *ACS Macro Lett.* **2022**, *11*, 1097−1101.[167] Copyright 2022 American Chemical Society.

properties, varies throughout the two phases of the final layered, biphasic thermoset. Propagation occurs through two separate modes of FP, with characteristic T_{max} and v_f values unique to each layer. Surprisingly, the boundary between FROMP and FRaP exhibits adhesion strengths of up to 3.6 MPa, as determined by tensile testing. The propagation behavior and subsequent mechanical properties of these mixed materials vary substantially with the location of the triggering event. For example, samples initiated in the bottom-most FRaP layer generate porous foams as the result of bubble formation. In contrast, samples initiated from the topmost FROMP layer provided welded thermosets without voids. Intriguingly, initiation at the interface or topmost FROMP layer generated periodic striations in the surface topology of the FRaP layer, presumably as the result of thermal (or convective) instabilities.

Precedent exists for organic/polymeric materials as fillers in radical polymerizations.[161] Similarly, frontally derived composite materials that contain biopolymeric fillers exist.[250,251] Early work from Mariani and co-workers[161] demonstrated that two modes of FP (radical and FROMP) occur simultaneously in mixtures of **MMA**, **DCPD**, and **G1** with either **BPO** or **AIBN**.

https://doi.org/10.1021/acs.chemrev.2c00686
Chem. Rev. 2023, 123, 3237−3298

One may view the p(**DCPD**) interpenetrating network as an organic filler, though the mechanical and thermochemical properties of such polymers remain unexplored.

4.4. Stoichiometric Frontal Curing

Unlike the aforementioned FP types (sections 4.1 through 4.3), several examples exist of frontal curing with stoichiometric curing agents. In 1975 (and later in 1978), Artuiunian et al.[111] and Davtyan et al.[112] first demonstrated frontal curing of bisphenol A-type resins with amines. Specifically, epoxydiane oligomers (i.e., ED-20, ED-6) reacted with *m*-phenylenediamine. Two decades later, Chekanov et al.[307] examined frontal curing of bisphenol F diglycidyl ether (**BFDGE**) with stoichiometric quantities of Epicure 3371, an aliphatic amine curing agent. Such systems exhibited short pot lives (≈1 h)—an unavoidable consequence of high concentrations of amine sufficiently reactive to support a front. The thermochemical and mechanical properties of products provided frontally were compared to analogous batch-cure conditions. By DSC and DMA, the two manufacturing methods provided similar T_g values. Specifically, the DSC-measured T_g values taken from the second heating cycle were 146 °C for both manufacturing methods. In contrast, DMA-derived T_g values of 151 and 156 °C were measured for FP and batch-cured samples, respectively. The glassy-modulus (E') at 25 °C and E of both samples were identical within error, with values of ≈2.2−2.4 GPa. The tensile strengths of these materials, however, varied to a larger extent. Frontally derived amine-cured epoxy exhibited strengths of 68.2 ± 0.8 MPa, whereas the batch-cured samples were nearly 10% stronger (75.9 ± 3.6 MPa). Nevertheless, FP curing occurred nearly 10x faster ($\nu_f \approx 0.4$ cm min^{-1}) than batch curing, which highlights the practical advantage of frontal methods. The authors also studied composites derived from the addition of rubber particle fillers from ground car tires.

Mariani and co-workers[82,191] reported an effective strategy to bypass the decrease in ν_f observed in resins doped with inert poly(silicate) additives. Hybrid materials comprised of silicates obtained from suitable precursors (i.e., 3-glycidoxypropyl trimethoxysilane (**GPTMS**) or epoxycyclohexyl-POSS) and **BADGE** were synthesized with stoichiometric **DETA**. The copolymerization with **GPTMS** afforded fronts with typical T_{max} values in the range of 225 to 240 °C, which is far hotter than the UV-triggered systems reported in Table 7.[191] While frontal temperatures did not display a dependency on the molar fraction of **GPTMS**, a slight decrease in ν_f occurred with this monomer. Specifically, frontal velocities were measured to be 0.9 and 0.6 cm min^{-1} at 0 and 100 mol % **GPTMS**, respectively. Similar trends were observed in the copolymerization of **BADGE**, **DETA**, and a monomer derived from epoxycyclohexyl appended poly(silsesquioxane) cages ($C_{80}H_{130}O_{25}Si_{10}$, 1791 g mol^{-1}).[82] Frulloni et al.[308] developed a phenomenological model of front propagation for this system.

Table 7. Transition Temperatures for Copolymers of BADGE and GPTMS Initiated by Stoichiometric DETA[a,b]

[GPTMS]/[BADGE] (%)	T_{max} (°C)	ν_f (cm min^{-1})	T_g (°C)
0	232	0.8	51
2.5	225	0.8	60
5	237	0.8	63
10	235	0.8	58 and 77
50	228	0.6	59 and 86
100	235	0.5	70 and 150

[a]Conditions: Equimolar quantities of **BADGE** and **DETA** with varying [**GPTMS**] were ignited by soldering iron. [b]Data found *J. Polym. Sci., Part A: Polym. Chem.* **2010**, 48, 4721−4725.[191]

The hybrid organic−inorganic copolymers derived from **BADGE** and **GPTMS** displayed interesting glass-transition temperature behavior (Table 7). A single T_g exists at low loadings of **GPTMS**, which monotonically increases with additional monoglycidyl monomer. At variance, as indicated by the occurrence of two T_g features, phase separation occurs at a critical concentration of **GPTMS**. The lower value corresponds to a purely organic domain, whereas the higher T_g results from a silicate-rich region.[191] Unfortunately, the mechanical properties of these hybrid materials were not reported. The formation of hybrid organic−inorganic phases derived from frontal geopolymerization reactions are discussed in more detail in section 5.4.2. A subsequent report from Gill et al.[309] prepared polymer-dispersed liquid crystals from the frontal curing of **BADGE** with **DETA**.

Stoichiometric reaction types exhibit two key limitations. First, the frontal process parameters are difficult to modulate. As the reaction occurs at stoichiometric loadings of monomer to curing agent, a narrow window of accessible ν_f values exists. The concentration of curing agent cannot be varied without significantly impacting the reaction conversion and product material properties. Second, resins employed in this class of FP reaction typically suffer from poor pot lives. This presents a practical challenge for large-scale applications.

5. APPLICATIONS OF FRONTAL POLYMERIZATION

Several key aspects of FP enable a variety of intriguing applications that are otherwise inaccessible or impractical with traditional batch processes. The rapid reaction rate and low energy input cause FP reactions to outperform bulk analogues in terms of time, energy, and cost efficiencies. The temperature uniformity of the reaction zone for stable propagation provides polymers with homogeneous properties; in contrast, bulk methods often suffer from localized hot spots. Moreover, the fast curing achieved in frontal systems can "freeze" out unusual and well-defined microstructures (e.g., microporosity); the extended reaction times in classical techniques often impedes uniform microstructures. Additionally, the processing window of frontal formulations, as measured by the storage lifetime, may enable integration into several technologies (e.g., 3D printing) that cannot employ traditional methods. Given these considerations, most application driven reports fail to highlight in which ways FP is more advantageous than batch methods.

Earlier reviews in this field focused primarily on polymer chemistry and instabilities associated with FP.[29,45,124] Moreover, a large volume of applied frontal systems have been reported over the last 5 years, particularly toward the development of novel materials. A need exists, therefore, to document and analyze all the potential applications in order to highlight successful design parameters for future studies in the field. This section of the review aims to fill the aforementioned absence to inspire new and creative possibilities for FP.

5.1. Hydrogels

FP exhibits promise toward hydrogel synthesis—that is, materials characterized by reversible swelling behavior in the presence of a liquid medium (often water). The swelling ratio (SR%) describes the degree of solvent incorporation into a

https://doi.org/10.1021/acs.chemrev.2c00686
Chem. Rev. 2023, 123, 3237−3298

material, and typically compares the mass (or volume) of the dried polymer (M_d) to that of the solvent swollen sample (M_s), as illustrated in eq 13:

$$\mathrm{SR\%} = \frac{(M_s - M_d)}{M_d} \times 100 \tag{13}$$

Hydrogels are typically composed of highly cross-linked, semiporous hydrophilic polymers and often exploit bioderived components (e.g., β-cyclodextrin) to impart biomimetic functionality. Frontally prepared hydrogel materials, therefore, have proven useful toward a variety of applications, ranging from shape persistent gels to drug delivery agents.[208,310,311] Given the wide functional diversity, it is essential to control pore-size and morphology while also retaining desirable mechanical properties (e.g., flexibility, toughness).[310] The exothermicity of traditional batch polymerization methods limit the uniformity within hydrogels; phase separation, for example, occurs in copolymers derived from *N*-isopropylacrylamide (**NIPAm**) via high temperature curing.[49] Reducing the curing temperature in the batch reactors mitigates these effects somewhat; unfortunately, lower cure temperatures diminish the degree of gelation as well as the polymerization rate, which hampers practical implementation. In contrast, FP reactions offer uniform temperature control within the reaction zone without sacrificing reaction rate. The latter also circumvents phase segregation, as clearly demonstrated by Alzari et al.,[312] wherein uniformly dispersed graphene-containing nanocomposites of p(**NIPAm**) were synthesized. Compared to traditional BP methods that resulted in graphene reaggregation during polymerization, FP occurred far faster and therefore limited accumulation of the compositing filler. It is unclear, however, whether larger scale implementation of this frontal approach is compatible with economical manufacturing.

The physical properties of hydrogels synthesized frontally are comparable, if not better than, traditional synthesized analogues. To date, more than 30 reports detailing the synthesis and properties of frontally prepared hydrogels exist (refs 61, 84−90, 206−209, 212, 213, 220, 228, 229, 232, 233, 236, 237, 239, 243, 244, 249, 252, 254, 256, 258, 263−267, 270, 271, 306, 313).

5.1.1. Synthesis, Porosity, and Swelling. Nearly all hydrogels synthesized frontally employ free-radical polymerization processes, as discussed in section 4.3. To achieve the desired degree of porosity, the synthesis requires a high boiling solvent, typically DMSO. Solvent incorporates into the gel during polymerization, and after reaction completion, it is rigorously removed to reveal void space capable of reversibly housing liquids. Washington and Steinbock[49] described an early example that consisted of **NIPAm** (5 g) and **APS** (20 mg) in DMSO (2.5 mL); cross-linking occurred by inclusion of **MBAm** (50 mg) into the reaction mixture. Polymers derived from conventional batch techniques at 60 °C were synthesized for comparison and the morphologies of the resultant batch and frontally prepared polymers are depicted in Figure 22. While both samples display porous microstructures, only the frontally synthesized material exhibits a uniform pore size distribution. The conventionally prepared hydrogel contains a microaggregate phase interlaced into the pore structure. The difference in microstructure results from the nature of the reaction zone. In frontal processes, localized, rapid temperature changes occur to lock-in a single microstructure on a faster time-scale than phase separation. Batch reactor conditions, however, occur via multiple reaction zones with lower localized temperatures. As a consequence, the polymeric microstructure suffers due to phase separation processes enabled by the longer required curing times.

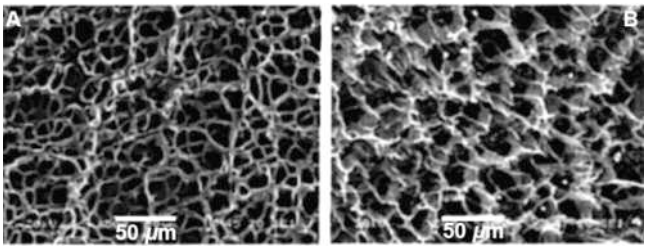

Figure 22. Scanning electron micrographs (SEM) of hydrogel polymers derived from frontal (A) or conventional curing (B) polymerization methods. Frontal formulation consisted of **NIPAm** (5 g), **APS** (20 mg), **MBAm** (50 mg), and DMSO (2.5 mL). Front initiation occurred via thermal ignition. Figure reprinted and adapted with permission from *J. Am. Chem. Soc.* **2001**, *123*, 7933−7934.[49] Copyright 2001, American Chemical Society.

The microstructural differences are borne out in the swelling ability of the two hydrogels (Figure 23), in that frontal samples exhibit increased SR% than batch polymers. Interestingly, temperature influences the swelling properties for both samples. Below 32 °C, these polymers absorb roughly 10 times their own weight in water, though superabsorbent materials (i.e., with SR% in water up to 35000%) were also synthesized (*vide infra*).[87,314] Increases in temperature, however, inhibit the swelling behavior of both samples. Such thermoresponsive swelling properties are well understood, and the inflection point of this plot (≈32 °C) is known as the lower critical solution temperature (LCST).[315] This phenomenon is generally ascribed to a decrease in hydrogen-bonding capability of the polymer that results from the thermodynamics associated with mixing. Water adsorption into the hydrogel occurs with a favorable enthalpic term, but at an entropic cost inherent to a highly ordered state (i.e., $\Delta S < 0$). At high temperatures, therefore, entropic factors are prevalent and induce water phase separation from the polymer in the form of deswelling.[315] Numerous literature examples of temperature responsive hydrogels generated frontally exist (refs 49, 85−90, 220, 228−230, 237, 312, 313, 316−321).

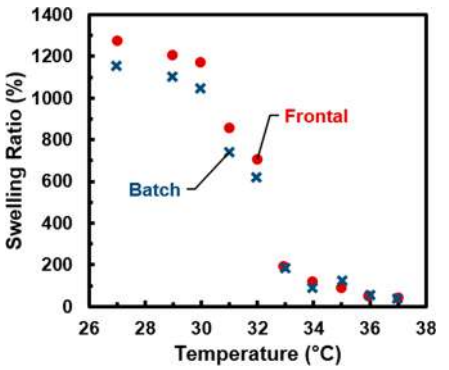

Figure 23. Plot of the temperature dependent aqueous swelling ratio for hydrogels consisting of p(**NIPAm**) generated frontally or via traditional batch methods (at 60 °C). Both samples display a LCST at ≈32 °C. Figure reprinted and adapted with permission from *J. Am. Chem. Soc.* **2001**, *123*, 7933−7934.[49] Copyright 2001, American Chemical Society.

https://doi.org/10.1021/acs.chemrev.2c00686
Chem. Rev. 2023, 123, 3237−3298

Monomer composition influences the swellability of the hydrogel since solvent incorporation is an enthalpically driven process, governed primarily by monomer−solvent hydrogen bonding networks. Unsurprisingly, polar or charged monomers offer the strongest hydrogen bonding capabilities. The most common formulations include mixtures of monomers bearing nitrogenous functionalities (e.g., acrylamide, imidazole, lactam). Alzari et al.[90] explicitly described the compositional effects on swelling of hydrogels, which provides several representative trends (Table 8). The specific formulations were derived from a mixture of **NIPAm** and **NVCL** in DMSO, with added **TEGDA** as a cross-linking agent and **APS** as the radical initiator. In this study, the homopolymers (Table 8, entries 1 and 2) displayed reduced swelling capacity at 25 °C than the copolymers (Table 8, entries 3 and 4).[90] Composition did not greatly affect the observed LCST values; all of the thermoresponsive hydrogels in this study exhibited LCST behavior in the range of 25−35 °C. Interestingly, the transition temperatures for the copolymers (Table 8, entries 3 and 4) exceeded those of the homopolymers (Table 8, entries 1 and 2), which illustrates nonlinear mixing behavior. Unsurprisingly, increases in the **TEGDA** concentration reduced the porosity of the resultant cross-linked polymer, thereby diminishing the SR % (Table 8, entry 5 vs 4).

Table 8. Swelling Ratios, LCST Values, and T_g for Various Frontally Derived Hydrogel Compositions Derived from Monomers NIPAm, TEGDA, and NVCL[a]

entry	NVCL: NIPAm[b]	TEGDA (mol %)	SR_{25} (%)[c]	LCST (°C)	T_g (°C)
1	1:0	2.5	280	31	147
2	0:1	2.5	480	28	142
3	1:3	2.5	690	30	146
4	1:1	2.5	590	31	153
5	1:1	10	180	27	154

[a]As reported in *Biomacromolecules* **2009**, *10*, 2672−2677.[90] [b]Ratio of **NVCL** to **NIPAm**. The combined molar amount of **NVCL** and **NIPAm** was fixed at 7.2×10^{-2} mol. Formulations included DMSO (2.5 mL) and **APS** (0.5 mol %). [c]Aqueous swelling ratio measured at 25 °C.

Indeed, the compositionally dependent swelling behavior arises as a result of the microstructural differences, as observed by SEM.[90] The homopolymer derived from **NIPAm** (Table 8, entry 2 and Figure 24A) exhibits pores with diameters nearly 10 times smaller than those obtained in the 1:1 copolymer (Table 8, entry 4 and Figure 24B). Porosity is lost upon addition of 10 mol % cross-linker, and only a smooth cross-section exists (Table 8, entry 5 and Figure 24C).

Hydrogels derived from charged monomers demonstrate superb absorbency. Formulations reported Scognamillo et al.[87] utilized the potassium salt of 3-sulfopropyl acrylate (**SPAK**) in the copolymerization with **Am** to generate "super" absorbent hydrogels. Samples comprised of at least 60 mol % **SPAK** displayed SR% at 25 °C in the range of 3000−14000%. Increases in **SPAK** content translated into enhanced swelling and higher LCST values (up to ≈36 °C). The hydrophilicity of the copolymers, as measured by water contact angle, offers a plausible explanation for the observed swelling behavior; the homopolymer of **Am** is reasonably hydrophobic with a large angle of 87°. In contrast, **SPAK** copolymers are characterized by contact angles as low as 33°. Interestingly, the reverse trend

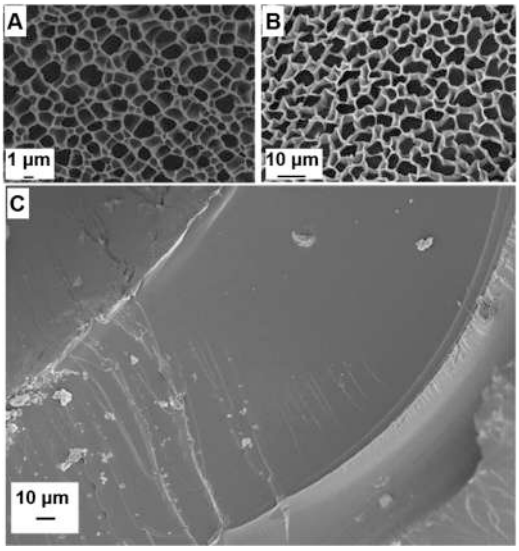

Figure 24. Scanning electron micrographs (SEM) of hydrogel polymers with varying monomer composition. The compositions are reported in Table 8, Entries 2 (A), 4 (B), and 5 (C). Figure reprinted and adapted with permission from *Biomacromolecules* **2009**, *10*, 2672−2677.[90] Copyright 2009, American Chemical Society.

occurred with the frontal parameters T_{max} and ν_f; addition of **SPAK** to the hydrogel formulations depressed both values.[87] It is unclear, however, if the swelling properties are directly correlated to these values.

In a subsequent research effort, a thermoresponsive p(**NIPAm**-*co*-**SPAK**) superabsorbent hydrogel was frontally prepared in the presence of **MBAm** as a cross-linker.[314] By properly changing the ratio between the three components, the swelling behavior of such **NIPAm**-derived hydrogels ranged from about 1000% (**MBAm**, 5 mol %) to 35000% (**SPAK**, 87.5 mol %; **MBAm**, 1 mol %). The absorbent features of these hydrogels were ascribed to different affinities toward water, as assessed by contact angle measurements. Specifically, these angles ranged from 37 to 74°.

Solvent and initiator concentration influenced the swelling ability of frontally prepared hydrogels, as described by Caria et al.[89] Homopolymer hydrogels of *N*,*N*-dimethylacrylamide (**NDMAm**) were prepared with varying amounts of **APS** under three solvent conditions (solvent-free, aqueous, and DMSO). Polymers prepared in DMSO or without solvent adsorb nearly twice as much as those derived from aqueous mixtures. The reason for the solvent effect is straightforward from a microstructural perspective. Hydrogels prepared in water in this study displayed dense structures with minimal porosity. In contrast, samples prepared either neat or in DMSO afforded porous structures akin to those described for related systems in Figures 22 and 24. All three solvent environments afforded homopolymers with LCST values of ≈33 °C. The homopolymer swelling capacity only displays a strong correlation to initiator content in certain solvents (Figure 25). The hydrogels derived from neat or aqueous formulations display an exceedingly weak dependency on the initiator content. In contrast, mixtures prepared in DMSO exhibit a positive correlation for **APS** loadings between 0.5 and 2.0 wt %. The underlying cause of the solvent-initiator synergistic effect on swelling remains unknown.

A related class of stimuli responsive hydrogels exists, wherein changes in pH dictate the swelling behav-

https://doi.org/10.1021/acs.chemrev.2c00686
Chem. Rev. 2023, 123, 3237−3298

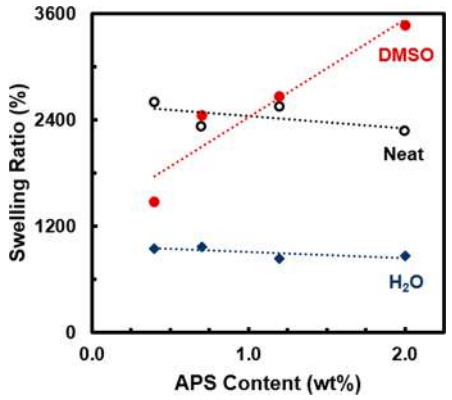

Figure 25. Plot of the aqueous swelling ratio measured at 26 °C for homopolymers of **NDMAm** prepared frontally as a function of **APS** content and formulation solvent. Formylations included 1 wt % of **MBAm** as a cross-linking reagent. Dotted lines correspond to the linear regression for each solvent employed in the frontal formulation. Figure adapted with permission from *J. Polym. Sci., Part A: Polym. Chem.* **2009**, *47*, 1422−1428.[89] Copyright 2009, Wiley Periodicals, Inc.

ior.[84,85,233,236,239,244,264−267,270] Such polymers require monomer compositions that contain Brønsted acidic or basic functionalities; the protonation state of these side chains dictates the hydrophilicity (or hydrophobicity) of the polymer, since charged species afford enhanced hydrogen bonding. Monomers bearing basic amine (e.g., **Am**, **NIPAm**) or *N*-substituted heterocyclic (e.g., **VI**, **NVP**) side chains swell in low pH solutions. Conversely, carboxylic acid containing monomers (e.g., itaconic acid, **AA**, **MAA**, or **HEMA**) swell under basic conditions. Copolymers comprised of *both* basic and acidic monomers, such as p(**VI**-*co*-**AA**), are swollen at non-neutral pH values.[85] Figure 26 depicts a representative

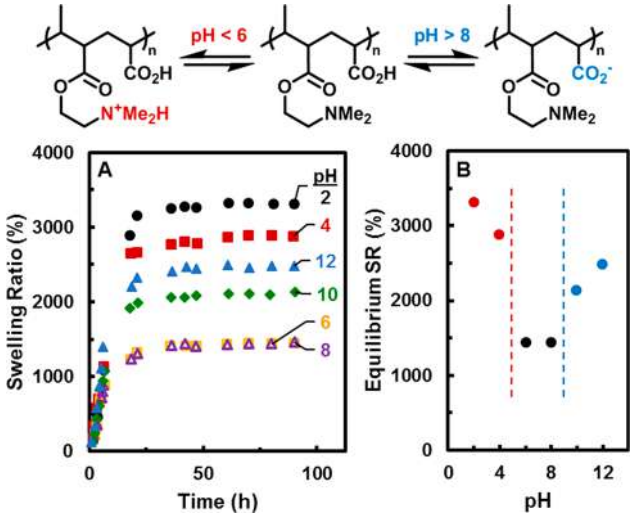

Figure 26. Aqueous swelling of poly(**DMAEMA**-*co*-**AA**) hydrogels prepared frontally. A: Plot of the aqueous swelling ratio as a function of time and solution pH. Hydrogels were kept at room temperature. B: Final equilibrated swelling ratio versus solution pH. The red region corresponds to amine protonation, whereas the blue region corresponds to carboxylic acid deprotonation. Improved swelling occurs in both of these regions compared to neutral pH values (black region). Data adapted from *RSC Adv.* **2015**, *5*, 30154−30521.[266] Copyright 2015, Royal Society of Chemistry.

example of pH dependent swelling for a copolymer comprised of **AA** and dimethylaminoethyl methacrylate (**DMAEMA**) prepared via laser ignition.[266] While traditional solution-state polymerization methods allow the synthesis of such polymers, frontally generated hydrogels exhibit stronger pH dependencies as minimal side chain aggregation occurs, thereby providing finer control over pore-size distribution.

5.1.2. Ion Removal Reagents. Stimuli-responsive hydrogels are promising candidates for a number of practical applications. The removal of toxic heavy metal ions from water sources, for example, highlights one such area of research that benefits from FP.[233,236] Such polymers contain Lewis basic side chains (i.e., imidazole, carboxylate), which strongly bind metal ions in a fashion reminiscent of natural metalloproteins and cofactors (e.g., hemoglobin, photosystem II).[322] An efficient, multiuse ion removal reagent, however, must also desorb efficiently under a different set of conditions. For this reason, frontally derived hydrogels with refined pH dependent swelling properties are an attractive sol−gel material for reversible ion capture, as detailed in several reports from Chen and co-workers.[46,233,236,263−266]

In an initial study, Chen and co-workers[263] described the laser-ignited FP of formulations comprised of **NMAm** and **NVCL** with added solution- or solid-state Pb^{2+} ions; efficient Pb removal occurred due to complete incorporation into the polymeric network. This precedent enabled the design of swellable hydrogels for metal sequestration, as illustrated in a representative example by Fan et al.[265] (Figure 27). Copolymer hydrogels of the type p(**VI**-*co*-**Am**) were synthesized by laser-ignited frontal radical polymerization. The resultant polymers exhibit shape persistence and retain the geometry of the mold-like reaction vessels to give a variety of topologies (e.g., hearts, stars, letters).[265] Ion sequestration studies employed colorless cylindrical hydrogel tubes, which were immersed in 10 mM aqueous MCl_2 [M = Mn, Co, Ni, Cu, Zn, Cd] solutions. Ion adsorption into the hydrogel networks induced surprising volume contractions of the materials despite increases in their masses (Figure 27A), which resulted from metal assisted cross-linking. The functional groups on the polymer side chains (i.e., imidazole, acrylamide) act as Lewis basic ligands which form complexes with the added metal ion. Hence, the radius of the cylindrical cross-section exhibited an inverse dependence on the strength of metal coordination. For example, closed shell d^{10} (Zn^{2+} and Cd^{2+}) and high-spin d^5 (Mn^{2+}) ions exhibit the largest radii as a result of poor complexation with the imidazole side-chains.

Color changes occurred from the adsorbed metal complexes. The efficiency of adsorption was determined by concentration changes in the solution mixture after equilibration. To determine the reversibility of ion sequestration, hydrogels containing the adsorbed ions were submerged in aqueous HCl (0.5 M) for 5 h. Under acidic conditions, the metal ions reformed the solvated MCl_2 species and desorbed from the polymer. The efficiencies of adsorption and desorption were relatively similar (Figure 27B); near quantitative desorption occurred. Indeed, these hydrogel samples could undergo multiple adsorb−desorb cycles without significant loss in efficiency; after 4 cycles, 87% of adsorbed ions were removed by HCl treatment. The kinetics of the adsorption process (Figure 27C) indicated that saturation occurs after ≈10 h.[265] It is unclear, however, how the ion capture would behave under practical conditions such as a continuous flow apparatus.

https://doi.org/10.1021/acs.chemrev.2c00686
Chem. Rev. 2023, 123, 3237−3298

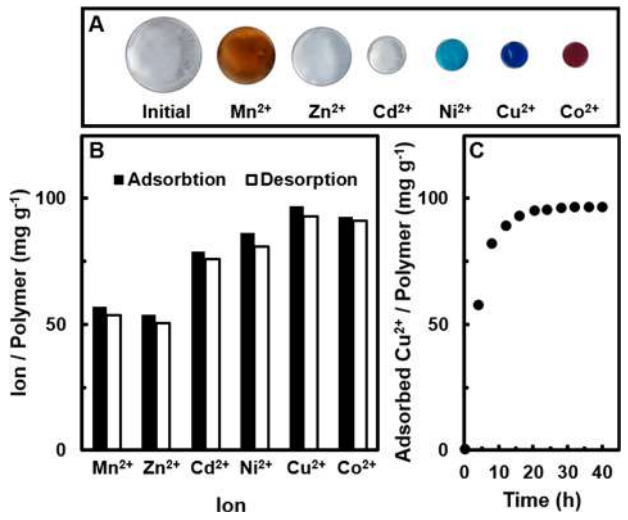

Figure 27. Ion adsorption and desorption data for a frontal hydrogel copolymer consisting of equimolar amounts of **Am** and **VI** synthesized by laser-ignition. A: Photographs of the cylindrical cross-section of the hydrogels before and after metal ion absorption. The diameter of the cross-section decreases after absorption due to chelation assisted cross-linking. The color of the adsorbed polymers results from the chelation complexes generated within the polymer. B: Adsorption (filled) and desorption (unfilled) data for each metal ion measured by the following equation: $Q_a = (C_0 \times V_0 - C_f \times V_s) \times (MW/M_p)$, where Q_a is the adsorption capacity of the polymer (mg g^{-1}); C_0 and C_f are the concentrations of metal ion in the adsorption medium before and after swelling, respectively; V_0 and V_s are the volume of the adsorption medium before and after swelling, respectively; MW (g mol^{-1}) is the molecular mass of the metal ion; M_p (g) is the mass of the unswollen polymer. Desorption is measured with an analogous equation. Note that incomplete desorption occurs after 1 cycle. C: Kinetic profile of Cu^{2+} adsorption versus time. The hydrogel reaches saturation in Cu^{2+} after ≈20 h. Figure adapted and reprinted with permission from *Applied Physics A* **2016**, *122*, 599.[265] Copyright 2016, Springer-Verlag Berlin Heidelberg.

Similar hydrogel compositions were reported by Wang et al.[236] for desalinization purposes.

Similar to heavy metal contamination, dye waste streams generated by the textile industry often infiltrate local water supplies, which adversely impact human health and the environment.[323] Liu et al.[266] extended the capabilities of swellable hydrogels toward the removal of charged organic dyes; specifically hydrogels composed of **AA** and **DMAEMA** exhibit a pH dependent adsorption behavior with cationic (methylene blue) or anionic (orange G) dyes. In this example, adsorption occurs via charge paired complexation of the dye to a specific receptor-like side chain. Cationic analytes bind the most strongly to negatively charged fragments (i.e., carboxylate), whereas the inverse trend occurs with anionic dyes. Hence, the pH dependency of each class of dye correlates to the protonation state of just one of the monomer side chains; cationic dyes adsorb more strongly in basic conditions, whereas the anionic dyes are best incorporated at low pH.[266] Interestingly, incorporation of activated carbon into the frontal formulation enhances the total swelling capacity for crystal violet removal.[213]

5.1.3. Drug Encapsulation and Delivery. Controlled drug delivery is perhaps the most topical application of frontally prepared hydrogels, as a need exists for targeted and robust drug administration technologies.[324] Traditional oral drug delivery methods rely on frequent patient participation to maintain a steady-state concentration within the body, which introduces the possibility for the patient to accidentally over- or underdose. The mechanism for drug decomposition within the body introduces an additional challenge; concentration spikes occur immediately after consumption, followed by a slower decay process as the body breaks degrades the drug. Finally, ingestion precludes targeted, site-specific drug delivery, thereby limiting the concentration at the desired organ.[324]

Hydrogel polymers offer an intriguing solution to the problems inherent with traditional administration methods.[324] By incorporating drugs into a hydrogel network through adsorption, an additional kinetic step must occur for drug release; moreover, stimuli-responsive hydrogels moderate the drug release rate and provide a control mechanism for the location of drug desorption. For instance, certain drug-hydrogel composites may only desorb in basic conditions, thereby circumventing adventitious release within the stomach. Additionally, the typical water content within a hydrogel allows for varied drug encapsulation due to hydrophilic interactions between the polymer host and the drug guest.[324] Indeed, these advantages are exploited for several hydrogels for controlled drug release.[91,208,237,313]

Gavini et al.[208] described the application of a hydrogel comprised of **Am** and prepared frontally toward the slow-release of the NSAID (nonsteroidal anti-inflammatory drug) diclofenac sodium and were compared to traditional batch polymers impregnated with drug. The drug release kinetics from the loaded hydrogels with varying cross-linker quantities were examined *in vitro* in aqueous phosphate buffered solutions (pH = 7.4). Unfortunately, the frontal and batch prepared hydrogels from this study underwent rapid and quantitative desorption at neutral pH after 2 h.

Modifications to the monomer composition outlined above, as well as the drug molecule, exhibited marked improvements in the controllability of drug release, as reported by Feng et al.[313] In this example, hydrogels comprised of **NIPAm** and **MBAm** as a cross-linker exhibited both drug adsorption and desorption properties. Drug loading into the polymer occurred over 3 days of treatment in a solution of aspirin (0.8 g) in ethanol (20 mL). In this example, substantial differences in drug storage capacity between frontal and batch synthesized hydrogels existed. Frontal systems contained 770 mg of aspirin (per g polymer), whereas the conventional analogue adsorbed nearly 25% less (590 mg g^{-1}). Indeed, these differences also exist in the desorption kinetics, as observed in Figure 28. The drug release rates vary with temperature; below the LCST of the polymer (i.e., 30−32 °C), complete drug release occurs within 15 h for frontally derived polymers. This value is extended somewhat to ≈40 h for the conventionally generated hydrogel, likely due to differences in porosity between the two materials (see section 5.1.1). At elevated temperatures such as those relevant to body temperature, the drug release rates substantially decrease to result in a complete desorption time of nearly 400 h. The dosage achievable with these materials exhibits promise for medicinal applications. Specifically, aspirin loaded hydrogels deliver ≈50−350 mg over a 12 h time span, whereas the batch polymers release only 50−200 mg. These values compare reasonably well to recommended dosage for regular consumption (50−325 mg), and are well below the maximum daily intake of 4000 mg.[313]

While the results for frontally synthesized hydrogels exhibit promise as candidates for controlled drug release agents, only a

https://doi.org/10.1021/acs.chemrev.2c00686
Chem. Rev. 2023, 123, 3237−3298

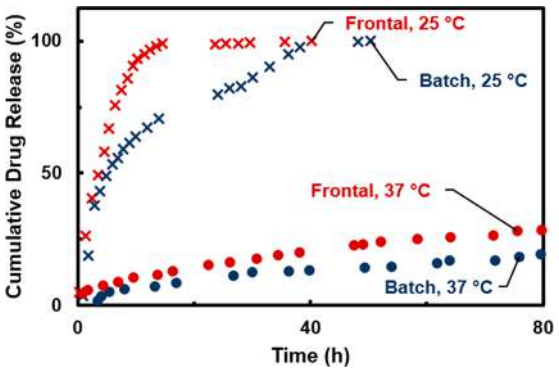

Figure 28. Aspirin desorption kinetics at 25 and 37 °C for hydrogels generated frontally (red) or through conventional batch processes (blue). Desorption occurred by immersion of the loaded hydrogel into 40 mL of a simulated body fluid solution. Hydrogels comprised of p(**NIPAm**) with added **MBAm** as a cross-linker. Figure adapted and reprinted with permission from *Colloid Polym. Sci.* **2010**, *288*, 915−921.[313] Copyright 2010, Springer-Verlag.

handful of pharmaceuticals have been explored.[91,208,237,313] Additionally, commercial-scale implementation requires a comprehensive study on the cytotoxicity of the hydrogel materials themselves; indeed, *in vivo* studies are necessary to gather further information useful to design biocompatible materials. To date, only a single study by Wang and co-workers[237] has investigated drug delivery kinetics within laboratory rats. For sustainable purposes, the hydrogel must undergo degradation only after expulsion from the patient. Comprehensive studies are required to fully develop frontally prepared hydrogels as practical, controlled drug delivery agents.[324] Purification of materials for medical applications, however, presents a major challenge for future advances. Biocompatibility requires complete removal of unreacted monomer (and solvent). It is unclear whether the economics of purification outweigh the benefits provided by the rapid frontal synthesis.

5.1.4. Synthesis of Interpenetrating and Supramolecular Polymer Networks. Some applications of hydrogels require structural properties to achieve the requisite degree of reliability and robustness. For example, reusable materials must display resistance to sustained conditions without loss of macroscopic structure or physical properties. On their own, hydrogels typically do not exhibit large tensile strengths, and are easily deformed, as observed in their stress−strain curves. In conjunction with an added material, a hydrogel composite exhibits enhanced durability without loss of swelling ability. Most hydrogel composites exist as interpenetrating polymer networks (IPNs) or supramolecular polymer networks (SPNs). According to IUPAC, IPNs are polymer systems comprised of two or more networks that are at least partially interlaced on a molecular scale, but not covalently bonded. Moreover, individual components of an IPN cannot be separated without breaking chemical bonds. On the other hand, SPNs result from spontaneous association of a large number of groups belonging to macromolecular chains.

The syntheses of INPs and SPNs (or binary systems more generally) occur by the concurrent generation of two discrete polymeric materials in the same reaction vessel (i.e., one-pot). Early work focused on FP of binary epoxy/acrylate resins.[325−327] A single thermal front propagates through monomer mixtures of **BADGE** and **TGDMA**, which suggested that radical and cationic polymerization mechanisms occurred simultaneously.[325] Recent developments in binary FP have primarily focused on the inclusion of thermoset polyurethane,[75,267] β-cyclodextrin[61,86,206,212,220,228,229,232] or SiO_2[84] as the secondary network.

Chen and collaborators[267] described the synthesis and mechanical properties of a compositionally complex composite material. Macromonomers of p**MMA** were block copolymerized with **VI** to afford p(p**MMA**-*b*-**VI**) via RAFT polymerization. Next, a mixture of this macromonomer, **AA**, **MBAm**, **BPO**, and presynthesized thermoplastic polyurethane (**TPU**) in *N*-methylpyrrolidinone was frontally polymerized after thermal ignition. The resultant IPN, p((p**MMA**-*b*-**VI**)-*co*-**AA**)/**TPU**, exhibited microscopic architectures dependent on the **TPU** composition, as observed by SEM. Samples composed primarily of poly(acrylates) displayed uniform macroporous structures. Addition of **TPU** (<12 wt %) to the formulation filled these large pores to afford a microporous morphology. While the pure hydrogel displayed a single T_g value (39.3 °C), an IPN with **TPU** (8 wt %) exhibited two T_g values that correspond to soft and hard segments of the polymer (−29.0 and +33.5 °C, respectively), the latter of which likely originates from pure **TPU**. Regardless, the two components were compatible as phase separation did not occur. The mechanical behavior of these polymers correlated to the quantity of **TPU** contained in the network, as is observed in Figure 29. The added **TPU** imparts the polymer

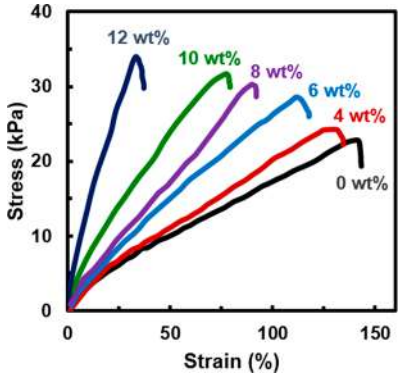

Figure 29. Stress−strain curves for IPNs comprised of thermoplastic polyurethane (**TPU**) and polymers derived from macromolecular monomers. The wt % corresponds to the **TPU** content in the final polymeric mixture. Increases to **TPU** wt % correspond to more rigid polymers, with high tensile strengths. Figure adapted and reprinted with permission from *J. Polym. Sci., Part A: Polym. Chem.* **2016**, *54*, 1210−1221.[267] Copyright 2015, Wiley Periodicals, Inc.

with increased structural stiffness (i.e., larger E values) as well as increases the IPN tensile strength. In exchange, the ductility is strongly reduced.

Cyclodextrin (**CD**) is a common additive in the preparation of SPNs, particularly in its β-form, as it imparts several desirable properties to the resultant materials. For example, **CD** is hydrophilic, and therefore attractive toward swelling hydrogels. Incorporation of **CD** also imparts enhanced rigidity and mechanical strength in a similar fashion to that of polyurethane-based IPNs. The uniform incorporation of this cyclic oligosaccharide requires either a direct covalent linkage[206,212] or host−guest[232] type interaction to avoid phase separation within the final polymer. Treatment of β-**CD** with maleic anhydride affords derivatized macromolecular

https://doi.org/10.1021/acs.chemrev.2c00686
Chem. Rev. 2023, 123, 3237−3298

monomers, which bear dangling cyclodextrin moieties.[206,212] Alternatively, inclusion of β-**CD** into formulations containing **VI** and **VCL** affords bound complexes of imidazole groups buried within the cyclic sugar-cage.[232] Indeed, this latter method presents the possibility of self-healing applications (see section 5.1.6).

The mechanical properties of p(**HEA**)/β-**CD** composites were investigated by Nuvoli and colleagues.[220] Samples comprised of 5 mol % β-**CD** exhibited unusual nonlinear stress−strain behavior (Figure 30A), with an estimated

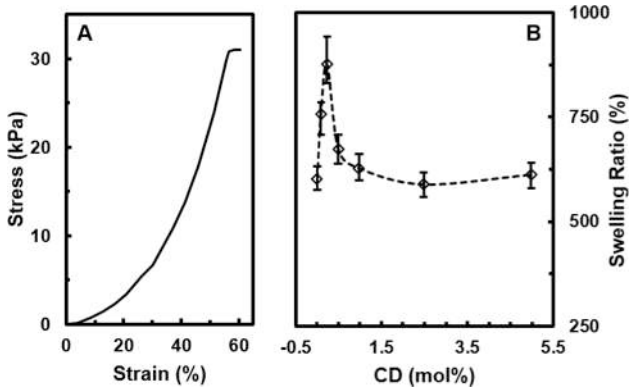

Figure 30. Mechanical and swelling properties of hydrogel composites comprised p(**HEA**)/β-**CD**. A: Nonlinear stress−strain behavior of a composite with 5 mol % β-**CD**. The Young's modulus is approximated as the slope of the tangent line at 30% strain (E_{t30} = 635 kPa). Fracture stress occurs at 30 kPa. B: Aqueous swelling behavior as a function of β-**CD** composition. Maximum SR% occurs with ≈1 mol % β-**CD** in the formulation. Figure adapted and reprinted with permission from *Carbohydr. Polym.* **2016**, *150*, 166−171.[220] Copyright 2016, Elsevier, Ltd. All rights reserved.

Young's modulus of 635 kPa as determined by the slope of a tangent at 30% strain (E_{t30}). Similar to other hydrogels discussed in section 5.1, these composite hydrogels exhibit compositionally dependent swelling of water (Figure 30B). Maximum swelling is achieved in formulations with ≈1 mol % β-**CD** due to its enhanced hydrophilicity when compared to virgin polymers. Further increases, however, result in consolidation of the microporous morphology and thereby reduce the accessibility of water and free volume for adsorption. Other IPN or SPN systems with β-**CD** exhibit similar swelling properties, though the specific nature of the frontally derived polymer dictates the total swellability in these hydrogels.[61,86,228,229]

5.1.5. Chemical Sensors. Stimuli-responsive swelling hydrogels (Section 5.1.1) exhibit interesting possibilities as chemical sensing materials, and several reported examples exist.[212,239,252,254,267,285] Effective chemical sensors rely on substantial differences of some quantifiable physical parameters (e.g., light absorbance/emission, resistivity, capacitance) when in the presence of an analyte.[328] Indeed, this type of behavior occurs for ion adsorbing hydrogels, as observed in Figure 27A, but adaptation to a quantifiable sensor has not yet occurred for metal ion detection. In the simplest sense, hydrogel polymers are moisture "sensors," as their size and mass change in response to humidity. For example, Zhao et al.[254] synthesized hydrogels of the type p(**Am**-*co*-2-acrylamido-2-methyl-1-propanesulfonate)-Zr^{4+} that self-actuate in the presence of water. Similarly, a recent paper by Gupta et al.[252] described the preparation of p(**Am**) hydrogels containing Sc^{3+} containing and their potential application in humidity sensing. Further work by Singh et al.[285] demonstrated that p(**Am**) materials produced from metal-containing monomers of Cd are effective sensors for liquefied petroleum gas.

A report by Yu et al.[239] described hydrogel composites which exhibit tongue-like sensing properties. Namely, stimuli-responsive hydrogels prepared by FP (see section 5.1.1) swell differently in the presence of flavor-like molecules. In this context, molecules associated with certain flavor sensations (e.g., citric acid = sour, sodium chloride = salty) are adsorbed to different degrees depending on the solution concentration. Adsorption occurs via electrostatic complexation, as well as H-bonding, between the charged polymer side chains and the flavor molecule, in a fashion similar to that described in section 5.1.2.

Interestingly, hydrogels saturated in flavor molecule exhibit unusual bending behavior when in the presence of an applied electric field.[212,239,267] While the charged side chains within the polymer are fairly immobile, the weakly adsorbed flavor molecules form a concentration gradient along the applied electric field. Overall, the charge-driven density differences within the hydrogel act as an actuator for a bending motion. The degree of bending directly relates to the concentration of adsorbed material, which provides a quantifiable sensing metric. The reported composites contain **TPU**[267] or β-**CD**[212] as an IPN or a covalent/supramolecular cross-linked polymer, respectively, to enhance the sensitivity, though another example employs embedded graphene-oxide.[239]

The results reported by Chen et al.[267] provide a representative example of this behavior, as is summarized in Figure 31 with five different "flavor" molecules. Specifically, analytes from four taste sensation classes (sour, sweet, umami, and salty) displayed concentration dependent swelling; the hydrogels adsorb less in high concentration solutions. The authors[267] suggest concentration dependent pH changes may account for the observed swelling, though a rigorous investigation into the operative origin is warranted. Under an applied DC potential of 25 V, the degree of bending correlates reasonably well with the solution concentration for most of the analytes, except for gluconic acid. Devices constructed from these hydrogels, however, likely cannot effectively differentiate analytes from one another given the narrow range of bending angles achievable.

5.1.6. Self-Healing Materials. Self-healing materials capable of repairing microscopic damage (e.g., cracks, fissures) present an intriguing avenue for applied polymer research.[329] The overabundance of single-use, disposable plastics pollutes the environment at an unsustainable rate; indeed, many polymers are discarded due to structural defects incurred under ambient conditions. Improved product longevity is obtained in materials that can effectively mitigate structural damage through a self-healing mechanism.[329] The mechanical properties of an effectively self-healed material must approach that of the virgin, undamaged one. To date, several concepts exist as guiding principles for the development of self-healing plastics. Researchers at the University of Illinois have successfully employed several strategies, which include polymers embedded beads[330] or microvascular channels[331] filled with fresh monomer or catalyst solutions. Upon damage, the space separating the two reagents ruptures, and rapid repolymerization occurs to fill the damage induced vacancy. In such examples, the healing chemistry involves ROMP of **DCPD** with Grubbs-type catalysts.

https://doi.org/10.1021/acs.chemrev.2c00686
Chem. Rev. 2023, 123, 3237−3298

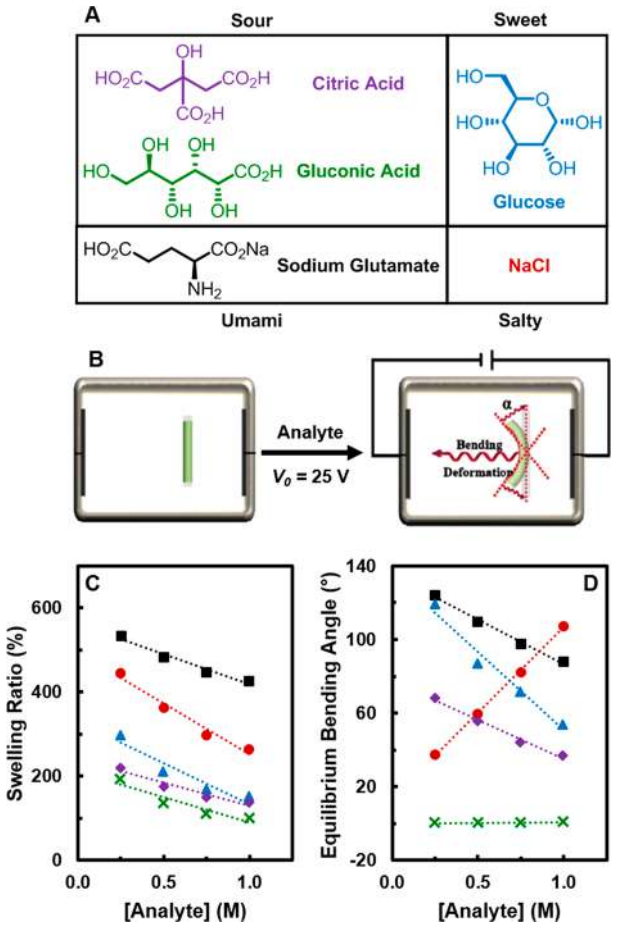

Figure 31. Chemical sensing abilities for an **IPN** hydrogel comprised of p((p**MMA**-*b*-**VI**)-*co*-**AA**)/**TPU**. The hydrogel material was suspended in an aqueous solution of analyte, and was subjected to a DC potential of 25 V. A: Chart of flavor-like analytes. B: Schematic of the bending behavior of hydrogels after adsorbing analyte in the presence an electric field. C: Plot of swelling ratios of the IPN hydrogels as a function of analyte concentration in solution. D: Equilibrium bending angle (α) after adsorption. Colors in **A** correspond to those of the data depicted in **C** and **D**. Note that for all analytes except gluconic acid, a linear dependency exists between solution concentration and bending angle. Figure adapted and reprinted with permission from *J. Polym. Sci., Part A: Polym. Chem.* **2016**, *54*, 1210−1221.[267] Copyright 2015, Wiley Periodicals, Inc.

In the context of FP, composite hydrogels are potential candidates for effective self-healing.[206,212,232,236,239,258] In contrast to the thermosetting self-healing with **DCPD**, hydrogels rely on weak side chain interactions to induce a repairing event. Indeed, H-bonding between side-chains in copolymers comprised of donor (2-hydroxypropyl acrylate, **HPA**) and acceptor (**NVP**) monomers can repair freshly cut samples.[239] Composites bearing β-**CD** undergo self-healing by host−guest interactions between imidazole-containing side chains and the inner cavity of the cyclic-oligosaccharide.[206,212,232,236] One potential limit with these materials, however, is that the mechanical properties of the undamaged polymers resemble those of elastomers.

Three recent representative examples from Chen and coworkers[212,232,258] highlight the efficiency of self-healing. The first report by Tsegay et al.[232] investigated self-healing behavior in p(**VI**-*co*-**NVCL**-*co*-**AA**)/β-**CD** supramolecular systems. The initial healing across two cut sections occurred within 30 s of being pressed back together. Full healing, however, required more than 12 h of undisturbed setting, which indicates that the temporal efficiency is governed by the kinetics associated with host−guest encapsulation. The tensile strength and elongation at fracture were examined for the pristine and fully self-healed samples, as summarized in Figure 32. Maximal self-healing

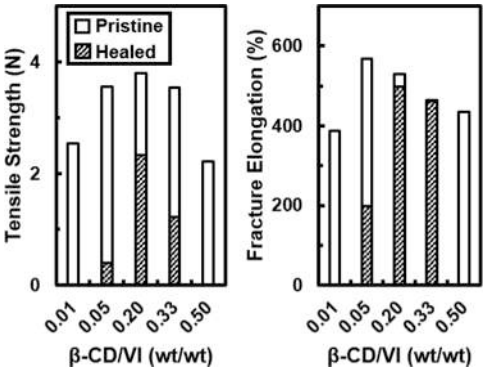

Figure 32. Tensile strengths (left) and elongation at break (right) for pristine (empty) and healed (filled) p(**VI**-*co*-**NVCL**-*co*-**AA**)/β-**CD** polymers. The best efficiencies occur at compositional ratios of 0.2 to 0.3 β-**CD**/**VI** (w/w). Figure adapted and reprinted with permission from *J. Polym. Sci., Part A: Polym. Chem.* **2018**, *56*, 1412−1423.[232] Copyright 2018, Wiley Periodicals, Inc.

occurred when the tensile strength and elongation at fracture of the two samples were closely matched. Interestingly, a compositional dependency on both mechanical properties exists. Indeed, polymers with β-**CD**/**VI** ratios of ≈0.2−0.3 exhibited the best self-healing abilities for both mechanical metrics. The authors also utilized microfluidic techniques in conjunction with FP to generate hydrogel supraballs from resins with methylsilicone oil as a diluent.

The same group[212] further examined the effect of healing time on the stress−strain behavior of repaired samples comprised of **AA** and β-**CD** grafted on maleic anhydride. Faster healing occurred by directly tethering the **CD** into the extended covalent network; efficiencies greater than 80% were observed after only 4 h. In this system, however, H-bonding appears to be the dominant pathway for healing as a pH dependency exists; efficient self-healing occurs only at pH <3. Repair does not need to occur between two flat surfaces. As observed in Figure 33, self-healing along curved edges afforded a variety of shapes and letters.[212]

Figure 33. Upper Left: Self-healing between two colored hydrogel cylinders comprised of **AA** and β-**CD** grafted on maleic anhydride. Lower Left: Stretching properties of the repaired polymer. Right: Shapes and letters accessible from self-healing between multiple segments. Figure reprinted and adapted with permission from *Ind. Eng. Chem. Res.* **2019**, *58*, 3885−2892.[212] Copyright 2019, American Chemical Society.

https://doi.org/10.1021/acs.chemrev.2c00686
Chem. Rev. 2023, 123, 3237−3298

5.2. Functionally Gradient Materials

Several niche applications require polymers with nonuniform properties throughout the bulk of the material, particularly those that exhibit an easily controlled gradient.[332−336] These so-called functional gradient materials (FGM) were first explored in Japan toward the fabrication of heat resistant composites for aerospace applications.[333] Spacecraft, such as the space shuttle orbiter formerly employed by NASA, require the usage of multiple layers of materials to ensure that its exterior can tolerate temperatures of ≈1800 °C without flambéing the personnel housed within.[333] An additional constraint requires the usage of lightweight, reusable, and highly durable materials.[337] Typically, a ceramic composite tiling serves as the heat resistant exterior layer atop a strong, thermally conductive metallic inner layer. The front edges of the shuttle employ all-carbon composites consisting of a rigid polymer resin reinforced with carbon fiber and painted with a black borosilicate glass coating.[337] In contrast to these layered composites, FGMs with a continuous compositional gradient may expand the potential uses beyond niche applications. Currently, some development of FGMs toward biomedical implants exists.[334,335]

Three reports (and one patent) highlight the adaptation of FP toward FGM synthesis.[149,204,221,338] Notably, the design of FGMs motifs is likely complicated or even inaccessible via classical polymerization as prolonged curing enables adventitious mass transport, which disrupts the desired gradation. An initial report by Chekanov and Pojman[204] explored FP reactions of resins with graded refractive indices toward the possible implementation in fiber optic applications. The authors developed a modified reaction apparatus to achieve a polymer with a color gradient. Two mixtures comprised **TEGDMA** and **Aliquat-PS** were prepared, and only differed in that one contained aluminum phthalocyanine chloride as a colorant. A computer-controlled feedback system regulated the quantity of each mixture transferred into a mixing chamber via two separate peristaltic pumps. The final mixture was then deposited atop a thermally ignited front in real time with a deposition speed approximately matched to the velocity of the front. Two equations governed the flow rates from each pump; the first ensured that the sum of the two pump rates was fixed at a constant value. The second dictated the quantity of colored resin such that a hyperbolic gradient of dye concentration existed. Indeed, the observed color gradient in the samples matched the desired input value reasonably well, as depicted in the differences in gray level (Figure 34).[204]

Mariani, Pojman, and co-workers[221] described a compositionally graded polymer fabricated frontally in a manner similar to that described above. In this study, each pump transferred a different monomer solution into the mixing chamber; one pump transferred a mixture consisting of **TEGDMA**, whereas the second pump transferred **HMA**. Both monomer mixtures employed **APS** (1 wt %) as the radical initiator. Linear and hyperbolic compositional gradients (χ as a function of position) induced variance in the polymer mechanical properties (*i.e.*, T_g, Shore A hardness, Young's modulus E, and SR%) in a complex manner. These polymers are not defined by a single value for each property; instead, the distance dependent functions provide a more meaningful description of the polymer, as summarized in Figure 35.[221]

Out of the four mechanical properties tested, only the T_g obey a bijective, one-to-one dependency on the compositional gradient. That is, a linear $\chi_{HMA}(x)$ gradient generates a linear

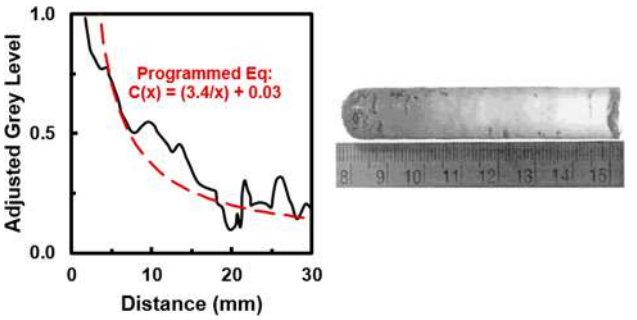

Figure 34. Left: Adjusted gray level (gray level/maximum gray value) as a function of distance within the frontally polymerized p-(**TEGDMA**) with a dye concentration gradient defined by the programmed equation. The largest gray value corresponds to an adjusted gray level of 1, while values of 0 reflect the absence of dye. The red fit line represents the input gradient, whereas the black trace is the observed color distribution. Right: Image of the corresponding polymer sample. Each number on the ruler corresponds to units of cm. Figure reprinted and adapted with permission from *J. Appl. Polym. Sci.* **2000**, *78*, 2398−2404.[204] Copyright 2000, John Wiley & Sons, Inc.

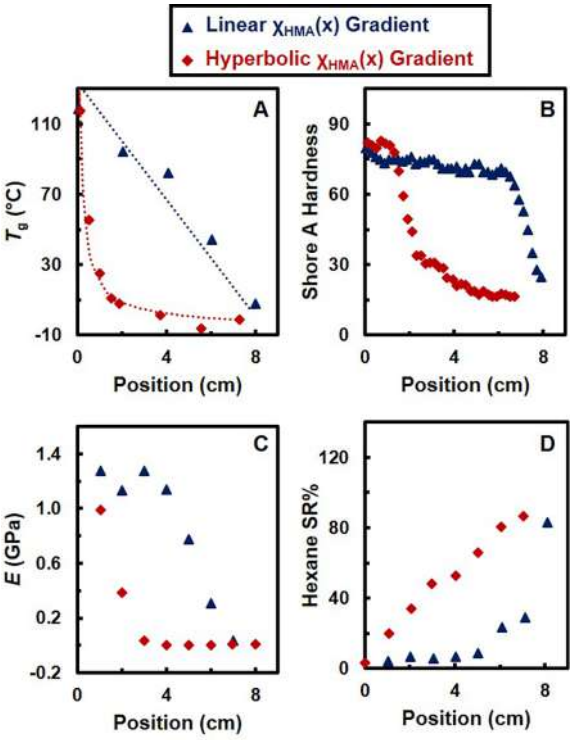

Figure 35. Mechanical properties of frontally synthesized FGM as a function of position in the polymer. The polymers were synthesized with varying **HMA**:**TEGDMA** ratios, which were defined either by a linear (blue) or hyperbolic (red) gradient functions, $\chi_{HMA}(x)$. For example, the composition is heavily weighted toward **TEGDMA** at lower position values. A: Glass transition temperature gradient. Dotted lines correspond to linear (blue) or hyperbolic (red) fits. B: Shore A Hardness gradient. C: Young's modulus gradient. D: Swelling ratio gradient. Each slice was soaked in hexanes to assess the swellability changes as a function of composition. Figure reprinted and adapted with permission from *ACS Appl. Mater. Interfaces* **2015**, *7*, 3600−3606.[221] Copyright 2015, American Chemical Society.

https://doi.org/10.1021/acs.chemrev.2c00686
Chem. Rev. 2023, 123, 3237−3298

$T_g(x)$ function (Figure 35A). This observation results from mixing behavior modeled by the Fox equation (eq 14) for a 2-component polymer blend:

$$\frac{1}{T_{g,\text{blend}}} = \frac{\omega_1}{T_{g,1}} + \frac{\omega_2}{T_{g,2}} \tag{14}$$

where $T_{g,\text{blend}}$ is the glass-transition temperature of the copolymer, ω_1 and ω_2 are the weight fractions of the first and second component, respectively, and $T_{g,1}$ and $T_{g,2}$ are the glass transition temperatures for each homopolymer. In the case of this FGM, ω_1 and ω_2 are defined directly by the chosen compositional gradient. In contrast, the other three mechanical properties exhibit complex positional dependencies. Two discrete regimes exist in the polymer hardness polymer (Figure 35B).[221] The first contains primarily the highly cross-linking monomer **TEGDMA**, which imparts toughness and stiffness. At a certain dilution with added **HMA**, insufficient cross-linking occurs, and the polymer softens. A similar effect is observed in the elastic modulus gradient in the FGM copolymers (Figure 35C).[221] The swelling behavior of the copolymer slices in hexane exhibits a complex positional gradation (Figure 35D) that likely exists due to differences in the microscopic morphology.[221]

Recently, Dean et al.[149] described the adaptation of FROMP toward FGM fabrication. Formulations consisting of **DCPD** and cyclooctadiene (**COD**) exhibited T_g values that obeyed the Fox equation (eq 14). Glass-transition temperatures in the range of −100 to 150 °C were accessible in copolymers with an appropriate dilution with **COD**. In contrast to the other frontal FGM systems, sheets of p(**DCPD**-*co*-**COD**) with a step-like T_g gradation were prepared in a layered fashion by the exploitation of density differences afforded by dilution with **COD**. The resultant sheets exhibited temperature sensitive shape persistence behavior (Figure 36) as a result of the differences in elastomeric properties throughout the FGM. Specifically, three separate compositional regimes existed, as depicted in Figure 36A; the three layers contained compositions with 10, 15, and 25% **COD**, with T_g values of 94, 74, and 40 °C, respectively. A cut-out of the graded sheet provided a patterned "thumbs-up" shape, which was deformed into a fist at 120 °C. Subsequently, the shape was cooled to ambient temperature and slowly heated back to 120 °C. Over the course of the heating process, the fist unfolded in a finger-by-finger fashion to regenerate the initial thumbs up shape (Figure 36B).

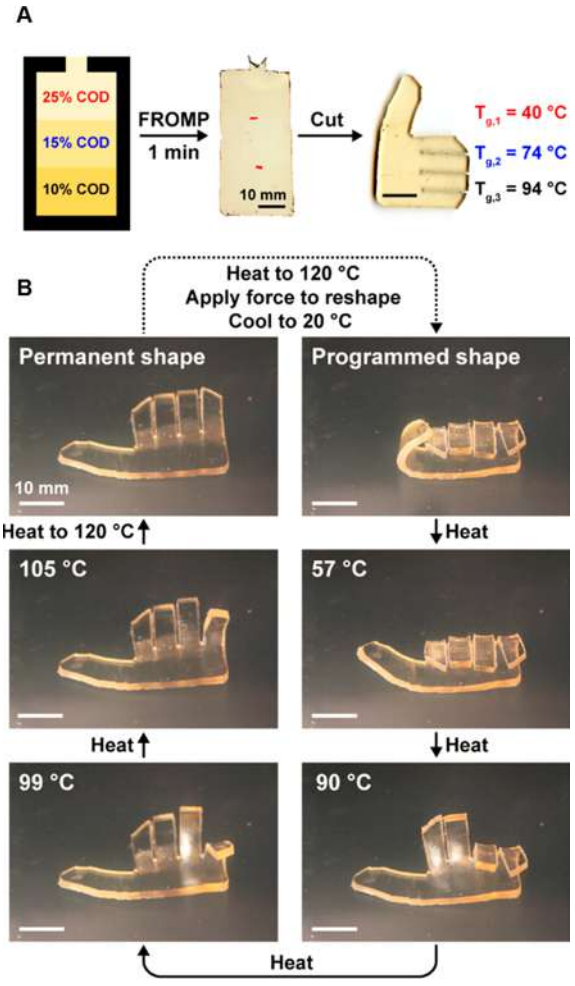

Figure 36. Fabrication of patterned FGMs via the FROMP of **DCPD** and **COD**. A: Synthesis of a three-layer sheet with a transition temperature gradient through the sheet. A patterned "thumbs-up" shape was prepared from the FGM sheet. B: Time point images of the shape persistent behavior of the patterned shape. A permanent shape was initially set and deformed at 120 °C. Rapid cooling to 20 °C temporarily altered the shape, which then underwent temperature triggered actuation to regenerate the permanent shape. Figure reprinted and adapted with permission from *ACS Macro Lett.* **2020**, *9*, 819−824.[149] Copyright 2020, American Chemical Society.

5.3. Instability Driven Spontaneous Patterning

As mentioned previously in section 3, thermal (e.g., spin modes) and buoyancy-driven convective instabilities in FP present a unique challenge with exciting ramifications. Current computational efforts focus on modeling this fluctional behavior so that future endeavors may exploit them productively. Indeed, the modeling efforts have borne exciting experimental fruit. Recent work by Lloyd et al.[51] and Gao et al.[126] leveraged thermally coupled convective instabilities that exist in open-mold FP experiments toward the generation of patterned materials (Figure 37). In this work, resins consisting of either **DCPD** or **COD** underwent FROMP in a geometry with nonuniform boundary conditions. In this configuration, the surface of the resin is exposed to atmosphere and therefore undergoes thermal cooling faster than monomers below the surface. As a result, the maximum reaction temperature undulates as a function of both space and time, which manifests as localized hotspots within the propagating front (Figure 37A). Furthermore, thermal diffusion within the resin occurs concurrently with mass transport of monomer ahead of the front. The pulsations in thermal and mass transport become "frozen" as the resin cures to generate a final polymer material with well-defined striation, as observed in optical and topographic images (Figure 37B and C). Indeed, this behavior is best described by analogy to the patterns formed in splashes of water by a single droplet.

Pattern formation in FROMP may also occur through localized disruption of thermal or mass transport. Recent work from Gao et al.[155,156] demonstrated that the inclusion of poly(caprolactone) microparticles in **COD** or **DCPD** resins introduces bias into the introduces periodic features in the temperature and velocity profiles of the front. During polymerization, the microparticles undergo an endothermic solid to liquid phase change that redirects thermal energy away from the reaction front. Intriguingly, the oscillations in T_{max} are reminiscent of patterns generated in the classical single- and

https://doi.org/10.1021/acs.chemrev.2c00686
Chem. Rev. 2023, 123, 3237−3298

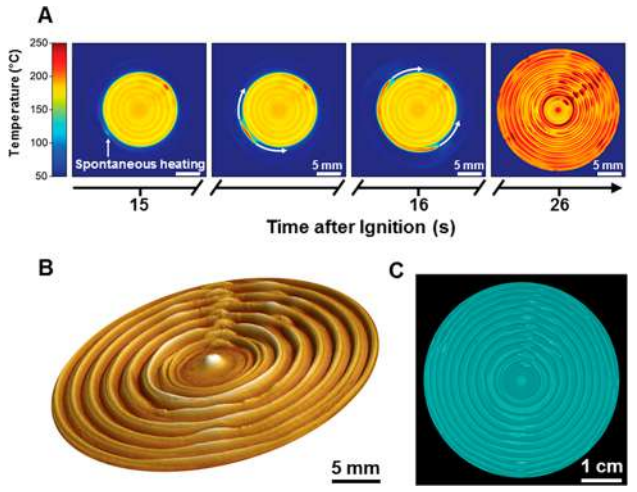

Figure 37. Spontaneous patterning during FROMP driven by thermal instabilities. A: IR thermographs of a radially propagating FROMP reaction of **DCPD** catalyzed by **G2** as a function of time. The reaction occurred in an open mold geometry. B: Topographic profile generated by optical profilometry of the postpolymerization product. C: Optical photograph of the postpolymerization product under UV-irradiation (365 nm). The frontally derived polymer contained 1,1,2,2-tetraphenylethylene, which enabled fluorescence upon photoexcitation. Figure reprinted and adapted with permission from *ACS. Cent. Sci.* **2021**, *7*, 603−612.[51] Copyright 2021, The Authors. Published by American Chemical Society.

multislit diffraction experiments; constructive and destructive interference of propagating waves provides a unique splitting pattern!

Recently, Alzate-Sanchez and co-workers[154] demonstrated that well-defined pattern formation occurs in FROMP resins with high concentration of added solvent. In this system, FP is triggered at the base of the resin inside a test tube; the heat of the reaction induces solvent boiling. The escaping gas propels monomer ahead of the reaction front to generate anisotropic voids in the resultant polymeric foam. Intriguingly, the specific nature of the reaction formulation (i.e., solvent identity, solvent concentration, resin rheology) dictates the alignment of the voids in the foam. The authors employed multivariant statistical analysis to identify correlations between formulation conditions and foam topology within the ≈70 formulations tested. Similar polymer self-organization behavior in FP was also observed in early work by Pojman and co-workers[339,340]

5.4. Composite Materials and Additive Manufacturing

5.4.1. Substrate Consolidation and Reinforcement.

One intriguing application of FP is structural rigidification of otherwise porous or weakened materials.[44,50,53,55,186,210,234,238,245,247,341−343] Extensive use of polymers exists toward the consolidation of materials, with uses including adhesives, fillers, and sealants. These examples, however, typically modify the surface material properties by providing a protective coating layer. Other purposes require that consolidation occurs *within* the material, particularly in architectural settings.[186,234,245,247,341,344] For instance, structural reinforcement of stones in historical sites must not perturb the surface as to minimize deviations from the original object.[234,344] Additionally, maximum structural effectiveness takes place when bulk consolidation occurs in the interior of the material; polymer detachment from the object may also result from surface adhesion. In contrast, polymer-filled stones exhibit enhancement of the structural properties, while also imparting potentially beneficial features, such as hydrophobicity, to mitigate erosion damage. Inserting preformed polymers into a porous network, however, is not a simple task. Large, high molecular weight polymers are similarly sized to the pore size of the substrate material; in addition, the viscosity of fluid polymers (or their solutions) strongly limits the penetration depth of the consolidating agent, which limits the practical application of a traditional protocol.

Visualization within nontransparent materials presents a challenge for the development of new structural consolidation techniques. Nevertheless, significant advances by Brunetti et al.[50] and Proietti et al.[342] enabled the analysis of FP within stone materials. In the former example,[50] X-ray tomography techniques enabled *post facto* analysis to determine the degree of consolidation within stonework after FP. In the latter example, magnetic resonance imaging (MRI) and unilateral NMR spectroscopy provided precise information about the nature of the stone-polymer composite.[342] In a separate work, Brunetti et al.[55] described the use of X-ray tomography as a valuable technique to estimate monomer absorption and FP within wood-based materials.

Cuccuru et al.[341] examined FP within a wide variety of stone materials employed in medieval structures in northern Sardinia, Italy. This study focused on common degradation and decay motifs within stonework to develop a relationship between the petrophysical properties of the substrate and the FP consolidation process. Several subsequent reports applied FP toward the consolidation of tiles crafted from calcareous sedimentary rock.[50,234] Specifically, historical Ligurian tiles, also known as *Pietra di Finale*, exhibit highly porous microstructures. The stone samples absorbed solutions comprised of **HDDA** and 2,2,2-trifluoroethyl methacrylate (**TFEMA**) as a hydrophobic comonomer via capillary action. The absorption process required 4 h, and the material was kept cold and in the dark to avoid polymerization induced by the decay of the radical initiator, **AIBN**. Hot ignition (at ≈200 °C) perpetuated a thermal front within the stone substrate; as a comparison, control samples were heated to 50 °C for 1 d in an oven to perform batch polymerization.

The efficiency of the substrate reinforcement was quantified by three metrics: weight variation, abrasion resistance, and water adsorption. By necessity, samples with a larger weight deviation after treatment absorbed more monomer, though this result does not necessarily reflect the degree of polymerization within the sample. Frontally polymerized samples displayed an average of 7.0 ± 0.2% increase in weight, whereas batch samples exhibited slightly lower gains at 6.0 ± 0.3%. Indeed, the weight gains only reflect the efficiency of capillary action and not the polymerization method. Abrasion tests were performed on these samples by subjecting them to repeated frictional stress on sandpaper, at a driving force of 2.5 kg. After 30 runs, the untreated stone samples exhibited ≈1.1% mass loss. In contrast, stones reinforced by frontally derived polymers exhibited only ≈0.3% mass loss. The efficiency of aggregation (EA%) afforded by structural consolidation was calculated by comparing the weight loss of untreated stones (WL_0) to the treated analogues (WL_t) as defined in eq 15.

$$EA\% = \frac{WL_0 - WL_t}{WL_t} \times 100 \tag{15}$$

https://doi.org/10.1021/acs.chemrev.2c00686
Chem. Rev. 2023, 123, 3237−3298

By this metric, frontal reinforcement outperformed traditional batch polymerization to a reasonable degree (62 ± 2 vs. 54 ± 2%, respectively). Similar trends were observed in hydrophobicity of the reinforced substrate. Indeed, FP provides a more energy efficient method for such an application, with modest enhancements in performance.[234] It is unclear, however, whether removal of the cured resin from the substrate is possible at a later date. Eventual removal of the consolidation agent is a requirement of historical restoration to avoid unexpected damage to the host material. Nevertheless, FP exhibits promise as a method of repairing stone-based artwork and historical architecture.

Structural reinforcement may also occur within a pre-existing polymer scaffold. Robertson et al.[44] illustrated that flexible poly(dimethylsiloxane) (**PDMS**) sheets, bearing microfluidic channels filled with **TMPTA** and **Luperox-231**, underwent rapid structural stiffening as a result of a thermal triggering. The channel dimensions ranged from ≈700 to 1100 μm, which are significantly narrower than most other cm scale systems. The large surface area to volume ratio in the microchannel exacerbates premature front termination as a direct result of magnified heat-loss. Additionally, adventitious bubble formation generates trapped gas pockets within the microfluidic network. Unable to escape the confines of the closed system, bubble aggregation and expansion occurs to provide a physical, insulating barrier that precludes heat transfer and prohibits front propagation. The dimensions of the microchannel, therefore, dictated the efficacy of front propagation, as well as the efficiency of rigidification. Remarkably, an increase of only 100 μm in vessel diameter induces nearly an order of magnitude difference in average propagation distance, as summarized in Table 9. A variety of unusual microchannel shapes and geometries were tolerated in this system, which included 90° angles as well as single-point branching.

Table 9. Effects of Microfluidic Channel Diameter on Frontal Propagation Distances, Rates, and Completion within a Microvascular Network Reinforced by FP[a]

channel diameter (μm)	propagation distance (mm)	completed propagations (%)[d]	ν_f (cm min^{-1})[e]
723	1[b]	0	–
762	6[b]	13	15.9 ± 1.5
838	16[b]	63	17.4 ± 0.4
1120	50[c]	quant.	21.0 ± 0.2

[a]As reported in *ACS Appl. Mater. Interfaces* **2014**, *6*, 18469−18474.[44] **PDMS** sheets with patterned microfluidic channels were filled with **TMPTA** and subjected to FP conditions. [b]Determined as the average of 20 to 25 trials including those that were unable to propagate. [c]Defined as the average of 10 trials. [d]Defined as the fraction of 8 trials which consumed all available monomer within a single frontal event. [e]Determined from samples which traversed at least 10 mm. The values were averaged from 3, 5, and 10 trials for 762, 838, and 1100 μm, respectively.

Structural reinforcement by FP within the microvascular network of the **PDMS** sheets greatly amplified the observed rigidity, as observed in the Young's modulus.[44] The effective *E* of the whole sheet material obeyed the rule of mixtures, and was equal to the weighted average of the *E* values of the unfilled **PDMS** and frontally derived polymer. An order of magnitude of *E* values are accessible from a small range of frontally derived polymer volume fractions, as illustrated in Figure 38A. In fact, the structural rigidification provided a

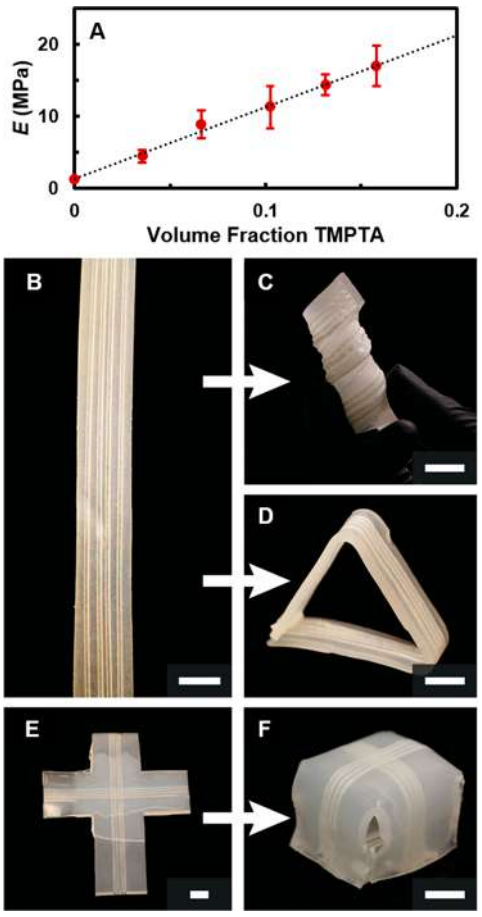

Figure 38. Rigidification of **PDMS** sheets with microvascular networks filled with frontal p(**TMPTA**) generated *in situ*. A: Effective increases in Young's moduli occur after FP within the microchannels. Measured in samples with 1−5 channels. Error bars calculated from the standard deviation of 3 experiments. The dotted trend line represents the values obtained from the rule of mixtures. B: Flat sheet of Ecoflex **PDMS** that contains 4 linear microchannels, each with a diameter of 1120 μm. FP has not yet occurred. C: Sample generated after being frontally polymerized. The sheet was wrapped around a rod of 3/4 in diameter prior to thermal ignition. FP occurred within 1 min flash cure to stiffen the material and afford a helical shape after rod removal. D: Triangular shape generated by flash curing. E: A multilayered **PDMS** sheet with 2 sets of linear channels in arranged in a t-shaped orientation. **F:** After flash curing, the patterned shape assembled into a cube-like structure. **B−F:** All scale bars correspond to 1 cm. Figure adapted and reprinted with permission from *ACS Appl. Mater. Interfaces* **2014**, *6*, 18469−18474.[44] Copyright 2014, American Chemical Society.

unique method to synthesize shape persistent materials on demand. Several 3D shapes were produced via FP within the 2D microvascular **PDMS** sheets (Figure 38B−F).[44]

Reinforcement of wood-based substrates is also accessible with FP chemistries. For example, Pojman[345] adapted and commercialized a cure-on-demand filler for wood repair. The resultant product, 3P QuickCure WoodFiller, rapidly cures upon heating. The adhesive strength of the filled section rivals that of a screw. Specifically, a traditional metal screw embedded in a section of wood filled with QuickCure WoodFiller breaks after impact from a hammer; the filler remains intact and fully bonded to the host substrate.

5.4.2. Frontal Geopolymerization. Civil engineering projects extensively employ ordinary Portland concrete

https://doi.org/10.1021/acs.chemrev.2c00686
Chem. Rev. 2023, 123, 3237−3298

(OPC) for structural (and nonstructural) components. The production process, however, produces considerable pollution. For example, OPC manufacturing emits ≈0.6 to 0.8 kg of CO_2 per kg concrete produced.[346,347] Nearly half of emitted CO_2 is obtained as a stoichiometric biproduct of limestone calcination.[347,348] The energy costs associated with heating the raw materials to 1400 °C (typically inside a rotating kiln) account for ≈11% of the total emissions.[347] In addition to CO_2, dust and particulate inhalation presents a safety concern; nearly 2.6 kg of dusty materials are emitted per kg concrete.[347] In contrast, geoplolymers (i.e., cross-linked inorganic materials) are attractive alternatives to OPC.[349] Geopolymerization reactions with metakaolin (or other common aluminosilicates) produces these eco-friendly materials after treatment with aqueous NaOH and $NaSiO_3$ at ambient temperature. Moreover, geopolymers exhibit outstanding physicochemical features comparable to OPC.[349]

In this context, the merger of FP with geopolymerization is an attractive new direction. Indeed, the energy efficiency of FP further reduces the time and energy costs associated with solidification and curing geopolymers. This new approach, as proposed by Alzari et al.[247] in a forward-looking report, combines FP of **HDDA** with geopolymerization of metakaolin (**MK**), as highlighted in Table 10. As control experiments, FP and geopolymerization were performed separately. The former provided p(**HDDA**) with T_{max} and ν_f values typical of acrylate monomers (see section 4.3). The latter involved a 2:1 wt/wt mixture of **MK** with an alkaline activated solution (**AAS**, 8 M $NaOH_{(aq)}$ with 35% Na_2SiO_3, 1:1 v/v). After 24 h at ambient temperature, successful curing provided a cross-linked inorganic network. Next, a composite material that contained **HDDA** with **MK** (44 wt %) as a filler was frontally polymerized. Similar to other filled materials, the addition of **MK** depresses T_{max}. Nevertheless, this composite material did not exhibit phase separation.

Table 10. Development of Frontal Geopolymerization

reagents	reaction type[d]	notes	T_{max} (°C)	ν_f (cm min^{-1})
HDDA	FP	p(**HDDA**) produced	192	4.0
MK/AAS[a]	GP	geopolymer produced	–	–
HDDA/MK[b]	FP	composite produced	160	3.8
HDDA/MK/AAS[c]	FP/GFP	hybrid material produced	119	4.0
	BP (ambient)	phase separation	–	–
	BP (80 °C)	gas formed; no hybrids	–	–

[a]**MK** = metakaolin; **AAS** = alkaline activated solution (8 M $NaOH_{(aq)}$ + 35% Na_2SiO_3, 1:1 v/v). **MK/AAS** = 2:1 wt/wt. [b]**MK** included as a filler (44 wt %) without water. [c]Contains **HDDA** and mixture of **MK/AAS** (44 wt % with respect to **HDDA**; **MK/AAS** = 2:1 wt/wt). [d]**FP** = frontal polymerization; **GP** = geopolymerization at ambient temperatures for 24 h; **FP/FGP** = frontal polymerization coupled with frontal geopolymerization; **BP** = bulk polymerization at either ambient temperature or 80 °C.

Concurrent FP and geopolymerization successfully occurred in resins containing **HDDA**, **MK**, and **AAS**. The resultant hybrid composites exhibited remarkably higher stiffnesses compared to its constituent components (i.e., p(**HDDA**) and **MK** geopolymer). The presence of water surprisingly did not affect the radical initiation or propagation steps associated with acrylate FP. The exothermicities of FP and geopolymerization overcame heat dissipation from water boiling and the inert filler. On the basis of the data in Table 10, as well as ^{27}Al and ^{29}Si MAS NMR spectroscopy, the authors confirmed that the exothermicity of FP triggers frontal geopolymerization. Two separate BP control experiments (i.e., ambient temperature or 80 °C for 1 h) highlighted this result; at temperatures below ≈100 °C, composite formation does not occur and instead the materials undergo phase separation or explosive gas release.

More recently, Alam et al.[245] exploited frontal geopolymerization to produce composites of **MMA** with fly ash and sand. Complete conversion occurred within an hour. The composite materials, however, exhibit extended porosity likely the result of monomer evaporation. Correspondingly, such materials display a decreased potential compressive strength. These first pioneering reports provide a good starting point for future endeavors. Indeed, these works may aid in the design of frontally geopolymerized composites with a host of advanced properties found in other mixed materials (e.g., thermal resistance,[350−352] self-healing,[330,331,352] or flame retardance[353]).

5.4.3. Frontally-Derived Adhesives. Pojman and coworkers[53,210] reported the use of FP to generate cure on demand wood adhesives. In the first study,[210] a mixture of **Luperox 231**, **TMPTA**, and filler was applied as an adhesive between two pine wood blocks. After application and pressing, thermally ignited FP occurred to fully join the two blocks. The efficacy of the frontal adhesive system was measured by shear strength tests to determine the stress necessary to break the physical bond between the two blocks. The filler identity, as well as initiator loading, affected the overall strength as an adhesive. Silica (6 phr by mass) loaded with initiator (7 phr by mass) provided the strongest shear strength of 1.9 MPa, though addition of **AA** as a comonomer enhanced this value to ≈10 MPa. For comparison, typical epoxy adhesives exhibit shear strengths ranging from 1 to 50 MPa, depending on the thickness of the glue. A subsequent report successfully employed these formulations toward frontally cured wood coatings containing either calcium carbonate or graphene as fillers.[53] Indeed, the coated wood samples received moderate increases in hardness, as determined by König pendulum tests.

Recent work from Turani et al.[184] developed UV-triggered FP resins as adhesives (Figure 39). A mix of two separate cross-linkable diepoxy monomers (namely, **BADGE** and **CE**) provided a desirable balance of reactivity and adhesion; **BADGE** promoted adhesion to different substrates (Al alloy, EN AW 7075; or porous glass-based Foamglas). In contrast, **CE** improved the exothermicity of the FP reaction and modulated the resin rheology to achieve a desirable viscosity suitable for coating purposes. The inclusion of **IOC-8 SbF_6** and **TPED** into the resin enabled UV-triggered FP to bond two independent substrates within seconds. Figure 39 describes this process to prepare lap shear samples and resultant apparent shear strengths as a function of **CE:BADGE** weight ratio. The strengths of samples prepared through this method match those of samples prepared through a traditional oven cure method at 110 °C for 1 h, but with significantly lower energy inputs. Additionally, employing this strategy in more complex substrate orientations (e.g., step lap joint) exhibits promise for commercial applications.[354,355]

https://doi.org/10.1021/acs.chemrev.2c00686
Chem. Rev. 2023, 123, 3237−3298

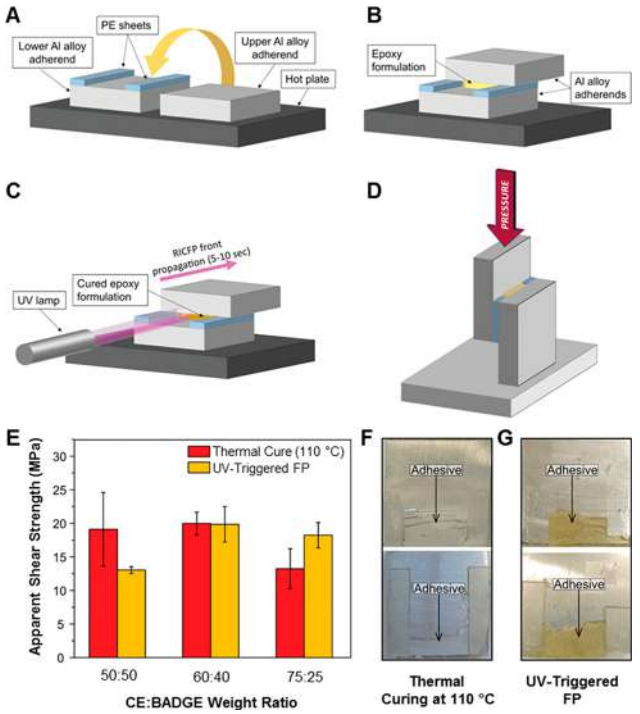

Figure 39. Epoxy-based adhesives generated by UV-triggered cationic FP. A: Preparation of substrates. Polyethylene gaskets were employed to control the thickness of the resin adhesive. B: The epoxy adhesive was applied to the bottom adherent and capped by the top substrate. C: UV-triggered FP occurred after irradiation, and fully cured the sample within seconds. D: Adhesion strength determined by single lap offset shear−compression tests. E: Apparent shear strength of the final joint as a function of monomer composition. Rapid FP curing provided similarly strong joints to those prepared by traditional thermal cure (110 °C for 1 h). F−G: Images of the joint samples after fracture. Figure adapted and reprinted with permission from *Macromol. Mater. Eng.* **2021**, *306*, 2100495.[184] Copyright 2021, Turani et al.

5.4.4. Frontally Polymerized Artwork. The intersection of art and science has existed long before the modern era; renaissance polymath Leonardo da Vinci is an instantly recognizable example of this interconnectedness. In this vein, one intriguing application of FP involves the creation of artwork, particularly sculptures. One of the authors of this review, John Pojman, became involved in the development of FP-based art media.[45,356] A fruitful conversation after a seminar at Portland State University in 2011 led Pojman to adapt radical FP for artistic purposes.

A mixture of acrylate and radical initiator thickened with a proprietary combination of inorganic fillers provides a moldable material. A judicious choice of initiator (i.e., long $t_{1/2}$ at room temperature) extends the lifetime of these sculpting clays to several years, which is an attractive trait for potential consumers.[45] Additionally, the persistence at ambient temperatures provides an artist sufficient time to sculpt. Unlike traditional ceramics used by artists, the FP approach requires significantly less thermal energy to set; kilns are no longer necessary to induce curing and structural rigidification. Instead, a heat-gun can quickly induce a self-sustaining polymerization front. The formulation of the clay ensures that T_{max} values are below 165 °C. Lower curing temperatures are desirable as they are compatible with other materials (e.g., wood, paper, plastics) and, therefore, allow the creation of mixed-media sculptures.[45] Impressively, the cured material after FP displays compressive strengths of around 40 MPa and significant resistance to shattering upon being dropped. The porosity of the set ceramic-like material aids in retaining paints (oil-, water-, or alcohol-based). This technology was later commercialized and marketed as QuickCure Clay by Ranger industries.[357] Interestingly, an exhibit in 2017 at the Louisiana Art and Science Museum[358] (organized in part by J.A.P.) highlighted several art pieces created by FP. Figure 40 highlights several example sculptures prepared with QuickCure Clay.

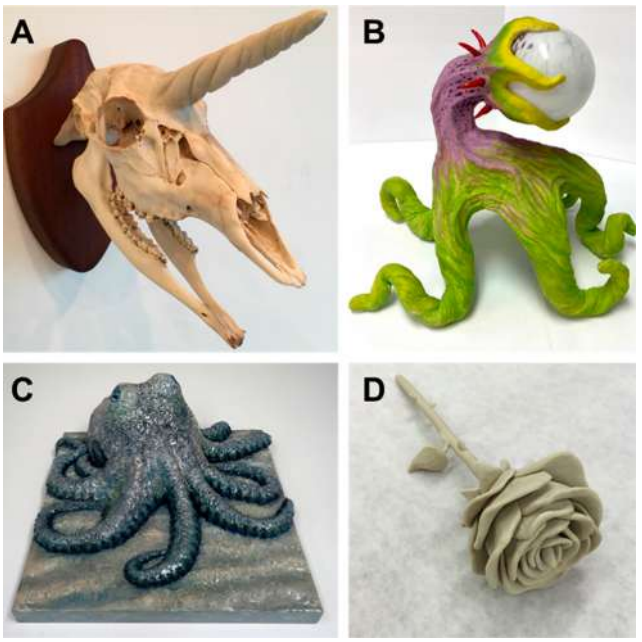

Figure 40. Sculptures prepared through frontal polymerization with QuickCure Clay. A: Mounted unicorn head created by Kevin Vanek. B: Painted fantasy plant created by Timothy Marsh. C: Painted octopus by Shelby Prindaville. D: Unpainted rose by Shaina LaCarbo. Images used with permission from the artists.

5.4.5. Photoluminescent and Thermochromic Composites. Inclusion of inorganic materials into frontally derived polymers accesses properties otherwise unattainable for a purely organic species. Adjusting the photophysical or electrical properties of easily synthesizable polymers represents an attractive alternative method to generate organic components for devices. A substantial volume of work has focused on the synthesis of frontally derived polymers embedded with colloidal quantum dots (CQDs),[77,262,270−272,306,359] carbon dots (CDots),[211,262] carbon nanotubes,[160] and other inorganic nanoparticles.[159,360] The light absorption behavior of these nanometer-sized inorganic clusters are easily modified;[361] as a result of quantum confinement, the size of the material directly impacts the λ_{max} as observed in an example where the size of PbS nanoparticles influenced the observed color.[362] Numerous applications and devices employ CQDs, which include LEDs,[363,364] photovoltaics,[361] and even televisions screens (QLED-TV).[365] Some applications are limited by the poor mechanical properties of these purely inorganic clusters. Flexible polymer−CQD composites, therefore, are appealing as they combine desirable mechanical and photophysical features.

https://doi.org/10.1021/acs.chemrev.2c00686
Chem. Rev. 2023, 123, 3237−3298

Practical integration of CQDs into polymers presents a synthetic challenge; traditional polymerization methods require sufficiently long curing times such that undesired photo oxidation quenches the absorbance properties of the inorganic component.[306] In contrast, the short time scale associated with FP avoids these effects to generate high-fidelity photoluminescent composites. An initial report by Fang and colleagues[306] reported the synthesis of CdS-poly(**NMAm**) materials. In this system, the CdS clusters were physically capped to the end of the polymeric backbone by (3-mercaptopropyl)trimethoxysilane (**MPS**) as a covalent bridge after condensation with the OH containing side chains. The absorption and photoluminescence profiles of the translucent composite material indicated that successful incorporation occurred. The **MPS** bound CdS particles display a characteristic absorption λ_{max} at 375 nm, whereas the CdS-poly(**NMAm**) composite possesses a red-shifted absorption band at 390 nm. The shift from 375 to 390 nm results from minute shape perturbations when CdS is incorporated into a polymeric host.[306] Similar behavior exists in copolymer composites, though the overall emission properties vary due to the innate photoluminescence afforded by different monomers.[272]

Another strategy for hybrid CQD-polymers involves reversible swelling into a frontally prepared, preformed hydrogel, as reported by Zhou et al.[271] Specifically, hydrogels comprised of p(**NMAm**-*co*-**NVP**) adsorbed CdTe particles capped with *N*-acetyl-L-cystine after immersion into an aqueous solution. Once adsorbed into the porous channels of the hydrogel, the CdTe CQDs coordinate irreversibly to the pyrrole side chains of the polymer. Interestingly, the photoluminescence behavior of the p(**NMAm**-*co*-**NVP**)/CdTe composites varies with water content within the hydrogel. Water swollen samples emit at 546 nm after excitation, which redshifts to 560 nm after desorption to generate a switchable photoluminescent polymer stable for at least five swell/deswell cycles with implications toward moisture detection. A related system employed an *in situ* CQD assembly strategy by first preparing a frontal formulation comprised of **MAA** and **VI** monomers and loaded with Cd^{2+} as a diacrylate salt.[270] Incorporation of Cd occurred via ligation with the carboxylate side chains of the polymer scaffold; subsequent treatment with aqueous Na_2S initiated crystallization of CdS within the confines of the polymer matrix to afford p(**MAA**-*co*-**VI**)/CdS. The initial concentration of Cd within the hydrogel modulated the photoluminescence intensity, and to a less extent, the λ_{max}.

Access to layered, biphasic photoluminescent polymers via FP enables several intriguing device applications.[77,262] Li et al.[262] described the fabrication of white LEDs synthesized from a layered, dual-component composite polymer (Scheme 10). Two frontal formulations (**AM**/**NVP** and **HEA**/**NVP**) were layered atop one another immediately prior to laser ignited FP. The first layer formed a composite with added CDots ($\lambda_{PL,1}$ = 471 nm), whereas the second phase included CdTe CDQs ($\lambda_{PL,2}$ = 587 nm). During photoluminescence, the inorganic components in each layer emitted light at the corresponding wavelengths to afford an observed white color. White LED devices were fabricated by combination of such biphasic composite polymers and UV-LEDs.[262]

This synthetic approach was also applied toward chemical detection of amines.[77] It is well established that photo quenching of CQDs by certain organic molecules occurs by surface modification after ligation, as observed in the interaction of organic amines with CdSe nanocrystals.[366] Chemical detectors for concentration quantification, however, require a mechanism for self-calibration. With this condition in mind, biphasic frontal composites were exploited by the Su and co-workers;[77] the first phase contained CdTe CQDs (λ_{CdTe} = 620 nm) as the amine sensing portion; a variety of amines were adsorbed into the polymer, which quenched the photoluminescent emission from the CdTe to dampen the intensity of photoluminescence from this phase (denoted as R_{CdTe}). The second layer contained the organic dye coumarin 6 (λ_{C6} = 523 nm), which does not undergo quenching phenomena as it is inert toward amines. Hence, the signal intensity (R_{C6}) from this layer is invariant of analyte and served as the reference signal. The ratio of the intensity of these two signals ($\gamma = R_{CdTe}/R_{C6}$) normalized the response across 4 amine analytes. Compared to the control sample, however, the mild sensitivity of the reported frontal composites precludes precise molecular recognition; for example, no discernible difference exists in the photoluminescence responses to Et_3N and $^iPr_3N$, but a substantial intensity change occurs with ethylenediamine.[77]

Verma and co-workers[367] described the frontal preparation of metal organic framework (MOF) composites of p(**Am**). In a typical reaction, WS_2 sheets, **APS**, and **Am** were mechanically ground, which facilitated **Am** coordination to W. The resultant metallomonomer pellet undergoes FP via a free-radical pathway to provide metallopolymer films. Based on SEM and TEM data, the frontally polymerized composites retain a sheet-like structure, with a domain size on the order of 150–

Scheme 10. Synthesis and Optoelectronic Properties of Dual-Component Frontally Derived Polymers[a]

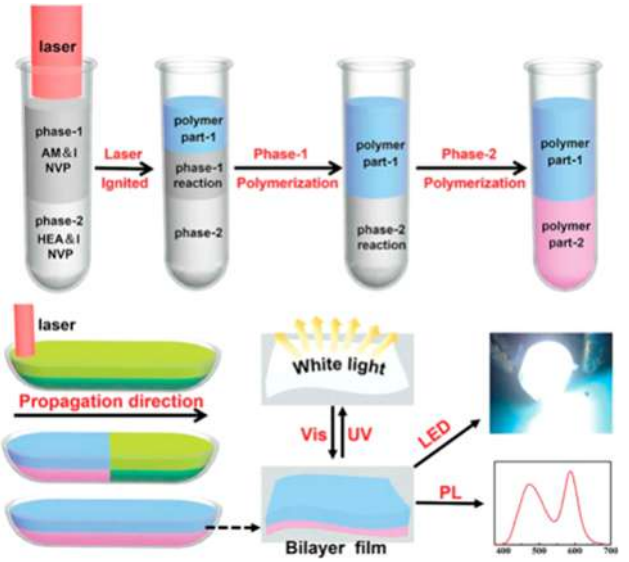

[a]Top: Two layers containing different compositions underwent FP after ignition by a CO_2 laser. Phase-1 and phase-2 are comprised of p(**AM**-*co*-**NVP**)/CDots and p(**HEA**-*co*-**NVP**)/CdTe. Bottom: The bilayer films emit white light after excitation by UV-wavelength light; these materials were incorporated into an LED device to provide white light classified by the chromaticity coordinates (0.31, 0.28) as defined by the Commission Internationale de l'Eclairage (CIE). This behavior results from emissions for each phase corresponding to the photoluminescence of CDots (λ = 471 nm) and CdTe (λ = 587 nm). Scheme reprinted and adapted with permission from *RSC Adv.* **2015**, *5*, 102294–102299.[262] Copyright 2015, Royal Society of Chemistry.

https://doi.org/10.1021/acs.chemrev.2c00686
Chem. Rev. 2023, 123, 3237–3298

300 nm wide by 10−20 nm thick. Powder X-ray diffraction experiments indicated that hexagonal orientation of the WS_2 fragment remains intact after FP. More interestingly, the photoabsorption properties of the WS_2 component in these MOF-polymer composites are ideal for photodetection applications. These composites exhibit remarkable flexibility due to the polymeric portion of the composite. As proof of concept, the authors fabricated photodetecting films from these composites on a paper-based substrate. Upon irradiation under an applied voltage, the WS_2 component of the device undergoes a change in current. Impressively, the detectors exhibit resistance to degradation after 100 cycles. Given the environmentally compatibility of the materials involved, the devices are compostable after combustion.

A related class of frontal composites exhibit temperature responsive color changes.[219] These thermochromic materials incorporated a simple inorganic salt, $CoCl_2{\cdot}6H_2O$, as the colorant embedded within p(**TEGDMA**-*co*-**Am**) with added glycerol. As a result of the heat of polymerization, the pink reaction mixture converted to a blue polymer, which underwent color reversion after cooling. The resultant rods underwent highly reversible (>100 cycles) pink to blue color changes upon warming (between ≈80 and 145 °C), which relates to the coordination sphere about the Co^{II} metal center. The machinability of the final polymer required glycerol incorporation into the cross-linked network.

As a result of the faster monomer-to-polymer conversion characteristic of FP, limited phase separation occurs in the synthesis of many composite materials. Conversely, phase-separated rubbery materials generated from traditional BP techniques are easily broken. It is noteworthy than an analogous observation was reported by the Mariani and co-workers,[312] who successfully prepared p(**NIPAm**)/graphene nanocomposite hydrogels that exhibit minimal graphene restacking during cross-linking.

In summary, frontal thermochromic polymers are suitable for temperature sensing applications.

5.4.6. Generation of Microvascular Networks and Microfluidic Devices. Precisely controlled vascularized polymer networks typically require an arduous fabrication strategy. Recent work by Garg and co-workers[158] employed a clever constructive-destructive approach to create well-defined channels within a thermoset matrix (Figure 41). Liquid- or gel-state **DCPD** resins contained thermally degradable poly(propylene carbonate) (**PPC**) fibers doped with 1% of a **PAG**. UV pretreatment of the sacrificial fibers reduced the decomposition onset temperature (T_d) from 200 to 93 °C compared to virgin **PPC**. Presumably, the UV-treated **PPC** templates undergo accelerated decomposition via an acid-mediated depolymerization reaction that produces propylene carbonate. FROMP of the **DCPD** resin provided sufficient heat to fully cure the matrix while also fully depolymerize the **PPC** fiber. Indeed, this strategy enabled the fabrication of "leaf-like" vascularized materials, with implications toward microfluidic device manufacturing. Shen and co-workers[249] described an alternative vascularization approach to generate hollow-tubes of p(**Am**-*co*-**HPA**-*co*- **NVP**) hydrogels.

An alternative (and quite elegant) vascularization approach was reported by Cabral and co-workers in the early 2000s.[278,279,282,368,369] In these works, photoinitiated thiol−ene FP generated micropatterned materials of various local topologies. Specifically, multilevel structured devices were fabricated in a single-step with clever application of photo-

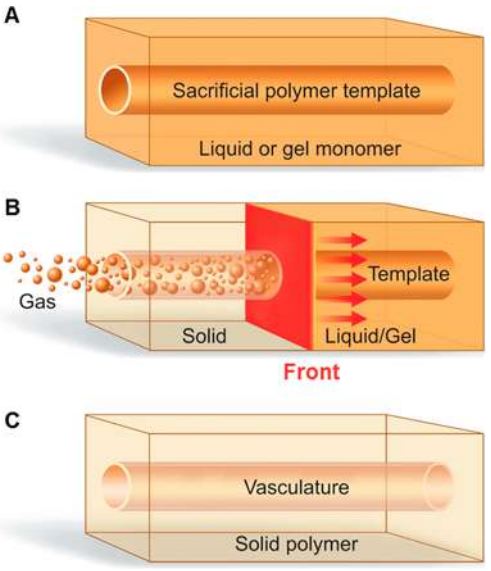

Figure 41. Preparation of microvascular structures. A: An embedded degradable polymer comprised of poly(propylene carbonate) and a **PAG** templated subsequent vasculature. B: During FP, the exothermicity afforded by the FROMP reaction of the host matrix induces thermal depolymerization of the templating polymer fiber. C: The small molecule products formed by depolymerization volatilize to reveal a well-defined channel within the solid thermoset host. Figure reprinted and adapted with permission from *Nat. Commun.* **2021**, *12*, 2836.[158] Copyright 2021, Garg et al.

lithography.[278] An object (such as that depicted in Figure 42A) of variable heights was produced using photomasks to alter the local UV-dose; the chosen resin underwent through-thickness, photoinitiated FP, whereby regions of low-UV doses underwent faster cure times. As a result, low-dose regions underwent faster FP to create taller structures (≈340 μm) compared to high-dose regions (≈190 μm). After curing, unreacted photoresist was washed away to fabricate a master pattern affixed to glass. The final microfluidic devices were replicated from the master pattern by molding PDMS and sealing with glass. The resultant devices (>1 mm tall; smallest line widths ≈50 μm) possessed microchannels with diameters identical with that of the height of the master pattern. The device presented in Figure 42B creates droplets of a predetermined size after mixing fluids from inputs A and B with an in-line static mixer and merging with a third flow from input C.[278] Subsequent studies characterized the flow-behavior of such microfluidic devices prepared by this method.[368,369] More recently, Hennessy and co-workers[280,281] studied the thermal and mass diffusion challenges associated with frontal photopolymerization on these small-scales. Nevertheless, it is evident that frontal photopolymerization can rapidly prototype new component designs, such as those utilized in the context of microfluidics.

5.4.7. Large-Scale Fabrication, 3D-Printing, and Additive Manufacturing. Many practical commercial and industrial applications rely on compositionally layered or patterned materials.[7] Nearly half of all aircraft structural components produced in 2017, for example, employed composite materials.[1] In this context, rigid polymer scaffolds, typically epoxy based, are reinforced with fibers of a secondary component. Glass fiber or strands of p(acrylonitrile) provide desirable mechanical and physical properties (i.e., strength, rigidity, thermal stability) without adding substantially to the

https://doi.org/10.1021/acs.chemrev.2c00686
Chem. Rev. 2023, 123, 3237−3298

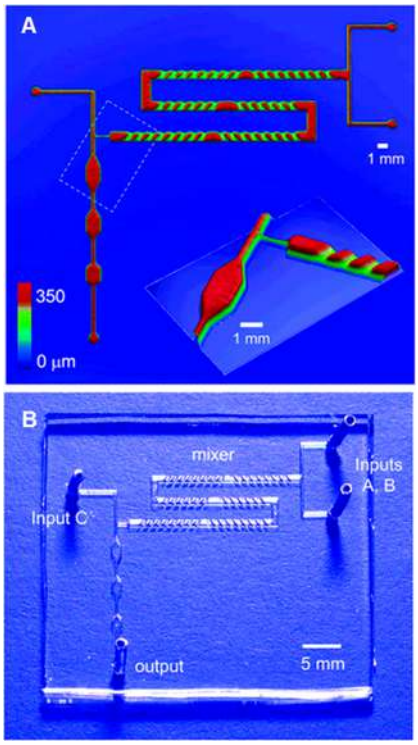

Figure 42. Preparation of a microfluidic device using photoinitiated thiol−ene FP. A: Topological image of the multilevel, patterned device negative. The use of photomasks modulated depth of cure in the prepolymerized resin to generate a single-component affixed to glass. The negative image possessed a bimodal distribution of heights (190 and 340 μm). B: Relief replica device generated by molding PDMS against the master pattern and sealed with glass. This device creates an immiscible flow where fluids from inputs A and B pass through an arduous path in-line static mixer and merge with a flow from input C to exude droplets of predetermined size at the output. Figure adapted and reprinted with permission from *Langmuir* **2004**, *20*, 10020−10029.[278] Copyright 2004, American Chemical Society.

weight of the composite. Despite this, practical limitations exist. Traditional batch syntheses require expensive, high temperature curing methods, which limit production to the size of the autoclave or oven used.[7] Moreover, the time and energy intensive batch curing processes currently employed are expensive and environmentally damaging as a result of the inherent efficiencies. Application of FP to such purposes, therefore, may fundamentally impact large-scale manufacturing techniques.

Despite the attractive rewards, only a handful of reports have attempted to adapt FP to such purposes.[32,64,69,105,195,370] An early theoretical study by Korotkov et al.[371] developed a model describing the relationship between temperature and conversion distribution for a hypothetical frontally cured fiber composite. Concurrently, a forward-thinking report in 1993 by White and Kim[372] described the hypothetical requirements and efficiency benefits for new composite fabrication methods, whereby the lay-up and cure events occur simultaneously. The authors fabricated 12 mm thick composite epoxy/graphite plates by simultaneously laying-up and curing precut prepregs in a metal mold heated to 177 °C. While not technically FP, this process occurs via a similar thermal propagation motif.[372] This report predates (and perhaps motivated) the explosive growth of FP derived composite fabrication. Subsequently, the same authors described a similar strategy to manufacture a 100 mm thickness composite in under 8 h comprised of prelaminated 32-ply prepregs (Hercules AS4/3501-6, 42% resin content).[373] This frontal curing process occurred without thermal spiking inherent to traditional autoclave condition. Moreover, the total manufacturing time was reduced by at least an order of magnitude compared to bulk curing.

Robertson et al.[32] demonstrated that fiber-reinforced composite materials are accessible via FROMP. The rheology of the frontal formulation directly influences the processability of the mixture. Remarkably, liquid solutions of **DCPD** with phosphite inhibited **G2** undergo slow conversion to a viscoelastic gel without inducing spontaneous polymerization. Moreover, the inhibitor concentration tunes the rheological properties of the mixture, which allows for precise control over the degree of gelation of the monomer mixture. Free-standing gels exist at certain phosphite concentrations and enable adaptation for the 3D printing and patterning purposes as depicted in Figure 43. These formulations are easily embossed

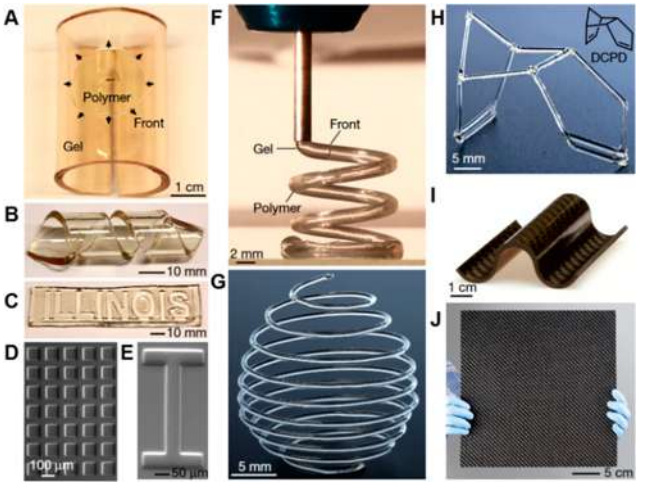

Figure 43. Patterning and 3D printing applications of FROMP. A: FROMP occurs from a single ignition point, and propagates radially throughout the free-standing gel. B: A reaction gel is rolled into a helical shape prior to polymerization. C: A flat gel sheet is embossed with "ILLINOIS" immediately before FROMP. D, E: Small μm-scale features are molded into a flat gel over the course of 1 d at ambient temperatures prior to solidification by FROMP. F: The free-standing gels allow for 3D printing via the depicted apparatus where polymerization occurs immediately after extrusion from the nozzle. G, H: Shaped structures produced by 3D-printed FROMP. I: Fiber-reinforced composite polymer of corrugated carbon produced by FROMP after vacuum-assisted resin-transfer molding (VARTM). J: A **DCPD**-carbon fiber panel is cured with ≈750 J of energy over 5 min. The panel is 51% fiber (by volume) and has an area of 900 cm.[2] Figure reprinted and adapted with permission from *Nature* **2018**, *557*, 223−227.[32] Copyright Macmillan Publishers Ltd., part of Springer Nature.

with shapes that range in size from μm- to mm-scale without significant shape defects (Figure 43D−E). Additionally, free-form structures are produced by integration of 3D-printing technology with FROMP (Figure 43F−H). The carbon-fiber reinforced composite polymers depicted in Figure 43I−J were rapidly produced (within 5 min) with a low-energy thermal trigger (750 J). Further, the tensile strengths and E values of the frontally prepared p(**DCPD**) samples are comparable to traditionally cured epoxy materials; the FP specimens also exhibit substantially larger fracture toughnesses.[32]

https://doi.org/10.1021/acs.chemrev.2c00686
Chem. Rev. 2023, 123, 3237−3298

Recent work from Noè et al.[195] fabricated biobased epoxy composites using radical-induced cationic FP with **DGEVA** as the monomer. Fabrics derived from biocompatible fibers from flax or cellulose served as the compositing material (either single or dual plied). The material properties of the resultant composites were probed with DMA and tensile testing. Typical T_g values existed between ≈90 and 140 °C, which increased with larger number of plies in the compositing filler. These materials exhibited E values between 0.6 and 1.2 GPa, with maximum tensile strengths of ≈10 mPa. The material properties are comparable with other bioderived epoxy composites but cure substantially faster than traditional thermal curing (i.e., 1 min vs 24 h).[195]

The scalability of efficient heat-transfer, however, is a key hurdle toward the implementation of FROMP to industrial-scale manufacturing applications. Subsequent reports demonstrated that such effects are mitigated by the inclusion of thermally conductive elements into the frontal system.[32,69,105] Microchannels within a **PDMS** matrix were filled with FROMP formulations and threaded with either stainless steel or copper wire (as well as single fiber carbon tows) to act as the conductive element. Samples embedded with copper exhibited substantial faster v_f than wireless samples; computational modeling indicated that the conductive fiber preheats monomer in advance of the propagating front, which results in more rapid thermal transfer throughout the system. These results present one possible method to overcome heat-loss limitations of FP. These effects were also observed in acrylate-derived FP resins.[246,253] A commonality among these examples relates to the shape of the front. Due to the thermal conductivity properties of the embedded material, propagation is accelerated at the interface of the element, which results in a V-shaped conical front (Figure 44).

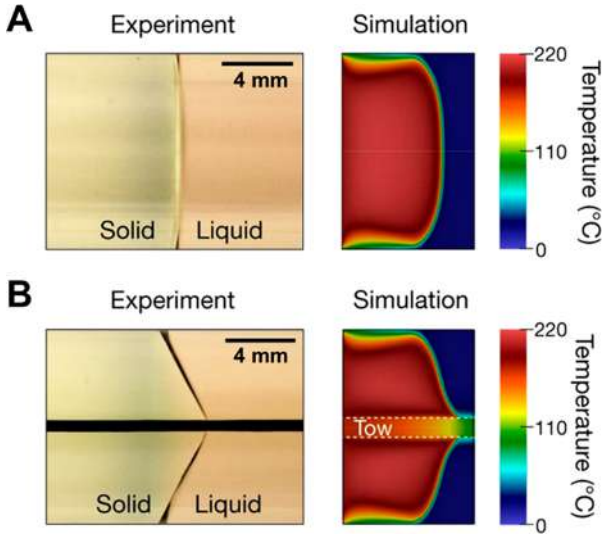

Figure 44. Experimentally and computationally observed effects on front shape in FROMP resins with a thermally conductive carbon fiber. A: Planar front propagation occurs in the absence of a conductive element. B: The inclusion of a single-fiber carbon tow alters heat-transfer throughout the resin media, and accelerates front propagation proximal to the interface of the tow. This perturbation results in a V-shaped conical reaction front. Figure reprinted and adapted with permission from *Nature* **2018**, *557*, 223−227.[32] Copyright Macmillan Publishers Ltd., part of Springer Nature.

Additionally, practical implementation in large-scale industrial settings requires multisite ignition in order to reasonably and quickly cure massive materials and components.[32,69,105,168,268] The dynamics of multifront systems create several key dilemmas; when two fronts meet, for example, heat dissipation becomes problematic as there is no longer a cold monomer heat sink to prevent uncontrolled spontaneous polymerization. As a result, the front junction displays significantly less desirable mechanical properties than the other portions of the polymer. One potential solution involves planar rather than point-based front initiation. This through-thickness curing approach involves exposure of a liquid, gel, or composite-containing resin to a planar heat source. While this requires a larger initial energy input than point-source, the increased heat-flux over a large area shortens the time-to-cure without compromising the material properties.

An alternative approach to large-scale manufacturing involves continuous flow-type methods (e.g., 3D printing, extrusion, flow reactors). Such additive manufacturing strategies, however, require a judicious choice in resin formulation. Fabrication of free-standing objects via 3D printing or extrusion necessitates appropriately modified resin rheologies.[157,162,163,166,374] Specifically, printing inks must exhibit shape retention after pressurized extrusion (i.e., low mechanical flow). The following materials properties address the aforementioned printing criterion; resins must exhibit shear yielding, shear thinning, and fast thixotropic recovery behavior.[374] For FP, these properties may result from rheological modification with a filler (e.g., fumed silica, nanoclays) or controlled prepolymerization of a liquid resin into a gel state. Recently, Ziaee and Yourdkhani[157] described the effects of controlled temperature incubation of **DCPD** resins to achieve such rheological properties for FROMP based printing. Subsequent work from the same group demonstrated that FROMP-based 3D-printing can fabricate thermoset composites reinforced by short carbon-fibers.[163] More recently, An and co-workers[162] employed FROMP to 3D-print shape memory polymers in resins containing cyclooctene as a comonomer. Similar work from Appelhans and co-workers[375] demonstrated that stereolithographic additive manufacturing via photoROMP of **DCPD** can generate complex shapes with sub mm-scale resolution (e.g., chess pieces). While technically not a frontal process, adaptation of this system to FP may access new material spaces. Currently, FP printing is limited to relatively small volumes (<10 L). Nevertheless, exciting work from Tonoyan and co-workers[243] developed a continuous flow reactor for extrusion of **PA**-based hydrogels via FP. Future efforts to achieve large-scale FP extrusion, however, may benefit from earlier works described in this review.[32,157,162,243,374]

In contrast to large-scale manufacturing processes, one may imagine possible industrial applications to fabricate small parts and components, such as those produced in the context of microfluidic devices (section 5.4.6).[278] In such cases, front initiation is less problematic than front-quenching associated with high surface area to volume ratios. Section 4 highlights potential chemical modifications that can mitigate front quenching (e.g., increased initiator concentration, inclusion of monomers with larger ΔH_r values). In contrast, elevation of the ambient temperature (*i.e.*, T_s as defined in section 3.1) dampens heat lost to the surroundings. Indeed, FP initiated in an environmental chamber heated to 40 °C in narrow reaction

https://doi.org/10.1021/acs.chemrev.2c00686
Chem. Rev. 2023, 123, 3237−3298

vessels (such as an NMR tube) overcomes front-quenching without alterations to the resin composition.

While application to major industrial processes has *yet* to occur, significant efforts are ongoing to commercialize FP-derived technologies. As mentioned in sections 5.4.1 and 5.4.4, several commercially available products involving FP exist (i.e., QuickCure WoodFiller and Clay). As of 2022, the number of patents related to FP exceeds 40 and covers a diverse set of applications including adhesives,[376−378] material consolidations,[379−381] fabrication of optical lenses,[382] disinfectants,[383] 3D printing,[384] patterned materials,[338,385,386] structure fabrication,[381,387] and sorbents/hydrogels.[388,389] While the scientific barrier for granting patents is perhaps lower than that associated with academic publications, the existence of an extensive patent library suggests that industrial implementation may be imminent. As mentioned previously, the goal of this review is to inform the broader community about the advantages of FP in the hopes that future industrialists adopt this as a manufacturing technique.

6. SUMMARY AND OUTLOOK

6.1. Summary: Where are We Now?

Frontal polymerization (FP) addresses several major limitations of traditional bulk polymerizations (BP). This process requires an initial stimulus (mainly, thermal, photo) to ignite a hot reaction zone, aptly named the polymerization front. Effective generation and transfer of the heat of polymerization enables propagation of the front throughout the monomer media. Unlike other BPs, curing occurs rapidly with frontal velocities (ν_f) in the range of 0.1 to 10 cm min^{-1}, or even more. Hence, the energy and reaction time efficiencies of FP far exceed classical techniques. Visual detection of the hot fronts is typically possible by the human eye, though IR-thermographic imaging (or optical pyrometry) enables real-time determination of the thermal dynamics.[29,47,48,50]

As discussed in detail in section 3, FP requires heat transfer through the reaction media to occur faster than heat-loss; the only heat energy added to the propagating system after ignition originates from polymerization itself.[41,57] The generated heat is transferred in the monomer via conduction and advection phenomena to further propagate the front. In contrast, heat-loss to the surroundings occur at the system's boundary conditions (e.g., conduction through the container, convection through air/solvent/fillers). Imbalances of heat generation, transfer, and loss may result in undesired bulk polymerization (heat generation- or transfer-dominated), front quenching (heat loss-dominated), or thermal instabilities. Complete monomer consumption necessitates that the exothermicity and kinetics of polymerization match the front velocity and heat loss.[41,57] The geometry of the propagating front influences the frontal parameters (i.e., T_{max} and ν_f), and polymerization can occur in a descending or ascending manner in vertically aligned systems;[134] indeed, even horizontal and spherically propagating fronts are accessible.[67,135]

As discussed in section 4, several distinct chemistries provide stable frontal systems: frontal ring-opening metathesis polymerization (FROMP), cationic polymerization, free-radical polymerization, atom transfer radical polymerization (ATRP), polymerizations involving urethanes, and stoichiometric curing reactions. Apart from ATRP and polyurethanes, which have not been thoroughly investigated, only FROMP occurs catalytically with the use of the commercial Grubbs-type ruthenium alkylidene complexes (e.g., **G1** and **G2**; section 4.1; refs 32, 41, 51, 52, 69, 72, 73, 76, 105, 126, 147−149, 153, 154, 162, 164, 165). Highly strained, cyclic olefins undergo living catalytic polymerization; frontally derived polymers of dicyclopentadiene (**DCPD**) exhibit desirable mechanical properties via extensive cross-linking during catalysis. Perhaps counterintuitively to most catalyst design principles, FROMP and polyurethane-based systems[71,75,198−200] require *worse* catalysts to circumvent rapid background polymerization. Frontal epoxy polymers, as discussed in section 4.2.1, are obtainable through cationic polymerizations, whereby the addition of acid activates the monomer for polymerization (refs 34, 62, 64, 74, 80, 82, 83, 133, 181, 182, 188, 189, 191, 192). For control over the polymerization event, acid generation must occur *in situ* from thermal or photothermal acid sources.

The majority of published reports employ frontal free-radical polymerization (Section 4.3; refs 29, 33, 34, 44, 47−50, 53, 60−63, 70, 77−79, 81, 84−93, 95, 114, 127, 134, 199, 201−241, 249−254, 256, 257). The addition of a thermal radical source induces a series of radical chain reactions of acrylate or acrylamide derived monomers. The nature of the initiator dictates several key features. Many radical sources have the potential to exude gaseous side products. The resultant bubbles within the polymer reduce the structural properties of the polymer, and can negatively impact the perpetuation process by insulating the monomers from the hot polymerization front. Development of persulfate-based initiators has largely circumvented these undesired effects, since decomposition occurs without gas generation. The identity of the monomers in frontal free-radical polymerization impacts the structural features of the final product. Typically, the addition of cross-linking monomers (often di- or triacrylates) generates polymers with good mechanical properties. Substantial research efforts have focused on the effects of embedded inert materials. Such fillers depress the frontal parameters, ν_f and T_{max}, but provide polymer composites with highly desirable mechanical properties.

There exist numerous potential applications for FP as a result of the rapid rate of polymerization. Swellable hydrogels (section 5.1) with well-defined pore sizes are easily obtained with frontal free-radical polymerization techniques (refs 61, 84−90, 206−209, 212, 213, 220, 228, 229, 232, 233, 236, 237, 239, 252, 254, 256, 259, 263−267, 270, 271, 306, 313), which is in stark contrast to batch-scale methods. These frontally derived hydrogels exhibit stimuli responsive behavior, wherein the swelling properties vary with nature of the surroundings (e.g., temperature, pH). Several appealing uses of these stimuli-responsive polymers exist (sections 5.1.2 through 5.1.6), ranging from heavy metal ion removal[233,236,263−266] to controlled drug delivery[91,208,237,313] or chemical detection.[212,239,267] Besides hydrogel generation, functionally gradient polymers (refs 149, 204, 221) and composite materials (refs 32, 44, 50, 53, 64, 69, 77, 210, 234, 238, 250, 251, 253, 262, 268, 270−272, 306) are easily obtained via FP (sections 5.2 and 5.4, respectively). Successful reactivity within a semiporous substrate (e.g., wood, stone), for example, provides structural reinforcement, which has direct implications for consolidation and conservation purposes.[44,50,53,55,210,234,238,341−343] Embedding frontally derived polymers with inorganic components imparts unique electronic and photophysical properties with reasonable retention of the desirable polymer mechanical features. Indeed, photolumines-

https://doi.org/10.1021/acs.chemrev.2c00686
Chem. Rev. 2023, 123, 3237−3298

cent polymers exist and are compatible with existing devices, such as LEDs (section 5.4.5).[77,211,262,270−272,306] Perhaps the most promising application of FP involves on-demand curing of thermoset plastics and composites.[32,64,69,105] For example, micropatterned and glass-fiber reinforced frontal p(**DCPD**) thermoset composites are rapidly synthesized at a fraction of the energy costs required by traditional methods.[32,51,126]

6.2. Outlook: Where Do We Go from Here?

A need exists for efficient, low-energy alternatives to polymer material synthesis, especially in light of the massive scale that plastics are produced annually. For successful integration of FP into existing manufacturing technologies, the field must address and overcome several key challenges, the first of which involves scalability. FP necessitates efficient heat-transfer with minimal loss to the surroundings, as only the polymerization exothermicity provides the required driving energy. While cm to mm diameter scale reactions occur without much difficulty, industrially relevant reaction sizes still remain relatively unexplored. On the other hand, the synthesis of large but thin frontally derived polymer sheets is likely problematic given the excess surface area relative to volume, which favors rapid heat-loss from the system. At the other extreme, problems may arise from uncontrolled autoacceleration phenomena, which terminate the propagating front via spontaneous polymerization events. Hence, any solution that addresses heat-loss must also not favor uncontrollable rate increases.

One potential solution provided involves embedded conductive fibers (i.e., copper or stainless steel wires, carbon fibers) to aid in the heat transfer through the reaction media.[35,69,246,253] Other possible solutions may include multipoint ignition, whereby multiple sites undergo simultaneous initiation and propagation. The interfaces between the multiple propagation sites, however, must not introduce structural defects. Indeed, theoretical and experimental evidence indicates that complete monomer conversion occurs when samples are ignited at multiple locations.[32,41,69] Further study into the mechanical properties at the multifront junctions will aid in understanding the frontal dynamics of large-scale reactions.

The current circular economy concept requires the use of low environmental impact chemistries (e.g., biosourced), and drives both academic and industrial researchers toward the design, preparation, and application of new polymer materials.[390] In this context, FP may represent an effective and attractive alternative to existing technologies. The use of solvent-free, low-energy FP processes may advance this ecological transition. Moreover, the creation of deconstructible polymers through FP will benefit waste management and address the end-of-life problem that plagues most commodity plastics. In this concept, structurally robust materials undergo controlled disassembly reactions at targeted sites only in the presence of orthogonal chemistries. Indeed, several examples[170,172,173,175,391,392] demonstrated the feasibility of such a thermoset deconstruction strategy (section 4.1.3). Ideally, these smaller components may themselves act as monomers for future upcycling/polymerization reactions.

The economics of FP also represents a potential challenge for large-scale applications. The overall price of FP must not exceed existing technologies, otherwise the financial benefits afforded by the low-energy requirements are outweighed by the material costs. For example, FROMP requires a relatively expensive Ru-based catalyst, albeit in low loadings, for polymerization to occur (section 4.1). Alternatively, gas-free frontal free-radical polymerizations require pricy persulfate salts in addition to added cross-linking monomers to achieve desirable mechanical properties (section 4.3). Indeed, the solutions to these economic factors likely require creative engineering and chemical solutions. Significant chemical space exists, however, in the development of new frontally obtainable materials. While FP is compatible with a variety of filling materials (e.g., clays, biopolymers, graphite, to name a few), other FP-derived composites may extend the possible applications. For example, the inclusion of metals into frontally derived polymers, either as molecular species or as a bulk extended network, is relatively unexplored. Despite these challenges, great opportunities exist for FP (Figure 45) and those who seek to develop it further.

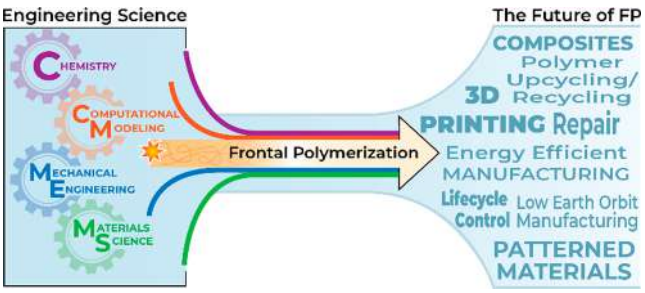

Figure 45. Merging tributary of interdisciplinary research feeds into an endless sea of future possibilities with FP.

AUTHOR INFORMATION

Corresponding Authors

Benjamin A. Suslick − *Beckman Institute for Advanced Science and Technology, University of Illinois at Urbana−Champaign, Urbana, Illinois 61801, United States; Department of Chemistry, University of Illinois at Urbana−Champaign, Urbana, Illinois 61801, United States;* orcid.org/0000-0002-6499-3625; Email: suslick@illinois.edu

Jeffrey S. Moore − *Beckman Institute for Advanced Science and Technology, University of Illinois at Urbana−Champaign, Urbana, Illinois 61801, United States; Department of Chemistry, University of Illinois at Urbana−Champaign, Urbana, Illinois 61801, United States;* orcid.org/0000-0001-5841-6269; Email: jsmoore@illinois.edu

Authors

Julie Hemmer − *Beckman Institute for Advanced Science and Technology, University of Illinois at Urbana−Champaign, Urbana, Illinois 61801, United States*

Brecklyn R. Groce − *Department of Chemistry, Louisiana State University, Baton Rouge, Louisiana 70803, United States*

Katherine J. Stawiasz − *Beckman Institute for Advanced Science and Technology, University of Illinois at Urbana−Champaign, Urbana, Illinois 61801, United States; Department of Chemistry, University of Illinois at Urbana−Champaign, Urbana, Illinois 61801, United States;* orcid.org/0000-0003-2518-0557

https://doi.org/10.1021/acs.chemrev.2c00686
Chem. Rev. 2023, 123, 3237−3298

Philippe H. Geubelle − *Beckman Institute for Advanced Science and Technology, University of Illinois at Urbana−Champaign, Urbana, Illinois 61801, United States; Department of Aerospace Engineering, University of Illinois at Urbana−Champaign, Urbana, Illinois 61801, United States;* orcid.org/0000-0002-4670-5474

Giulio Malucelli − *Department of Applied Science and Technology, Politecnico di Torino, 15121 Alessandria, Italy;* orcid.org/0000-0002-0459-7698

Alberto Mariani − *Department of Chemical, Physical, Mathematical and Natural Sciences, University of Sassari, 07100 Sassari, Italy; National Interuniversity Consortium of Materials Science and Technology, 50121 Firenze, Italy;* orcid.org/0000-0001-8973-4542

John A. Pojman − *Department of Chemistry, Louisiana State University, Baton Rouge, Louisiana 70803, United States;* orcid.org/0000-0003-4788-8767

Nancy R. Sottos − *Beckman Institute for Advanced Science and Technology, University of Illinois at Urbana−Champaign, Urbana, Illinois 61801, United States; Department of Materials Science and Engineering, University of Illinois at Urbana−Champaign, Urbana, Illinois 61801, United States;* orcid.org/0000-0002-5818-520X

Complete contact information is available at: https://pubs.acs.org/10.1021/acs.chemrev.2c00686

Author Contributions

CRediT: **Benjamin A Suslick** conceptualization, data curation, formal analysis, project administration, visualization, writing-original draft, writing-review & editing; **Julie Hemmer** writing-original draft, writing-review & editing; **Brecklyn R Groce** writing-review & editing; **Katherine J. Stawiasz** writing-review & editing; **Philippe H Geubelle** funding acquisition, writing-review & editing; **Giulio Malucelli** writing-review & editing; **Alberto Mariani** funding acquisition, writing-review & editing; **Jeffrey S. Moore** funding acquisition, supervision, writing-review & editing; **John Anthony Pojman** funding acquisition, writing-review & editing; **Nancy R. Sottos** funding acquisition, writing-review & editing.

Notes

The authors declare the following competing financial interest(s): J.A.P. declares a financial conflict of interest with QuickCure Clay and QuickCure WoodFiller. The other authors have no conflicts to declare.

Biographies

Benjamin A. Suslick was born in Urbana, IL, in 1992. He discovered his passion for chemistry while working as a high-school student in the Kenneth S. Suslick and Gregory S. Girolami research groups at the University of Illinois at Urbana−Champaign. He, then, received his B.S. in 2014 from the California Institute of Technology working with Prof. Robert H. Grubbs. As an NSF Graduate Research Fellow, he received his Ph.D. from the University of California, Berkeley under the direction of Prof. T. Don Tilley. After graduating in 2019, Ben returned to the University of Illinois to begin his current position as a postdoctoral research associate in the Jeffrey S. Moore group.

Julie Hemmer received her Ph.D. in mechanical and process engineering from the Ecole Centrale de Nantes (France) in 2018, under the direction of Prof. Binetruy and Prof. Comas-Cardona as a CIFRE-ANRT fellow. Passionate about interdisciplinary scientific subjects, she joined the Beckman Institute as a Postdoctoral Fellow in 2019. While at Illinois, she focused on the instabilities and fluid flow arising during frontal polymerization, in collaboration with the Philippe H. Geubelle and Nancy R. Sottos groups.

Brecklyn R. Groce obtained his B.S. in chemistry in 2019 from the University of West Florida in Pensacola, FL. He is currently a Ph.D. candidate and Louisiana Board of Regents Fellow at Louisiana State University working under the guidance of Dr. John Pojman. His research interests focus on the development and study of resins that utilize cationic frontal polymerization and their applications to cure on-demand materials and additive manufacturing.

Katherine J. Stawiasz graduated magna cum laude from Cornell University's chemistry department in 2018. While in Ithaca, she performed undergraduate research with Prof. Brett Fors and developed an interest in polymer chemistry. Katie then moved to Champaign, Illinois to pursue graduate studies with Prof. Jeff Moore as an NDSEG fellow. There, she focused on the fabrication of thermoset materials using frontal ring-opening metathesis polymerization with focuses in catalyst design and photoinitiation. After completing her Ph.D., Katie joined 3M's corporate research laboratories where she currently is a senior research chemist.

Philippe H. Geubelle is originally from Belgium; he received his B.Sc. in mechanical engineering at the Catholic University of Louvain in 1988, and his Ph.D. in aeronautics at the California Institute of Technology in 1993. After a year as postdoc at Harvard, he joined the faculty in 1995 at the University of Illinois, Urbana−Champaign, where he is currently the Bliss Professor in the Department of Aerospace Engineering, with a joint appointment at the Beckman Institute for Advanced Science and Technology. For the past four years, he has been serving as the Executive Associate Dean of the Grainger College of Engineering. His research interests pertain to the field of solid mechanics and materials with emphasis on composite manufacturing, multiscale analysis and design of materials, fracture mechanics, and multiphysics modeling of biomimetic multifunctional materials.

Giulio Malucelli was born in Cuneo (Italy) in 1967. He received his Master degree in Chemical Engineering in 1992 from Politecnico di Torino, Italy, and a Ph.D. in Chemistry in 1996 from the University of Genova (Italy) under the direction of Prof. A. Priola. At present, he is Professor of Materials Science and Technology at the Department of Applied Science and Technology, Alessandria branch, where he investigates the structure−property relationships in polymer systems, polymer blends, and their micro- and nanocomposites. He has coauthored more than 280 peer-reviewed papers (from Scopus database—accessed on 9 January 2023−9457 total citations by 5133 documents; h Index: 57), 40 book chapters, 1 book, and more than 260 Communications to National and International Congresses.

Alberto Mariani was born in Bressanone, a town in the very North of Italy, in 1963. He moved to Sassari (Sardinia island) during high school. While in Sassari, he also acquired his masters degree in Chemistry and a Ph.D. in Chemical Sciences under the direction of Prof. Saverio Russo on aromatic polyamides. In 1999, he met John A. Pojman who introduced him to Frontal Polymerization, which became his main research topic. At present, he is Professor of Industrial and Polymer Chemistry at the University of Sassari.

Jeffrey S. Moore received his B.S. in chemistry and Ph.D. in materials science and engineering from the University of Illinois, Urbana−Champaign. He then went to Caltech as an NSF Postdoctoral Fellow working with Robert Grubbs. In 1990, he joined the faculty at the University of Michigan, Ann Arbor, and returned to the University of Illinois in 1993, where he is currently the Stanley O. Ikenberry Research Professor of Chemistry. Jeff is a member of the National

https://doi.org/10.1021/acs.chemrev.2c00686
Chem. Rev. 2023, 123, 3237−3298

Academy of Sciences and a fellow of the American Academy of Arts & Sciences, the American Association for the Advancement of Science and the American Chemical Society; he has also received the Campus Award for Excellence in Undergraduate Teaching. For 14 years, he served as an associate editor for the Journal of American Chemical Society. In 2014, he was selected as a Howard Hughes Medical Institute Professor and received the 2016 ACS Edward Leete Award in Organic Chemistry. He received the RSC's Materials Chemistry Division 2018 Stephanie L. Kwolek Award and was part of a team that was honored with the Secretary of Energy Honor Award, Achievement Award the same year. Jeff was also awarded the 2019 National Award in Polymer Chemistry by the American Chemical Society. He has published over 400 articles covering topics from technology in the classroom to self-healing polymers, mechanoresponsive materials and shape-persistent macrocycles. From 2016 to 2022, he was the Director of the Beckman Institute for Advanced Science and Technology. In this role, he received the 2021 Executive Officer Distinguished Leadership Award from the UIUC Campus.

John A. Pojman was born in Cleveland, Ohio, in 1962. He received his B.S. in Chemistry (with a minor in Classics) from Georgetown University in 1984. He earned his doctorate in Chemical Physics in 1988 at the University of Texas at Austin under the direction of James Whitesell and Ilya Prigogine. Pojman then worked for two years at Brandeis University with Irving Epstein. In 1990, he joined the Chemistry & Biochemistry department at The University of Southern Mississippi, where he taught for 18 years. Dr. Pojman joined the Department of Chemistry at Louisiana State University in August 2008, where he is the William and Patricia Senn, Jr., Distinguished Professor & Chair. He is also the founder and CEO of Pojman Polymer Products, LLC.

Nancy R. Sottos holds the Maybelle Leland Swanlund Endowed Chair and is Head of the Department of Materials Science and Engineering at the University of Illinois, Urbana−Champaign. She is a member of the National Academy of Engineering, the National Academy of Science, and the American Academy of Arts and Sciences.

ACKNOWLEDGMENTS

B.A.S, J.H., K.J.S., P.H.G., N.R.S., and J.S.M acknowledge the National Science Foundation under award number NSF CMMI 19-33932, the Air Force Office of Scientific Research (Center of Excellence Phase II) under award number FA9550-20-1-0194, and the Department of Energy (Office of Basic Energy Sciences, Energy Frontier Research Center) under an Award titled Regenerative Energy-Efficient Manufacturing of Thermoset Polymeric Materials (REMAT). K.J.S. acknowledges the U.S. Department of Defense for an NDSEG fellowship. A.M. acknowledges FAR-UNISS 2019-21 for funding. B.R.G. and J.A.P acknowledge the National Science Foundation EPSCoR-Louisiana Materials Design Alliance (LAMDA) program under Award number OIA-1946231. We also acknowledge Dorothy Loudermilk for creating several figures in this work.

ABBREVIATIONS, TERMS, AND SYMBOLS

A	Arrhenius pre-exponential factor (s^{-1})
AA	acrylic acid
AAS	alkaline activated solution
AIBN	azobis(isobutyronitrile)
α	degree of conversion
AM	acrylamide
APS	ammonium persulfate
ATRP	atom transfer radical polymerization
BADGE	bisphenol A diglycidyl ether
BFDGE	bisphenol F diglycidyl ether
β	Zeldovich number
β_c	critical Zeldovich number
BP	bulk polymerization
BPO	benzoyl peroxide
CD	cyclodextrin
CDots	carbon dots
CE	3,4-epoxycyclohexylmethyl-3′,4′-epoxycyclohexanecarboxylate
CHDGE	cyclohexanedimethanol diglycidyl ether
CHP	cumene hydroperoxide
COD	cyclooctadiene
C_p	specific heat capacity (J kg^{-1} K^{-1})
CR	cited references
CQDs	colloidal quantum dots
CTA	chain-transfer agent
$Đ$	dispersity
DGEVA	diglycidyl ether of vanillyl alcohol
DBTDL	dibutyl tin dilaurate
DCPD	dicyclopentadiene
DETA	diethylenetriamine
DHF	2,3-dihydrofuran
DMA	dynamic mechanical analysis
DMAEMA	dimethylaminoethyl acrylate
DMAP	dimethylaminopyridine
DOX	3,3′-(oxybis(methylene))bis(3-ethyloxetane)
DSC	differential scanning calorimetry
E	Young's modulus (MPa or GPa)
E'	storage modulus (MPa or GPa)
E″	loss modulus (MPa or GPa)
E_a	activation energy (J mol^{-1})
ENB	5-ethylidene-2-norbornene
FGM	functionally gradient material
FP	frontal polymerization
FGP	frontal geopolymerization
FROMP	frontal ring-opening metathesis polymerization
FTIR	Fourier-transformed IR spectroscopy
G1	1st generation Grubbs catalyst [$(PCy_3)_2Ru(=CHPh)Cl_2$]
G2	2nd generation Grubbs catalyst [$(SIMes)Ru(=CHPh)(PCy_3)Cl_2$]
GP	geopolymerization
GPTMS	(3-glycidoxypropyl)trimethoxysilane
HA	hexyl acrylate
HDDA	1,6-hexanediol diacrylate
HDGE	1,6-hexanediol diglycidyl ether
HEA	hydroxyethyl acrylate
HOPH-SbF_6	[4-(2-hydroxytetradecyl)oxy]phenyliodonium-SbF_6
H_r or ΔH_p	heat of polymerization (J g^{-1})
HPA	2-hydroxypropyl acrylate
IOC-8-SbF_6	[(4-(octyloxy)phenyl]phenyliodonium-SbF_6
IPN	interpenetrating network
κ	thermal conductivity (W m^{-1} K^{-1})
KPS	potassium persulfate
LCST	lower critical solution temperature (°C)
LSA	linear stability analysis
L_θ	characteristic front length
M	molar (mol L^{-1})
MA	methyl acrylate
MAA	methyacrylic acid
MBAm	N,N'-methylenebis(acrylamide)

https://doi.org/10.1021/acs.chemrev.2c00686
Chem. Rev. 2023, 123, 3237−3298

MK	metakaolin
MMA	methyl methacrylate
MPS	(3-mercaptopropyl)trimethoxysilane
NBE	norbornene
NHC	*N*-heterocylic carbene
NIPAm	*N*-isopropylacrylamide
NMAm	*N*-methylolacrylamide
NMR	nuclear magnetic resonance
NPDGE	neopentyl glycol diglycidyl ether
NVC	*N*-vinylcarbazole
NVP	*N*-vinylcaprolactam
OPC	ordinary Portland concrete
PAG	photoacid generator
PDMS	poly(dimethylsiloxane)
φ	heat flux (W m^{-2})
phr	per hundred rubber
POX	3-ethyl-3-(phenoxymethyl)oxetane
PPC	poly(propylene carbonate)
Q	total heat energy per volume (W m^{-3})
R	universal gas constant (J mol^{-1} K^{-1})
RPYS	reference publication year spectroscopy
ρ	density (kg m^{-3})
SEM	scanning electron microscopy
SIMes	1,3-bis(2,4,6-trimethylphenyl)-4,5-dihydroimidazol-2-ylidene
SP	spontaneous polymerization
SPAK	3-sulfopropyl acrylate
SPION	super paramagnetic Fe_3O_4 nanoparticles
SPN	supramolecular penetrating network
SR%	swelling ratio (%)
TBPPS	tetra-butyl phosphonium persulfate
TEGDA	triethylene glycol diacrylate
TEGDMA	triethylene glycol dimethacrylate
TFEMA	2,2,2-trifluoroethyl methacrylate
T_g	glass-transition temperature (°C)
TGA	thermogravimetric analysis
θ	normalized temperature
t_{ignite}	ignition time (s)
T_m	melting temperature (°C)
T_{max}	maximum front temperature (°C)
TMEDA	*N,N,N′,N′*-tetramethylethylenediamine
TMPTA	trimethylolpropane triacrylate
TMPTGE	trimethylolpropane triglycidyl ether
TPED	1,1,2,2-tetraphenylethylenediol
TPU	thermoplastic polyurethane
TREN	tris(2-aminoethyl)amine
t_{ss}	presteady state time (s)
VARTM	vacuum-assisted resin transfer molding
ν_f	steady-state frontal velocity (mm s^{-1} or cm s^{-1})
VI	1-vinyl imidazole
WoS	Web of Science

REFERENCES

(1) Bachmann, J.; Hidalgo, C.; Bricout, S. Environmental Analysis of Innovative Sustainable Composites with Potential Use in Aviation Sector—a Life Cycle Assessment Review. *Sci. China Technol. Sci.* **2017**, *60*, 1301−1317.

(2) Giurgiutiu, V. Chapter 1—Introduction. In *Structural Health Monitoring of Aerospace Composites*; Giurgiutiu, V., Ed.; Academic Press: Oxford, 2016; pp 1−23.

(3) Timmis, A. J.; Hodzic, A.; Koh, L.; Bonner, M.; Soutis, C.; Schäfer, A. W.; Dray, L. Environmental Impact Assessment of Aviation Emission Reduction through the Implementation of Composite Materials. *Int. J. Life Cycle Assess.* **2015**, *20*, 233−243.

(4) Friedrich, K.; Almajid, A. A. Manufacturing Aspects of Advanced Polymer Composites for Automotive Applications. *Appl. Compos. Mater.* **2013**, *20*, 107−128.

(5) Karbhari, V. M.; Seible, F. Fiber Reinforced Composites - Advanced Materials for the Renewal of Civil Infrastructure. *Appl. Compos. Mater.* **2000**, *7*, 95−124.

(6) Brøndsted, P.; Lilholt, H.; Lystrup, A. Composite Materials for Wind Power Turbine Blades. *Annu. Rev. Mater. Res.* **2005**, *35*, 505−538.

(7) Abliz, D.; Duan, Y.; Steuernagel, L.; Xie, L.; Li, D.; Ziegmann, G. Curing Methods for Advanced Polymer Composites - a Review. *Polym. Polym. Compos.* **2013**, *21*, 341−348.

(8) Herrmann, C.; Dewulf, W.; Hauschild, M.; Kaluza, A.; Kara, S.; Skerlos, S. Life Cycle Engineering of Lightweight Structures. *CIRP Annals* **2018**, *67*, 651−672.

(9) Bhat, G.; Kandagor, V. 1—Synthetic Polymer Fibers and Their Processing Requirements. In *Advances in Filament Yarn Spinning of Textiles and Polymers*; Zhang, D., Ed.; Woodhead Publishing: 2014; pp 3−30.

(10) Elias, H.-G.; Mülhaupt, R. Plastics, General Survey, 2. Production of Polymers and Plastics. In *Ullmann's Encyclopedia of Industrial Chemistry*; Wiley-VCH: Weinheim, Germany, 2015; pp 1−38.

(11) IPCC, 2021: Summary for Policymakers. In *Climate Change 2021: The Physical Science Basis. Contriution of Working Group I to the Sixth Assessment Report of the Intergovernmental Panel on Climate Change*; Masson-Delmotte, V., Zhai, P., Pirani, A., Connors, S. L., Péan, C., Berger, S., Caud, N., Chen, Y., Goldfarb, L., Gomis, M. I., et al., Eds.; Cambridge University Press: Cambridge, UK, 2021; pp 1−3949.

(12) Elias, H.-G.; Mülhaupt, R. Plastics, General Survey, 5. Plastics and Sustainability. In *Ullmann's Encyclopedia of Industrial Chemistry*; Wiley-VCH: Weinheim, Germany, 2015; pp 1−7.

(13) Marx, W.; Bornmann, L.; Barth, A.; Leydesdorff, L. Detecting the Historical Roots of Research Fields by Reference Publication Year Spectroscopy (RPYS). *J. Assoc. Inf. Sci. Technol.* **2014**, *65*, 751−764.

(14) Chechilo, N. M.; Enikolopyan, N. S. Structure of the Polymerization Wave Front and Propagation Mechanism of the Polymerization Reactions. *Dolk. Phys. Chem.* **1974**, *214*, 174−176.

(15) Chechilo, N. M.; Khvilivitskii, R. J.; Enikolopyan, N. S. Propagation of the Polymerization Reaction. *Dolk. Akad. Nauk SSSR* **1972**, *204*, 1180.

(16) Shkadinskii, K. G.; Khaikin, B. I.; Merzhanov, A. G. Propagation of a Pulsating Exothermic Reaction Front in the Condensed Phase. *Combust. Explos. Shock Waves* **1973**, *7*, 15−22.

(17) Varma, A.; Lebrat, J.-P. Combustion Synthesis of Advanced Materials. *Chem. Eng. Sci.* **1992**, *47*, 2179−2194.

(18) Surkov, N. F.; Davtyan, S. P.; Rozenberg, B. A.; Enikolopyan, N. S. Calculation of the Steady-State Velocity of the Reaction Front During the Curing of Epoxy Olgiomers by Diamines. *Dolk. Akad. Nauk SSSR* **1976**, *228*, 141−144.

(19) Sivashinsky, G. On Spinning Propagation of Combustion Waves. *SIAM J. Appl. Math.* **1981**, *40*, 432−438.

(20) Vol'pert, V. A.; Megrabova, I. N.; Davtyan, S. P.; Begishev, V. P. Propagation of the Caprolactam Polymerization Wave. *Combust. Explos. Shock Waves* **1985**, *21*, 443−447.

(21) Maksimov, Y. M.; Merzhanov, A. G.; Pak, A. T.; Kuchkin, M. N. Unstable Combustion Modes of Gasless Systems. *Combust. Explos. Shock Waves* **1982**, *17*, 393−400.

(22) Shkiro, V. M.; Nersisyan, G. A. Structure of Fluctuations Occurring in the Burning of Tantalum-Carbon Mixtures. *Combust. Explos. Shock Waves* **1978**, *14*, 121−122.

(23) Khanukaev, B. B.; Kozhushner, M. A.; Enikolopyan, N. S.; Chechilo, N. M. Theory of the Propagation of a Polymerization Front. *Combust. Explos. Shock Waves* **1974**, *10*, 17−21.

(24) Khanukaev, B. B.; Kozhushner, M. A.; Enikolopyan, N. S. Theory of Polymerization-Front Propagation. *Combust. Explos. Shock Waves* **1974**, *10*, 562−568.

https://doi.org/10.1021/acs.chemrev.2c00686
Chem. Rev. 2023, 123, 3237−3298

(25) Maksimov, Y. M.; Pak, A. T.; Lavrenchuk, G. B.; Naiborodenko, Y. S.; Merzhanov, A. G. Spin Combustion of Gasless Systems. *Combust. Explos. Shock Waves* **1979**, *15*, 415−418.
(26) Chechilo, N. M.; Enikolopyan, N. S. Structure of a Polymerization Wave Front and Mechanism of Polymerization Propagation. *Dolk. Akad. Nauk SSSR* **1974**, *214*, 1131−1133.
(27) Merzhanov, A. G.; Filoneko, A. K.; Borovinskaya, I. P. New Phenomena in Combustion of Condensed Systems. *Dolk. Akad. Nauk SSSR* **1973**, *208*, 892−894.
(28) Kojevnikov, A. The Phenomenon of Soviet Science. *Osiris* **2008**, *23*, 115−135.
(29) Pojman, J. A.; Ilyashenko, V. M.; Khan, A. M. Free-Radical Frontal Polymerization: Self-Propagating Thermal Reaction Waves. *J. Chem. Soc., Faraday Trans.* **1996**, *92*, 2825−2837.
(30) Pojman, J. A. 4.38—Frontal Polymerization. In *Polymer Science: A Comprehensive Reference*; Matyjaszewski, K., Möller, M., Eds.; Elsevier: Amsterdam, 2012; pp 957−980.
(31) Davtyan, S. P.; Zhirkov, P. V.; Vol'fson, S. A. Problems of Non-Isothermal Character in Polymerisation Processes. *Russ. Chem. Rev.* **1984**, *53*, 150−163.
(32) Robertson, I. D.; Yourdkhani, M.; Centellas, P. J.; Aw, J. E.; Ivanoff, D. G.; Goli, E.; Lloyd, E. M.; Dean, L. M.; Sottos, N. R.; Geubelle, P. H.; Moore, J. S.; White, S. R. Rapid Energy-Efficient Manufacturing of Polymers and Composites Via Frontal Polymerization. *Nature* **2018**, *557*, 223−227.
(33) Fortenberry, D. I.; Pojman, J. A. Solvent-Free Synthesis of Polyacrylamide by Frontal Polymerization. *J. Polym. Sci., Part A: Polym. Chem.* **2000**, *38*, 1129−1135.
(34) Bomze, D.; Knaack, P.; Koch, T.; Jin, H.; Liska, R. Radical Induced Cationic Frontal Polymerization as a Versatile Tool for Epoxy Curing and Composite Production. *J. Polym. Sci., Part A: Polym. Chem.* **2016**, *54*, 3751−3759.
(35) Vyas, S.; Zhang, X.; Goli, E.; Geubelle, P. H. Frontal Vs. Bulk Polymerization of Fiber-Reinforced Polymer-Matrix Composites. *Compos. Sci. Technol.* **2020**, *198*, 108303.
(36) By analogy, one may consider supercritical nuclear fission as an extreme example of an uncontrolled propagation process; without a proper moderator, the chain-propagation accelerates and becomes a "run-away" reaction.
(37) Odian, G. *Principles of Polymerization*, 4th ed.; John Wiley & Sons, Inc.: Hoboken, NJ, 2004.
(38) Trommsdorff, E.; Kohle, H.; Lagally, P. Polymerization of Methyl Methacrylates. *Makromol. Chem.* **1948**, *1*, 169−198.
(39) Norrish, R. G. W.; Smith, R. Catalyzed Polymerization of Methylmethacrylate in the Liquid Phase. *Nature* **1942**, *150*, 336−337.
(40) Comissiong, D. M. G.; Gross, L. K.; Volpert, V. A. Nonlinear Dynamics of Frontal Polymerization with Autoacceleration. *J. Eng. Math.* **2005**, *53*, 59−78.
(41) Goli, E.; Robertson, I. D.; Geubelle, P. H.; Moore, J. S. Frontal Polymerization of Dicyclopentadiene: A Numerical Study. *J. Phys. Chem. B* **2018**, *122*, 4583−4591.
(42) Goli, E.; Gai, T.; Geubelle, P. H. Impact of Boundary Heat Losses on Frontal Polymerization. *J. Phys. Chem. B* **2020**, *124*, 6404.
(43) Pojman, J. A.; Masere, J.; Petretto, E.; Rustici, M.; Huh, D.-S.; Kim, M. S.; Volpert, V. The Effect of Reactor Geometry on Frontal Polymerization Spin Modes. *Chaos* **2002**, *12*, 56−65.
(44) Robertson, I. D.; Hernandez, H. L.; White, S. R.; Moore, J. S. Rapid Stiffening of a Microfluidic Endoskeleton Via Frontal Polymerization. *ACS Appl. Mater. Interfaces* **2014**, *6*, 18469−18474.
(45) Pojman, J. A. Cure-on-Demand Composites by Frontal Polymerization. In *Reference Module in Materials Science and Materials Engineering*; Hashmi, M. S. J., Li, G., Eds.; Elsevier: Amsterdam, 2022; pp 85−100.
(46) Li, Q.; Shen, H.-X.; Liu, C.; Wang, C.-F.; Zhu, L.; Chen, S. Advances in Frontal Polymerization Strategy: From Fundamentals to Applications. *Prog. Polym. Sci.* **2022**, *127*, 101514.
(47) Pojman, J. A.; West, W. W.; Simmons, J. Propagating Fronts of Polymerization in the Physical Chemistry Laboratory. *J. Chem. Educ.* **1997**, *74*, 727.
(48) Masere, J.; Pojman, J. A. Free Radical-Scavenging Dyes as Indicators of Frontal Polymerization Dynamics. *J. Chem. Soc., Faraday Trans.* **1998**, *94*, 919−922.
(49) Washington, R. P.; Steinbock, O. Frontal Polymerization Synthesis of Temperature-Sensitive Hydrogels. *J. Am. Chem. Soc.* **2001**, *123*, 7933−7934.
(50) Brunetti, A.; Princi, E.; Vicini, S.; Pincin, S.; Bidali, S.; Mariani, A. Visualization of Monomer and Polymer inside Porous Stones by Using X-Ray Tomography. *Nucl. Instrum. Methods Phys. Res. B* **2004**, *222*, 235−241.
(51) Lloyd, E. M.; Feinberg, E. C.; Gao, Y.; Peterson, S. R.; Soman, B.; Hemmer, J.; Dean, L. M.; Wu, Q.; Geubelle, P. H.; Sottos, N. R.; Moore, J. S. Spontaneous Patterning During Frontal Polymerization. *ACS Cent. Sci.* **2021**, *7*, 603−612.
(52) Robertson, I. D.; Dean, L. M.; Rudebusch, G. E.; Sottos, N. R.; White, S. R.; Moore, J. S. Alkyl Phosphite Inhibitors for Frontal Ring-Opening Metathesis Polymerization Greatly Increase Pot Life. *ACS Macro Lett.* **2017**, *6*, 609−612.
(53) Bansal, K.; Pojman, J. A.; Webster, D.; Quadir, M. Frontal Polymerization of a Thin Film on a Wood Substrate. *ACS Macro Lett.* **2020**, *9*, 169−173.
(54) Usamentiaga, R.; Venegas, P.; Guerediaga, J.; Vega, L.; Molleda, J.; Bulnes, F. G. Infrared Thermography for Temperature Measurement and Non-Destructive Testing. *Sensors* **2014**, *14*, 12305−12348.
(55) Brunetti, A.; Mariani, A.; Bidali, S. X-Ray Tomography as an Estimation Technique for Wood Consolidation by Frontal Polymerization. *Il Nuovo Cimento C* **2007**, 407−413.
(56) Novozhilov, B. V. Propagation Rate of the Front of an Exothermic Reaction in Condensed Phase. *Dolk. Akad. Nauk SSSR* **1961**, *141*, 151−153.
(57) Solovyov, S. E.; Ilyashenko, V. M.; Pojman, J. A. Numerical Modeling of Self-Propagating Polymerization Fronts: The Role of Kinetics on Front Stability. *Chaos* **1997**, *7*, 331−340.
(58) Potzmann, P. M.; Lopez Villanueva, F. J.; Liska, R. UV-Initiated Bubble-Free Frontal Polymerization in Aqueous Conditions. *Macromolecules* **2015**, *48*, 8738−8745.
(59) Nason, C.; Roper, T.; Hoyle, C.; Pojman, J. A. UV-Induced Frontal Polymerization of Multifunctional (Meth)Acrylates. *Macromolecules* **2005**, *38*, 5506−5512.
(60) Nason, C.; Pojman, J. A.; Hoyle, C. The Effect of a Trithiol and Inorganic Fillers on the Photo-Induced Thermal Frontal Polymerization of a Triacrylate. *J. Polym. Sci., Part A: Polym. Chem.* **2008**, *46*, 8091−8096.
(61) Yan, Q.-Z.; Zhang, W.-F.; Lu, G.-D.; Su, X.-T.; Ge, C.-C. Frontal Polymerization Synthesis of Starch-Grafted Hydrogels: Effect of Temperature and Tube Size on Propagating Front and Properties of Hydrogels. *Chem. Eur. J.* **2006**, *12*, 3303−3309.
(62) Bomze, D.; Knaack, P.; Liska, R. Successful Radical Induced Cationic Frontal Polymerization of Epoxy-Based Monomers by C−C Labile Compounds. *Polym. Chem.* **2015**, *6*, 8161−8167.
(63) Evstratova, S. I.; Antrim, D.; Fillingane, C.; Pojman, J. A. Isothermal Frontal Polymerization: Confirmation of the Isothermal Nature of the Process and the Effect of Oxygen and Polymer Seed Molecular Weight on Front Propagation. *J. Polym. Sci., Part A: Polym. Chem.* **2006**, *44*, 3601−3608.
(64) Sangermano, M.; D'Anna, A.; Marro, C.; Klikovits, N.; Liska, R. Uv-Activated Frontal Polymerization of Glass Fibre Reinforced Epoxy Composites. *Compos. Part B. Eng.* **2018**, *143*, 168−171.
(65) Ritter, L. R.; Volpert, V. A.; Olmstead, W. E. Initiation of Free-Radical Polymerization Waves. *SIAM J. Appl. Math.* **2003**, *63*, 1831−1848.
(66) Inamdar, S. R.; Pujari, N. S.; Karimi, I. A.; Ponrathnam, S.; Tayal, R. K.; Kulkarni, B. D. Spinning Wave Motion in Frontal Polymerization. *Chem. Eng. Sci.* **2007**, *62*, 1448−1455.
(67) Urdiales, E.; Volpert, V. A. Linear Stability Analysis of Spherically Propagating Thermal Frontal Polymerization Waves. *J. Eng. Math.* **2011**, *71*, 279−290.
(68) Goldfeder, P. M.; Volpert, V. A.; Ilyashenko, V. M.; Khan, A. M.; Pojman, J. A.; Solovyov, S. E. Mathematical Modeling of Free-

https://doi.org/10.1021/acs.chemrev.2c00686
Chem. Rev. 2023, 123, 3237−3298

Radical Polymerization Fronts. *J. Phys. Chem. B* **1997**, *101*, 3474−3482.
(69) Goli, E.; Robertson, I. D.; Agarwal, H.; Pruitt, E. L.; Grolman, J. M.; Geubelle, P. H.; Moore, J. S. Frontal Polymerization Accelerated by Continuous Conductive Elements. *J. Appl. Polym. Sci.* **2019**, *136*, 47418.
(70) Parrinello, C. A.; Bounds, C. O.; Liveri, M. L. T.; Pojman, J. A. Thermal Frontal Polymerization with a Thermally Released Redox Catalyst. *J. Polym. Sci., Part A: Polym. Chem.* **2012**, *50*, 2337−2343.
(71) Fiori, S.; Mariani, A.; Ricco, L.; Russo, S. First Synthesis of a Polyurethane by Frontal Polymerization. *Macromolecules* **2003**, *36*, 2674−2679.
(72) Mariani, A.; Fiori, S.; Chekanov, Y.; Pojman, J. A. Frontal Ring-Opening Metathesis Polymerization of Dicyclopentadiene. *Macromolecules* **2001**, *34*, 6539−6541.
(73) Robertson, I. D.; Pruitt, E. L.; Moore, J. S. Frontal Ring-Opening Metathesis Polymerization of Exo-Dicyclopentadiene for Low Catalyst Loadings. *ACS Macro Lett.* **2016**, *5*, 593−596.
(74) Scognamillo, S.; Bounds, C.; Luger, M.; Mariani, A.; Pojman, J. A. Frontal Cationic Curing of Epoxy Resins. *J. Polym. Sci., Part A: Polym. Chem.* **2010**, *48*, 2000−2005.
(75) Chen, S.; Tian, Y.; Chen, L.; Hu, T. Epoxy Resin/Polyurethane Hybrid Networks Synthesized by Frontal Polymerization. *Chem. Mater.* **2006**, *18*, 2159−2163.
(76) Alzari, V.; Nuvoli, D.; Sanna, D.; Ruiu, A.; Mariani, A. Effect of Limonene on the Frontal Ring Opening Metathesis Polymerization of Dicyclopentadiene. *J. Polym. Sci., Part A: Polym. Chem.* **2016**, *54*, 63−68.
(77) Zhang, W.; Yang, S.; Wang, C.-F.; Chen, S. Anisotropic Biphase Frontal Polymerization toward in Situ Generation of Dual-Component Polymers. *Macromolecules* **2015**, *48*, 5543−5549.
(78) McFarland, B.; Popwell, S.; Pojman, J. A. Free-Radical Frontal Polymerization with a Microencapsulated Initiator: Characterization of Microcapsules and Their Effect on Pot Life, Front Velocity, and Mechanical Properties. *Macromolecules* **2006**, *39*, 55−63.
(79) Illescas, J.; Ortíz-Palacios, J.; Esquivel-Guzmán, J.; Ramirez-Fuentes, Y. S.; Rivera, E.; Morales-Saavedra, O. G.; Rodríguez-Rosales, A. A.; Alzari, V.; Nuvoli, D.; Scognamillo, S.; Mariani, A. Preparation and Optical Characterization of Two Photoactive Poly(Bisphenol a Ethoxylate Diacrylate) Copolymers Containing Designed Amino-Nitro-Substituted Azobenzene Units, Obtained Via Classical and Frontal Polymerization, Using Novel Ionic Liquids as Initiators. *J. Polym. Sci., Part A: Polym. Chem.* **2012**, *50*, 1906−1916.
(80) Mariani, A.; Bidali, S.; Fiori, S.; Sangermano, M.; Malucelli, G.; Bongiovanni, R.; Priola, A. Uv-Ignited Frontal Polymerization of an Epoxy Resin. *J. Polym. Sci., Part A: Polym. Chem.* **2004**, *42*, 2066−2072.
(81) Illescas, J.; Ramirez-Fuentes, Y. S.; Rivera, E.; Morales-Saavedra, O. G.; Rodríguez-Rosales, A. A.; Alzari, V.; Nuvoli, D.; Scognamillo, S.; Mariani, A. Synthesis and Optical Characterization of Photoactive Poly(2-Phenoxyethyl Acrylate) Copolymers Containing Azobenzene Units, Prepared by Frontal Polymerization Using Novel Ionic Liquids as Initiators. *J. Polym. Sci., Part A: Polym. Chem.* **2012**, *50*, 821−830.
(82) Mariani, A.; Alzari, V.; Monticelli, O.; Pojman, J. A.; Caria, G. Polymeric Nanocomposites Containing Polyhedral Oligomeric Silsesquioxanes Prepared Via Frontal Polymerization. *J. Polym. Sci., Part A: Polym. Chem.* **2007**, *45*, 4514−4521.
(83) Zhou, J.; Jia, S.; Fu, W.; Liu, Z.; Tan, Z. Fast Curing of Thick Components of Epoxy Via Modified Uv-Triggered Frontal Polymerization Propagating Horizontally. *Mater. Lett.* **2016**, *176*, 228−231.
(84) Illescas, J.; Sanna, R.; Alzari, V.; Nuvoli, D.; Casu, M.; Sanna, R.; Rivera, E.; Mariani, A. Organic-Inorganic Interpenetrating Polymer Networks and Hybrid Polymer Materials Prepared by Frontal Polymerization. *J. Polym. Sci., Part A: Polym. Chem.* **2013**, *51*, 4618−4625.
(85) Nuvoli, L.; Sanna, D.; Alzari, V.; Nuvoli, D.; Sanna, V.; Malfatti, L.; Mariani, A. Double Responsive Copolymer Hydrogels Prepared by Frontal Polymerization. *J. Polym. Sci., Part A: Polym. Chem.* **2016**, *54*, 2166−2170.
(86) Mariani, A.; Nuvoli, L.; Sanna, D.; Alzari, V.; Nuvoli, D.; Rassu, M.; Malucelli, G. Semi-Interpenetrating Polymer Networks Based on Crosslinked Poly(N-Isopropyl Acrylamide) and Methylcellulose Prepared by Frontal Polymerization. *J. Polym. Sci., Part A: Polym. Chem.* **2018**, *56*, 437−443.
(87) Scognamillo, S.; Alzari, V.; Nuvoli, D.; Mariani, A. Thermoresponsive Super Water Absorbent Hydrogels Prepared by Frontal Polymerization. *J. Polym. Sci., Part A: Polym. Chem.* **2010**, *48*, 2486−2490.
(88) Alzari, V.; Mariani, A.; Monticelli, O.; Valentini, L.; Nuvoli, D.; Piccinini, M.; Scognamillo, S.; Bon, S. B.; Illescas, J. Stimuli-Responsive Polymer Hydrogels Containing Partially Exfoliated Graphite. *J. Polym. Sci., Part A: Polym. Chem.* **2010**, *48*, 5375−5381.
(89) Caria, G.; Alzari, V.; Monticelli, O.; Nuvoli, D.; Kenny, J. M.; Mariani, A. Poly(N,N-Dimethylacrylamide) Hydrogels Obtained by Frontal Polymerization. *J. Polym. Sci., Part A: Polym. Chem.* **2009**, *47*, 1422−1428.
(90) Alzari, V.; Monticelli, O.; Nuvoli, D.; Kenny, J. M.; Mariani, A. Stimuli Responsive Hydrogels Prepared by Frontal Polymerization. *Biomacromolecules* **2009**, *10*, 2672−2677.
(91) Mota-Morales, J. D.; Gutiérrez, M. C.; Ferrer, M. L.; Sanchez, I. C.; Elizalde-Peña, E. A.; Pojman, J. A.; Monte, F. D.; Luna-Bárcenas, G. Deep Eutectic Solvents as Both Active Fillers and Monomers for Frontal Polymerization. *J. Polym. Sci., Part A: Polym. Chem.* **2013**, *51*, 1767−1773.
(92) Cai, X.; Chen, S.; Chen, L. Solvent-Free Free-Radical Frontal Polymerization: A New Approach to Quickly Synthesize Poly(N-Vinylpyrrolidone). *J. Polym. Sci., Part A: Polym. Chem.* **2008**, *46*, 2177−2185.
(93) Chen, L.; Hu, T.; Yu, H.; Chen, S.; Pojman, J. A. First Solvent-Free Synthesis of Poly(N-Methylolacrylamide) Via Frontal Free-Radical Polymerization. *J. Polym. Sci., Part A: Polym. Chem.* **2007**, *45*, 4322−4330.
(94) Callister, W. D., Jr. *Materials Science and Engineering an Introduction*; 7th ed.; John Wiley & Sons, Inc.: New York, NY, 2007.
(95) Mariani, A.; Fiori, S.; Bidali, S.; Alzari, V.; Malucelli, G. Frontal Polymerization of Diurethane Diacrylates. *J. Polym. Sci., Part A: Polym. Chem.* **2008**, *46*, 3344−3352.
(96) Shercliff, H. R.; Ashby, M. F. Elastic Structures in Design. In *Reference Module in Materials Science and Materials Engineering*; Elsevier: 2016.
(97) Ashby, M. F. *Materials Selection in Mechanical Design*, 2nd ed.; Butterworth-Heinemann: Oxford, 1999.
(98) Comissiong, D. M. G.; Gross, L. K.; Volpert, V. A. Bifurcation Analysis of Polymerization Fronts. In *Nonlinear Dynamics in Polymeric Systems*; American Chemical Society: 2003; Vol. *869*, pp 147−159.
(99) Lewis, L. L.; DeBisschop, C. A.; Pojman, J. A.; Volpert, V. A. Evolution of Isothermal Polymerization Fronts Via Laser Line Deflection and Predictive Modeling. In *Nonlinear Dynamics in Polymeric Systems*; American Chemical Society: 2003; Vol. *869*, pp 169−183.
(100) Pumir, A.; Barelko, V. V.; Barkalov, I. M.; Kiryukhin, D. P. "Cold" Ignition of Combustionlike Waves of Cryopolymerization and Other Reactions in Solids. In *Nonlinear Dynamics in Polymeric Systems*; American Chemical Society: 2003; Vol. *869*, pp 160−168.
(101) Epstein, I. R.; Pojman, J. A. *An Introduction to Nonlinear Chemical Dynamics: Oscillations, Waves, Patterns, and Chaos*; Oxford University Press, Inc.: Oxford, UK, 1998.
(102) Kessler, M. R.; White, S. R. Cure Kinetics of the Ring-Opening Metathesis Polymerization of Dicyclopentadiene. *J. Polym. Sci., Part A: Polym. Chem.* **2002**, *40*, 2373−2383.
(103) Vyas, S.; Goli, E.; Zhang, X.; Geubelle, P. H. Manufacturing of Unidirectional Glass-Fiber-Reinforced Composites Via Frontal Polymerization: A Numerical Study. *Compos. Sci. Technol.* **2019**, *184*, 107832.

https://doi.org/10.1021/acs.chemrev.2c00686
Chem. Rev. 2023, 123, 3237−3298

(104) Kumar, A.; Gao, Y.; Geubelle, P. H. Analytical Estimates of Front Velocity in the Frontal Polymerization of Thermoset Polymers and Composites. *J. Polym. Sci.* **2021**, *59*, 1109−1118.
(105) Goli, E.; Parikh, N. A.; Yourdkhani, M.; Hibbard, N. G.; Moore, J. S.; Sottos, N. R.; Geubelle, P. H. Frontal Polymerization of Unidirectional Carbon-Fiber-Reinforced Composites. *Compos. Part A Appl. Sci. Manuf.* **2020**, *130*, 105689.
(106) Goli, E.; Peterson, S. R.; Geubelle, P. H. Instabilities Driven by Frontal Polymerization in Thermosetting Polymers and Composites. *Compos. Part B. Eng.* **2020**, *199*, 108306.
(107) *Computational Design of Microvascular Biomimetic Materials*. http://hdl.handle.net/2142/18271 (accessed 07/26/2020).
(108) Tiani, R.; Pojman, J. A.; Rongy, L. Critical Role of Layer Thickness in Frontal Polymerization. *J. Phys. Chem. B* **2022**, *126*, 3607−3618.
(109) Pojman, J. A. A New Approach to Manufacturing with Frontal Polymerization to Generate Patterned Materials. *ACS Cent. Sci.* **2021**, *7*, 534−535.
(110) Zeldovich, Y. B.; Frank-Komenetskii, D. A. A Theory of Thermal Propagation of Flame. *Acts Physicochim. U.R.S.S.* **1938**, *9*, 341−350.
(111) Arutiunian, K. A. D. S. P.; Rozenberg, B. A.; Enikolopyan, N. S. Curing of Epoxy Resins of Bis-Phenol a by Amines under Conditions of Reaction Front Propagation. *Dokl. Akad. Nauk SSSR* **1975**, *223*, 667−660.
(112) Davtyan, S.P.; Abutyunyan, Kh. A.; Shkadinskii, K.G.; Rozenberg, B.A.; Yenikolopyan, N.S. The Mechanism of Epoxide Oligomer Hardening by Diamines under Advancing Reaction Front Conditions. *Poly. Sci. U.S.S.R* **1977**, *19*, 3149−3154.
(113) Lemaigre, L.; Budroni, M. A.; Riolfo, L. A.; Grosfils, P.; De Wit, A. Asymmetric Rayleigh-Taylor and Double-Diffusive Fingers in Reactive Systems. *Phys. Fluids* **2013**, *25*, 014103.
(114) Nagy, I. P.; Pojman, J. A. Suppressing Convective Instabilities in Propagating Fronts by Tube Rotation. *J. Phys. Chem.* **1996**, *100*, 3299−3304.
(115) Belk, M.; Kostarev, K. G.; Volpert, V.; Yudina, T. M. Frontal Photopolymerization with Convection. *J. Phys. Chem. B* **2003**, *107*, 10292−10298.
(116) Bowden, G.; Garbey, M.; Ilyashenko, V. M.; Pojman, J. A.; Solovyov, S. E.; Taik, A.; Volpert, V. A. Effect of Convection on a Propagating Front with a Solid Product: Comparison of Theory and Experiments. *J. Phys. Chem. B* **1997**, *101*, 678−686.
(117) Downey, J. P.; Pojman, J. A. Polymer Processing in Microgravity: An Overview. In *Polymer Research in Microgravity*; American Chemical Society: 2001; Vol. *793*, pp 2−15.
(118) Clavin, P. Dynamic Behavior of Premixed Flame Fronts in Laminar and Turbulent Flows. *Prog. Energy Combust. Sci.* **1985**, *11*, 1−59.
(119) Masere, J.; Stewart, F.; Meehan, T.; Pojman, J. A. Period-Doubling Behavior in Frontal Polymerization of Multifunctional Acrylates. *Chaos* **1999**, *9*, 315−322.
(120) Begishev, V. P.; Volpert, V. A.; Davtyan, S. P.; Malkin, A. Y. Some Features of the Anionic Activated E-Caprolactam Polymerization under Wave Propagation Conditions. *Dokl. Phys. Chem.* **1984**, *29*, 1075−1077.
(121) Volpert, V. A.; Volpert, V. A.; Pojman, J. A. Effect of Thermal Expansion on Stability of Reaction Front Propagation. *Chem. Eng. Sci.* **1994**, *49*, 2385−2388.
(122) Pojman, J. A.; Craven, R.; Khan, A.; West, W. Convective Instabilities in Traveling Fronts of Addition Polymerization. *J. Phys. Chem.* **1992**, *96*, 7466−7472.
(123) Texier-Picard, R.; Pojman, J. A.; Volpert, V. A. Effect of Interfacial Tension on Propagating Polymerization Fronts. *Chaos* **2000**, *10*, 224−230.
(124) Pojman, J. A. Frontal Polymerization. In *Polymer Science: A Comprehensive Reference*; Matyjaszewski, K.; Möller, M., Eds.; Elsevier BV: Amsterdam, 2012; Vol. *4*, p 957−980.
(125) Van Gorder, R. A.; Kim, H.; Krause, A. L. Diffusive Instabilities and Spatial Patterning from the Coupling of Reaction—Diffusion Processes with Stokes Flow in Complex Domains. *J. Fluid Mech.* **2019**, *877*, 759.
(126) Gao, Y.; Rodriguez Koett, L. E.; Hemmer, J.; Gai, T.; Parikh, N. A.; Sottos, N. R.; Geubelle, P. H. Frontal Polymerization of Thin Layers on a Thermally Insulating Substrate. *ACS Appl. Polym. Mater.* **2022**, *4*, 4919.
(127) Viner, V.; Viner, G. Effect of Filler Choice on a Binary Frontal Polymerization System. *J. Phys. Chem. B* **2011**, *115*, 6862−6867.
(128) Pojman, J. A.; Gunn, G.; Patterson, C.; Owens, J.; Simmons, C. Frontal Dispersion Polymerization. *J. Phys. Chem. B* **1998**, *102*, 3927−3929.
(129) Xu, X.; Zhou, L.; Liang, B.; Wu, Y.; Wang, C. Synthesis of Copolymers Containing Double Spiro Orthocarbonate and Used as Anti-Shrinkage Additives in Epoxy Resin Composite. *Polym.-Plast. Technol. Eng.* **2014**, *53*, 753−759.
(130) Sadhir, R. K.; Luck, R. M. *Expanding Monomers: Synthesis, Characterization, and Applications*; 1st ed.; CRC Press: Boca Raton, 1992.
(131) Takata, T.; Endo, T. Recent Advances in the Development of Expanding Monomers: Synthesis, Polymerization and Volume Change. *Prog. Polym. Sci.* **1993**, *18*, 839−870.
(132) Bidali, S.; Ducrot, A.; Mariani, A.; Rustici, M. Self-Ignition of Polymerization Fronts with Convection: The "Rainstorm Effect". *e-Polymers* **2005**, 044.
(133) Scognamillo, S.; Bounds, C.; Thakuri, S.; Mariani, A.; Wu, Q.; Pojman, J. A. Frontal Cationic Curing of Epoxy Resins in the Presence of Defoaming or Expanding Compounds. *J. Appl. Polym. Sci.* **2014**, *131*, 40339−40340.
(134) Bazile Jr, M.; Nichols, H. A.; Pojman, J. A.; Volpert, V. Effect of Orientation on Thermoset Frontal Polymerization. *J. Polym. Sci., Part A: Polym. Chem.* **2002**, *40*, 3504−3508.
(135) Binici, B.; Fortenberry, D. I.; Leard, K. C.; Molden, M.; Olten, N.; Popwell, S.; Pojman, J. A. Spherically Propagating Thermal Polymerization Fronts. *J. Polym. Sci., Part A: Polym. Chem.* **2006**, *44*, 1387−1395.
(136) Wu, Z.; Benedicto, A. D.; Grubbs, R. H. Living Ring-Opening Metathesis Polymerization of Bicyclo[3.2.0]Heptene Catalyzed by a Ruthenium Alkylidene Complex. *Macromolecules* **1993**, *26*, 4975−4977.
(137) Schrock, R. R.; Feldman, J.; Cannizzo, L. F.; Grubbs, R. H. Ring-Opening Polymerization of Norbornene by a Living Tungsten Alkylidene Complex. *Macromolecules* **1987**, *20*, 1169−1172.
(138) Sutthasupa, S.; Shiotsuki, M.; Sanda, F. Recent Advances in Ring-Opening Metathesis Polymerization, and Application to Synthesis of Functional Materials. *Polym. J.* **2010**, *42*, 905−915.
(139) Choi, T.-L.; Grubbs, R. H. Controlled Living Ring-Opening-Metathesis Polymerization by a Fast-Initiating Ruthenium Catalyst. *Angew. Chem., Int. Ed.* **2003**, *42*, 1743−1746.
(140) Leitgeb, A.; Wappel, J.; Slugovc, C. The Romp Toolbox Upgraded. *Polymer* **2010**, *51*, 2927−2946.
(141) Autenrieth, B.; Jeong, H.; Forrest, W. P.; Axtell, J. C.; Ota, A.; Lehr, T.; Buchmeiser, M. R.; Schrock, R. R. Stereospecific Ring-Opening Metathesis Polymerization (ROMP) of Endo-Dicyclopentadiene by Molybdenum and Tungsten Catalysts. *Macromolecules* **2015**, *48*, 2480−2492.
(142) Herbert, M. B.; Suslick, B. A.; Liu, P.; Zou, L.; Dornan, P. K.; Houk, K. N.; Grubbs, R. H. Cyclometalated Z-Selective Ruthenium Metathesis Catalysts with Modified N-Chelating Groups. *Organometallics* **2015**, *34*, 2858−2869.
(143) Keitz, B. K.; Endo, K.; Patel, P. R.; Herbert, M. B.; Grubbs, R. H. Improved Ruthenium Catalysts for Z-Selective Olefin Metathesis. *J. Am. Chem. Soc.* **2012**, *134*, 693−699.
(144) Herbert, M. B.; Grubbs, R. H. Z-Selective Cross Metathesis with Ruthenium Catalysts: Synthetic Applications and Mechanistic Implications. *Angew. Chem., Int. Ed.* **2015**, *54*, 5018−5024.
(145) Love, J. A.; Morgan, J. P.; Trnka, T. M.; Grubbs, R. H. A Practical and Highly Active Ruthenium-Based Catalyst That Effects the Cross Metathesis of Acrylonitrile. *Angew. Chem., Int. Ed.* **2002**, *41*, 4035−4037.

https://doi.org/10.1021/acs.chemrev.2c00686
Chem. Rev. 2023, 123, 3237−3298

(146) Walsh, D. J.; Lau, S. H.; Hyatt, M. G.; Guironnet, D. Kinetic Study of Living Ring-Opening Metathesis Polymerization with Third-Generation Grubbs Catalysts. *J. Am. Chem. Soc.* **2017**, *139*, 13644−13647.
(147) Liu, H.; Wei, H.; Moore, J. S. Frontal Ring-Opening Metathesis Copolymerization: Deviation of Front Velocity from Mixing Rules. *ACS Macro Lett.* **2019**, *8*, 846−851.
(148) Ruiu, A.; Sanna, D.; Alzari, V.; Nuvoli, D.; Mariani, A. Advances in the Frontal Ring Opening Metathesis Polymerization of Dicyclopentadiene. *J. Polym. Sci., Part A: Polym. Chem.* **2014**, *52*, 2776−2780.
(149) Dean, L. M.; Wu, Q.; Alshangiti, O.; Moore, J. S.; Sottos, N. R. Rapid Synthesis of Elastomers and Thermosets with Tunable Thermomechanical Properties. *ACS Macro Lett.* **2020**, *9*, 819−824.
(150) Ivanoff, D. G.; Sung, J.; Butikofer, S. M.; Moore, J. S.; Sottos, N. R. Cross-Linking Agents for Enhanced Performance of Thermosets Prepared Via Frontal Ring-Opening Metathesis Polymerization. *Macromolecules* **2020**, *53*, 8360−8366.
(151) Stawiasz, K. J.; Paul, J. E.; Schwarz, K. J.; Sottos, N. R.; Moore, J. S. Photoexcitation of Grubbs' Second-Generation Catalyst Initiates Frontal Ring-Opening Metathesis Polymerization. *ACS Macro Lett.* **2020**, *9*, 1563−1568.
(152) Dean, L. M.; Ravindra, A.; Guo, A. X.; Yourdkhani, M.; Sottos, N. R. Photothermal Initiation of Frontal Polymerization Using Carbon Nanoparticles. *ACS Appl. Polym. Mater.* **2020**, *2*, 4690−4696.
(153) Suslick, B. A.; Stawiasz, K. J.; Paul, J. E.; Sottos, N. R.; Moore, J. S. Survey of Catalysts for Frontal Ring-Opening Metathesis Polymerization. *Macromolecules* **2021**, *54*, 5117−5123.
(154) Alzate-Sanchez, D. M.; Cencer, M. M.; Rogalski, M.; Kersh, M. E.; Sottos, N.; Moore, J. S. Anisotropic Foams Via Frontal Polymerization. *Adv. Mater.* **2022**, *34*, 2105821.
(155) Gao, Y.; Dearborn, M. A.; Vyas, S.; Kumar, A.; Hemmer, J.; Wang, Z.; Wu, Q.; Alshangiti, O.; Moore, J. S.; Esser-Kahn, A. P.; Geubelle, P. H. Manipulating Frontal Polymerization and Instabilities with Phase-Changing Microparticles. *J. Phys. Chem. B* **2021**, *125*, 7537−7545.
(156) Gao, Y.; Dearborn, M. A.; Hemmer, J.; Wang, Z.; Esser-Kahn, A. P.; Geubelle, P. H. Controllable Frontal Polymerization and Spontaneous Patterning Enabled by Phase-Changing Particles. *Small* **2021**, *17*, 2102217.
(157) Ziaee, M.; Yourdkhani, M. Effect of Resin Staging on Frontal Polymerization of Dicyclopentadiene. *J. Polym. Sci.* **2021**, *59*, 1732−1739.
(158) Garg, M.; Aw, J. E.; Zhang, X.; Centellas, P. J.; Dean, L. M.; Lloyd, E. M.; Robertson, I. D.; Liu, Y.; Yourdkhani, M.; Moore, J. S.; Geubelle, P. H.; Sottos, N. R. Rapid Synchronized Fabrication of Vascularized Thermosets and Composites. *Nat. Commun.* **2021**, *12*, 2836.
(159) Chen, L.; Wang, P.; Yang, L.; Ling, J.; Liu, C.; Wang, Y.; Zhang, S.; Feng, S.; Wu, X.; Xu, P.; Ding, Y. Enhanced Dielectric Properties of High Glass Transition Temperature Pdcpd/Batio3 Composites by Frontal Ring-Opening Metathesis Polymerization. *Mater. Lett.* **2022**, *310*, 131492.
(160) Wang, P.; Yang, L.; Gao, S.; Chen, X.; Cao, T.; Wang, C.; Liu, H.; Hu, X.; Wu, X.; Feng, S. Enhanced Dielectric Properties of High Glass Transition Temperature Pdcpd/Cnt Composites by Frontal Ring-Opening Metathesis Polymerization. *Advanced Composites and Hybrid Materials* **2021**, *4*, 639−646.
(161) Fiori, S.; Mariani, A.; Ricco, L.; Russo, S. Interpenetrating Polydicyclopentadiene/Polyacrylate Networks Obtained by Simultaneous Non-Interfering Frontal Polymerization. *e-Polymers* **2002**, *2*, 029.
(162) An, Y.; Jang, J. H.; Youk, J. H.; Yu, W.-R. Frontally Polymerizable Shape Memory Polymer for 3d Printing of Free-Standing Structures. *Smart Mater. Struct.* **2022**, *31*, 025013.
(163) Ziaee, M.; Johnson, J. W.; Yourdkhani, M. 3d Printing of Short-Carbon-Fiber-Reinforced Thermoset Polymer Composites Via Frontal Polymerization. *ACS Appl. Mater. Interfaces* **2022**, *14*, 16694−16702.
(164) Stawiasz, K. J.; Wendell, C. I.; Suslick, B. A.; Moore, J. S. Photoredox-Initiated Frontal Ring-Opening Metathesis Polymerization. *ACS Macro Lett.* **2022**, *11*, 780−784.
(165) Suslick, B. A.; Yazdani, A. N.; Cencer, M. M.; Paul, J. E.; Parikh, N. A.; Stawiasz, K. J.; Qamar, I. P. S.; Sottos, N. R.; Moore, J. S. Storable, Dual-Component Systems for Frontal Ring-Opening Metathesis Polymerization. *Macromolecules* **2022**, *55*, 5459−5473.
(166) Aw, J. E.; Zhang, X.; Nelson, A. Z.; Dean, L. M.; Yourdkhani, M.; Ewoldt, R. H.; Geubelle, P. H.; Sottos, N. R. Self-Regulative Direct Ink Writing of Frontally Polymerizing Thermoset Polymers. *Adv. Mater. Technol.* **2022**, *7*, 2200230.
(167) Lessard, J. J.; Kaur, P.; Paul, J. E.; Chang, K. M.; Sottos, N. R.; Moore, J. S. Switching Frontal Polymerization Mechanisms: Fromp and Frap. *ACS Macro Lett.* **2022**, *11*, 1097−1101.
(168) Centellas, P. J.; Yourdkhani, M.; Vyas, S.; Koohbor, B.; Geubelle, P. H.; Sottos, N. R. Rapid Multiple-Front Polymerization of Fiber-Reinforced Polymer Composites. *Compos. Part A Appl. Sci. Manuf.* **2022**, *158*, 106931.
(169) Suslick, B. A.; Alzate-Sanchez, D. M.; Moore, J. S. Scalable Frontal Oligomerization: Insights from Advanced Mass Analysis. *Macromolecules* **2022**, *55*, 8234−8241.
(170) Davydovich, O.; Paul, J. E.; Feist, J. D.; Aw, J. E.; Balta Bonner, F. J.; Lessard, J. J.; Tawfick, S.; Xia, Y.; Sottos, N. R.; Moore, J. S. Frontal Polymerization of Dihydrofuran Comonomer Facilitates Thermoset Deconstruction. *Chem. Mater.* **2022**, *34*, 8790−8797.
(171) Rule, J. D.; Moore, J. S. Romp Reactivity of Endo- and Exo-Dicyclopentadiene. *Macromolecules* **2002**, *35*, 7878−7882.
(172) Lloyd, E. M.; Cooper, J. C.; Shieh, P.; Ivanoff, D. G.; Parikh, N. A.; Mejia, E. B.; Husted, K. E. L.; Costa, L. C.; Sottos, N. R.; Johnson, J. A.; Moore, J. S. Efficient Manufacture, Deconstruction, and Upcycling of High-Performance Thermosets and Composites. *ACS Appl. Eng. Mater.* **2022**, DOI: 10.1021/acsaenm.1022c00115.
(173) Husted, K. E. L.; Brown, C. M.; Shieh, P.; Kevlishvili, I.; Kristufek, S. L.; Zafar, H.; Accardo, J. V.; Cooper, J. C.; Klausen, R. S.; Kulik, H. J.; Moore, J. S.; Sottos, N. R.; Kalow, J. A.; Johnson, J. A. Remolding and Deconstruction of Industrial Thermosets Via Carboxylic Acid-Catalyzed Bifunctional Silyl Ether Exchange. *J. Am. Chem. Soc.* **2023**, *145*, 1916.
(174) Vidavsky, Y.; Navon, Y.; Ginzburg, Y.; Gottlieb, M.; Lemcoff, N. G. Thermal Properties of Ruthenium Alkylidene-Polymerized Dicyclopentadiene. *Beilstein J. Org. Chem.* **2015**, *11*, 1469−1474.
(175) Shieh, P.; Zhang, W.; Husted, K. E. L.; Kristufek, S. L.; Xiong, B.; Lundberg, D. J.; Lem, J.; Veysset, D.; Sun, Y.; Nelson, K. A.; Plata, D. L.; Johnson, J. A. Cleavable Comonomers Enable Degradable, Recyclable Thermoset Plastics. *Nature* **2020**, *583*, 542−547.
(176) Fouquet, T. N. J. The Kendrick Analysis for Polymer Mass Spectrometry. *J. Mass Spectrom.* **2019**, *54*, 933−947.
(177) Suslick, B. A.; Klok, H.-A.; Moore, J. S. There Is Signal in Your Noise: A Case for Advanced Mass Analysis. *ACS Polymers Au* **2022**, *2*, 392−396.
(178) Pham, H. Q.; Marks, M. J. Epoxy Resins. *Ullmann's Encyclopedia of Industrial Chemistry* **2005**, *13*, 154.
(179) Plommer, H.; Reim, I.; Kerton, F. M. Ring-Opening Polymerization of Cyclohexene Oxide Using Aluminum Amine-Phenolate Complexes. *Dalton Trans.* **2015**, *44*, 12098−12102.
(180) Leonard, J. Heats and Entropies of Polymerization. In *Polymer Handbook*, 4th ed.; Brandrup, J., Immergut, E. H., Grulke, E. A., Abe, A., Bloch, D. R., Eds.; John Wiley & Sons: 1999; pp 363−407.
(181) Crivello, J. V. Investigation of the Photoactivated Frontal Polymerization of Oxetanes Using Optical Pyrometry. *Polymer* **2005**, *46*, 12109−12117.
(182) Švajdlenková, H.; Kleinová, A.; Šauša, O.; Rusnák, J.; Dung, T. A.; Koch, T.; Knaack, P. Microstructural Study of Epoxy-Based Thermosets Prepared by "Classical" and Cationic Frontal Polymerization. *RSC Adv.* **2020**, *10*, 41098−41109.
(183) Groce, B. R.; Gary, D. P.; Cantrell, J. K.; Pojman, J. A. Front Velocity Dependence on Vinyl Ether and Initiator Concentration in Radical-Induced Cationic Frontal Polymerization of Epoxies. *J. Polym. Sci.* **2021**, *59*, 1678−1685.

(184) Turani, M.; Baggio, A.; Casalegno, V.; Salvo, M.; Sangermano, M. An Epoxy Adhesive Crosslinked through Radical-Induced Cationic Frontal Polymerization. *Macromol. Mater. Eng.* **2021**, *306*, 2100495.
(185) Taschner, R.; Knaack, P.; Liska, R. Bismuthonium- and Pyrylium-Based Radical Induced Cationic Frontal Polymerization of Epoxides. *J. Polym. Sci.* **2021**, *59*, 1841−1854.
(186) Maugeri, D.; Sangermano, M.; Leterrier, Y. Radical Photo-induced Cationic Frontal Polymerization in Porous Media. *Polym. Int.* **2021**, *70*, 269−276.
(187) Wu, Q. Uv-Activated Frontal Polymerization for Preparation of Magnetically Oriented Graphene Nanoplatelets/Epoxy Composites. *Mater. Lett.* **2022**, *321*, 132370.
(188) Tran, A. D.; Koch, T.; Liska, R.; Knaack, P. Radical-Induced Cationic Frontal Polymerisation for Prepreg Technology. *Monatsh. Chem.* **2021**, *152*, 151−165.
(189) Malik, M. S.; Schlögl, S.; Wolfahrt, M.; Sangermano, M. Review on Uv-Induced Cationic Frontal Polymerization of Epoxy Monomers. *Polymers* **2020**, *12*, 2146.
(190) Gachet, B.; Lecompère, M.; Croutxé-Barghorn, C.; Burr, D.; L'Hostis, G.; Allonas, X. Highly Reactive Photothermal Initiating System Based on Sulfonium Salts for the Photoinduced Thermal Frontal Cationic Polymerization of Epoxides: A Way to Create Carbon-Fiber Reinforced Polymers. *RSC Adv.* **2020**, *10*, 41915−41920.
(191) Scognamillo, S.; Alzari, V.; Nuvoli, D.; Mariani, A. Hybrid Organic/Inorganic Epoxy Resins Prepared by Frontal Polymerization. *J. Polym. Sci., Part A: Polym. Chem.* **2010**, *48*, 4721−4725.
(192) Mariani, A.; Bidali, S.; Caria, G.; Monticelli, O.; Russo, S.; Kenny, J. M. Synthesis and Characterization of Epoxy Resin-Montmorillonite Nanocomposites Obtained by Frontal Polymerization. *J. Polym. Sci., Part A: Polym. Chem.* **2007**, *45*, 2204−2211.
(193) Liao, Y. Design and Applications of Metastable-State Photoacids. *Acc. Chem. Res.* **2017**, *50*, 1956−1964.
(194) Crivello, J. V.; Lee, J. L. Photosensitized Cationic Polymerizations Using Dialkylphenacylsulfonium and Dialkyl(4-Hydroxyphenyl)Sulfonium Salt Photoinitiators. *Macromolecules* **1981**, *14*, 1141−1147.
(195) Noè, C.; Hakkarainen, M.; Malburet, S.; Graillot, A.; Adekunle, K.; Skrifvars, M.; Sangermano, M. Frontal-Photopolymerization of Fully Biobased Epoxy Composites. *Macromol. Mater. Eng.* **2022**, *307*, 2100864.
(196) Chabanne, P.; Tighzert, L.; Pascault, J.-P.; Bonnetot, B. Epoxy Polymerization Initiated by BF_3-Amine Complexes. I. Synthesis and Characterization of BF_3-Amine Complexes and BF_3-Amine Complexes Dissolved in γ-Butyrolactone. *J. Appl. Polym. Sci.* **1993**, *49*, 685−699.
(197) Brydson, J. A. 26—Epoxide Resins. In *Plastics Materials*, 7th ed.; Brydson, J. A., Ed.; Butterworth-Heinemann: Oxford, 1999; pp 744−777.
(198) Chen, S.; Sui, J.; Chen, L. Segmented Polyurethane Synthesized by Frontal Polymerization. *Colloid Polym. Sci.* **2005**, *283*, 932−936.
(199) Mariani, A.; Bidali, S.; Fiori, S.; Malucelli, G.; Ricco, L. New Vistas in Frontal Polymerization. *Macromol. Symp.* **2001**, *169*, 1−10.
(200) Mariani, A.; Bidali, S.; Fiori, S.; Malucelli, G.; Sanna, E. Synthesis and Characterization of a Polyurethane Prepared by Frontal Polymerization. *e-Polymers* **2003**, *3*, 044.
(201) Hu, T.; Chen, S.; Tian, Y.; Pojman, J. A.; Chen, L. Frontal Free-Radical Copolymerization of Urethane-Acrylates. *J. Polym. Sci., Part A: Polym. Chem.* **2006**, *44*, 3018−3024.
(202) Asakura, K.; Nihei, E.; Harasawa, H.; Ikumo, A.; Osanai, S. Spontaneous Frontal Polymerization: Propagating Front Spontaneously Generated by Locally Autoaccelerated Free-Radical Polymerization. In *Nonlinear Dynamics in Polymeric Systems*; American Chemical Society: 2003; Vol. *869*, pp 135−146.
(203) Bynum, S.; Tullier, M.; Morejon-Garcia, C.; Guidry, J.; Runnoe, E.; Pojman, J. A. The Effect of Acrylate Functionality on Frontal Polymerization Velocity and Temperature. *J. Polym. Sci., Part A: Polym. Chem.* **2019**, *57*, 982−988.
(204) Chekanov, Y. A.; Pojman, J. A. Preparation of Functionally Gradient Materials Via Frontal Polymerization. *J. Appl. Polym. Sci.* **2000**, *78*, 2398−2404.
(205) Chen, S.; Hu, T.; Tian, Y.; Chen, L.; Pojman, J. A. Facile Synthesis of Poly(Hydroxyethyl Acrylate) by Frontal Free-Radical Polymerization. *J. Polym. Sci., Part A: Polym. Chem.* **2007**, *45*, 873−881.
(206) Du, X.-Y.; Liu, S.-S.; Wang, C.-F.; Wu, G.; Chen, S. Facile Synthesis of Self-Healing Gel Via Magnetocaloric Bottom-Ignited Frontal Polymerization. *J. Polym. Sci., Part A: Polym. Chem.* **2017**, *55*, 2585−2593.
(207) Du, X.-Y.; Shen, J.; Zhang, J.; Ling, L.; Wang, C.-F.; Chen, S. Generation of a Carbon Dots/Ammonium Persulfate Redox Initiator Couple for Free Radical Frontal Polymerization. *Polym. Chem.* **2018**, *9*, 420−427.
(208) Gavini, E.; Mariani, A.; Rassu, G.; Bidali, S.; Spada, G.; Bonferoni, M. C.; Giunchedi, P. Frontal Polymerization as a New Method for Developing Drug Controlled Release Systems (DCRS) Based on Polyacrylamide. *Eur. Polym. J.* **2009**, *45*, 690−699.
(209) Ghazinezhad, M.; Grinyuk, E. V.; Krul', L. P. Chromium(III) Cross-Linked Poly(Acylamide Co-2-Acrylamido-2-Methyl-1-Propanesulfonic Acid) Hydrogels, Prepared by Frontal Polymerization in Aqueous Solutions. *Russ. J. Appl. Chem.* **2015**, *88*, 1368−1374.
(210) Holt, T.; Fazende, K.; Jee, E.; Wu, Q.; Pojman, J. A. Cure-on-Demand Wood Adhesive Based on the Frontal Polymerization of Acrylates. *J. Appl. Polym. Sci.* **2016**, *133*, 44064.
(211) Illescas, J.; Ramírez-Fuentes, Y. S.; Zaragoza-Galán, G.; Porcu, P.; Mariani, A.; Rivera, E. Pegda-Based Luminescent Polymers Prepared by Frontal Polymerization. *J. Polym. Sci., Part A: Polym. Chem.* **2015**, *53*, 2890−2897.
(212) Li, Q.; Liu, J.-D.; Liu, S.-S.; Wang, C.-F.; Chen, S. Frontal Polymerization-Oriented Self-Healing Hydrogels and Applications toward Temperature-Triggered Actuators. *Ind. Eng. Chem. Res.* **2019**, *58*, 3885−3892.
(213) Li, S.; Huang, H.; Tao, M.; Liu, X.; Cheng, T. Frontal Polymerization Preparation of Poly(Acrylamide-Co-Acrylic Acid)/Activated Carbon Composite Hydrogels for Dye Removal. *J. Appl. Polym. Sci.* **2013**, *129*, 3737−3745.
(214) Mariani, A.; Fiori, S.; Malucelli, G.; Pincin, S.; Ricco, L.; Russo, S. Recent Chemical Advances in Frontal Polymerization. In *Nonlinear Dynamics in Polymeric Systems*; American Chemical Society: 2003; Vol. *869*, pp 121−134.
(215) Mariani, A.; Nuvoli, D.; Alzari, V.; Pini, M. Phosphonium-Based Ionic Liquids as a New Class of Radical Initiators and Their Use in Gas-Free Frontal Polymerization. *Macromolecules* **2008**, *41*, 5191−5196.
(216) Masere, J.; Chekanov, Y.; Warren, J. R.; Stewart, F. D.; Al-Kaysi, R.; Rasmussen, J. K.; Pojman, J. A. Gas-Free Initiators for High-Temperature Free-Radical Polymerization. *J. Polym. Sci., Part A: Polym. Chem.* **2000**, *38*, 3984−3990.
(217) McFarland, B.; Popwell, S.; Pojman, J. A. Free-Radical Frontal Polymerization with a Microencapsulated Initiator. *Macromolecules* **2004**, *37*, 6670−6672.
(218) Morales, A.; Pojman, J. A. A Study of the Effects of Thiols on the Frontal Polymerization and Pot Life of Multifunctional Acrylate Systems with Cumene Hydroperoxide. *J. Polym. Sci., Part A: Polym. Chem.* **2013**, *51*, 3850−3855.
(219) Nagy, I. P.; Sike, L.; Pojman, J. A. Thermochromic Composite Prepared Via a Propagating Polymerization Front. *J. Am. Chem. Soc.* **1995**, *117*, 3611−3612.
(220) Nuvoli, D.; Alzari, V.; Nuvoli, L.; Rassu, M.; Sanna, D.; Mariani, A. Synthesis and Characterization of Poly(2-Hydroxyethylacrylate)/B-Cyclodextrin Hydrogels Obtained by Frontal Polymerization. *Carbohydr. Polym.* **2016**, *150*, 166−171.
(221) Nuvoli, D.; Alzari, V.; Pojman, J. A.; Sanna, V.; Ruiu, A.; Sanna, D.; Malucelli, G.; Mariani, A. Synthesis and Characterization of Functionally Gradient Materials Obtained by Frontal Polymerization. *ACS Appl. Mater. Interfaces* **2015**, *7*, 3600−3606.

https://doi.org/10.1021/acs.chemrev.2c00686
Chem. Rev. 2023, 123, 3237−3298

(222) Pojman, J. A. Traveling Fronts of Methacrylic Acid Polymerization. *J. Am. Chem. Soc.* **1991**, *113*, 6284−6286.
(223) Pojman, J. A.; Curtis, G.; Ilyashenko, V. M. Frontal Polymerization in Solution. *J. Am. Chem. Soc.* **1996**, *118*, 3783−3784.
(224) Pojman, J. A.; Nagy, I. P.; Salter, C. Traveling Fronts of Addition Polymerization with a Solid Monomer. *J. Am. Chem. Soc.* **1993**, *115*, 11044−11045.
(225) Pojman, J. A.; Popwell, S.; Fortenberry, D. I.; Volpert, V. A.; Volpert, V. A. Nonlinear Dynamics in Frontal Polymerization. In *Nonlinear Dynamics in Polymeric Systems*; American Chemical Society: 2003; Vol. *869*, pp 106−120.
(226) Pojman, J. A.; Varisli, B.; Perryman, A.; Edwards, C.; Hoyle, C. Frontal Polymerization with Thiol-Ene Systems. *Macromolecules* **2004**, *37*, 691−693.
(227) Pujari, N. S.; Inamdar, S. R.; Ponrathnam, S.; Kulkarni, B. D. Water-Triggered Frontal Polymerization. *Macromol. Rapid Commun.* **2007**, *28*, 109−115.
(228) Rassu, M.; Alzari, V.; Nuvoli, D.; Nuvoli, L.; Sanna, D.; Sanna, V.; Malucelli, G.; Mariani, A. Semi-Interpenetrating Polymer Networks of Methyl Cellulose and Polyacrylamide Prepared by Frontal Polymerization. *J. Polym. Sci., Part A: Polym. Chem.* **2017**, *55*, 1268−1274.
(229) Sanna, D.; Alzari, V.; Nuvoli, D.; Nuvoli, L.; Rassu, M.; Sanna, V.; Mariani, A. B-Cyclodextrin-Based Supramolecular Poly(N-Isopropylacrylamide) Hydrogels Prepared by Frontal Polymerization. *Carbohydr. Polym.* **2017**, *166*, 249−255.
(230) Sanna, R.; Sanna, D.; Alzari, V.; Nuvoli, D.; Scognamillo, S.; Piccinini, M.; Lazzari, M.; Gioffredi, E.; Malucelli, G.; Mariani, A. Synthesis and Characterization of Graphene-Containing Thermoresponsive Nanocomposite Hydrogels of Poly(N-Vinylcaprolactam) Prepared by Frontal Polymerization. *J. Polym. Sci., Part A: Polym. Chem.* **2012**, *50*, 4110−4118.
(231) Singh, S.; Singh, A.; Yadav, B. C.; Tandon, P.; Kumar, S.; Yadav, R. R.; Pomogailo, S. I.; Dzhardimalieva, G. I.; Pomogailo, A. D. Frontal Polymerization of Acrylamide Complex with Nanostructured Zns and Pbs: Their Characterizations and Sensing Applications. *Sens. Actuators, B* **2015**, *207*, 460−469.
(232) Tsegay, N. M.; Du, X.-Y.; Liu, S.-S.; Wang, C.-F.; Chen, S. Frontal Polymerization for Smart Intrinsic Self-Healing Hydrogels and Its Integration with Microfluidics. *J. Polym. Sci., Part A: Polym. Chem.* **2018**, *56*, 1412−1423.
(233) Tu, J.; Zhou, J.; Wang, C.-F.; Zhang, Q.; Chen, S. Facile Synthesis of N-Vinylimidazole-Based Hydrogels Via Frontal Polymerization and Investigation of Their Performance on Adsorption of Copper Ions. *J. Polym. Sci., Part A: Polym. Chem.* **2010**, *48*, 4005−4012.
(234) Vicini, S.; Mariani, A.; Princi, E.; Bidali, S.; Pincin, S.; Fiori, S.; Pedemonte, E.; Brunetti, A. Frontal Polymerization of Acrylic Monomers for the Consolidation of Stone. *Polym. Adv. Technol.* **2005**, *16*, 293−298.
(235) Viner, V. Frontal Polymerization of a Cyanate Ester. *J. Appl. Polym. Sci.* **2012**, *128*, 2208−2215.
(236) Wang, C.; Liu, J.-D.; Li, Q.; Chen, S. Self-Healing Hydrogel toward Metal Ion Rapid Removal Via Available Solar-Driven Fashion. *Ind. Eng. Chem. Res.* **2019**, *58*, 17067−17074.
(237) Wang, X.-L.; Yao, H.-F.; Li, X.-Y.; Wang, X.; Huang, Y.-P.; Liu, Z.-S. Ph/Temperature-Sensitive Hydrogel-Based Molecularly Imprinted Polymers (Hydromips) for Drug Delivery by Frontal Polymerization. *RSC Adv.* **2016**, *6*, 94038−94047.
(238) Yan, Q. Z.; Lu, G. D.; Zhang, W. F.; Ma, X. H.; Ge, C. C. Frontal Polymerization Synthesis of Monolithic Macroporous Polymers. *Adv. Funct. Mater.* **2007**, *17*, 3355−3362.
(239) Yu, C.; Wang, C.-F.; Chen, S. Facile Access to Versatile Hydrogels Via Interface-Directed Frontal Polymerization Derived from the Magnetocaloric Effect. *J. Mater. Chem. A* **2015**, *3*, 17351−17358.
(240) Yu, H.; Fang, Y.; Chen, L.; Chen, S. Investigation of Redox Initiators for Free Radical Frontal Polymerization. *Polym. Int.* **2009**, *58*, 851−857.
(241) Hu, T.; Fang, Y.; Yu, H.; Chen, L.; Chen, S. Synthesis of Poly(N-Methylolacrylamide)/Polymethylacrylamide Hybrids Via Frontal Free-Radical Polymerization. *Colloid Polym. Sci.* **2007**, *285*, 891−898.
(242) Gary, D. P.; Bynum, S.; Thompson, B. D.; Groce, B. R.; Sagona, A.; Hoffman, I. M.; Morejon-Garcia, C.; Weber, C.; Pojman, J. A. Thermal Transport and Chemical Effects of Fillers on Free-Radical Frontal Polymerization. *J. Polym. Sci.* **2020**, *58*, 2267−2277.
(243) Tonoyan, A. O.; Varderesyan, A. Z.; Ketyan, A. G.; Minasyan, A. H.; Hovnanyan, K. O.; Davtyan, S. P. Continuous Reactors of Frontal Polymerization in Flow for the Synthesis of Polyacrylamide Hydrogels with Prescribed Properties. *J. Polym. Eng.* **2020**, *40*, 601−606.
(244) Li, B.; Liu, J.; Fu, D.; Li, Y.; Xu, X.; Cheng, M. Rapid Preparation of Pam/N-Cnt Nanocomposite Hydrogels by Dem Frontal Polymerization and Its Performance Study. *RSC Adv.* **2021**, *11*, 35268−35273.
(245) Alam, S.; Manzur, T.; Banjara, A.; Eklund, S.; Radadia, A.; Johnston, W.; Hashm, H.; Williams, J.; Matthews, J. Rapid Curing Prospects of Geopolymer Cementitious Composite Using Frontal Polymerization of Methyl Methacrylate Monomer. *Constr. Build Mater.* **2021**, *309*, 125198.
(246) Gao, Y.; Shaon, F.; Kumar, A.; Bynum, S.; Gary, D.; Sharp, D.; Pojman, J. A.; Geubelle, P. H. Rapid Frontal Polymerization Achieved with Thermally Conductive Metal Strips. *Chaos* **2021**, *31*, 073113.
(247) Alzari, V.; Kamseu, E.; Leonelli, C.; Spinella, A.; Malucelli, G.; Bianco, G.; Nuvoli, D.; Sanna, D.; Armetta, F.; Rassu, M.; Mariani, A. Organic-Inorganic Materials through First Simultaneous Frontal Polymerization and Frontal Geopolymerization. *Mater. Lett.* **2021**, *295*, 129808.
(248) Bidali, S.; Fiori, S.; Malucelli, G.; Mariani, A. Frontal Atom Transfer Radical Polymerization of Tri(Ethylene Glycol) Dimethacrylate. *e-Polymers* **2003**, *3*, 060.
(249) Shen, H.; Wang, H.-P.; Wang, C.-F.; Zhu, L.; Li, Q.; Chen, S. Rapid Fabrication of Patterned Gels Via Microchannel-Conformal Frontal Polymerization. *Macromol. Rapid Commun.* **2021**, *42*, 2100421.
(250) Arellano-Cruz, D. C.; Illescas, J.; Martínez-Gallegos, S.; Díaz-Nava, M. d. C. Synthesis and Characterization of Nanocomposites with Nanocellulose Obtained through Frontal Polymerization and Study of Their Properties. *MRS Adv.* **2021**, *6*, 947−951.
(251) Jater-Ruiz, A. I.; Illescas, J.; del Carmen Díaz-Nava, M.; Martínez-Gallegos, S. Synthesis and Characterization of Clay Polymer Composites of Acrylamide and Starch Obtained by Frontal Polymerization. *MRS Adv.* **2022**, *7*, 63.
(252) Gupta, L. K.; Kumar, K.; Sikarwar, S.; Yadav, B. C.; Golubeva, N. D.; Shershnev, V. A.; Dzhardimalieva, G. I.; et al. Shripal Frontal Polymerization Synthesis of Scandium Polyacrylamide Nanomaterial and Its Application in Humidity Testing. *Colloid Polym. Sci.* **2022**, *300*, 191−202.
(253) Gao, Y.; Li, S.; Kim, J.-Y.; Hoffman, I.; Vyas, S. K.; Pojman, J. A.; Geubelle, P. H. Anisotropic Frontal Polymerization in a Model Resin-Copper Composite. *Chaos* **2022**, *32*, 013109.
(254) Zhao, J.; Liu, J.-D.; Shen, H.; Guo, M.; Li, Q.; Wang, C.-F.; Liu, C.; Chen, S. Rapid Preparation of Dual Cross-Linked Mechanical Strengthening Hydrogels Via Frontal Polymerization for Use as Shape Deformable Actuators. *ACS Appl. Polym. Mater.* **2022**, *4*, 1457−1465.
(255) Gary, D. P.; Ngo, D.; Bui, A.; Pojman, J. A. Charge Transfer Complexes as Dual Thermal/Photo Initiators for Free-Radical Frontal Polymerization. *J. Polym. Sci.* **2022**, *60*, 1624−1630.
(256) Li, B.; Xu, X.; Hu, Z.; Li, Y.; Zhou, M.; Liu, J.; Jiang, Y.; Wang, P. Rapid Preparation of N-CNTS/P(AA-co-Am) Composite Hydrogel Via Frontal Polymerization and Its Mechanical and Conductive Properties. *RSC Adv.* **2022**, *12*, 19022−19028.
(257) Ebner, C.; Mitterer, J.; Eigruber, P.; Stieger, S.; Riess, G.; Kern, W. Ultra-High through-Cure of (Meth)Acrylate Copolymers Via Photofrontal Polymerization. *Polymers* **2020**, *12*, 1291.
(258) He, Z.-L.; Liu, J.-D.; Hu, J.; Wang, C.-F.; Li, Q.; Wang, G.; Chen, S. Facile Synthesis of Self-Healing Gels Via Frontal Polymer-

https://doi.org/10.1021/acs.chemrev.2c00686
Chem. Rev. 2023, 123, 3237−3298

ization toward Acid-Base Regulatable Wound Dressing. *J. Mater. Sci.* **2022**, *57*, 12971.
(259) Ebner, C.; Mitterer, J.; Gonzalez-Gutierrez, J.; Riess, G.; Kern, W. Resins for Frontal Photopolymerization: Combinging Depth-Cure and Tunable Mechanical Properties. *Materials* **2021**, *14*, 743.
(260) Fiori, S.; Mariani, A.; Bidali, S.; Malucelli, G. Synthesis and Characterization of Unsaturated Polyester Resins Cured by Frontal Polymerization. *e-Polymers* **2004**, *4*, 001.
(261) Fiori, S.; Malucelli, G.; Mariani, A.; Ricco, L.; Casazza, E. Synthesis and Characterization of a Polyester/Styrene Resin Obtained by Frontal Polymerization. *e-Polymers* **2002**, *2*, 057.
(262) Li, Q.; Zhang, W.-c.; Wang, C.-F.; Chen, S. In Situ Access to Fluorescent Dual-Component Polymers Towards Optoelectronic Devices Via Inhomogeneous Biphase Frontal Polymerization. *RSC Adv.* **2015**, *5*, 102294−102299.
(263) Zhou, Z.-F.; Yu, C.; Wang, X.-Q.; Tang, W.-Q.; Wang, C.-F.; Chen, S. Facile Access to Poly(NMA-co-VCL) Hydrogels Via Long Range Laser Ignited Frontal Polymerization. *J. Mater. Chem. A* **2013**, *1*, 7326−7331.
(264) Li, Y.; Yang, S.; Wang, C.-F.; Chen, S. Facile Synthesis of Poly(DMC-co-HPA) Hydrogels Via Infrared Laser Ignited Frontal Polymerization and Their Adsorption-Desorption Switching Performance. *J. Polym. Sci., Part A: Polym. Chem.* **2015**, *53*, 2085−2093.
(265) Fan, S.; Liu, S.; Wang, X.-Q.; Wang, C.-F.; Chen, S. Laser-Ignited Frontal Polymerization of Shape-Controllable Poly(VI-co-Am) Hydrogels Based on 3d Templates toward Adsorption of Heavy Metal Ions. *Appl. Phys. A: Mater. Sci. Process.* **2016**, *122*, 599.
(266) Liu, Y.; Wang, C.-F.; Chen, S. Facile Access to Poly-(DMAEMA-co-AA) Hydrogels Via Infrared Laser-Ignited Frontal Polymerization and Their Polymerization in the Horizontal Direction. *RSC Adv.* **2015**, *5*, 30514−30521.
(267) Chen, T.; Li, Y.; Yang, S.-Y.; Wang, C.-F.; Chen, S. Synthesis of Versatile Poly(PMMA-B-VI) Macromonomer-Based Hydrogels Via Infrared Laser Ignited Frontal Polymerization. *J. Polym. Sci., Part A: Polym. Chem.* **2016**, *54*, 1210−1221.
(268) Petko, F.; Świeży, A.; Ortyl, J. Photoinitiating Systems and Kinetics of Frontal Photopolymerization Processes - the Prospects for Efficient Preparation of Composites and Thick 3d Structures. *Polym. Chem.* **2021**, *12*, 4593−4612.
(269) Gugg, A.; Gorsche, C.; Moszner, N.; Liska, R. Frontal Polymerization: Polymerization Induced Destabilization of Peracrylates. *Macromol. Rapid Commun.* **2011**, *32*, 1096−1100.
(270) Shao, H.; Wang, C.-F.; Chen, S.; Xu, C. Fast Fabrication of Superabsorbent Polyampholytic Nanocomposite Hydrogels Via Plasma-Ignited Frontal Polymerization. *J. Polym. Sci., Part A: Polym. Chem.* **2014**, *52*, 912−920.
(271) Zhou, J.; Shao, H.; Tu, J.; Fang, Y.; Guo, X.; Wang, C.-F.; Chen, L.; Chen, S. Available Plasma-Ignited Frontal Polymerization Approach toward Facile Fabrication of Functional Polymer Hydrogels. *Chem. Mater.* **2010**, *22*, 5653−5659.
(272) Zhou, J.; Tang, W.-Q.; Wang, C.-F.; Chen, L.; Chen, Q.; Chen, S. In Situ Access to White Light-Emitting Fluorescent Polymer Nanocomposites Via Plasma-Ignited Frontal Polymerization. *J. Polym. Sci., Part A: Polym. Chem.* **2012**, *50*, 3736−3742.
(273) Nania, M.; Matar, O. K.; Cabral, J. T. Frontal Vitrification of Pdms Using Air Plasma and Consequences for Surface Wrinkling. *Soft Matter* **2015**, *11*, 3067−3075.
(274) Mahmoudi, M.; Sant, S.; Wang, B.; Laurent, S.; Sen, T. Superparamagnetic Iron Oxide Nanoparticles (SPIONs): Development, Surface Modification and Applications in Chemotherapy. *Adv. Drug Delivery Rev.* **2011**, *63*, 24−46.
(275) Lewis, L. L.; DeBisschop, C. S.; Pojman, J. A.; Volpert, V. A. Isothermal Frontal Polymerization: Confirmation of the Mechanism and Determination of Factors Affecting the Front Velocity, Front Shape, and Propagation Distance with Comparison to Mathematical Modeling. *J. Polym. Sci., Part A: Polym. Chem.* **2005**, *43*, 5774−5786.
(276) Dixon, K. W. Decomposition Rates of Organic Free Radical Initiators. In *Polymer Handbook*, 4th ed.; Brandrup, J., Immergut, E. H., Grulke, E. A., Abe, A., Bloch, D. R., Eds.; John Wiley & Sons: 1999; pp 1−43.
(277) Kolthoff, I. M.; Miller, I. K. The Chemistry of Persulfate. I. The Kinetics and Mechanism of the Decomposition of the Persulfate Ion in Aqueous Medium1. *J. Am. Chem. Soc.* **1951**, *73*, 3055−3059.
(278) Cabral, J. T.; Hudson, S. D.; Harrison, C.; Douglas, J. F. Frontal Photopolymerization for Microfluidic Applications. *Langmuir* **2004**, *20*, 10020−10029.
(279) Vitale, A.; Hennessy, M. G.; Matar, O. K.; Cabral, J. T. A Unified Approach for Patterning Via Frontal Photopolymerization. *Adv. Mater.* **2015**, *27*, 6118−6124.
(280) Hennessy, M. G.; Vitale, A.; Matar, O. K.; Cabral, J. T. Controlling Frontal Photopolymerization with Optical Attenuation and Mass Diffusion. *Phys. Rev. E* **2015**, *91*, 062402.
(281) Hennessy, M. G.; Vitale, A.; Cabral, J. T.; Matar, O. K. Role of Heat Generation and Thermal Diffusion During Frontal Photopolymerization. *Phys. Rev. E* **2015**, *92*, 022403.
(282) Cabral, J. T.; Douglas, J. F. Propagating Waves of Network Formation Induced by Light. *Polymer* **2005**, *46*, 4230−4241.
(283) Perry, M. F.; Volpert, V. A.; Lewis, L. L.; Nichols, H. A.; Pojman, J. A. Free-Radical Frontal Copolymerization: The Dependence of the Front Velocity on the Monomer Feed Composition and Reactivity Ratios. *Macromol. Theory Simul.* **2003**, *12*, 276−286.
(284) Zakiev, S. E.; Dzhardimalieva, G. I.; Pomogailo, A. D. Nonthermal Model for Thermal Frontal Polymerization of Metal-Containing Monomers. *Polym. Sci. Ser. B* **2017**, *59*, 210−215.
(285) Singh, S.; Singh, M.; Yadav, B. C.; Tandon, P.; Pomogailo, S. I.; Dzhardimalieva, G. I.; Pomogailo, A. D. Experimental Investigations on Liquefied Petroleum Gas Sensing of $Cd(NO_3)_2{\cdot}(AAm)_4{\cdot}2H_2O$ and Cds/Polyacrylamide Synthesized Via Frontal Polymerization. *Sens. Actuators, B* **2011**, *160*, 826−834.
(286) Maciejewska, E.; Leonowicz, M.; Pomogailo, A. D.; Dzhardimalieva, G. I. Intermatrix Synthesis of Magnetic Nanocrystals by Frontal Polymerization and Subsequent Pyrolysis of Iron Containing Monomer. *IEEE Trans. Magn.* **2008**, *44*, 2764−2767.
(287) Sówka, E.; Leonowicz, M.; Kaźmierczak, J.; Ślawska-Waniewska, A.; Pomogailo, A. D.; Dzhardimalieva, G. I. Formation of Cobalt Nanoparticles in Inorganic Matrix by Frontal Polymerisation and Thermolysis of Metal-Containing Monomers. *Physica B Condens. Matter* **2006**, *384*, 282−285.
(288) Kholpanov, L. P.; Zakiev, S. E.; Pomogailo, A. D. Two-Phase Frontal Polymerization of Metal-Containing Monomers. *Polym. Sci. Ser. A* **2006**, *48*, 11−17.
(289) Pomogailo, A. D.; Dzhardimalieva, G. Frontal Polymerization of Metal-Containing Monomers: Achievements and Problems. *Polym. Sci. Ser. A* **2004**, *46*, 250−263.
(290) Kholpanov, L. P.; Zakiev, S. E.; Pomogailo, A. D. Modeling of Frontal Polymerization with Consideration of Phase Transitions in the Reaction Front. *Dokl. Phys. Chem.* **2004**, *395*, 84−87.
(291) Dzhardimalieva, G. I.; Golubeva, N. D.; Pomogailo, A. D. Frontal Polymerization of Metal-Containing Monomers as a Way for Synthesis of Polymer Nanocomposites. *Solid State Phenom.* **2003**, *94*, 323−328.
(292) Dzhardimalieva, G. I.; Pomogailo, A. D.; Volpert, V. A. Frontal Polymerization of Metal-Containing Monomers: A Topical Review. *J. Inorg. Organomet. Polym.* **2002**, *12*, 1−21.
(293) Barelko, V. V.; Pomogailo, A. D.; Dzhardimalieva, G. I.; Evstratova, S. I.; Rozenberg, A. S.; Uflyand, I. E. The Autowave Modes of Solid Phase Polymerization of Metal-Containing Monomers in Two- and Three-Dimensional Fiberglass-Filled Matrices. *Chaos* **1999**, *9*, 342−347.
(294) Savostyanov, V. S.; Kritskaya, D. A.; Ponomarev, A. N.; Pomogailo, A. D. Thermally Initiated Frontal Polymerization of Transition Metal Nitrate Acrylamide Complexes. *J. Polym. Sci., Part A: Polym. Chem.* **1994**, *32*, 1201−1212.
(295) McCurdy, K. G.; Laidler, K. J. Rates of Polymerization of Acrylates and Methacrylates in Emulsion Systems. *Can. J. Chem.* **1964**, *42*, 825−829.

https://doi.org/10.1021/acs.chemrev.2c00686
Chem. Rev. 2023, 123, 3237−3298

(296) Barner-Kowollik, C.; Beuermann, S.; Buback, M.; Castignolles, P.; Charleux, B.; Coote, M. L.; Hutchinson, R. A.; Junkers, T.; Lacík, I.; Russell, G. T.; Stach, M.; van Herk, A. M. Critically Evaluated Rate Coefficients in Radical Polymerization - 7. Secondary-Radical Propagation Rate Coefficients for Methyl Acrylate in the Bulk. *Polym. Chem.* **2014**, *5*, 204−212.
(297) Willemse, R. X. E.; van Herk, A. M. Determination of Propagation Rate Coefficients of a Family of Acrylates with PLP-MALDI-TOF-MS. *Macromol. Chem. Phys.* **2010**, *211*, 539−545.
(298) Beuermann, S.; Buback, M. Rate Coefficients of Free-Radical Polymerization Deduced from Pulsed Laser Experiments. *Prog. Polym. Sci.* **2002**, *27*, 191−254.
(299) Kamachi, M.; Yamada, B. Propagation and Termination Constants in Free Radical Polymerization. In *Polymer Handbook*, 4th ed.; Brandrup, J., Immergut, E. H., Grulke, E. A., Abe, A., Bloch, D. R., Eds.; John Wiley & Sons: 1999; pp 77−94.
(300) Moore, J. E.; Schroeter, S. H.; Shultz, A. R.; Stang, L. D. Calorimetric Analysis of Photopolymerizations. In *Ultraviolet Light Induced Reactions in Polymers*; American Chemical Society: 1976; Vol. *25*, pp 90−106.
(301) Lalevée, J.; Allonas, X.; Fouassier, J. P. Direct Measurements of the Addition and Recombination of Acrylate Radicals: Access to Propagation and Termination Rate Constants? *J. Polym. Sci., Part A: Polym. Chem.* **2006**, *44*, 3577−3587.
(302) Duran, H.; Meng, S.; Kim, N.; Hu, J.; Kyu, T.; Natarajan, L. V.; Tondiglia, V. P.; Bunning, T. J. Kinetics of Photopolymerization-Induced Phase Separation and Morphology Development in Mixtures of a Nematic Liquid Crystal and Multifunctional Acrylate. *Polymer* **2008**, *49*, 534−545.
(303) Mota-Morales, J. D.; Gutiérrez, M. C.; Ferrer, M. L.; Jiménez, R.; Santiago, P.; Sanchez, I. C.; Terrones, M.; Del Monte, F.; Luna-Bárcenas, G. Synthesis of Macroporous Poly(Acrylic Acid)-Carbon Nanotube Composites by Frontal Polymerization in Deep-Eutectic Solvents. *J. Mater. Chem. A* **2013**, *1*, 3970−3976.
(304) Mota-Morales, J. D.; Gutiérrez, M. C.; Sanchez, I. C.; Luna-Bárcenas, G.; del Monte, F. Frontal Polymerizations Carried out in Deep-Eutectic Mixtures Providing Both the Monomers and the Polymerization Medium. *Chem. Commun.* **2011**, *47*, 5328−5330.
(305) Fazende, K. F.; Phachansitthi, M.; Mota-Morales, J. D.; Pojman, J. A. Frontal Polymerization of Deep Eutectic Solvents Composed of Acrylic and Methacrylic Acids. *J. Polym. Sci., Part A: Polym. Chem.* **2017**, *55*, 4046−4050.
(306) Fang, Y.; Chen, L.; Wang, C.-f.; Chen, S. Facile Synthesis of Fluorescent Quantum Dot-Polymer Nanocomposites Via Frontal Polymerization. *J. Polym. Sci., Part A: Polym. Chem.* **2010**, *48*, 2170−2177.
(307) Chekanov, Y.; Arrington, D.; Brust, G.; Pojman, J. A. Frontal Curing of Epoxy Resins: Comparison of Mechanical and Thermal Properties to Batch-Cured Materials. *J. Appl. Polym. Sci.* **1997**, *66*, 1209−1216.
(308) Frulloni, E.; Salinas, M. M.; Torre, L.; Mariani, A.; Kenny, J. M. Numerical Modeling and Experimental Study of the Frontal Polymerization of the Diglycidyl Ether of Bisphenol a/Diethylenetriamine Epoxy System. *J. Appl. Polym. Sci.* **2005**, *96*, 1756−1766.
(309) Gill, N.; Pojman, J. A.; Willis, J.; Whitehead, J. B., Jr Polymer-Dispersed Liquid-Crystal Materials Fabricated with Frontal Polymerization. *J. Polym. Sci., Part A: Polym. Chem.* **2003**, *41*, 204−212.
(310) Fu, J.; in het Panhuis, M. Hydrogel Properties and Applications. *J. Mater. Chem. B* **2019**, *7*, 1523−1525.
(311) Mondal, S.; Das, S.; Nandi, A. K. A Review on Recent Advances in Polymer and Peptide Hydrogels. *Soft Matter* **2020**, *16*, 1404−1454.
(312) Alzari, V.; Nuvoli, D.; Scognamillo, S.; Piccinini, M.; Gioffredi, E.; Malucelli, G.; Marceddu, S.; Sechi, M.; Sanna, V.; Mariani, A. Graphene-Containing Thermoresponsive Nanocomposite Hydrogels of Poly(N-Isopropylacrylamide) Prepared by Frontal Polymerization. *J. Mater. Chem.* **2011**, *21*, 8727−8733.
(313) Feng, Q.; Li, F.; Yan, Q.-Z.; Zhu, Y.-C.; Ge, C.-C. Frontal Polymerization Synthesis and Drug Delivery Behavior of Thermo-Responsive Poly(N-Isopropylacrylamide) Hydrogel. *Colloid Polym. Sci.* **2010**, *288*, 915−921.
(314) Scognamillo, S.; Alzari, V.; Nuvoli, D.; Illescas, J.; Marceddu, S.; Mariani, A. Thermoresponsive Super Water Absorbent Hydrogels Prepared by Frontal Polymerization of N-Isopropyl Acrylamide and 3-Sulfopropyl Acrylate Potassium Salt. *J. Polym. Sci., Part A: Polym. Chem.* **2011**, *49*, 1228−1234.
(315) Zhang, Q.; Weber, C.; Schubert, U. S.; Hoogenboom, R. Thermoresponsive Polymers with Lower Critical Solution Temperature: From Fundamental Aspects and Measuring Techniques to Recommended Turbidimetry Conditions. *Mater. Horizons* **2017**, *4*, 109−116.
(316) Alzari, V.; Ruiu, A.; Nuvoli, D.; Sanna, R.; Martinez, J. I.; Appelhans, D.; Voit, B.; Zschoche, S.; Mariani, A. Three Component Terpolymer and Ipn Hydrogels with Response to Stimuli. *Polymer* **2014**, *55*, 5305−5313.
(317) Alzari, V.; Nuvoli, D.; Sanna, R.; Peponi, L.; Piccinini, M.; Bon, S. B.; Marceddu, S.; Valentini, L.; Kenny, J. M.; Mariani, A. Multistimuli-Responsive Hydrogels of Poly(2-Acrylamido-2-Methyl-1-Propanesulfonic Acid) Containing Graphene. *Colloid Polym. Sci.* **2013**, *291*, 2681−2687.
(318) Damonte, G.; Maddalena, L.; Fina, A.; Cavallo, D.; Müller, A. J.; Caputo, M. R.; Mariani, A.; Monticelli, O. On Novel Hydrogels Based on Poly(2-Hydroxyethyl Acrylate) and Polycaprolactone with Improved Mechanical Properties Prepared by Frontal Polymerization. *Eur. Polym. J.* **2022**, *171*, 111226.
(319) Sanna, R.; Alzari, V.; Nuvoli, D.; Scognamillo, S.; Marceddu, S.; Mariani, A. Polymer Hydrogels of 2-Hydroxyethyl Acrylate and Acrylic Acid Obtained by Frontal Polymerization. *J. Polym. Sci., Part A: Polym. Chem.* **2012**, *50*, 1515−1520.
(320) Sanna, R.; Fortunati, E.; Alzari, V.; Nuvoli, D.; Terenzi, A.; Casula, M. F.; Kenny, J. M.; Mariani, A. Poly(N-Vinylcaprolactam) Nanocomposites Containing Nanocrystalline Cellulose: A Green Approach to Thermoresponsive Hydrogels. *Cellulose* **2013**, *20*, 2393−2402.
(321) Malucelli, G.; Dore, J.; Sanna, D.; Nuvoli, D.; Rassu, M.; Mariani, A.; Alzari, V. Sliding Crosslinked Thermoresponsive Materials: Polypseudorotaxanes Made of Poly(N-Isopropylacrylamide) and Acrylamide-γ-Cyclodextrin. *Front. Chem.* **2018**, xx DOI: 10.3389/fchem.2018.00585.
(322) Liu, J.; Chakraborty, S.; Hosseinzadeh, P.; Yu, Y.; Tian, S.; Petrik, I.; Bhagi, A.; Lu, Y. Metalloproteins Containing Cytochrome, Iron-Sulfur, or Copper Redox Centers. *Chem. Rev.* **2014**, *114*, 4366−4469.
(323) Lellis, B.; Fávaro-Polonio, C. Z.; Pamphile, J. A.; Polonio, J. C. Effects of Textile Dyes on Health and the Environment and Bioremediation Potential of Living Organisms. *Biotechnol. Res. Int.* **2019**, *3*, 275−290.
(324) Li, J.; Mooney, D. J. Designing Hydrogels for Controlled Drug Delivery. *Nat. Rev. Mater.* **2016**, *1*, 16071.
(325) Pojman, J. A.; Elcan, W.; Khan, A. M.; Mathias, L. Binary Frontal Polymerization: A New Method to Produce Simultaneous Interpenetrating Polymer Networks (SINs). *J. Polym. Sci., Part A: Polym. Chem.* **1997**, *35*, 227−230.
(326) Perry, M. F.; Volpert, V. A. Self-Propagating Free-Radical Binary Frontal Polymerization. *J. Eng. Math.* **2004**, *49*, 359−372.
(327) Pojman, J. A.; Griffith, J.; Nichols, H. A. Binary Frontal Polymerization: Velocity Dependence on Initial Composition. *e-Polymers* **2004**, *4*, 13.
(328) Li, Z.; Askim, J. R.; Suslick, K. S. The Optoelectronic Nose: Colorimetric and Fluorometric Sensor Arrays. *Chem. Rev.* **2019**, *119*, 231−292.
(329) Wu, D. Y.; Meure, S.; Solomon, D. Self-Healing Polymeric Materials: A Review of Recent Developments. *Prog. Polym. Sci.* **2008**, *33*, 479−522.
(330) White, S. R.; Sottos, N. R.; Geubelle, P. H.; Moore, J. S.; Kessler, M. R.; Sriram, S. R.; Brown, E. N.; Viswanathan, S. Autonomic Healing of Polymer Composites. *Nature* **2001**, *409*, 794−797.

(331) Toohey, K. S.; Sottos, N. R.; Lewis, J. A.; Moore, J. S.; White, S. R. Self-Healing Materials with Microvascular networks. *Nat. Mater.* **2007**, *6*, 581−585.
(332) Groves, J. F.; Wadley, H. N. G. Functionally Graded Materials Synthesis Via Low Vacuum Directed Vapor Deposition. *Compos. Part B. Eng.* **1997**, *28*, 57−69.
(333) Koizumi, M. Fgm Activities in Japan. *Compos. Part B. Eng.* **1997**, *28*, 1−4.
(334) Watari, F.; Yokoyama, A.; Omori, M.; Hirai, T.; Kondo, H.; Uo, M.; Kawasaki, T. Biocompatibility of Materials and Development to Functionally Graded Implant for Bio-Medical Application. *Compos. Sci. Technol.* **2004**, *64*, 893−908.
(335) Watari, F.; Yokoyama, A.; Saso, F.; Uo, M.; Kawasaki, T. Fabrication and Properties of Functionally Graded Dental Implant. *Compos. Part B. Eng.* **1997**, *28*, 5−11.
(336) Zhang, Q.; Wang, P.; Zhai, Y. Refractive Index Distribution of Graded Index Poly(Methyl Methacrylate) Preform Made by Interfacial-Gel Polymerization. *Macromolecules* **1997**, *30*, 7874−7879.
(337) Heppenheimer, T. A. High-Temperature Structures and Materials. In *NASA's Contributions to Aeronautics*; Hallion, R. P., Ed.; National Aeronautics and Space Administration: Washington D.C., USA, 2010; Vol. *1*, pp 568−629.
(338) Pojman, J. A.; McCardle, T. W. Functionally Gradient Polymeric Materials. US Patent 6057406, May 2, 2000.
(339) Pojman, J. A. Self Organization in Synthetic Polymeric Systems. *Ann. N.Y. Acad. Sci.* **1999**, *879*, 194−214.
(340) Ainsworth, W. J.; Pojman, J. A.; Chekanov, Y. A.; Masere, J. Bubble Behavior in Frontal Polymerization:Results from Kc-135 Parabolic Flights. In *Polymer Research in Microgravity*; American Chemical Society: 2001; Vol. *793*, pp 112−125.
(341) Cuccuru, S.; Mameli, P.; Mariani, A.; Meloni, P.; Oggiano, G. Contrasting Decay of Historical Building Stone: Relationships between Petrophysical Features and Frontal Polymerization Treatment Suitability on Medieval Buildings of North Sardinia, Italy. *Bull. Eng. Geo. Environ.* **2019**, *78*, 1669−1682.
(342) Proietti, N.; Capitani, D.; Cozzolino, S.; Valentini, M.; Pedemonte, E.; Princi, E.; Vicini, S.; Segre, A. L. In Situ and Frontal Polymerization for the Consolidation of Porous Stones: A Unilateral NMR and Magnetic Resonance Imaging Study. *J. Phys. Chem. B* **2006**, *110*, 23719−23728.
(343) Mariani, A.; Bidali, S.; Cappelletti, P.; Caria, G.; Colella, A.; Brunetti, A.; Alzari, V. Frontal Polymerization as a Convenient Technique for the Consolidation of Tuff. *e-Polymers* **2009**, *9*, 064.
(344) Amoroso, G. G.; Fassina, V. *Stone Decay and Conservation*; Elsevier: Losanna, 1983.
(345) *3p Quickcure Woodfiller*. https://3pquickcurewoodfiller.com/product/3p-quick-cure-woodfiller/ (accessed: 8/31/2022).
(346) Li, C.; Gong, X. Z.; Cui, S. P.; Wang, Z. H.; Zheng, Y.; Chi, B. C. Co2 Emissions Due to Cement Manufacture. *Mater. Sci. Forum* **2011**, *685*, 181−187.
(347) Sprung, S. Cement. In *Ullmann's Encyclopedia of Industrial Chemistry*; Wiley-VCH: Weinheim, 2012; Vol. *7*, pp 399−461.
(348) Turner, L. K.; Collins, F. G. Carbon Dioxide Equivalent (Co2-E) Emissions: A Comparison between Geopolymer and Opc Cement Concrete. *Constr. Build Mater.* **2013**, *43*, 125−130.
(349) Komnitsas, K.; Zaharaki, D. Geopolymerisation: A Review and Prospects for the Minerals Industry. *Miner. Eng.* **2007**, *20*, 1261−1277.
(350) Zhang, R.; Qiu, Z.; Qiu, H.; Zhang, X. Frontal Polymerization of Superabsorbent Nanocomposites Based on Montmorillonite and Polyacrylic Acid with Enhanced Soil Properties. *J. Appl. Polym. Sci.* **2014**, xxx DOI: 10.1002/app.39825.
(351) Parker, D.; Bussink, J.; van de Grampel, H. T.; Wheatley, G. W.; Dorf, E.-U.; Ostlinning, E.; Reinking, K.; Schubert, F.; Jünger, O.; Wagener, R. Polymers, High-Temperature. In *Ullmann's Encyclopedia of Industrial Chemistry*; Wiley-VCH: Weinheim, Germany, 2012; pp 1−42.
(352) Yuan, Y. C.; Ye, X. J.; Rong, M. Z.; Zhang, M. Q.; Yang, G. C.; Zhao, J. Q. Self-Healing Epoxy Composite with Heat-Resistant Healant. *ACS Appl. Mater. Interfaces* **2011**, *3*, 4487−4495.
(353) Shi, Y.; Yu, B.; Wang, X.; Yuen, A. C. Y. Editorial: Flame-Retardant Polymeric Materials and Polymer Composites. *Front. Mater.* **2021**, DOI: 10.3389/fmats.2021.703123.
(354) Campbell, F. C. Chapter 8—Adhesive Bonding and Integrally Cocured Structure: A Way to Reduce Assembly Costs through Parts Integration. In *Manufacturing Processes for Advanced Composites*; Campbell, F. C., Ed.; Elsevier Science: Amsterdam, 2004; pp 241−301.
(355) Raos, G.; Zappone, B. Polymer Adhesion: Seeking New Solutions for an Old Problem. *Macromolecules* **2021**, *54*, 10617−10644.
(356) *3p Quickcure Clay*. http://pojman.com/3PQCC/3Pquickcureclay.html (accessed: 3/2/2022).
(357) *Ranger Ink: Quickcure Clay*. https://rangerink.com/collections/ranger-quickcure-clay (accessed: 3/2/2022).
(358) *Polymers in Art through the Centuries*. https://www.lasm.org/exhibitions/art-exhibitions/polymers-in-art-through-the-centuries (accessed: 3/2/2022).
(359) Liu, C.; Li, Q.; Wang, H.; Wang, G.; Shen, H. Quantum Dots-Loaded Self-Healing Gels for Versatile Fluorescent Assembly. *Nanomaterials* **2022**, *12*, 452.
(360) Gupta, L. K.; Kumar, K.; Yadav, B. C.; Yadav, T. P.; Dzhardimalieva, G. I.; Uflyand, I. E.; et al. Shripal Comparative Study on Humidity Sensing Abilities of Synthesized Mono and Poly Rhodium Acryl Amide Tin Oxide (Rhaam/Sno2) Nanocomposites. *Sens. Actuators, A Phys.* **2021**, *330*, 112839.
(361) Carey, G. H.; Abdelhady, A. L.; Ning, Z.; Thon, S. M.; Bakr, O. M.; Sargent, E. H. Colloidal Quantum Dot Solar Cells. *Chem. Rev.* **2015**, *115*, 12732−12763.
(362) Moreels, I.; Justo, Y.; De Geyter, B.; Haustraete, K.; Martins, J. C.; Hens, Z. Size-Tunable, Bright, and Stable Pbs Quantum Dots: A Surface Chemistry Study. *ACS Nano* **2011**, *5*, 2004−2012.
(363) Kim, L.; Anikeeva, P. O.; Coe-Sullivan, S. A.; Steckel, J. S.; Bawendi, M. G.; Bulović, V. Contact Printing of Quantum Dot Light-Emitting Devices. *Nano Lett.* **2008**, *8*, 4513−4517.
(364) Anikeeva, P. O.; Halpert, J. E.; Bawendi, M. G.; Bulović, V. Quantum Dot Light-Emitting Devices with Electroluminescence Tunable over the Entire Visible Spectrum. *Nano Lett.* **2009**, *9*, 2532−2536.
(365) *Qled Vs. Oled Tvs: Which Tv Technology Is Better in 2022?* https://www.cnet.com/tech/home-entertainment/qled-vs-oled-samsung-and-lg-tv-technologies-explained/ (accessed: 5/16/2022).
(366) Nazzal, A. Y.; Qu, L.; Peng, X.; Xiao, M. Photoactivated Cdse Nanocrystals as Nanosensors for Gases. *Nano Lett.* **2003**, *3*, 819−822.
(367) Verma, A.; Chaudhary, P.; Tripathi, R. K.; Yadav, B. C. Flexible, Environmentally-Acceptable and Long-Durable-Energy-Efficient Novel Ws2-Polyacrylamide Mofs for High-Performance Photodetectors. *Mater. Adv.* **2022**, *3*, 3994.
(368) Cabral, J. T.; Hudson, S. D. Microfluidic Approach for Rapid Multicomponent Interfacial Tensiometry. *Lab Chip* **2006**, *6*, 427−436.
(369) Cygan, Z. T.; Cabral, J. T.; Beers, K. L.; Amis, E. J. Microfluidic Platform for the Generation of Organic-Phase Microreactors. *Langmuir* **2005**, *21*, 3629−3634.
(370) Chen, Z.; Liu, P.; Shi, L.; Huang, Z. X.; Jiang, B. Y. Preparation of Nano Carbon Black/Epoxy Composite by Frontal Polymerization. *Appl. Mech. Mater.* **2014**, *692*, 416−419.
(371) Korotkov, V. N.; Chekanov, Y. A.; Rozenberg, B. A. The Simultaneous Process of Filament Winding and Curing for Polymer Composites. *Compos. Sci. Technol.* **1993**, *47*, 383−388.
(372) White, S. R.; Kim, C. A Simultaneous Lay-up and in Situ Cure Process for Thick Composites. *J. Reinf. Plast. Compos.* **1993**, *12*, 520−535.
(373) Kim, C.; Teng, H.; Tucker, C. L.; White, S. R. The Continuous Cuing Process for Thermoset Polymer Composites. Part

https://doi.org/10.1021/acs.chemrev.2c00686
Chem. Rev. 2023, 123, 3237−3298

1: Modeling and Demonstration. *J. Comp. Mater.* **1995**, *29*, 1222−1253.
(374) Dean, L. M. Rapid on-Demand Polymerization for Multifunctional Materials. Ph.D. Dissertation, University of Illinois at Urbana-Champaign, 2021.
(375) Leguizamon, S. C.; Monk, N. T.; Hochrein, M. T.; Zapien, E. M.; Yoon, A.; Foster, J. C.; Appelhans, L. N. Photoinitiated Olefin Metathesis and Stereolithographic Printing of Polydicyclopentadiene. *Macromolecules* **2022**, *55*, 8273−8282.
(376) Schnoell, C.; Liska, R.; Knaack, P.; Mitterbauer, M.; Grunenberg, D. Process for Producing Adhesive Tapes or Molding Compounds. Patent WO 2021148602 A1, July 29, 2021.
(377) Xie, T.; Nowak, A. P.; Boundy, T. Compositions, Methods, and Apparatus for Remote Triggering of Frontally Curable Adhesives. US Patent US 20150152215 A1, June 4, 2015.
(378) He, W.; Ao, Y. Dual-Curing Frontal Polymerization Conductive Silver Adhesive and Its Preparation Method. Patent CN 105062398 A, November 18, 2015.
(379) Bidali, S.; Fiori, S.; Mariani, A.; Moggi, G.; Pedemonte, E.; Princi, E.; Russo, S.; Vicini, S.; Vigo, D. Mortar Composition with Acrylic-Based Binder Obtained by Frontal Polymerization and Prepared in the Resence of Inorganic Compounds. Patent IT 2004GE0029 A1, July 14, 2004.
(380) Hoyle, C. E.; Pojman, J. A. Rapid Curing Wood Putty Based on Frontal Polymerization. US PatentUS 20090155485 A1, June 18, 2009.
(381) Buergel, T.; Pfeil, A. Reactive Resin Mortar That Can Be Cured by Means of Frontal Polymerization and Method for Fastening Anchor Rods. Patent WO 2015040143 A1, March 26, 2015.
(382) Jethmalani, J. M.; Warden, L.; Lai, S. T.; Dreher, A. W. Method of Manufacturing an Optical Lens. Patent US8753551B2, June 17, 2014.
(383) Banish, M.; Banish, R.; Crandal, D. Disinfectant System. Patent WO2021237024 A1, November 25, 2021.
(384) Moore, J. S.; White, S. R.; Robertson, I. D.; Sottos, N. R.; Aw, J. E. 3d Printing of Thermoset Polymers and Composites. US Patent US20180327531 A1, November 15, 2018.
(385) Moore, J. S.; Sottos, N. R.; Suslick, B. A.; Stawiasz, K.; Paul, J. E. Frontally Polymerized Polymeric Body and Method of Producing a Polymeric Body Having Spatially Varying Properties. US Patent US20220235173 A1, July 28, 2022.
(386) Moore, J. S.; Geubelle, P. H.; Sottos, N. R.; Feinberg, A. M.; Lloyd, E. M. Method of Spontaneously Patterning a Polymer During Frontal Polymerization. Patent WO2022125437 A1, June 16, 2022.
(387) Mackay, B. A.; Sullivan, P. F. D.; Droger, N.; D'Angelo, R. M.; Miller, D. E. Method for Treating Well Bore within a Subterranean Formation. Patent WO2011042826 A2, April 14, 2011.
(388) Ge, C.; Yan, Q. Method for Preparing Superabsorbent Resin Via Frontal Polymerization. Patent CN1648137 A, August 8, 2005.
(389) Davtyan, D. S.; Tonoyan, A. O.; Davtyan, S. P. Method for Producing Polyacrylamide Hydrogels by Continuous Frontal Polymerization. Patent RU2681212 C1, March 5, 2019.
(390) Kalmykova, Y.; Sadagopan, M.; Rosado, L. Circular Economy - from Review of Theories and Practices to Development of Implementation Tools. *Resour. Conserv. Recycl.* **2018**, *135*, 190−201.
(391) Johnson, A. M.; Husted, K. E. L.; Kilgallon, L. J.; Johnson, J. A. Orthogonally Deconstructable and Depolymerizable Polysilylethers Via Entropy-Driven Ring-Opening Metathesis Polymerization. *Chem. Commun.* **2022**, *58*, 8496−8499.
(392) Husted, K. E. L.; Shieh, P.; Lundberg, D. J.; Kristufek, S. L.; Johnson, J. A. Molecularly Designed Additives for Chemically Deconstructable Thermosets without Compromised Thermomechanical Properties. *ACS Macro Lett.* **2021**, *10*, 805−810.
(393) Alzate-Sanchez, D. M.; Yu, C. H.; Lessard, J. J.; Paul, J. E.; Sottos, N. R.; Moore, J. S. Rapid Controlled Synthesis of Large Polymers by Frontal Ring-Opening Metathesis Polymerization. *Macromolecules* **2023**, x DOI: 10.1021/acs.macromol.2c01892.

Recommended by ACS

Enzymes' Power for Plastics Degradation
Vincent Tournier, Isabelle André, *et al.*
MARCH 14, 2023
CHEMICAL REVIEWS
READ

Biobased, Degradable, and Conjugated Poly(Azomethine)s
Azalea Uva, Helen Tran, *et al.*
FEBRUARY 07, 2023
JOURNAL OF THE AMERICAN CHEMICAL SOCIETY
READ

A Single-Atom Upgrade to Polydicyclopentadiene
Benjamin Godwin, Jeremy E. Wulff, *et al.*
FEBRUARY 08, 2023
MACROMOLECULES
READ

Catalytic Chemical Recycling of Post-Consumer Polyethylene
Alejandra Arroyave, Geoffrey W. Coates, *et al.*
DECEMBER 16, 2022
JOURNAL OF THE AMERICAN CHEMICAL SOCIETY
READ

Get More Suggestions >